To the Graduate Council:

I am submitting herewith a thesis written by Christopher L. Lewis entitled "Isothermal and Nonisothermal Crystallization Kinetics of 2-Methyl-1,3-Propanediol Substituted Poly(ethylene terephthalate)." I have examined the final paper copy of this thesis for form and content and recommend that it be accepted in partial fulfillment of the requirements for the degree of Master of Science, with a major in Polymer Engineering.

Joseph E. Spruiell, Major Professor

We have read this thesis and
recommend its acceptance:

Acceptance for the Council:

Vice Provost and Dean of
Graduate Studies

ISOTHERMAL AND NONISOTHERMAL CRYSTALLIZATION KINETICS OF 2-METHYL-1,3-PROPANEDIOL SUBSTITUTED POLY(ETHYLENE TEREPHTHALATE)

A Thesis
Presented for the
Master of Science
Degree

The University of Tennessee, Knoxville

Christopher L. Lewis

May, 2002

DEDICATION

This thesis is dedicated to my wife

Aimee J. Lewis

whose love and support has made this work possible

ACKNOWLEDGEMENTS

First and foremost I would like to express my sincere gratitude to Dr. Joseph E. Spruiell who has provided me with much guidance in both this research and the preparation of this manuscript. I am also grateful to all of the members of Dr. Spruiell's research group, particularly Gary Holt and Jaein Suh, for their guidance and willingness to devote much of their time discussing this research.

I would also like to express my sincere gratitude to the ATHAS research group, particularly Dr. Marek Pyda and Dr. Joengihm Pak, for allowing me to use their DSC and for their many hours of discussion related to this work.

I would also like to thank the members of the electronics shop and Doug Fielden's group for all of their help related to the maintenance of the experimental equipment.

To my parents, H. Lloyd and Diana Lewis, and my sister, Tracie Lewis, I owe many thanks for the great support they have shown me throughout my life and for making me believe that I can be anything that I want to be. I would also like to express my thanks to Albert and Diane Horning for their strong belief in education and faith in my abilities.

And to my wife Aimee, whose continued support and belief in my abilities has allowed this work to become a reality. For the many hours that she spent with me discussing this work and reviewing this manuscript, and for her genuine belief in me, I am sincerely grateful.

And last but certainly not least to my Lord Jesus Christ, for by his grace I am.

ABSTRACT

Differential Scanning Calorimetry (DSC) and a modified Light Depolarizing Microscopy (LDM) technique, capable of producing controlled cooling rates up to 5,000°C/min, was used to evaluated the isothermal and nonisothermal crystallization kinetics of poly(ethylene terephthalate) (PET) copolymers containing 2-methyl-1,3-propanediol (MPDiol) as a comonomer unit. The results of these experiments indicate that both the isothermal and nonisothermal crystallization kinetics are reduced by the addition of this comonomer. In this case it appears that the more flexible glycol group does not increase crystallization rates by promoting chain folding during crystallization, as has been suggested for some other glycol modified PET copolyesters. The melting behavior was also examined where it was found that the inclusion of these comonomers served to decrease the observed melting temperature. The isothermal melting behavior was examined using a Hoffman-Weeks approach, showing very good linearity for all copolymers tested and predicted an equilibrium melting temperature of 280.0°C for PET homopolymer. The remaining copolymers showed a marked decrease in T_m^0 with increasing copolymer composition. The results of the analysis of the melting behavior support the claim that these comonomers are excluded from the polymer crystal during growth. Nonisothermal crystallization experiments showed similar results, both at moderate cooling rates examined using DSC and at high cooling rates using the modified LDM technique. The experimental data were examined both as a function of cooling rate and temperature where in both cases it was shown that the incorporation of MPDiol

results in the reduction of the rate of crystallization. Likewise, the cooling rate required to quench the materials to the glassy state (QCR) was estimated using the LDM technique where it was shown that an increase in MPDiol content reduces QCR. From this experiment, Continuous Cooling Transform (CCT) diagrams were proposed for each of the three materials.

TABLE OF CONTENTS

Chapter Page

Chapter Page

Chapter Page

LIST OF TABLES

Table Page

Table Page

LIST OF FIGURES

Figure Page

Figure Page

Figure Page

Figure Page

Figure Page

Figure Page

Figure Page

Figure Page

CHAPTER 1: INTRODUCTION

Poly(ethylene terephthalate) (PET) is a polymer that has found widespread use and has established itself as arguably one of the most industrially important polyester materials. Many investigators have attempted to improve upon the base PET architecture through copolymerization with other glycols to produce glycol modified PET copolyesters. One such case is that of the 2-methyl-1,3-propanediol (MPDiol) substituted PET copolymers recently studied by Suh (2001). In this study, Suh (2001) found that for melt spun fibers, an increase in the MPDiol content up to 7mol% allowed for the maximum take-up velocities to be increased at a given mass throughput, thus allowing for increased productivity. In this study it was also found that the crystallinity and birefringence of the MPDiol substituted copolyesters fibers decreased with increasing comonomer concentrations.

The purpose of this study is to further examine the effect of the incorporation of MPDiol, partially substituted for ethylene glycol in the manufacture of these PET copolyesters, on the crystallization kinetics under isothermal and nonisothermal conditions. In particular the crystallization kinetics of samples containing 4, 7, and 10 mol% MPDiol will be compared to PET homopolymer samples.

In this study the isothermal crystallization kinetics will be examined using a Differential Scanning Calorimeter (DSC) where the rates of crystallization will be determined using the Avrami equation. The melting behavior, upon subsequent reheating of the isothermally crystallized samples, will also be examined with the equilibrium melting temperatures determined using the Hoffman-Weeks approach. Using this data

the isothermal crystallization kinetics, as determined using the Avrami equation, will then be used to compare these materials on the basis of undercooling ($\Delta T=T_m^0-T_m$). In addition, the activation energy of the crystallization process for each material will be estimated both by a phenomenological approach, as well as by the more traditional Avrami approach.

Nonisothermal crystallization experiments will be conducted using both a DSC as well as a modified Light Depolarizing Microscopic (LDM) technique developed in the labs at the University of Tennessee by Ding and Spruiell (1996). For moderate cooling rates, a DSC will be used to evaluate the crystallization kinetics from 1-12.5°C/min with the resulting data analyzed using the Avrami and Ozawa equations. Also the activation energy of crystallization will be approximated using the Kissinger equation and compared to that found in isothermal experiments. Additionally, the nonisothermally crystallized materials will be subsequently reheated in the DSC so as to examine the melting behavior and compared to that found in the isothermal crystallization experiment.

The modified LDM technique, capable of producing cooling rates in excess of 5,000°C/min, will be used to examine the nonisothermal crystallization kinetics of these polymers under conditions that are more realistic to that which would occur under normal polymer processing conditions. All samples will be cooled from a standard temperature in the melt (ca. 290°C) at increasing cooling rates until the material has been quenched to the glassy state. The resulting data will then be examined using the traditional Avrami approach. Additionally, Continuous Cooling Transformation (CCT) diagrams for each of the four materials will be generated and compared.

CHAPTER 2: LITERATURE REVIEW

2.1 Polyethylene Terephthalate

2.1.1. Uses of Polyethylene Terephthalate

Poly(ethylene terephthalate) (PET) is a polymer that has become of great industrial significance. Due to its excellent barrier properties, PET is used in the packaging industry primarily as films or as the raw material for bottles. In fact, it was reported that in 1994 the U.S. consumption of PET for bottling applications alone was estimated at 702,000 tons (Mitchell 1994). PET has also found widespread use as the raw material for melt-spun fibers used extensively in the textiles industry.

In many cases the physical and/or chemical properties of PET homopolymer are insufficient in satisfying the requirements of all potential applications. PET can be modified by copolymerization to improve these properties. For example, copolyesters of glycol-modified PET have been used for many years in the bottling industry. The presence of the comonomer decreases the rate of crystallization, thus allowing for clearer bottles to be produced (Richardson 1989). Other properties affected by copolymerization include glass transition temperature, melting point, degree of crystallinity, mechanical properties, dyeing behavior, and moisture absorption (Varma et al 1986).

2.1.2. Preparation of PET

The basic preparation and chemical structure of PET is shown in Figure 2.1. As is depicted, PET is most commonly prepared by the transesterification reaction of

dimethyl terephthalate and ethylene glycol (Stevens 1990, Ulrich 1993). In this process, dimethyl terephthalate is heated with ethylene glycol to yield a mixture of dihydroxyethyl terephthalate and low molecular weight oligomers. A final polycondensation reaction is performed by further heating under vacuum to approximately 270°C in the presence of a catalyst (in this case Sb_2O_3) to produce the final polymer through a second interchange reaction. The final product is then extruded and pelletized.

During the polymerization of PET it is important to point out that a small amount (≈ 2-4 mol%) of the dimer diethylene glycol (DEG) is incorporated into the main chain of the final product (Fakirov 1997, Bouma et al 2001).

It has been reported that PET copolymers containing 2-methyl-1,3 propanediol have been produced that increase the dyeability of melt spun fibers, while exhibiting

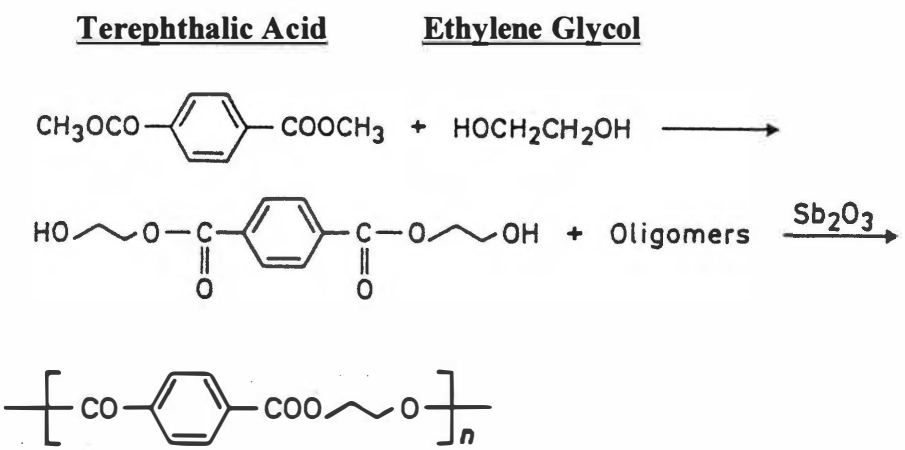

Figure 2.1: Schematic of Preparation of Polyethylene Terephthalate
Adapted from: Ulrich, H.; "Introduction to Industrial Polymers", 2nd ed., Hanser, NY (1993).

greater strength and less elongation (Chen et al 2000). These PET copolymers were prepared in a similar fashion to that suggested for PET homopolymer, as is depicted in Figure 2.2. A slurry mixture composed of excess mixed glycols (ethylene glycol and 2-methyl-1,3 propanediol) and terephthalic acid was first prepared. An esterification reaction of the slurry mixture then took place at 250°C under pressure (absolute pressure = 2 kg/cm^2) at a conversion rate of 95% to yield a low-polymerized product. Antimony trioxide (350 ppm) was then added and polycondensation was carried out for 3 hours at 280°C and an absolute pressure of 1 torr. Since the reactivities of the polymerizing species in a step polymerizing reaction depend primarily on the reactivity of the functional groups, and not on the actual monomers, it is assumed that the resultant polyesters are random copolymers (Boyd and Phillips 1993).

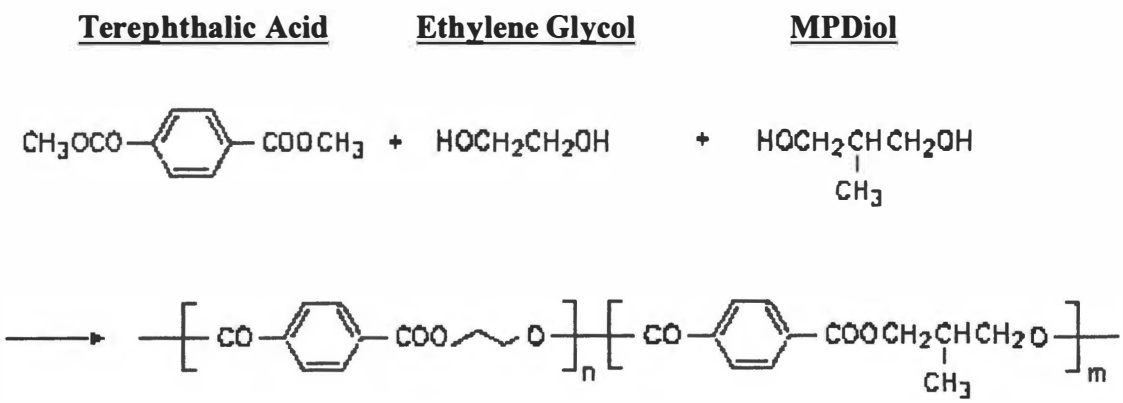

Figure 2.2: Schematic of Preparation of MPDiol Modified PET Copolymers
Adapted from: Ulrich, H.; "Introduction to Industrial Polymers", 2nd ed., Hanser, NY (1993).

2.1.3. Crystal Structure of PET

The unit cell structure of polyethylene terephthalate, as shown in Figure 2.3, is triclinic with cell dimensions of a=4.56Å, b=5.94Å, c=10.75Å, α=98.5°, β=118°, and γ=112° (Daubeny et al 1954). PET is a very stiff macromolecule primarily due the existence of benzene rings in the main polymer chain. As is shown in Figure 2.3 the aromatic, carboxyl, and aliphatic groups lie in a nearly planar configuration and exist in a side-by-side arrangement. Departure from complete linearity was determined by the fact that the measured repeat distance of PET is 10.75Å compared to 10.9Å for a completely flat molecule. This departure from complete planarity is most likely due to rotations about the O-CH_2 bond. No structural evidence was found to suggest the existence of any unusually strong forces between molecules, but rather that the atomic distances between neighboring molecules were characteristic of normal Van der Waals attractive forces (Daubeny et al 1954). These Van der Waals interactions are primarily responsible for the unusually high melting point of PET. The cohesion of PET occurs as a result Van der Waals interactions, caused by dipole interactions, induction, and dispersion forces among the chains (Gupta 1983).

The density of PET homopolymer is reported as being in the range 1.36-1.38 g/cm^3 (Ulrich 1993), while unit cell calculations suggests that 100% crystalline PET will have a density of 1.455 g/cm^3 (Daubeny et al 1954). Completely amorphous PET has a density in the range of 1.328 – 1.341 g/cm^3, depending on the DEG content (1.83-14.90 mol%) (Fakirov et al 1985, Fakirov 1985).

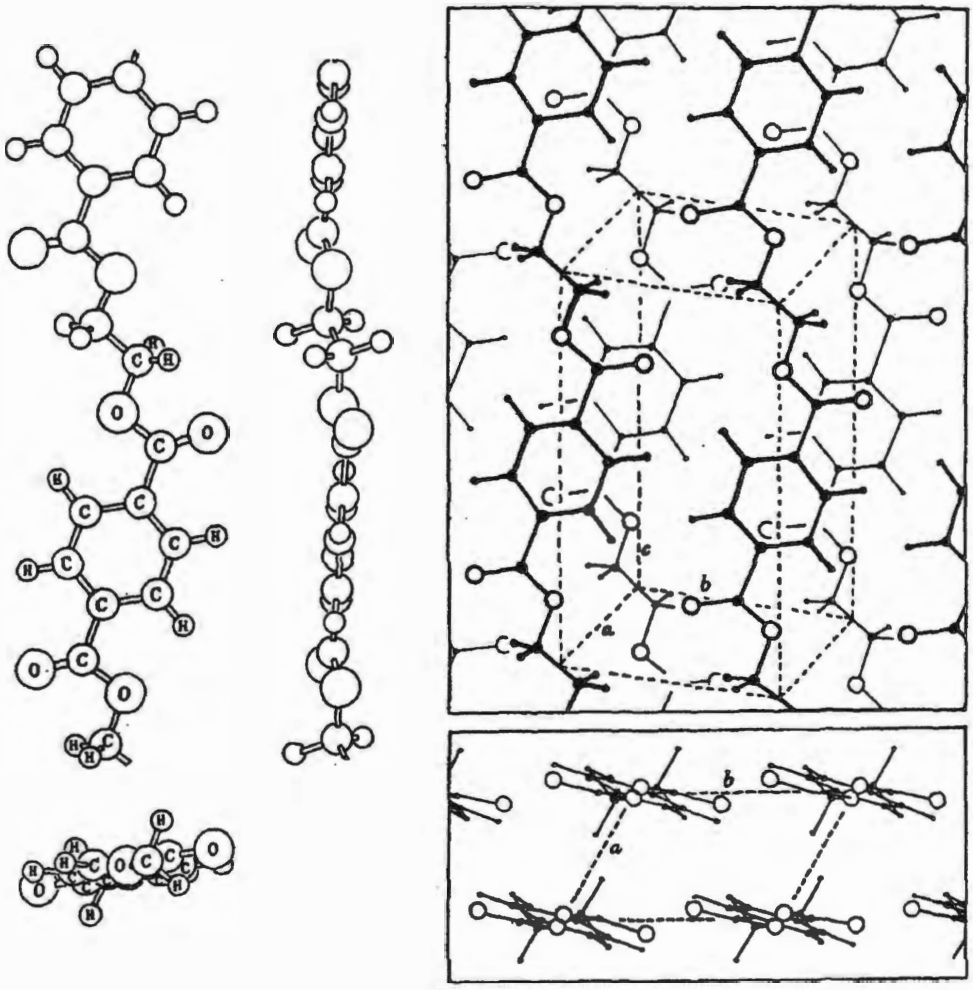

Figure 2.3: Schematic Drawing of PET Crystal Structure
Source: Daubeny, R. P., Bunn, C.W., and Brown, C. J., Proc. Roy. Soc., Ser. A, 226, 531 (1954).

In a general sense, the crystallization of PET is slow compared to other polymers. In many cases, this allows for it to be quenched to the amorphous state. This is thought to be due to the preference for the gauche conformation of the CH_2-CH_2 bonds.

2.2. Basic Concepts of Polymer Crystallization

2.2.1. Degree of Crystallinity

One of the most fundamental concepts in polymer crystallization is the degree of crystallinity, which is often defined based on the assumption that a polymer is composed of an ideal crystalline phase and an ideal amorphous phase whose properties are additive. As a result, the degree of crystallinity can be defined as follows:

$$P^0 = X \cdot P_c^0 + (1 - X) \cdot P_a^0 \qquad (2.1)$$

where P^0 is a particular measurable intensive property, P^0_c and P^0_a are the partial properties of the crystalline and amorphous components respectively, and X is the apparent degree of crystallinity. The degree of crystallinity of semicrystalline polymers usually varies from less than 0.5 to as high as 0.95 (Bovey 1979).

There are may techniques commonly employed to determine the degree of crystallinity in polymers. A Density Gradient Column (DGC) can be used to determine the density of a polymer sample, with the degree of crystallinity given by the following formula:

$$X = \left(\rho / \rho_a\right) \times \left[(\rho - \rho_a) / (\rho_c - \rho_a)\right] \qquad (2.2)$$

where ρ is the density of the sample, ρ_a is the density of a 100% amorphous sample, and ρ_c is the density of a 100% crystalline sample.

The degree of crystallinity, as determined by Differential Scanning Calorimetry (DSC), can be determined by using the following Equation:

$$X = \Delta H_f / \Delta H_f^0 \qquad (2.3)$$

where ΔH_f is the heat of fusion of the sample, and ΔH_f^0 is the heat of fusion of a 100% crystalline sample.

Several other techniques have been used to determine the degree of crystallinity of polymers, such as Wide Angle X-Ray diffraction (WAXD) (Kampf 1986) and Fourier Transform Infrared Spectroscopy (FTIR) (Stevens 1991). It has been shown by Stevens (1991) that the aforementioned techniques do not yield an absolute value of the degree of crystallinity. Although the values obtained from each technique were slightly different, the same trends were witnessed when comparing samples prepared by different thermal treatments.

2.2.2. Fringed Micelle Model

Since the early 1900's scientists have been exploring the concept of polymer crystallinity and therefore several models have been developed in the past century to describe the morphology of semi-crystalline polymers. One of the earliest of these models is the Fringed Micelle Model. In this model, small polymer crystals—called crystallites—are assumed to be approximately 100 Angstroms in length and the polymer chains are assumed to pass from one crystalline region to another with the intermediary

regions being amorphous. This model predicts that one polymer chain may be incorporated into many crystal regions therefore "tying" the crystals together. Although this model is outdated it is important to note that it still has some utility because it recognizes that polymers are composed of a highly ordered crystalline phase and a random amorphous phase (Sperling 1992).

2.2.3. Single Polymer Crystals and the Nature of Chain Folding

In 1957, Keller proposed that polymer crystals folded back upon themselves. His conclusion came from the study of single crystals of polyethylene prepared by precipitation from dilute solutions. Electron microscopy showed that the chains were parallel to the thickness direction in the thin lamella shaped single crystals. Keller recognized that the polyethylene chains were known to have a contour length much greater than the thickness of the polymer crystals and thus concluded that the chains must be folding back upon themselves. This conclusion led to the development of what is known as the folded chain model. In this model, the polymer molecule folds back and forth throughout the matrix of the crystal (Sperling 1992).

An adaptation of the folded chain model is the switchboard model. In this model, polymer chains do not have regular reentry into the lamellae, but are believed to enter in and out of the crystal randomly (Flory 1962, Fischer et al 1962). It is likely that a polymer single crystal likely resembles something intermediate to these last two models (Mandelkern 1982).

Hoffman et al (1959) suggested that the free energy of a fold surface could be expressed in the following simple equation:

$$\sigma_E = \frac{\varphi}{2A_0} \qquad (2.4)$$

where φ is the energy required for chain folding and A_0 is the chain cross-section in the crystal. According to this equation the ease with which folding occurs is dependent upon the energy-barrier to fold-formation. It has been argued that chain flexibility and pendent groups can sometimes serve to decrease φ, thus promoting chain folding, which ultimately serves to enhance polymer crystallization (Bouma et al 2001).

2.2.4. Spherulites

2.2.4.1. Spherulite Morphology

Up to this point, the models presented have applied primarily to single crystals formed in solution. It is extremely important to consider models that apply to crystals formed from the molten state. In this regard, the most important model is that of the spherulite (see Figure 2.4). When polymers are crystallized from the bulk, spherulites are commonly encountered. Spherulites are sphere-shaped structures that are composed of many lamellae crystalline plates of equal thickness. Between these lamellae lies amorphous material and impurities rejected from the polymer crystal. Spherulite lamellae also contain low-angle branch points where new lamellae structures are initiated, which tend to keep the spacing between the crystallites constant. Spherulites also contain interlamellar links, sometimes referred to as tie molecules. Thus a spherulite itself is not a single crystal, but a polycrystalline entity (Sperling 1992).

Spherulites are birefringent entities. When viewed under crossed polars, a distinctive cross, centered at the origin of the spherulite, is witnessed which is often

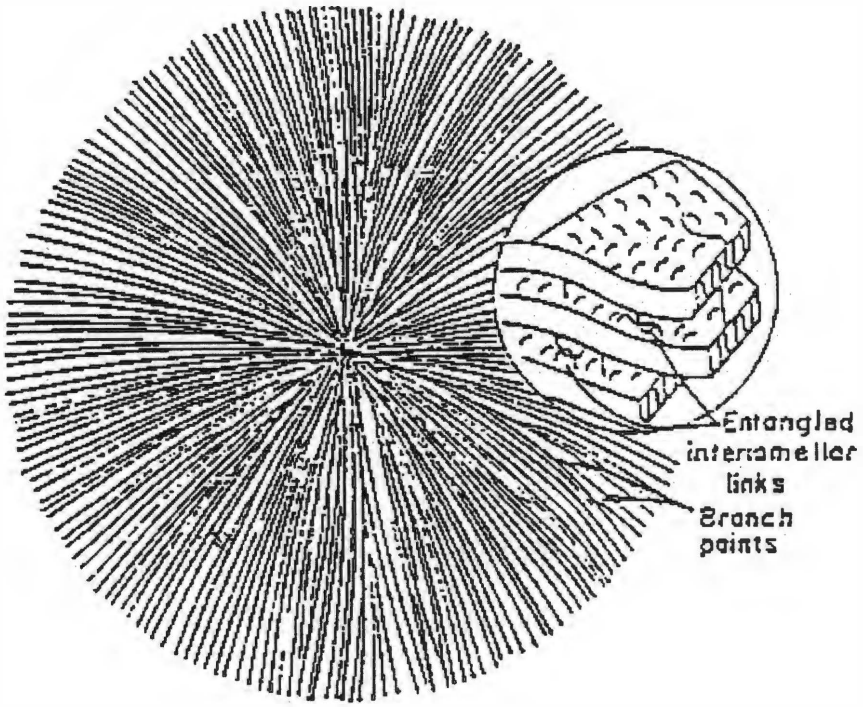

Figure 2.4: Schematic Representation of a Polymer Spherulite

Source: Hoffman et al; in "Treatise on Solid State Chemistry," Vol. 3, Plenum Press, NY (1976)

called a Maltese cross. These extinction patterns are a manifestation of the ability of the individual crystals to reorient the directions of the polarization of a beam of light into a specific crystallographic direction. A typical spherulite, as viewed under crossed polars, is shown in Figure 2.5.a. In many cases, if a thin section of a bulk-crystallized sample of polyethylene, polyamide, or polyester is examined under crossed polars, all that is witnessed is a birefringent mass, such as shown in Figure 2.5.b. For this type of morphology, it is believed that such materials contain many spherulites, but due to an extremely high nucleation density, individual spherulites are not resolvable (Sharples 1966).

2.2.4.2. Basic Concepts of Spherulite Formation

Spherulites begin to form after a polymer melt has been cooled to some temperature below its melt temperature. This initial process is known as nucleation. Nucleation can be thought of as the initial stage of crystallization and occurs as a result of the formation of small, submicroscopic embryos. After the primary nucleus has formed a stable crystal a sheaf-like structure begins to form, which has been called an axialite and/or a hedrite. New lamellae develop on either side of a central reference plane and fan out progressively, growing away from the plane. Gradually, lamellae in the hedrite fan outward, which eventually leads to the spherical shape of the spherulite (Sperling 1992).

It has been observed that once an observable spherulite has formed, it will tend to grow in a linear fashion given by:

$$r = Gt \qquad (2.5)$$

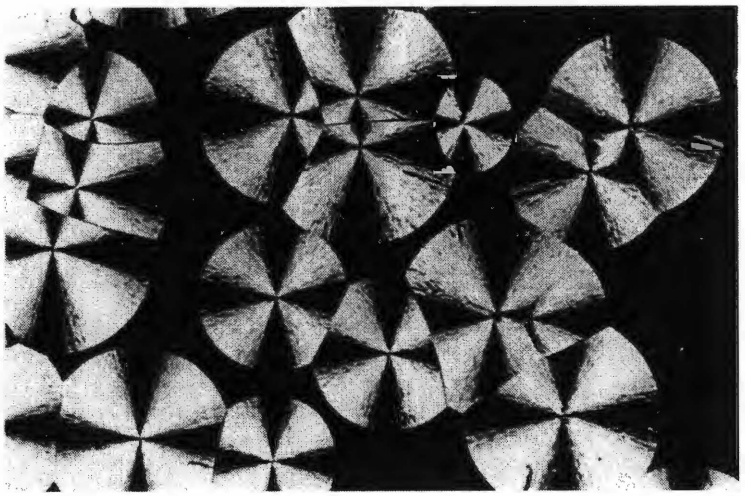

Figure 2.5.a.

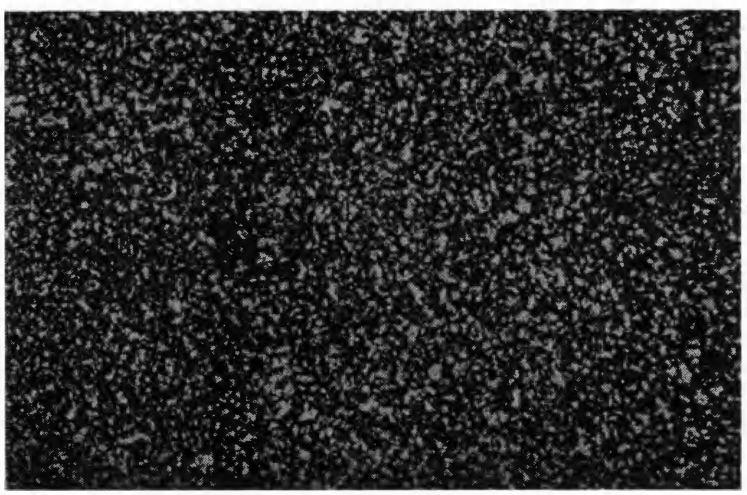

Figure 2.5.b.

Figure 2.5: Optical Photographs of Polymer Spherulites

a.) Isotactic Polystyrene Spherulite Growth as viewed under crossed polars (115X)

b.) High Density Polyethylene (HDPE) melted at 200°C and crystallized slowly at 129°C (200X)

Source: a.) Bovey, F.A., and Winslow, F.H., "Macromolecules: An introduction to Polymer Science," Academic Press, NY (1979).

b.) Sharples, A., "Introduction to Polymer Crystallization," St. Martins Press, NY (1966).

where r is the spherulite radius, G is the linear growth rate of the spherulite, and t is the time allowed for spherulite growth. Equation 2.5 holds true for the growth of a spherulite until impingement with neighboring spherulites occurs. At this stage, the Avrami-type crystallization (see section 2.2.6.1.1.) has ended, though secondary crystallization may continue to occur. Secondary crystallization can be loosely described as any increase in crystallization that occurs after the initial formation of the lamellae has completed. As will be shown in later sections, this type of crystallization occurs as a result of crystal perfection (i.e. the reorganization of polymer molecules to form more perfect crystals) and the crystallization of initially rejected macromolecular segments.

2.2.5 Fundamentals of Polymer Crystallization

Polymer crystallization from the bulk can be described as occurring in a series of fundamental steps. These steps are listed below and will be discussed in more detail in the next few sections:

1. Primary Crystallization
    a.) Primary nucleation
    b.) Secondary nucleation
2. Secondary Crystallization

2.2.5.1. Primary Nucleation

Upon cooling of a polymer melt, it might first be expected that crystallization would occur at the same temperature as melting. Under these conditions, the Gibbs free energy would follow the familiar expression:

$$\Delta G = G_{crystal} - G_{melt} = \Delta H - T\Delta S \qquad (2.6)$$

Thus at the condition where the Gibb's free energy is equal to zero, Equation 2.6 predicts that the melt temperature, and the crystallization temperature, would simply be given by the condition $T_m = T_c = \Delta S/\Delta H$. It is well known, however, that polymers do not crystallize at the temperature implied by this equation, but only crystallize after a sufficient amount of cooling below its melt temperature (i.e. supercooling). This is due to the fact that for a small crystal to be formed (i.e. a nucleus) enough polymer molecules must pack together to form a small, crystalline embryo. Thus there is an additional energy barrier to nucleation caused by the formation of an embryo with a surface energy that initially increases the Gibb's free energy of formation. Therefore there must be a sufficient thermodynamic driving force to cause the embryo to grow to a critical size, whereupon the continued growth of the nucleus will occur in a spontaneous manner (Young 1981).

The classical theory of nucleation is often used to illustrate primary nucleation. This is accomplished by viewing a primary nucleus as a simple three-dimensional block with lateral dimensions a and b and length l and side and end surface free energies σ and σ_e. Thus the change in Gibbs free energy of the nucleus (with dimensions a = b) will be given by the expression:

$$\Delta G = -a^2 l \Delta g_f + 4al\sigma + 2a^2\sigma_e \qquad (2.7)$$

where Δg_f is the bulk free energy of a perfect crystal per unit volume and can be approximated by the following relationship:

$$\Delta g_f \approx \Delta h_f \rho_c \left(\frac{\Delta T}{T_m^0} \right) \tag{2.8}$$

where Δh_f is the heat of fusion per unit volume, ρ_c is the density of the crystal, T_m^0 is the equilibrium melt temperature, and ΔT is the supercooling given by $\Delta T = T_m^0 - T$. The concept of the equilibrium melt temperature will be dealt with in a later section (see section 2.2.8.) but can be defined for this purpose as the melting temperature of an infinitely thick crystal with no surface (i.e. the crystal becomes so large that surface energy is negligible).

The critical nucleus dimensions, a* and l*, can be determined by combining Equations 2.7 and 2.8, differentiating with respect to a and l and setting these equations equal to zero, leading to the following equations:

$$l^* = \frac{4\sigma_e T_m^0}{\left(\Delta h_f \Delta T \rho_c\right)} \tag{2.9}$$

and

$$a^* = \frac{4\sigma T_m^0}{\left(\Delta h_f \Delta T \rho_c\right)} \tag{2.10}$$

Finally, Equations 2.9 and 2.10 can be substituted into Equation 2.6 to obtain an expression for the critical Gibb's free energy of formation of a primary nucleus:

$$\Delta G^* = \frac{32\sigma^2 \sigma_e \left(T_m^0\right)^2}{\left(\Delta H_f \Delta T \rho_c\right)^2} \tag{2.11}$$

It is important to point out that Equation 2.11 is somewhat of an oversimplification of the actual primary nucleation process (Wunderlich 1976). Nevertheless, it is evident from this equation that the Gibb's free energy of formation of a

critical nucleus decreases with increasing supercooling. Likewise, Equations 2.9 and 2.10 suggest that the critical nucleus size decreases with increasing supercooling.

2.2.5.1.1. Primary Nucleation Types

When discussing the crystallization of polymers there are three main types of nucleation: homogeneous, heterogeneous, and orientation-induced nucleation. The first two are concerned with the primary nucleation of polymer crystals in an unstrained state (i.e. under quiescent conditions), while the latter applies only to deformed macromolecules oriented in the presence of an elongational flow field.

Homogeneous nucleation involves the spontaneous formation of nuclei after a sufficient degree of supercooling. This type of nucleation process occurs randomly throughout the bulk of the polymer and typically exhibits a first-order time dependence (Sharples 1966). Homogeneous nucleation is unlikely to occur in real systems, since it is virtually impossible to prepare a polymer sample containing no impurities.

Heterogeneous nucleation is most common with polymers crystallized in the bulk and makes use of a surface to reduce the free energy opposing nucleation. This can occur on the surface of impurities present in the bulk material or on fixed surfaces, such as the surface of a reaction vessel or a DSC pan for example. With this type of nucleation there are a limited number of growth centers becoming instantaneously effective at the crystallization temperature (with a zeroth order time dependence) (Sharples 1966).

The rate of primary nucleation of polymers is often manipulated by the use of nucleating agents, which are impurities intentionally added to the bulk polymer to initiate heterogeneous nucleation. Groeninckx et al (1974) showed that several nucleating agents

could be added to PET to enhance nucleation, including titanium dioxide, talc, kaolin, and silicon dioxide. It has also been shown that residual catalysts can have an effect on the nucleation rate of PET. For example, antimony glycolate, added as a polycondensation catalyst (Di Fiore et al 1993), and Calcium Acetate, added as a transesterification catalyst (Weigel and Zimmerman 1979, Gumther and Zachmann 1983, Asano et al 1989), have both been shown to increase the nucleation rate of PET.

Orientation-induced nucleation, as the name implies, occurs as a result of macromolecular extension in pure elongational flow, such as that encountered in fiber spinning. This molecular alignment in the fluid more closely resembles the conformation of the polymer molecules in the crystalline state, causing an enhanced rate of nucleation to be observed (Wunderlich 1976).

2.2.5.2. Theories of Polymer Crystal Growth

2.2.5.2.1. Keith and Padden Theory of Spherulite Crystallization

When examining the radial growth rate of polymer spherulites as a function of supercooling, a maximum is encountered somewhere between T_g and T_m as is shown in Figure 2.6. In their examination of the influence of fractionation and impurity segregation on the melt crystallization of spherulites, Keith and Padden (1964, 1964b) attempted to explain this phenomena by suggesting that there are two competing processes during spherulite formation: 1.) the rate of molecular transport (i.e. diffusion) and; 2.) the rate of nucleation. It was suggested that as the temperature is lowered below the melt temperature, a further decrease in temperature supplies more of a driving force for crystallization, causing an increase in the spherulite growth rate. However, as the

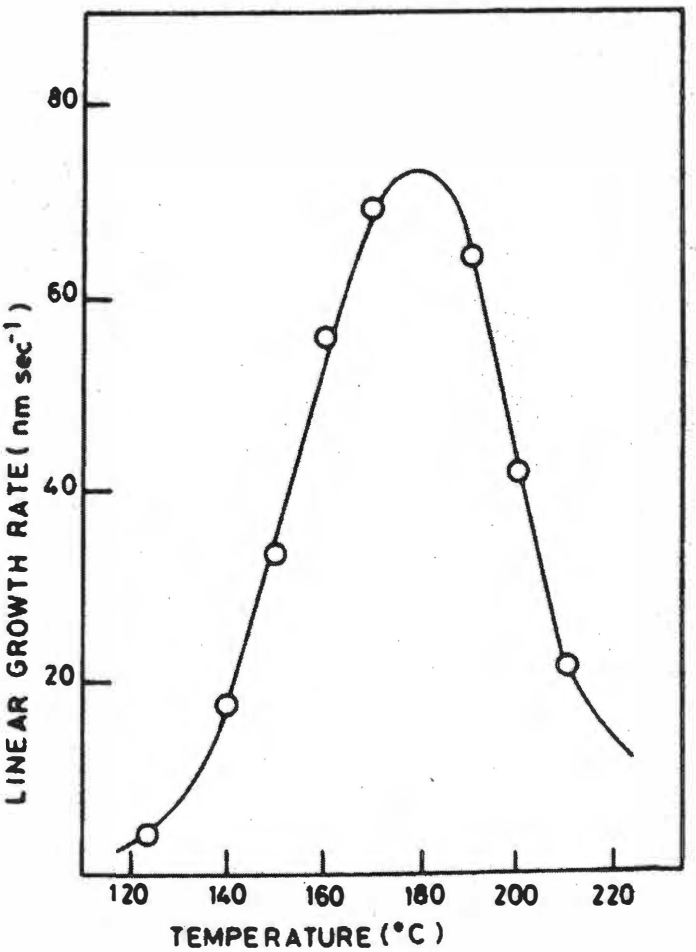

Figure 2.6: Schematic of Spherulite Growth Rate as a Function of Temperature for PET

Source: Palys, L.H. and Phillips, P.J., J. Polym. Sci. Polym. Phys. Ed., 18, 829 (1980).

temperature is decreased molecular motions become more sluggish as the glass transition temperature is approached, and the crystallization rate begins to decrease again until crystallization is essentially halted.

Keith and Padden suggested that a simple parameter, δ, could be defined that is essentially a measure of the internal structure of the spherulite as:

$$\delta = D/G \qquad (2.12)$$

where D is the diffusion coefficient for impurity in the melt and G is the radial spherulite growth. Thus as the temperature is decreased, the rate of nucleation increases while the rate of molecular transport decreases. At intermediate temperatures these two processes are on the same order and therefore a maximum is achieved. Thus to the left of the maxima on the growth rate curve the growth rate is controlled by the diffusion rate whereas to the right of the maxima the process is under nucleation control.

This phenomena is also explained by the examination of the simple equation often used to describe spherulite growth which is an extension of the Turnbull-Fischer equation (Turnbull and Fischer 1949):

$$G = G_0 e^{\Delta E/RT} e^{-\Delta F/RT} \qquad (2.13)$$

where ΔF^* is the free energy of formation of a critical sized nucleus, and ΔE is the free energy of activation for a chain crossing the barrier to the crystal. Thus Equation 2.13 further supports the idea that spherulite growth rate is governed by two competing rate processes (Sperling 1992).

2.2.5.2.2. Theory of Secondary Nucleation

Upon primary nucleation of a polymer crystal, the growth stage of the spherulite then ensues in a space-filling mode. In this mode polymer stems are added to the surface of the growing crystal lamellae as shown in Figure 2.7. In this figure, a is the width of the molecular stem, b is the thickness of a surface nucleus, l is the height of the nucleus which is fixed at a specific undercooling, L is the width of the crystal, and σ and σ_e are the lateral and fold surface free energies respectively. In this figure it can also be noted that a new molecular layer is formed in the g direction, while overall crystal growth occurs in the G direction.

After the addition of a surface nucleus there are three possible ways by which the remaining portion of the molecular layer can fill in that depend on the rate of secondary nucleation and the rate of spreading. Secondary nucleation is the term often used to describe the process of laying down the first stem onto the lamellae growth surface. The rate of spreading refers to the rate at which subsequent stems add to the nucleus. As a result there are three possible ways with which a crystal can grow: 1.) dominant secondary nucleation; 2.) dominant spreading mechanism; or 3.) combined mechanism. Thus the mode of crystallization is dependent on two competing processes: the rate of secondary nucleation, **i**, and the rate of spreading, **g**. These three mechanisms are often referred to as regimes (Hoffman et al 1976).

In regime I the rate of spreading, g, is dominant (i.e. **g>>i**). Upon laying down one nucleus, the remainder of crystal formation for that layer is dominated by a space filling spreading mode. In this regime, the rate-limiting step is the deposition of the first stem on the surface. This regime also occurs at the lowest degree of supercooling. The

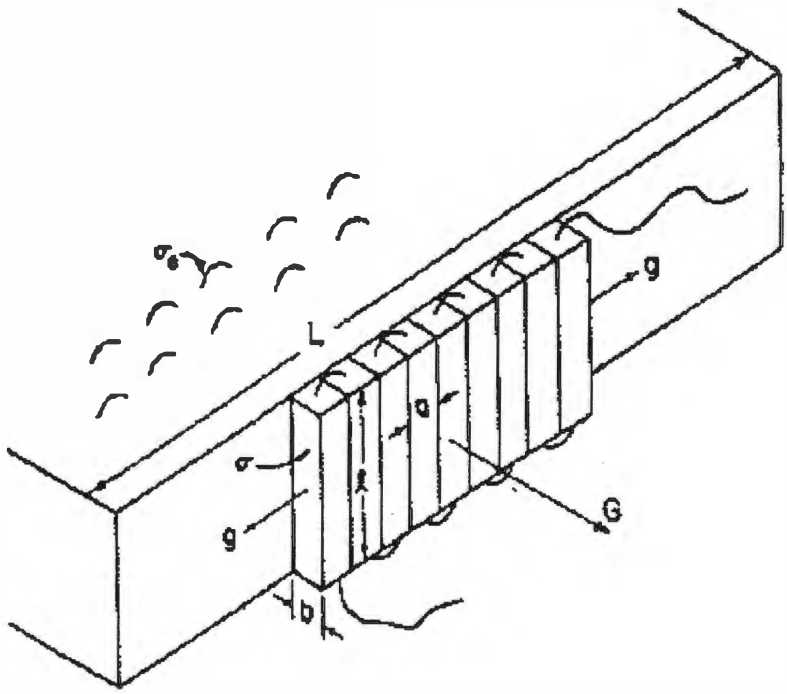

Figure 2.7: Schematic Diagram of Hoffman's Lamellar Crystal Growth

Source: Hoffman et al; in "Treatise on Solid State Chemistry," Vol. 3, Plenum Press, NY (1976)

reason for this will become apparent as the other regimes are discussed. What is also important to note about this mechanism is that it is assumed that adjacent reentry occurs in this regime since it is the most energetically favorable form of spreading. It can be inferred then that what results is a spherulite where stem reentry is so dominant that individual crystal lamellae are divided by amorphous regions with little to no tie molecules formed between adjacent lamellae. In regime II the rate of spreading becomes on the same order as the rate of secondary nucleation. As a result, multiple surface nuclei can occur on the same surface. Since a certain amount of energy is required for secondary nucleation to occur, it should be no surprise that regime II is encountered at a higher degree of supercooling. In regime III the rate of secondary nucleation is much greater than the rate of spreading and therefore requires the highest degrees of supercooling (Phillips 1990).

The secondary nucleation theory of Hoffman, Lauritzen, et al (1961, 1962, 1962b 1976, 1983, 1985, 1988, 1989, 1992) can be expressed as follows:

$$G = G_0 \exp\left[-\frac{U^*}{R(T - T_\infty)}\right]\exp\left[-\frac{K_g}{T\Delta Tf}\right] \qquad (2.14)$$

where G is the growth rate, G_0 is the growth rate constant, U* is the activation energy for the transport of segments to the site of crystallization, R is the gas constant, T is the crystallization temperature, T_∞ is the temperature where all molecular motions associated with viscous flow are thought to cease ($T_\infty \cong Tg - 30°$), ΔT is the undercooling ($\Delta T = T_m° - T$), f is a correction factor that accounts for the change in the heat of fusion, Δh_f, at high undercoolings ($f = 2T/T+T°_m$), and K_g is the nucleation rate constant, given by:

$$K_g = jb_0\sigma\sigma_e T_m^0 / k\Delta h_f \qquad (2.15)$$

where b_0 is the width of the chain, T^0_m is the equilibrium melt temperature (in Kelvins), k is Boltzmann's constant, and j is a constant that is dependent on the crystallization temperature and is equal to 4 for regimes I and III and 2 for regime II.

It has been suggested that the degree of supercooling has a strong influence on the crystallization mechanism and thus the regime in which crystallization occurs. This is illustrated schematically in Figure 2.8 where $\log G + U^*/2.303(T-T_\infty)$ is plotted as a function of $1/T(\Delta T)f$. Thus according to Equation 2.14, for each specific regime, this plot should be linear with slope = $-K_g$ and y-intercept = G_0. Also, note that by Equation 2.15 regimes I and III should, theoretically, have the same slope. From Figure 2.8 it evident that the growth rate of the crystal, G, is strongly influenced by the degree of supercooling. Provided that the supercooling does not exceed that temperature where maximum crystallization occurs (see Figure 2.6) a higher supercooling should produces the highest crystallization rates. From Figure 2.8 it is also evident that each mechanism has a particular temperature dependence, suggesting that a different morphology is formed for each regime.

It is important to mention that the initial development of the secondary nucleation theory was based on the assumption that chain folding was dominant, regardless of the degree of supercooling. As is pointed out by Phillips (1990), it is very likely that for molecules crystallizing in regime III, and deep into regime II, there will be nuclei whose chains are already a part of previously formed crystals. This implies that, in these regimes, tie molecules will be formed between lamellae.

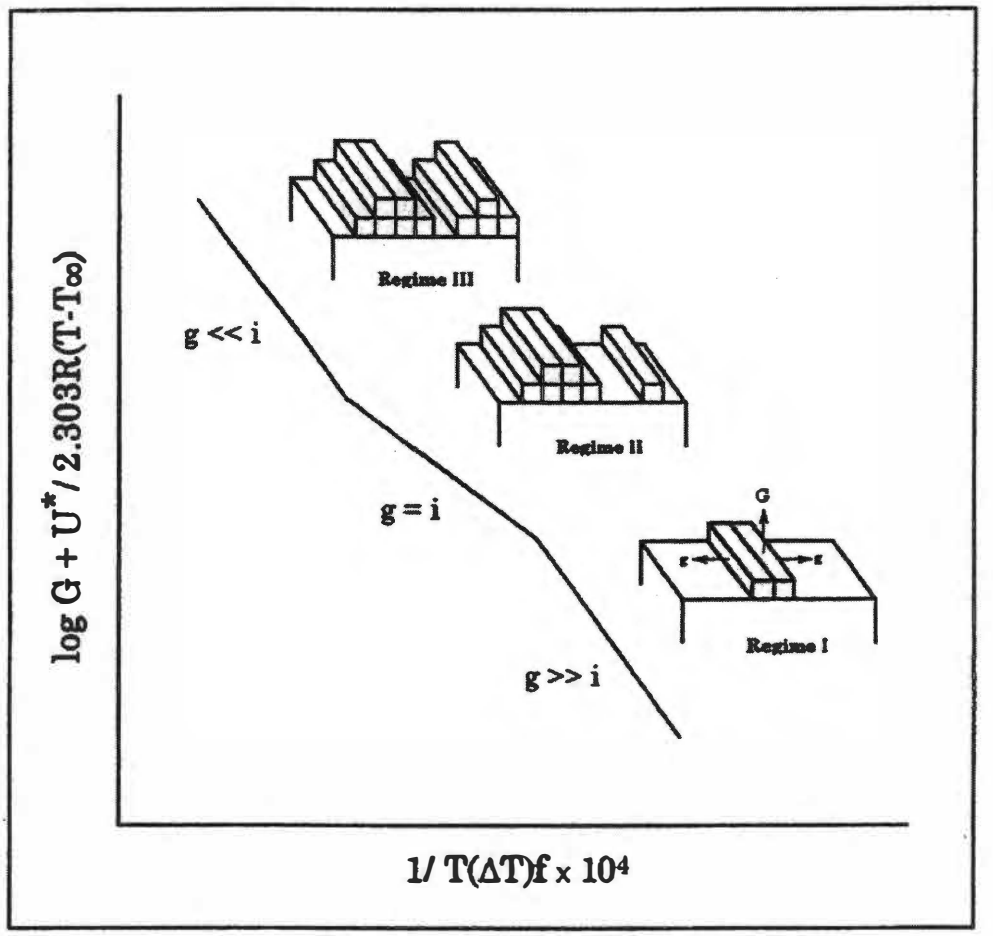

Figure 2.8: Plot Illustrating Regime I, Regime II, and Regime III Crystallization Kinetics

Source: Supaphol, P., MS Thesis, University of Tenn. (1996).

Lauritzen and Hoffman (1973) defined a parameter, Z, governing the difference between regimes I and II as:

$$Z = \frac{iL^2}{4g} \qquad (2.16)$$

If Z is 0.01 or less it is expected that regime I will be operative, while regime II will be operative for $Z \geq 1$. As previously mentioned, the slopes of the plots shown in Figure 2.8 can be used to determine K_g, which in turn can be used to estimate the quantity $\sigma\sigma_e$. The Thomas-Stavely relation, modified by Hoffman, can then be used to determine σ independently:

$$\sigma = \alpha \Delta h_f \sqrt{a_0 b_0} \qquad (2.17)$$

where α is taken as 0.1 for most polymers. Finally, once the fold surface energy is known, the work of chain folding, q, can be calculated directly using the following equation:

$$q = 2a_0 b_0 \sigma_e \qquad (2.18)$$

Experimentally, it is sometimes preferred to express Equation 2.14 in terms of the half-times of crystallization (Ross and Frolen 1975, 1980, Supaphol 1996). This is accomplished by noting that, for spherulite growth with instantaneous nucleation, the crystallization half time, $t_{½}$, is directly proportional to the crystallization rate constant, k, which is given by (see section 2.2.6.):

$$k = \frac{4}{3}\pi G^3 N \qquad (2.19)$$

where G is the linear growth rate from Equation 2.5 and N is the number of nuclei. Since $t_{½}$ is also directly proportional to G^3 we obtain the following:

$$t_{1/2} = A_1\left\{G_0 \exp\left[-\frac{U^*}{R(T-T_\infty)}\right]\exp\left[-\frac{K_g}{T\Delta Tf}\right]\right\}^3 \qquad (2.20)$$

where A_1 is a constant of proportionality. Taking logarithms of Equation 2.20 and rearranging leads to following:

$$\frac{1}{3}\log(t_{1/2}) + \frac{U^*}{R(T-T_\infty)} = A_2 - \frac{K_g}{2.303T(\Delta T)f} \qquad (2.21)$$

where $A_2=(1/3)\log A_1+\log G_0$. Thus in this case, a plot of $(1/3)\log t_{1/2} + U^*/R(T-T_\infty)$ as a function of $1/2.303T(\Delta T)f$ should yield a straight line with slope = $-K_g$ and y-intercept = A_2.

This experimental technique was used by Supaphol (1996) to investigate the regime II to regime III transition of High Density Polyethylene (HDPE) using the Light Depolarizing Microscope technique developed by Ding and Spruiell (1996).

2.2.5.3. Secondary Crystallization and Crystal Perfection

Secondary crystallization represents that stage of crystallization that continues after spherulite impingement has occurred and as mentioned previously, is that portion of the crystallization curve not adequately described by the Avrami equation (see section 2.2.6.). As suggested by Strobl (1997), this process is also partially responsible for broadening of the melting peak temperature, especially for polymers containing non-crystallizable entities such as branches or comonomer units.

As is pointed out by Wang et al (1999) the secondary crystallization process is still quite unclear and could include the thickening of lamellae, perfection of the crystals, or the growth of defective crystallites. Wunderlich (1976) suggests that generally this

delayed crystallization can be broken down into two main types: secondary crystallization and crystal perfection. Secondary crystallization, as he describes, involves the further crystallization of amorphous molecules, or portions of molecules that were initially rejected or unable to diffuse to the growth site from the crystal during primary crystallization. Crystal perfection involves the further perfection of initially poorly crystallized macromolecules. It is most likely that both of these processes are often responsible for the increasing crystallinity after primary crystallization has completed.

Many experimenters have investigated the secondary crystallization of PET. Hartely et al (1954) observed a small, slow, linear increase in density when PET was held at the initial crystallization temperature for longer periods of time. More recently, several studies have focused on Small Angle X-Ray Scattering (SAXS) experiments used in conjunction with isothermal DSC experiments to examine the nature of the secondary crystallization of PET. Two such studies were performed by Medellin-Rodriguez et al (1997, 1998) and Wang et al (1999). Both authors verified that increasing the time of isothermal crystallization, the amount of secondary crystallization increased substantially. Since both of these authors conclusions were strongly based on the multiple melting peaks observed immediately following isothermal crystallization in a DSC this subject will be discussed further in the context of crystal melting in a later section (see section 2.2.8.).

Most recently, Lu and Hay (2001) studied the isothermal crystallization and melting behavior of PET using DSC and Scanning Electron Microscopy (SEM) where it was again shown that secondary crystallization continued after the primary crystallization process. Direct observation, using SEM, showed that the primary crystallization process

occurred by heterogeneous nucleation, followed by three-dimensional spherical growth, while secondary crystallization followed a one-dimensional growth involving fibrillar growth between the primary lamellae.

2.2.6. Crystallization Kinetics

2.2.6.1. Isothermal Crystallization Kinetics

There are a variety of models that are used to aid in the experimental determination of the isothermal kinetics of polymer crystallization. One of the earliest and still most popular methods of studying the isothermal, bulk crystallization kinetics is to use the Avrami equation (Avrami 1939, 1940, 1941).

Following that of Evans (1945) the derivation of the Avrami equation can be performed by first imagining the process of primary nucleation and crystal growth as raindrops falling in a puddle. As the raindrops make contact with the puddle, a circular wave front is produced from each raindrop such that the wave fronts will intersect and eventually cover the whole surface of the puddle. It is assumed that whether the raindrops hit the puddle all at the same time or sporadically, they must strike the surface of the puddle at random points. In this example, the points of impact in the puddle are the analog of primary crystal nuclei and the expanding wave fronts are analogous to the growth fronts of spherulites. Thus the first assumption involved in deriving the Avrami equation is that nucleation occurs randomly. Mathematically, the probability, p_x, that a point P is crossed by x fronts of growing spherulites can be expressed by an equation originally derived by Poisson (1837):

$$p_x = e^{-E} E^x / x! \qquad (2.22)$$

where E is the average number of wave fronts in the system. By Equation 2.22, the probability that a point P is not crossed by any fronts (and consequently is still amorphous) will result when x=0, thus:

$$p_0 = e^{-E} \tag{2.23}$$

The relative crystallinity, at any time t, θ(t), is defined by the relation:

$$\theta(t) = \frac{X(t)}{X(t=\infty)} \tag{2.24}$$

where X(t) is the degree of crystallinity at time t and X(t=∞) is the final degree of crystallinity. Thus the quantity p_0 will also be equal to the volume fraction of amorphous material, namely 1-θ(t), resulting in:

$$1-\theta(t) = e^{-E} \tag{2.25}$$

Note that at low degree of crystallinity, θ(t) ≅ E therefore

$$1-\theta(t) = e^{-V_t} \tag{2.26}$$

where V_t is the volume of crystallized material, which must be evaluated for both the shape of the growth entity, as well as situations where the nuclei are: 1.) predetermined (all nuclei form at once upon cooling to the crystallization temperature, i.e. instantaneous nucleation) and 2.) there is sporadic nucleation (nuclei form more or less at random times). It is important to note that, from a practical standpoint, these two nucleation types will result in crystalline entities of different forms. In the case of predetermined nucleation, upon impingement all growth entities will be more or less the same size, while sporadic nucleation will create growth entities of various sizes.

Considering the case of predetermined nucleation of a spherulite, the volume increase in crystallinity for the time period t to t+dt for N spherical nuclei will be:

$$dV_t = 4\pi r^2 N dr \tag{2.27}$$

where r is the radius of the spheres at time t and the spherulite growth rate is linear and given by Equation 2.5 (i.e. r = Gt). Therefore the total volume can be determined by substituting Equation 2.5 into 2.27 and integrating to obtain:

$$V_t = \frac{4}{3}\pi \cdot G^3 \cdot N \cdot t^3 \tag{2.28}$$

It can also be shown that for the sporadic nucleation of spheres, with the number of nuclei increasing linearly at a rate s that the volume, V_t, is given by:

$$V_t = \frac{2}{3}\pi \cdot G^3 \cdot s \cdot t^3 \tag{2.29}$$

Equations 2.27 or 2.28 can be substituted back into Equation 2.26 to obtain the general form of the Avrami equation:

$$\theta(t) = 1 - \exp\left(-kt^n\right) \tag{2.30}$$

where k is the overall crystallization rate constant, and n is the Avrami exponent. In practice, the time, t, is determined as the time to reach a particular reduced crystallinity, $\theta(t)$, excluding the time taken to begin the crystallization process, t_i. The time t_i is often referred to as the induction time, or incubation time, of crystallization. The Avrami exponent is a function of both growth and nucleation of the crystal and varies between the values of 1 and 4. Table 2.1 shows that for a particular growth type (i.e. spheres, disks, or rods) the Avrami exponent reveals something about the type of nucleation (sporadic or predetermined) and the growth rate. It is important to note that the Avrami

Table 2.1: Theoretical Description of Avrami Exponent

Geometry	Crystallization Mechanism	Avrami Constant k	Avrami Constant n	Restrictions
Spheres	Sporadic	$(2/3)\pi G^3 s$	4.0	3 dimensions
	Predetermined	$(4/3)\pi G^3 N$	3.0	3 dimensions
Discs[a]	Sporadic	$(1/3)\pi G^2 sd$	3.0	2 dimensions
	Predetermined	$\pi G^2 Nd$	2.0	2 dimensions
Rods[b]	Sporadic	$(1/4)\pi G s d^2$	2.0	1 dimension
	Predetermined	$(1/2)\pi G N d^2$	1.0	1 dimension

[a]Constant thickness d
[b]Constant radius d

Source: Hay, J.N., Br. Polym. J., 3, 74 (1971).

exponent, n, can also take on half values. This occurs in the case where the rate of crystallization is diffusion controlled, such as when there is a high concentration of noncrysallizable impurities and thus the radial growth rate is given by the equation (Keith and Padden 1964, 1964b, Sperling 1992):

$$r = Gt^{1/2} \tag{2.31}$$

Taking logarithms of both sides of Equation 2.30 results in the more useful form of the Avrami equation, which allows for the experimental determination of both n and k:

$$\ln[-\ln(1-\theta(t))] = \ln k + n \ln t \tag{2.32}$$

Equation 2.32 suggests that a plot of ln[-ln (1-θ(t)] vs. ln(t) should be linear with slope= n and y-intercept = lnk.

The Avrami rate constant evaluated at the half-time of crystallization, $k_{t_{1/2}}$, can also be calculated using the following equation:

$$k_{t_{1/2}} = \frac{\ln 2}{t_{1/2}^{\,n}} = \frac{0.693}{t_{1/2}^{\,n}} \tag{2.33}$$

Although the Avrami equation is often used to study the crystallization kinetics of polymers, it is important to note that it does have its limitations. One of the most significant limitations of the Avrami equation is that it assumes the growth process ceases upon impingement of the growth units. Thus the Avrami equation does not account for the often times subtle, yet significant secondary crystallization process that occurs with many polymers. Also, fractional values of the Avrami index can lead to difficulties in data interpretation. Since the Avrami equation is based upon geometric considerations, fractional values of the Avrami index do not allow for inferences to be made about the

actual structure of the growth units. A third source of error is the assumption that the growth rates are always linear. Although, in general, linear growth is observed, there are instances where nonlinear growth rates have been reported (Wunderlich 1976).

An implicit assumption in the derivation of the Avrami equation is that there can be an infinite number of nucleation sites. From a practical standpoint, the number of primary nucleation sites may decrease with time as heterogeneous nucleation sites are used up. This would be especially important when considering the case of sporadic nucleation. Additionally, there are instances where nucleation may not always occur randomly (such as with heterogeneous nucleation on the surface of a reaction vessel) (Sharples 1966).

2.2.6.2. Nonisothermal Crystallization

The isothermal crystallization of polymers is an important area of research, in that it provides information related to the fundamental crystallization process. Its utility as a means for predicting and understanding the crystallization process during polymer processing however is of major concern. As a result, much work has been done in the area of nonisothermal crystallization so as to better predict the kinetics of crystallization under these conditions.

The Avrami equation can easily be extended to the nonisothermal case by noting that, if sample cooling is constant, the temperature domain can be easily transformed to the time domain by the equation:

$$t = \frac{T_0 - T}{\phi} \tag{2.34}$$

where T_0 is the initial temperature, T is the current temperature, and ϕ is the cooling rate. Thus the Avrami equation as expressed in Equation 2.30 can be applied directly to nonisothermal crystallization at a constant cooling rate.

One of the most well-known theories relating to the nonisothermal crystallization of polymers is that provided by Nakamura et al (1973). Here Avrami's theory was extended to the nonisothermal case by the use of an "isokinetic approximation" which simply states that the ratio of the rate of primary nucleation and crystal growth rate is constant and independent of temperature. The governing equation is given by:

$$\theta(t) = 1 - \exp\left[-\left(\int_0^t K(T)dt'\right)^n\right] \qquad (2.35)$$

where as before, $\theta(t)$ is the reduced crystallinity at any time t, n is the Avrami index determined from isothermal experiments, and K(T) is a nonisothermal rate constant and is related to the Avrami rate constant, k, by:

$$K(T) = k(T)^{1/n} \qquad (2.36)$$

Another extension of the Avrami theory was offered by Ozawa (1971). In his theory the relative crystallinity at any temperature T is expressed as a function of cooling rate and is given by:

$$\theta(T) = 1 - \exp\left(-\frac{\alpha_0}{\phi^{n_0}}\right) \qquad (2.37)$$

where α_0 is the non-isothermal cooling crystallization function, ϕ is the cooling rate, and n_0 is the Ozawa exponent, which is similar to the Avrami exponent. Taking logarithms of Equation 2.37 leads to the following more useful form:

$$\ln\{-\ln[1-\theta(T)]\} = \ln(\alpha_0) - n_o \ln(\phi) \qquad (2.38)$$

thus a plot of $\ln\{-\ln[1-\theta(T)]\}$ as a function of $\ln(\phi)$ is predicted to yield a straight line with slope = n_0 and y-intercept = $\ln(\alpha_0)$.

Ozawa's original work was with PET and appeared to show quite good linearity. Many investigators, with some marginal success, however, have used the Ozawa equation. In some cases, the Ozawa equation appears to fit experimental data quite well such as that found for syndiotactic PP (Supaphol 2000), and PET (Jayakannan and Ramakrishnan 1999), while in other cases it did not appear to fit very well at all, such as was found for Nylon 11 (Liu et al 1998) and Poly(ε-caprolactone) / Poly(ethylene oxide) Diblock copolymers (Gan et al 1997) for example.

As is pointed out by Gan et al (1997) one reason for deviations from Ozawa's theory may be attributed to the fact that this equation is only applicable to primary crystallization. Ozawa (1971) argued that the slow secondary crystallization process becomes even slower by the time the temperature at which secondary crystallization would occur and thus could be neglected. Verhoyen et al (1998) also points out that one of the major limitations of Ozawa's equation is that it is restricted to constant cooling rates and that it does not consider the effect of thermal history on the ultimate degree of crystallinity. Likewise, Patel and Spruiell (1991) suggest that over predictions of non-isothermal data can be attributed to the fact that traditional kinetic models do not account for the induction time.

As is the case of the Avrami equation, many investigators have attempted to refine and/or develop new models that might more adequately describe the nonisothermal crystallization of polymers. Verhoyen et al (1998) developed a macro-kinetic model considering induction time, final degree of crystallinity, and secondary crystallization that

appears to describe both the isothermal and non-isothermal crystallization of PET quite well. Numerous other models have grown in popularity including those offered by Tobin (1974, 1976, 1977), Ziabicki (1967, 1967b, 1976), Dietz (1981), and Kamal and Chu (1983), to name a few. A nice review of some of the more common nonisothermal theories, including their application, can be found in Supaphol (2000).

Patel and Spruiell (1991) examined many of the more common polymer crystallization models with regard to their utility in polymer process modeling. It was found that the most satisfactory results for application to polymer process modeling could be obtained by the use of a nonlinear regression method to fit the nonisothermal crystallization data using a simplified differential form of the Nakamura model.

2.2.7. Factors that Influence Polymer Crystallinity

There are many factors that influence polymer crystallinity. In order for a polymer (or any material for that matter) to crystallize, the molecules must be arranged in a regular, and periodic way to form the more thermodynamically favorable crystal structure. If any sort of molecular disorder exists, the irregular portion of the molecule must be excluded from the crystal. Some of the more important factors that influence the ability of a polymer to crystallize (i.e. the crystallizability) are: molecular structure, stereoisomerism, geometric isomerism, steric order, polarity, and the inclusion of a comonomer.

2.2.7.1. Molecular Structure

Molecular structure is one of the most influential characteristics of a polymer that determines its ability to crystallize. For example, linear polymers such as High Density Polyethylene (HDPE) are capable of obtaining a much greater degree of crystallinity than the branched Low Density Polyethylene (LDPE) (Ulrich 1993). Another example of the effect of molecular structure on the ability of a polymer to crystallize is witnessed when comparing polyethylene with similar vinyl derivatives such as polymethylmethacrylate (PMMA), polystyrene (PS), and polyvinylchloride (PVC). Due to the existence of these side groups, the attainment of any significant crystallinity is hindered due to their inability to effectively pack in an ordered way (Sharples 1966).

2.2.7.2. Geometric Isomerism

The cis and trans isomers of polyisoprene are excellent examples of how geometric isomerism can affect polymer crystallizability. Cis-1,4 polyisoprene (natural rubber) is known to form a coiled structure, while the trans isomer, trans-1,4 polyisoprene (gutta-percha) is known to form a rod-like structure. The regular structure of gutta-percha therefore allows for more efficient molecular packing and thus has a higher degree of crystallinity than natural rubber (Gowariker et al 1986).

2.2.7.3. Stereoregularity & Steric Order

The stereoregularity of polymers can also have a strong influence on the crystallizability of a polymer. It is well established that isotactic and syndiotactic polymers are often able to crystallize, while atactic polymers are typically amorphous.

This again, is witnessed for polystyrene (PS), where atactic PS is completely amorphous, while isotactic polystyrene forms well-defined spherulites with a degree of crystallinity of approximately 50% (Sharples 1966).

One of the most common examples of steric order is that of the head-to-head defects that occur with some vinyl polymers. While the head-to-tail arrangement is the most probable conformation, head-to-head defects can occur which disrupts the regularity of the chain, reducing the degree of crystallinity.

2.2.7.4. Polarity

Polarity can also be a significant factor that determines the crystallizability of a polymer. Nylon 6 for example is known to form hydrogen bonds between the carbonyl oxygen group of one nylon molecule and the amine hydrogen on an adjacent molecule thus facilitating tighter packing of the chains (Gowaricker 1986). Polyesters, such as PET, are also dependent upon polarity to crystallize. Like nylons, polyesters must not only line up in a periodic fashion, but must also line up adjacent polar groups to form crystals. This explains, in part, why PET crystallizes more slowly, than polyethylene for example (Sharples 1966). Additionally, the stiffness of the PET chains is also believed to be partially responsible for its relatively slow crystallization rate.

2.2.7.5. Copolymerization

Although copolymerization could be, arguably, placed under the heading of Molecular structure, it seems more appropriate in the context of this research to include it

under its own heading. In general, a copolymer, can be classified as one of three types: random, alternating, or graft.

For a copolymer containing A and B comonomer units, a random copolymer is one of the form: -AABBABBBBABA-. Thus a random copolymer is one where along any point in the macromolecular chain, the probability of finding either an A or B unit is dependent on the concentration of each unit. Alternating copolymers are those that in general have a repeating structure of A and B units of the form: -ABABABABABAB-. When alternating copolymers contain several A and/or several B units in sequence they are referred to as block copolymers with the general formula: -AAAAAABBBBBB-. Finally, graft copolymers are those that contain a polymer chain comprised solely of A units with a side-chain composed solely of B units.

As a general rule, adding a comonomer reduces the crystallinity and rate of crystallization. This is much the same phenomenon that occurs when discussing any other type of defect. Thus a second comonomer is typically rejected from the homopolymer crystal, just as with a head-to-head defect for example, until at even moderate concentrations, little to no crystallinity is encountered. Because of this effect, the addition of a comonomer, even in relatively low concentrations, can have a very dramatic effect on the overall physical properties of the material.

Many investigators have verified this effect. For example, Righetti et al (1998) observed a decrease in the overall rate of crystallization of copolymers of poly(butylene adipate) and poly(butylene isophthalate). Likewise, Hybart and Pepper (1969) found that for Nylon 11 copolymers containing up to 20 mol% ω-aminocaprioc acid the half-time of

crystallization was increased and the degree of crystallinity decreased with increasing comonomer content.

There are numerous examples pertaining to the decrease in the crystallizability of random PET copolymers as well. For example, this includes PET copolymerized with 4,4'-bis[(4-carbo-2-hydroxyethoxy)phthaolimido] diphenylmethane]) (Park and Lee 1995), and polyethylene isophthalate (Li et al 1999).

It is important to note, however, that many investigators have found evidence suggesting that copolymerizing PET with certain species actually increases the rate of crystallization. Connor et al (2001) found that copolymerizing PET with one of three different comonomers (dimethyl-4-4'-biphenyldicarboxylate, 2,7-dimethyl-4,5,9,10-tetrahydropyrenedicarboxylate, or dimethyl-2,7-pyrenedicarboxylate) reduced the overall rate of crystallization. However, it was found that when perylene was added to the copolymers containing pyrene the rate of crystallization was apparently enhanced. It was suggested that this might be due to the formation of π-stacked assemblies of perylene with pyrene thus forming aggregates that serve as seeds for crystallization. An alternative explanation given was that perylene, upon cooling, first crystallizes, thus acting as a phase-separated, heterogeneous nucleation agent. PET copolymerized with ethylene diamine has also been shown to improve crystallizability (Bouma et al 2000). Here it is speculated that the entropy of crystallization is decreased by the preferential self-assembly of diamide units facilitated by hydrogen bonding.

Of notable applicability to this study, Bier et al (1977) found that PET copolymers containing approximately 5-mol% of branched codiols, such as 2,5-hexanediol and 3-methyl-2,4-pentanediol, crystallized much more rapidly than PET homopolymer. In a

related study, Bouma et al (2001) found that PET copolymers containing low concentrations of 1,5-pentanediol, 1,8-octanediol, 2,5-hexanediol, or 1,3-dihydroxymethyl benzene were able to enhance nucleation.

It is also notable to mention that Bouma et al (2001) found the optimum concentration of 2,5-hexanediol to be 1mol%, much lower than that suggested by Bier et al (1977). Likewise, it was shown that copolymers containing a branched olefinic diol (C_{36}-diol) were also able to improve crystallizability (Bouma et al 2001). Codiols with greater than 4 carbons are known to fold easily and have a lower surface energy than ethanediol (Bier et al 1977, Eisenbach et al 1995, Bouma et al 2001). As a result, it was speculated that the short codiols, assumed to be rejected from the parent homopolymer crystal but possibly included in the chain fold, enhanced nucleation by decreasing the surface fold free energy. It was further suggested that the inclusion of short methyl groups would decrease the surface free energy to an even greater extent, thus further enhancing this nucleation effect (Bouma et al 2001).

On a related matter, Suh (2001) found that fibers produced from PET copolymerized with 2-methyl-1,3-propanediol (MPDiol) showed a marked decrease in crystallinity with increasing comonomer content at a given spinning speed. Thus, at least under conditions of elongational flow, the crystallizability of these particular copolymers appears to be reduced.

2.2.8. Polymer Crystal Melting

As is pointed out by Young (1981) there are several differences between the melting behavior of polymer crystals and crystals of lower molecular weight materials, including:

1. The melting temperature of polymers is broad, and therefore it is not possible to define a single melt temperature;
2. The melt temperature is dependent upon the specimen history, particularly the crystallization temperature; and
3. The melt temperature is dependent upon the rate at which the polymer is heated.

This melting variability is a direct reflection of the fact that polymer crystals are quite thin and that sample preparation, previous melt history, and experimental technique can influence the melting behavior of polymers (Young 1981). As a result of this variability the concept of an equilibrium melt temperature is introduced. The equilibrium melt temperature, as will be shown in the next few sections, can be defined as the melting temperature of an infinitely thick crystal with a negligible surface energy.

2.2.8.1. Relationship between Melt Temperature, Lamellae Thickness, and Surface Area

Thermodynamically, the overall change in Gibb's free energy of melting a lamellae crystal with lateral dimensions, x and y, and thickness, l, is given by:

$$\Delta G = xyl\Delta g_f - 2l(x+y)\sigma - 2xy\sigma_e \qquad (2.39)$$

where Δg_f is the Gibb's free energy per unit volume (the same general form as that given in Equation 2.8), and the side and end surface free energies are given by σ and σ_e, respectively.

For lamellar crystals, the top and bottom surfaces will be much larger than the side surfaces, and therefore the second term of Equation 2.39 can be neglected. Since the melting point occurs when ΔG=0, the melting temperature is therefore given by:

$$T_m = T_m^0 - \frac{2\sigma_e T_m^0}{l\Delta h_f} \qquad (2.40)$$

Equation 2.40, known as the Thomson-Gibbs equation, shows that the melting temperature will always be less than the equilibrium melt temperature and that only when the lamellae thickness, l, approaches ∞ will the two melt temperatures be equal. Likewise, this equation illustrates that surface energy also serves to decrease the melt temperature.

2.2.8.2. Copolymer Melt Temperature

One of the earliest theories that pertains to the lowering of the melt temperature dates back to 1947 when Flory suggested that comonomer units, which are excluded from the crystal, change the configurational entropy of the system and therefore influence the melt temperature (Flory 1947, 1955). In his theory, Flory determined the upper bound of the copolymer melting temperature by considering the melting of crystals built up from "infinitely long" homopolymer sequences of A units in a copolymer. Flory developed an equation to examine the melting point depression as a function of comonomer concentration (Flory 1947, 1955, Wendling and Suter 1998):

$$\frac{1}{T_m^0} - \frac{1}{T_m(x_B)} = \left(\frac{R}{\Delta H_f}\right) \times \ln(1 - x_B) \qquad (2.41)$$

where $T_m(x_B)$ is the equilibrium melting temperature of a copolymer with mole fraction x_B, T_m^0 is the equilibrium melting temperature of the homopolymer, R is the universal gas constant and ΔH_f is the heat of fusion.

It is important to note that in some cases Flory's equation does not adequately describe experimental data. As a result, Baur (1966) further developed Flory's model to suggest a "hindered equilibrium" concept, which considers the average length of homopolymer chain sections that can segregate and crystallize (Wendling and Suter 1998). Thus Baur offered the following equation:

$$\frac{1}{T_m^0} - \frac{1}{T_m(x_B)} = \left(\frac{R}{\Delta H_m^0}\right) \times [\ln(1 - x_B) - \langle \xi \rangle] \qquad (2.42)$$

where $\langle \xi \rangle = [2x_B(1-x_B)]^{-1}$ is the average length of the homopolymer sequence in the melt. While Baur's model does take into account crystal thickness and has been shown in some instances to fit experimental data better than Flory's equation, it is still often very inadequate in describing the melting behavior of copolymers. As a result, much work continues to be conducted to better understand the crystallization process associated with copolymers (Wendling and Suter 1998, Helfand and Lauritzen 1973). Even still, these models provide a certain amount of insight into the actual crystallization process of copolymers. As comonomer content increases, the number of crystallizable units decreases, therefore resulting in a "thinner" crystal, which serves to ultimately reduce the melt temperature.

2.2.8.3. Determination of The Equilibrium Melting Temperature

The equilibrium melting temperature can be determined by several techniques. Two of the most common techniques involve an extrapolation method. Equation 2.40 suggests that there should be a linear relationship between the experimentally determined melt temperature and the reciprocal of the lamellae thickness. Thus both T_m^0 and σ_e can be experimentally determined by plotting T_m as a function of the reciprocal lamellae thickness, 1/l, where the slope is equal to $-(2\sigma_e T_m^0)/h_f$ and the y-intercept = T_m^0.

A second method to determine the equilibrium melting temperature is the Hoffman-Weeks plot. It was witnessed that the temperature of crystallization, T_c, was always lower than the melt temperature, T_m. It was also noticed that as the isothermal crystallization temperature was increased, the subsequent melting temperature also increased and that the two temperatures were apparently directly proportional. This observation led to the conclusion that the lower limit of the melting temperature should be observed when $T_m=T_c$ (Young 1981). Thus it is suggested that the experimentally determined value of T_m can be plotted as a function of T_c. The best-fit line can be extrapolated to the intersection of the line given by the equation $T_m=T_c$ thus leading to the determination of the melting temperature for a polymer that was crystallized infinitely slowly at the melting temperature. Thus the intercept of these two lines must represent the equilibrium melting temperature (Hoffman and Weeks 1962).

Many other methods have been proposed for determining the equilibrium melting temperature and as a result the appropriate method is still somewhat disputed. As a result, the equilibrium melting temperature and the heat of fusion for 100% crystalline PET are also somewhat in question.

Many experimenters have observed somewhat high melting temperatures of highly annealed PET samples. Melting temperatures of 278°C (Taylor 1962) and as high as 280°C (Myagi and Wunderlich 1972) have been observed. The equilibrium melt temperature of PET was determined by Wlochowicz and Przygocki (1973) using both the Thomson-Gibbs method (Equation 2.34) and the Hoffman-Weeks approach where the two methods showed good agreement yielding values of 278 and 279°C. These experiments, along with the work of many others, have resulted in the commonly accepted value of T_m^0=280°C for PET. In a like manner, the heat of fusion for a 100% crystalline sample of PET, ΔH_f^0, is commonly accepted to be 140 J/g (Wunderlich 1980).

One difficulty in determining the equilibrium melt temperature of PET by an extrapolation method involving the measured melting temperature is the fact that upon melting of isothermally crystallized samples at certain crystallization temperatures, multiple melting peaks are observed (see Chapter 4-Figures 4.26-4.29). This has been reported by many investigators and has been suggested to result from the melting of crystals produced during primary and secondary crystallization. Using this assumption, each peak has been attributed to a particular crystallization mechanism. Zhou and Clough (1988), Wang et al (1999), and Lu and Hay (2001) have all suggested that the first melting peak is assigned to melting of subsidiary lamellae formed during secondary crystallization, the second melting peak is assigned to the melting of the primary lamellae formed during isothermal crystallization, and the third melting peak is attributed to recrystallization during subsequent DSC heating of material formed at the crystallization temperature.

However, it is important to note that there is an alternative explanation for this phenomenon. Medellin-Rodriguez et al (1997, 1998) have suggested that the first melting peak was attributed to the final stage of secondary crystallization (small branches of metastable crystalline material), the second melting peak was associated with secondary crystallization (metastable secondary branches), and the third melting peak was attributed to crystals formed during primary crystallization that have recrystallized during reheating in the DSC.

2.2.9. Practical Significance of Polymer Crystallinity

Polymer crystallinity is an important parameter that significantly affects many of the properties of polymers including the mechanical, optical, and chemical properties of the material.

2.2.9.1. Mechanical Properties

The degree of crystallinity is known to significantly affect the mechanical properties of polymers. For example, uncrystallized rubber can be reversibly extended many times its own length, but has a very low modulus. However, it has been shown that rubbers with approximately 24% crystallinity have a modulus approximately 100X that of the uncrystallized rubber (Sharples 1966).

In general, as crystallinity increases, modulus, yield strength, density, and hardness also increase. In fact, modulus typically increases linearly with density, apparently independent of crystallization conditions. Annealing of unstrained polymers typically increases modulus, increases ultimate tensile strength, and reduces ultimate

elongation which is just the opposite of that encountered for metals or other lower molecular weight materials (Schultz 1974). In general the quality, size of spherulites, and number of tie molecules may also play an important role in determining mechanical properties of polymers. Refinement of spherulites results in higher yield and ultimate strength, and an increase in ultimate elongation in the case of isotactic polypropylene and polystyrene (Sogolava 1965). Likewise, many investigators have found evidence that spherulite size refinement also improves impact strength (Kargin et al 1966, Dixon and Jackson 1968, Ohlberg et al 1959).

Since the degree of crystallinity is typically reduced by the addition of a comonomer it is expected that the mechanical properties will also be affected. Karayannidis et al (2000) verified this relationship by examining the thermal and tensile properties of poly(ethylene terephthalate-co-ethylene isophthalate) with comonomer content ranging from 0 to 100% ethylene isophthalate. It was determined that increasing polyethylene isophthalate content reduces both the rate of crystallization as well as the overall degree of crystallinity (Li et al 1999). As would be expected, PET homopolymer showed a much higher Young's modulus (610 MPa) as compared to a copolyester containing 10 mole% polyethylene isophthalate (242 MPa). It was also shown that elongation at yield was significantly increased up to 30 mol% comonomer and elongation at break was maximized by the addition of 10% comonomer. It is also notable that copolyesters containing more than 20mol% comonomer were found to be amorphous. Since the glass transition temperature for all of the copolyesters was well above room temperature (65-82°C), copolyesters that were completely amorphous were quite brittle with relatively low elongation at break (13-38%).

A study by Varma et al (1986) examined how increasing both comonomer content and the length of the methylene groups in the comonomer affect the mechanical and physical properties of PET/Poly(alkylene terephthalate) copolyester fibers. As with the previous study, it was witnessed in drawn fibers that the tenacity and modulus of copolyester fibers were lower than PET homopolymer. It was also observed that percent elongation increased with an increase in the number of methylene groups contained in the polymer (i.e. increasing comonomer content). As is suggested here, this is probably due to the lower degree of crystallinity caused by the incorporation of flexible groups in the PET backbone. Upon drawing of these fibers, it was also observed that there was a decrease in birefringence and crystalline orientation with an increase in the number of methylene groups incorporated in the chain.

2.2.9.2. Chemical Properties

The degree of crystallinity is known to strongly influence the chemical reactivity of a polymer. In fact, the amorphous content of a material largely determines both the rate and extent of reaction (Sharples 1966). Polystyrene, for example, is an amorphous material easily attacked by solvents. On the other hand, at room temperature, crystalline PET is resistant to water, weak acids and bases, ketones, alcohols, glycols, ethers, aliphatic hydrocarbons, and chlorinated aliphatic hydrocarbons, and gasoline, motor oil, and brake and transmission fluids at temperatures up to 60°C (Arroyo 1997). Water absorption, in general, also is known to decrease with increasing crystallinity.

Copolymerization of PET is sometimes used to improve the chemical properties of PET. An example of this is shown for PET fibers copolymerized with 2-methyl-1,3-

propanediol. Incorporation of the comonomer in this case has been shown to greatly improve the dyability of the fibers (Chen et al 2000). Kiyotsukuri et al (1994) also showed that copolymerizing PET with 1,3-propanediol and 2,2-dialkyl-1,3-propanediols (where the dialkyl groups were dimethyl, diethyl, and butyl-ethyl) improved the dyeability and alkali resistance of the polymer.

2.2.9.3. Optical Properties

The optical properties of a polymer are significantly affected by the degree of crystallinity, in particular by the size of the spherulites. It is well established that the light scattering from polymer crystals severely affects the clarity of the material, in that the ordered crystals alter the refractive index in a given direction. As a result, the transmission of light through a polymer sample significantly decreases with increasing crystallinity. There are many ways that the optical properties of a polymeric material can be manipulated. One obvious way is to prepare a copolymer with a sufficient amount of irregularity (i.e. high comonomer content) so as to eliminate crystallinity altogether. However, in some cases this may not be desirable due to other design constraints (such as the retention of mechanical properties and/or chemical resistance characteristics). A second method then might be to use nucleating agents, which can improve clarity, by reducing spherulite size (Sharples 1966).

CHAPTER 3: EXPERIMENTAL

3.1 Materials

In this experiment Poly(ethylene terephthalate) (PET) homopolymer and PET copolymers containing 2-methyl-1,3-propanediol (MPDiol) were supplied by Wellman, Inc. As described by Chen et al (2000), these copolymers could be produced by preparing a slurry mixture composed of excess mixed glycols (ethylene glycol and 2-methyl-1,3 propanediol) and terephthalic acid, as previously illustrated in Figure 2.2. An esterification reaction of the slurry mixture is carried out at 250°C under pressure (absolute pressure = 2 kg/cm^2) at a conversion rate of 95% to yield a low-polymerized product. Antimony trioxide (350 ppm) was then added and polycondensation was carried out for 3 hours at 280°C and an absolute pressure of 1 torr (Chen et al 2000).

The copolymers used in this study were prepared with nominal glycol feed compositions of 4, 7, and 10 mol% MPDiol. Since the reactivities of the polymerizing species in a step polymerizing reaction depend primarily on the reactivity of the functional groups, and not on the actual monomers, it is assumed that the resultant polyesters are random copolymers containing roughly the same composition as in the feed. NMR was used to verify the copolymer composition, where it was found that the actual MPDiol content in these copolymers was slightly higher than in the feed (5, 9, and 12 mol%). However, the correlation between them was quite good and it was decided to use the nominal composition when reporting the experimental results.

All copolymers were supplied in pellet form and were reported as having intrinsic viscosities of 0.61 $\pm$0.01 dl/g.

3.2 Experimental Procedure

3.2.1. Sample Preparation

3.2.1.1. DSC Sample Preparation

All samples were first dried at 100°C in vacuo for at least 12 hours. Thin films were then prepared by melt pressing four to seven sliced pellets of each copolymer in a Wabash compression molding machine. The sliced pellets were placed between two sheets of Teflon film, which were then sandwiched between two preheated metal plates. The plates were then placed on the platens of the Wabash compression molding machine and allowed to remain at the set temperature (approximately 10-20°F above the material's melt temperature) for three minutes. The samples were then melt pressed at 5 tons/in^2 for four minutes. The plates were then immediately taken from the machine and the pressed films, still sandwiched between the two sheets of Teflon film, were taken from between the two metal plates and allowed to cool to room temperature. The films were then immediately placed in a dessicator until use. Samples were then cut from the film using a standard size paper punch and trimmed (if needed) to size.

As will be described later, the isothermal crystallization experiment was carried out in a Perkin Elmer DSC7 differential scanning calorimeter, while the nonisothermal crystallization experiment and the thermal characterization of these copolymers was carried out in a the Mettler-Toledo DSC820 differential scanning calorimeter. Due to the

different types of sample pans for each experiment, the resulting sample sizes were slightly different. Samples used in isothermal crystallization experiments were cut to a sample mass of 4.50 ± 0.20 mg, while samples for nonisothermal crystallization and for thermal characterization were cut to 4.00 ± 0.11 mg.

3.2.1.2. Light Depolarizing Microscope Sample Preparation

A Mettler-Toledo FP82 hotstage with a Mettler-Toledo FP80 programmable controller was used to prepare the Light Depolarizing Microscope (LDM) samples. Several pellets (at least 20) of each copolymer, dried at 100°C in vacuo for at least 12 hours, were sliced into small pieces (weighing about 6 mg each) and mixed together. Three to four of the sliced pellet pieces were then randomly chosen and placed between two 24 x 60 mm glass slide cover slips. A 76.2 μm (0.003 in) diameter J-type iron constantan thermocouple was embedded into the material. With the aid of two spacers the sample was then melt-pressed into a thin film of 150 μm in thickness as is shown in Figure 3.1. The thermocouple wires were then insulated and the leads connected to a standard thermocouple plug. Several samples were prepared for each copolymer in this manner.

3.2.2. Experimental Techniques

3.2.2.1. Differential Scanning Calorimeter (DSC)

3.2.2.1.1. DSC –Description of Apparatus and Basic Theory

A Differential Scanning Calorimeter (DSC) works on the principle of differential heat flow between a sample and a reference. Because heat is measured by this technique,

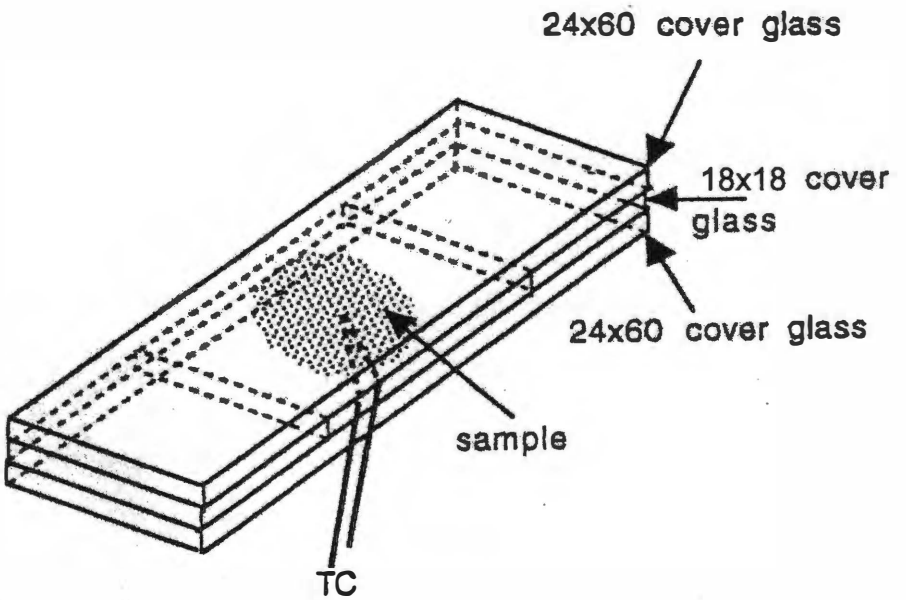

Figure 3.1: Sample Used in LDM Studies

Adapted from: Ding, Z. PhD. Dissertation, University of Tenn. (1995).

important quantitative thermodynamic measurements can be made. In contrast, a somewhat similar technique known as Differential Thermal Analysis (DTA) can be used to measures the difference in the temperatures of a known and reference sample when subjected to a linear heating program, with the result plotted as a function of temperature. The distinct advantage of DSC over DTA is that the area under a DSC transition peak is directly related to the heat of that transition, while in DTA the peak areas can only be converted to heat by use of a suitable calibration method where the temperature and sample-dependent thermal resistance of the system is taken into account (Kämpf 1986).

A DSC can be used to measure thermal transitions under both isothermal and nonisothermal conditions. In the case of nonisothermal conditions, DSC's can be programmed to heat or cool at a constant rate, where the desired thermal transition is measured.

There are essentially two different types of commercially available DSC's: a power compensating DSC and a heat-flux DSC. Since both types were used in this investigation, they are briefly described below. More detailed descriptions of the operation and mathematical treatments of DSC's are readily available, including those by Wunderlich (1990, 1997), Gallagher (1997), Boerio-Goates and Callanan (1992), and Hemminger and Höhne (1984).

The schematic of a typical power compensating DSC is shown in Figure 3.2. A power compensating DSC does not rely on differences in temperature between the sample and reference for its operation, but rather attempts to keep the difference in temperature, ΔT, nearly constant during operation. This is accomplished by placing Pt resistance thermometer temperature sensors into a bridge circuit such as is shown. Any

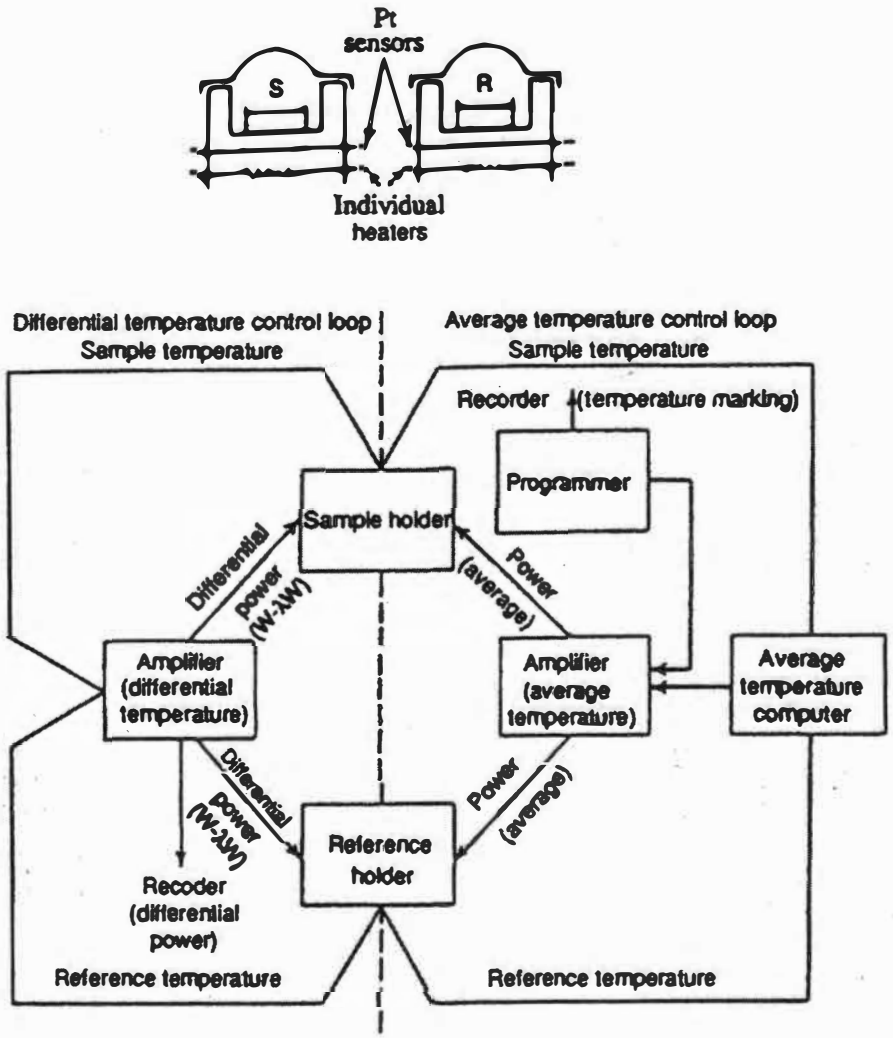

Figure 3.2: Schematic Representation of a Power Compensating DSC

Source: Watson et al., Anal. Chem., 36, 1233 (1964).

temperature imbalance is used to direct heat (in the form of electrical energy) to the appropriate portion of the cell. Thus the power compensating DSC is constantly compensating for changes in heat capacity between the sample and reference, as well as for any heat absorbed or evolved by the sample during a thermodynamic transition by continuously supplying the required electrical energy needed to balance the bridge circuit (Gallagher 1997).

In this investigation, a Perkin-Elmer DSC7, of the power compensation type, was used to study the isothermal crystallization and subsequent melting behavior of the PET copolymers examined.

The second main type of DSC, a heat-flux DSC, works on much the same principle as a conventional DTA except for one notable difference. Essentially, a heat-flux DSC measures the difference in temperature between the sample and reference (T_s-T_r) as a function of temperature. In this type of DSC, the peak area magnitudes are directly dependent on the magnitude of the thermal constants in the system, which change with temperature, much the same as with a conventional DTA. Thus quantitative compensation for the temperature dependence of thermal transport and sensor sensitivity must be built into the associated software and hardware (Gallagher 1997). This is in direct contrast to the power compensating DSC mentioned earlier, which measures heat in the form of electrical energy directly.

In this experiment a Mettler-Toledo DSC 820, based on the Boersma or heat-flux principle, was used for non-isothermal crystallization work and for the initial thermal characterization of these polymers. A schematic of a typical heat-flux DSC, showing

Boersma thermocouple placement, is shown in Figure 3.3. The model shown is based on the DuPont 910 DSC, but is common in basic operation to most heat-flux DSC's including those made by Mettler-Toledo. In this particular DSC, a constantan disk is used which serves multiple purposes. It serves not only as the primary means of heat transfer to the sample and reference pans, but also as one element of the temperature measuring thermoelectric junction. A chromel-constantan area thermocouple, formed by the constantan disk and a chromel wafer that covers the underside of each platform, is used to measure the differential heat flow to the sample and reference pans. The chromel and alumel wires are connected to the underside of chromel wafers thus forming a chromel-alumel thermocouple, which is used to measure the sample temperature directly (Wendlandt and Gallagher 1981).

3.2.2.1.2. DSC- Thermal Characterization of Copolymers

DSC samples, prepared as described earlier, were placed in a Mettler FP85 TA cell (equipped with an FP80 central processor) set at 290°C and allowed to sit at that temperature for 10 minutes. This step was performed not only to heat the sample above its melt temperature for subsequent quenching, but also to destroy any thermal and mechanical history imparted on the sample during melt pressing.

The DSC pans were then quickly submerged in liquid nitrogen and held there for 45 seconds. An effort was made to ensure that the pan was not tipped or inverted during quenching to guarantee that the melt solidified on the bottom surface of the DSC pan. After quenching, the samples were allowed to sit for no more than 45 minutes prior to testing to ensure that annealing effects remained minimal. Samples were then

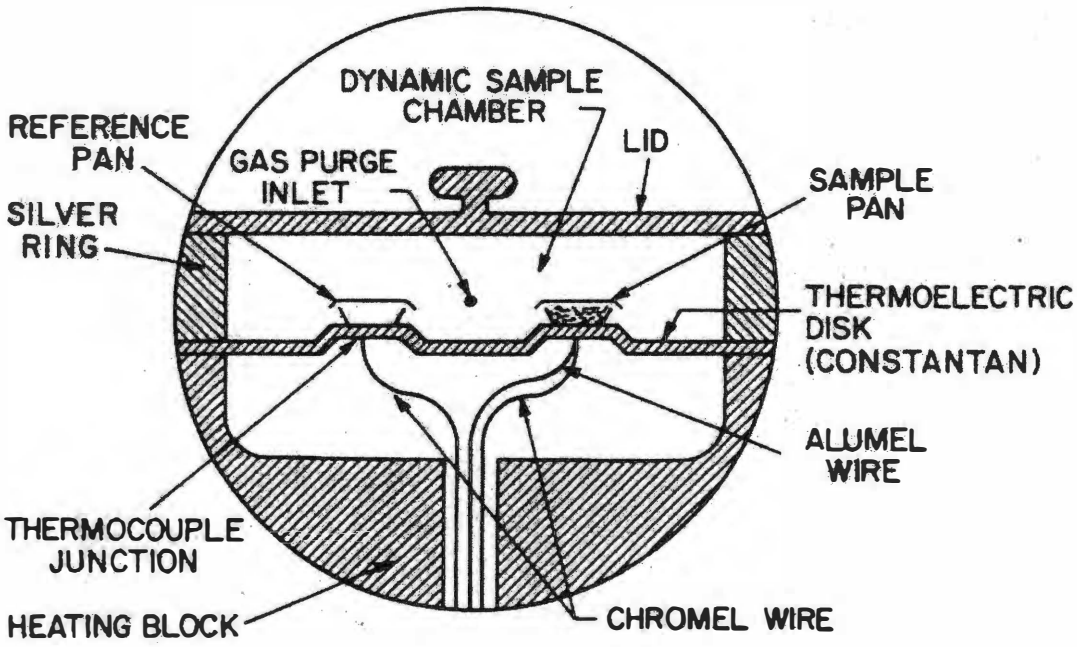

Figure 3.3: Schematic Representation of a Heat-Flux DSC

Source: Baxter, R.A., in "Thermal Analysis," Vol. 1, Academic Press, NY (1969).

transferred to the Mettler-Toledo DSC820 cell maintained at 25°C. The DSC was held at 25°C for 5 minutes to ensure thermal equilibrium was achieved and then heated from 25 to 300°C at a rate of 10°C/min. Three samples of each material were tested in this manner. A pure Indium standard, with an onset melting temperature of 156.60°C and a heat of fusion of 28.450 J/g, was used to perform periodic machine calibrations between experimental runs to ensure data precision.

It should be noted that all data for the thermal characterization and nonisothermal crystallization portions of this experiment are reported and examined in terms of the sample temperature, not reference temperature.

3.2.2.1.3. DSC -Isothermal Crystallization of Copolymers

The isothermal crystallization kinetics of PET and its copolymers of 2-methyl-1,3-propanediol were examined using a Perkin-Elmer DSC7 differential scanning calorimeter equipped with an FC-50-100-PE intercooler and using a dried nitrogen purge gas. The experimental procedure for determining the overall isothermal crystallization kinetics of PET and PET copolymers was based largely on similar studies performed by Park and Lee (1995) and Li et al (1999).

In this experiment, the samples were heated slightly above their observed melt temperature (T_{hold}) and held at that temperature for five minutes (see Table 3.1). This step was performed to erase the mechanical and thermal history of the polymer subjected during sample preparation. The next step was to quench the sample to the isothermal crystallization temperature at a scanning rate of 200°C/minute. The sample was allowed

Table 3.1: Hold Temperatures Used in Isothermal Crystallization Experiment

Sample	T_{hold} , °C
PET	280
PET-4	270
PET-7	270
PET-10	260

to remain at the desired isothermal crystallization temperature until returning to a horizontal baseline, thus indicating the end of crystallization. The samples were then reheated at a rate of 25°C/min back to the melt temperature to examine the resulting melting behavior. DSC calibration was performed periodically during testing using an Indium standard to ensure data precision.

3.2.2.1.4. DSC-Nonisothermal Crystallization of Copolymers

In this experiment a Mettler-Toledo DSC820 equipped with liquid nitrogen cooling and dried nitrogen purge gas was used to investigate the nonisothermal crystallization kinetics of the PET copolymers. The experimental procedure was based largely on similar studies performed by Park and Lee (1995), Li et al (1999), and Supaphol (2000).

In this experiment, the samples were heated to 290°C and held at that temperature for 10 minutes, again to ensure the achievement of thermal equilibrium as well as to erase the mechanical and thermal history, which the polymer was subjected to during sample preparation. The samples were then cooled to 30°C at rates of 1, 2.5, 5, 7.5, 10, and 12.5°C/minute. The samples were then held at 30°C for 10 minutes and then

immediately reheated to 290°C at 10°C/min to observe the resulting melting behavior. As before, DSC calibrations were performed periodically during testing using an Indium standard.

As was mentioned previously, all data for the nonisothermal crystallization portion of this experiment is reported and examined in terms of the sample temperature. It is assumed that thermal lag in this experiment is very small because sample sizes were not excessively large and because the cooling rates used were relatively moderate.

3.2.2.2. Light Depolarizing Microscope (LDM)

3.2.2.2.1. LDM –Description of Apparatus and Basic Theory

Much of the work that has been done in the area of nonisothermal crystallization of polymers has been done under moderate cooling conditions. Although this work is very important, it represents only the first step in really understanding the nonisothermal crystallization kinetics likely encountered during polymer processing. In the recent past, much of the difficulty in determining this behavior was due to the inadequacies of conventional methods to record and analyze data under more extreme cooling conditions. Recognizing that no technique was available to study the nonisothermal crystallization kinetics under these conditions, Ding and Spruiell (1996) developed a technique that allowed for the study of such phenomena at cooling rates up to 5,000°C/min.

As is shown in Figure 3.4 the modified LDM system consists of an Olympus BH2 optical microscope, a light source, a cooling unit, a heating coil, a specially made sample chamber, three amplifiers, a gas control board, and a personal computer equipped with an in-house developed data acquisition software package. As is shown, nitrogen gas,

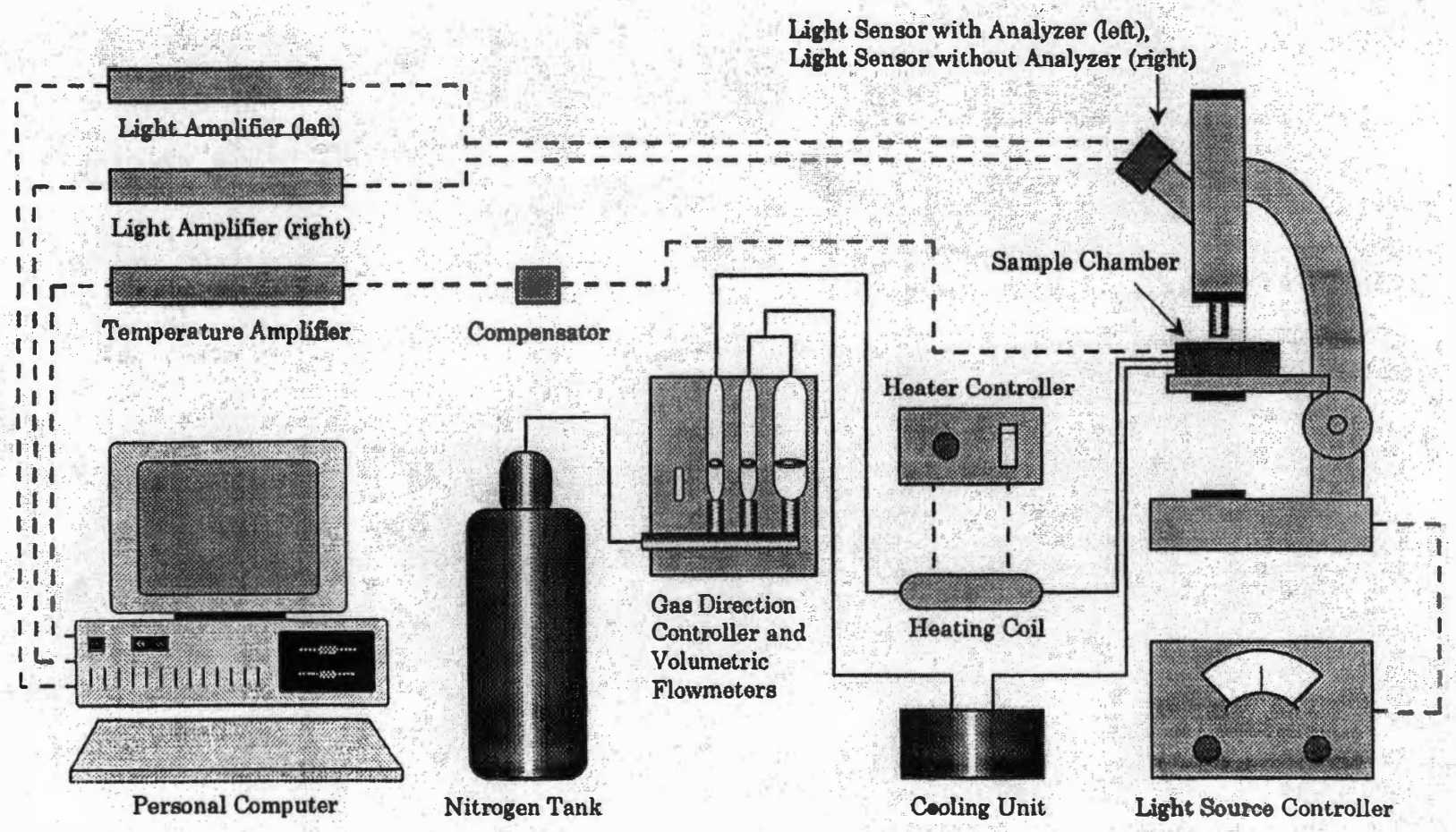

Figure 3.4: Schematic Diagram of the Light Depolarizing Microscope

Source: Supaphol, P., MS Thesis, University of Tenn. (1996).

passing through a gas direction controller, is used to heat and cool the sample. Sample heating is achieved by passing the nitrogen gas through a heating coil prior to reaching the sample chamber. In a like manner, sample cooling is achieved by bypassing the heating unit, delivering nitrogen gas directly to the sample chamber. For even higher cooling rates, a cooling unit such as is shown in Figure 3.4 can be used. A Mettler FP82 hotstage with a Mettler FP 80 programmable controller can also be used, in replacement of the gas heating and cooling system, to obtain more moderate cooling conditions (up to 20°C/min).

The light transmitted through the sample at any instant in time is recorded by two light sensors, which are in place of the eyepieces of the microscope. As will be described later, the purpose of simultaneously measuring the light intensity with and without a crossed analyzer is to minimize the effect of light scattering during crystallization. The signals from both light sensors, as well as the temperature signal from the thermocouple imbedded in the sample, are then amplified and sent to the PC where the signals are recorded by the data acquisition program.

One of the more important considerations in using this technique is to ensure that the sample thickness is maintained constant, and must be quite thin so that the temperature gradient across the thickness of the sample during rapid cooling is negligible. The governing heat transfer equation that was used to quantitatively study this system is given as:

$$b \cdot \rho \cdot Cp \cdot \left(\frac{dT}{dt} \right) = -H_{ga} \cdot (T - T_s) \qquad (3.1.)$$

where b is the half thickness of the polymer sample, Cp is the heat capacity, ρ is the density, T is the temperature of the polymer melt, T_s is the temperature of the immediate surroundings, and H_{ga} is the overall heat transfer coefficient of the air and cover glass given by:

$$H_{ga} = \frac{1}{\left(\frac{l}{k_g}\right) + \left[\left(\frac{1+2(l_g/2b)}{h_a}\right)\right]} \qquad (3.2.)$$

where l_g and k_g are the thickness and thermal conductivity of the cover glass respectively and h_a is the heat transfer coefficient for the air boundary layer. If ρ, Cp, and k_g are assumed to be constant during cooling to the temperature at which crystallization occurs then the analytical solution to Equation 3.1. is given by:

$$T - T_s = (T_0 - T_s)\exp\{-(CRF)\cdot t\} \qquad (3.3.)$$

where T_0 is the initial hold temperature prior to cooling and CRF is the cooling rate function given by:

$$CRF = \frac{H_{ga}}{b \cdot \rho \cdot Cp} \qquad (3.4.)$$

Under quiescent conditions it was observed that the light intensity was directly proportional to the absolute crystallinity, X_c, sample thickness, l, and the intensity of the incident light, I_0'. However, under high cooling rate conditions, the high nucleation rates caused a significant amount of light scattering that prevented the transmitted light intensity from varying in a manner directly related to the sample crystallinity. Simultaneously measuring the transmitted light intensity with and without an analyzer and using the following relation solved this problem:

$$I = C_1 I_0 X_c l + I_z \qquad (3.5.)$$

where C_1 is a constant related to the geometrical and optical quality of the sample, I is the transmitted light intensity measured with an analyzer, I_0 is the transmitted light intensity measured without an analyzer and I_z is a quantity that represents the light that leaks through the crossed polars when the sample is completely amorphous, or when no sample is present. Within an acceptable range of I and I_0 Equation 3.5 is given by:

$$I_z = R_0 I_0 + C_2 \qquad (3.6.)$$

where C_2 is a constant. Thus combining Equations 3.5. and 3.6. leads to the following important equation:

$$I = (C_1 X_c l + R_0) I_0 + C_2 \qquad (3.7.)$$

By noting that the term in brackets is a constant for a given degree of crystallinity leads to the following:

$$I = C_3 I_0 + C_2 \qquad (3.8.)$$

Equation 3.8 is an important result in that it provides a theoretical basis for the experimental determination of C_2. For any given polymer with a given degree of crystallinity, a plot of I as a function of I_0 for a variety of incident light intensities should yield a straight line with slope equal to the combined constant, C_3, and y-intercept equal to C_2.

Additionally, Equation 3.7 can also be written as:

$$R = C_1 X_c l + R_0 \qquad (3.9.)$$

where R is called the relative light intensity and is given by:

$$R = (I - C_2)/I_0 \qquad (3.10.)$$

By Equation 3.9. R_0 is equal to R when X_c is zero. In a similar fashion when $t=\infty$, $R=R_\infty$, leading to the following:

$$\theta = \frac{X_c}{(X_c)_\infty} = \frac{R - R_0}{R_\infty - R_0} \qquad (3.11.)$$

where θ is the relative crystallinity at any time t. Thus to determine the relative degree of crystallinity by this technique, I and I_0 must be measured simultaneously and corrected to determine the relative intensity at any time t.

3.2.2.2.2. LDM - Nonisothermal Crystallization of Copolymers

3.2.2.2.2.1. Determination of Universal Constant, C_2

As mentioned in the previous section, the light intensity transmitted through the sample must be measured simultaneously with and without an analyzer to minimze the effect of light scattering during crystallization. By Equation 3.10 in order to convert this raw data into a relative crystallinity, the universal constant, C_2, must be determined. Ding and Spruiell (1996) suggested that this correction factor could be determined by preparing samples with different crystallinity levels and measuring the light intensity with and without an analyzer at various incident light intensities and plotting I as a function of I_0 according to Equation 3.8. Thus several samples were prepared of each copolymer and subjected to different cooling conditions to obtain samples of varying crystallinity. The light intensity with and without an analyzer was measured at a variety of different incident light intensities to obtain a correction factor for each sample at a particular degree of crystallinity. Averaging all of the scattering correction factors for each copolymer then provided a universal scattering constant. The plots of light intensity

with an analyzer as a function of the light intensity without an analyzer for the four materials examined are shown in Figures 3.5 through 3.8. The "universal correction factors" for PET, and the 4, 7, and 10% copolyesters were found to be $-0.00583*10^{-6}$, $-0.00187*10^{-6}$, $0.00500*10^{-6}$, and $0.01718*10^{-6}$ W/cm^2 respectively.

As mentioned, Equation 3.5 suggests that a plot of I as a function of I_0 for a completely amorphous sample or when no sample is present should lead to a determination of I_z for that sample. This was tested by replacing the sample in one of the specimens with an extra cover slip (150μm in thickness) between two cover slips and measuring I and I_0 at a variety of incident light intensities. Thus the "glass" curves shown in Figures 3.5 through 3.8 are an experimental description of Equation 3.5 where I represents the magnitude of I_z at any point along that line.

The quenched curves for all of the materials tested closely resemble that of the glass samples, which suggest that, all of these materials are capable of being quenched to the amorphous state. Note also that for any given polymer that the slope increases as the cooling rate is decreased and that the y-intercept changes in sign from a positive to a negative value with decreasing cooling rate. Also note that the universal constants shift from negative to positive with increasing copolymer content. This is shown in Figure 3.9 where C_2 appears to exhibit a nearly perfect parabolic functionality with regard to the copolymer composition. Theoretically, this strong correlation is not understood but qualitatively shows that increasing copolymer content influences the value of C_2.
In this case, there appears to be a high level of uncertainty in the values for the four universal constants. Nevertheless, it is believed that because all of these values are centered around a value of $C_2 \approx 0$, and that a slight change in this value will not strongly

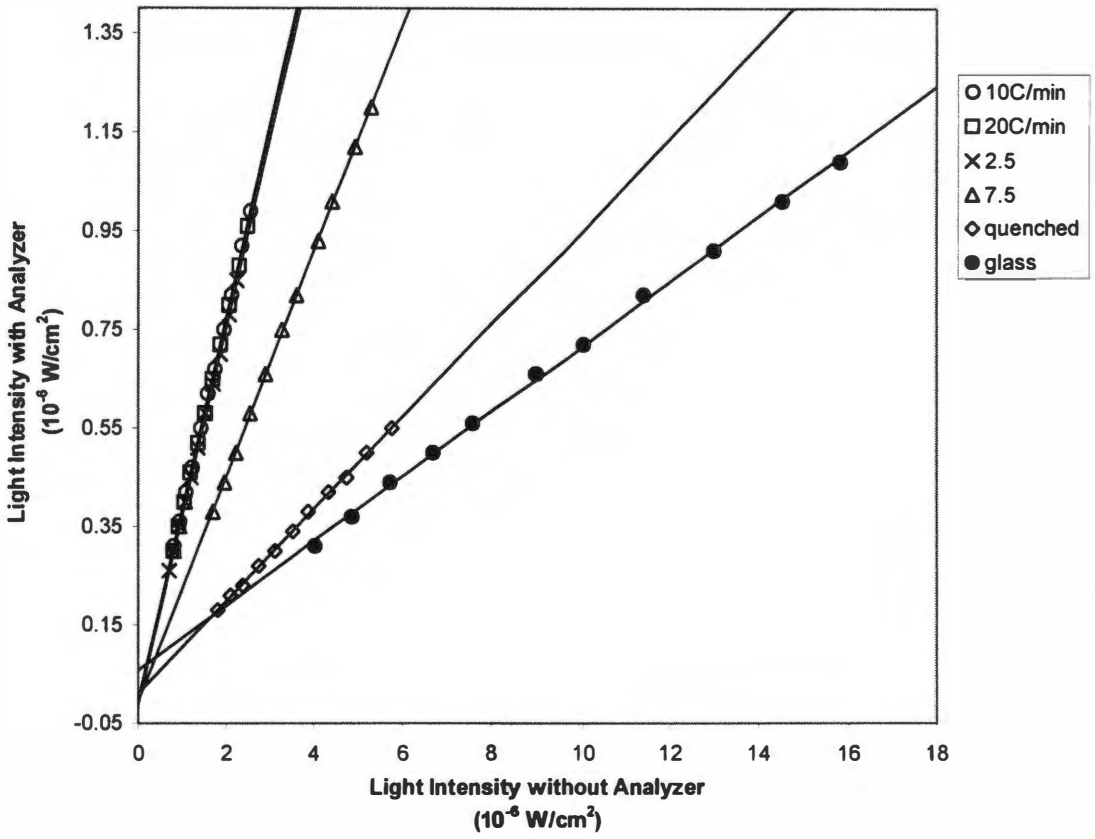

10°C/min:	y = 3.917E-01x - 1.095E-02	R^2 = 1.000
20°C/min:	y = 3.890E-01x - 8.257E-03	R^2 = 1.000
2.5:	y = 3.839E-01x - 1.319E-02	R^2 = 1.000
7.5:	y = 2.291E-01x - 6.999E-03	R^2 = 1.000
quenched:	y = 9.389E-02x + 1.025E-02	R^2 = 0.999
glass:	y = 6.585E-02x + 5.727E-02	R^2 = 0.999

Figure 3.5: Plot of the Light Intensity With an Analyzer, I, as a Function of the Light Intensity Without an Analyzer, I_0, for PET Homopolymer

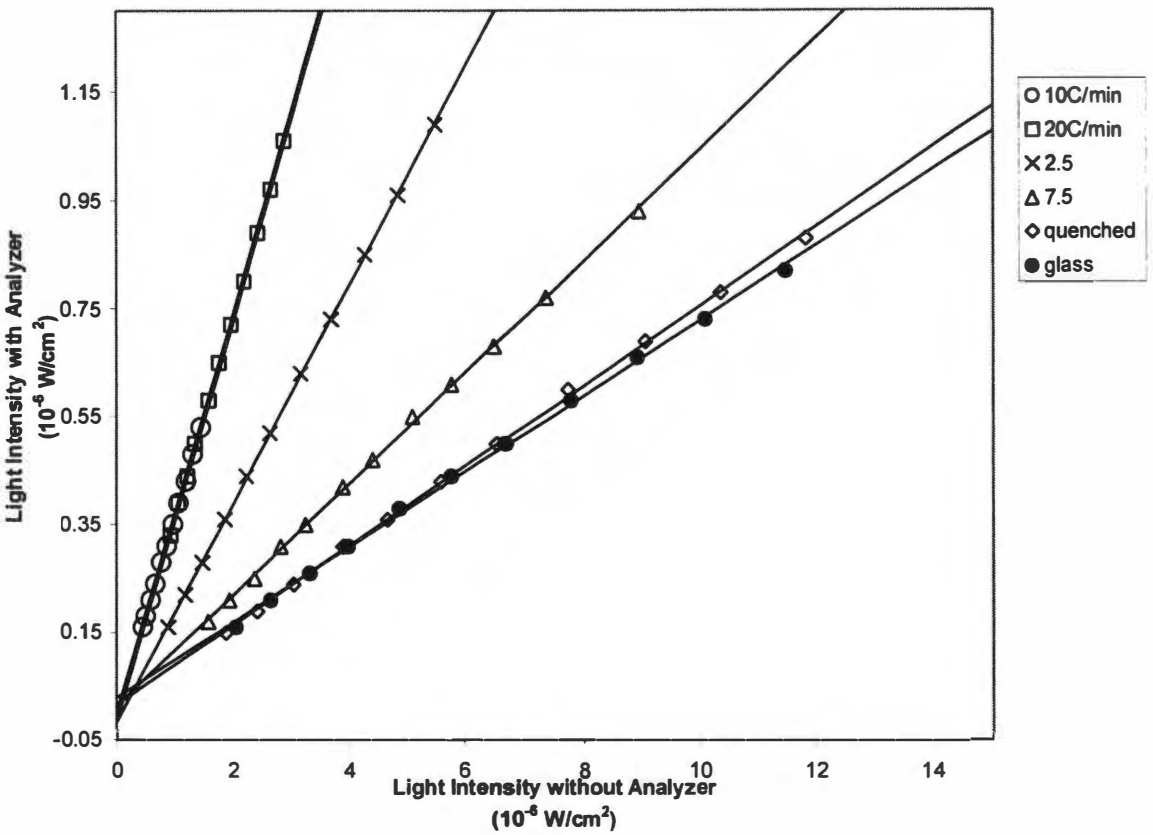

10°C/min:	y = 3.687E-01x - 9.847E-03	R^2 = 1.000
20°C/min:	y = 3.677E-01x - 6.947E-03	R^2 = 1.000
2.5:	y = 2.020E-01x - 1.760E-02	R^2 = 1.000
7.5:	y = 1.031E-01x + 1.274E-02	R^2 = 0.999
quenched:	y = 7.389E-02x + 1.555E-02	R^2 = 0.999
glass:	y = 6.996E-02x + 2.842E-02	R^2 = 0.999

Figure 3.6: Plot of the Light Intensity With an Analyzer, I, as a Function of the Light Intensity Without an Analyzer, I_0, for the 4% MPDiol Copolymer

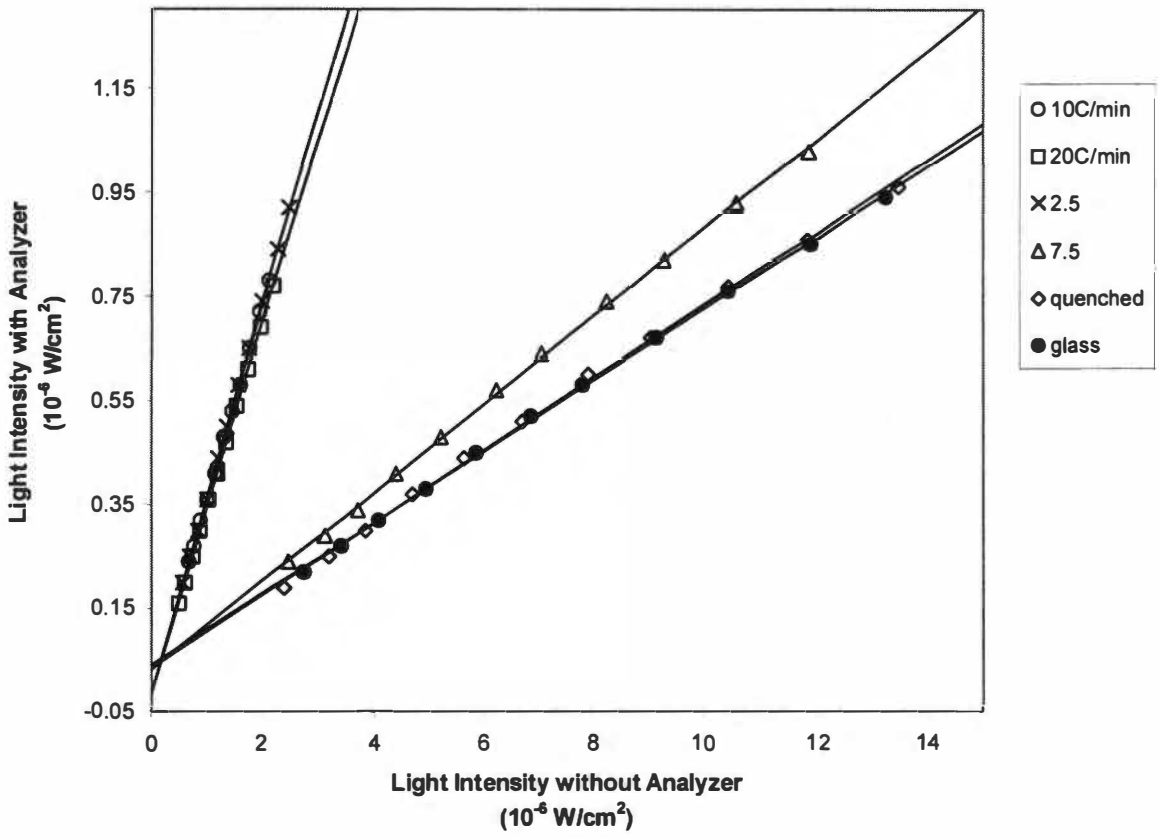

10°C/min:	y = 3.707E-01x - 1.398E-02	R^2 = 1.000
20°C/min:	y = 3.566E-01x - 1.588E-02	R^2 = 1.000
2.5:	y = 3.751E-01x - 1.473E-02	R^2 = 1.000
7.5:	y = 8.493E-02x + 3.343E-02	R^2 = 1.000
quenched:	y = 6.982E-02x + 3.615E-02	R^2 = 0.999
glass:	y = 6.854E-02x + 4.131E-02	R^2 = 0.999

Figure 3.7: Plot of the Light Intensity With an Analyzer, I, as a Function of the Light Intensity Without an Analyzer, I_0, for the 7% MPDiol Copolymer

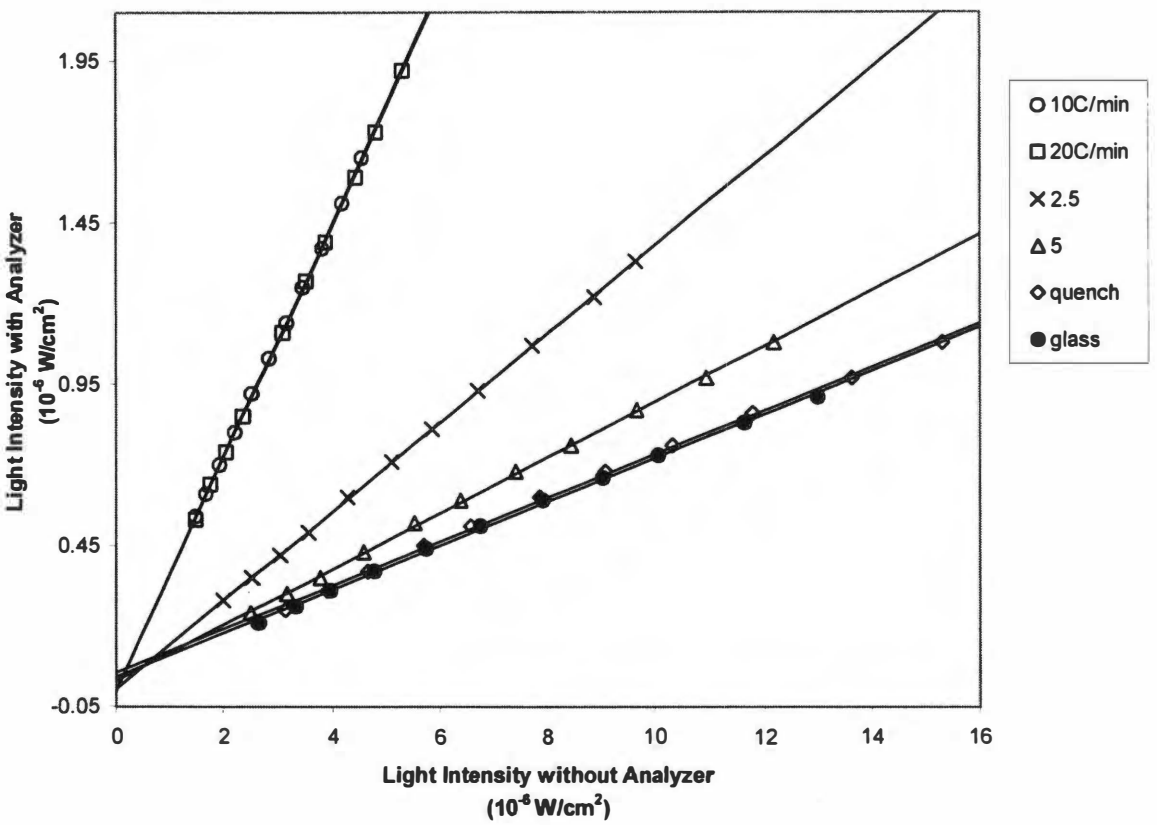

10°C/min:	y = 3.625E-01x - 1.885E-03	R^2 = 1.000
20°C/min:	y = 3.610E-01x - 3.125E-03	R^2 = 1.000
2.5:	y = 1.375E-01x + 4.861E-03	R^2 = 1.000
5:	y = 8.654E-02x + 3.067E-02	R^2 = 1.000
quenched:	y = 6.778E-02x + 5.537E-02	R^2 = 0.999
glass:	y = 6.792E-02x + 4.210E-02	R^2 = 0.999

Figure 3.8: Plot of the Light Intensity with an Analyzer, I, as a Function of the Light Intensity Without an Analyzer, I_0, for the 10% MPDiol Copolymer

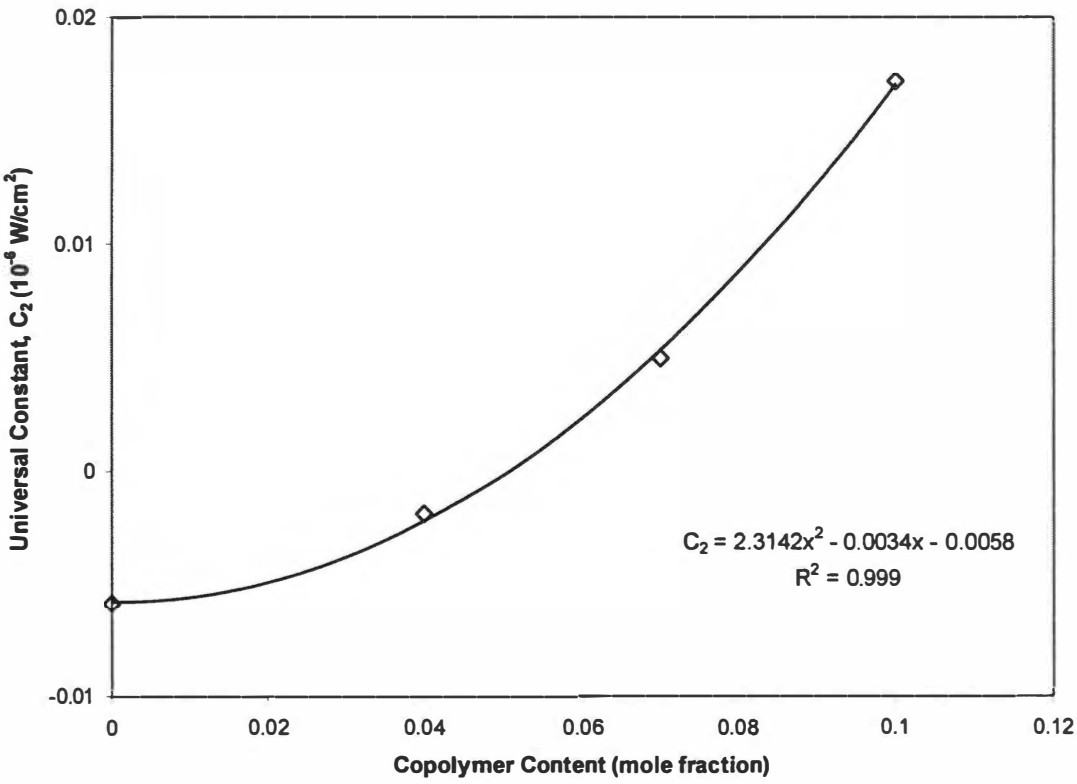

Figure 3.9: Plot of the Universal Constant, C_2, as a Function of Copolymer Content

influence the final results, it was decided that the values listed previously could be used to correct the experimental data over the range tested.

3.2.2.2.2.2. LDM System Calibration and Operating Procedure

Prior to sample testing a calibration technique was performed to ensure the light intensity was always set at a constant level and that the polarizer and analyzer were completely crossed. Prior to calibration the light source was turned on and allowed to equilibrate for 20 minutes. After light source equilibrium had been achieved, a cover slip that had been marked with a black pen was then placed on the microscope stage. Once the microscope had been focused on the black line, the cover slip was removed from the microscope stage. The eyepieces were then removed from the microscope and replaced with the light intensity sensors. The connector of the light intensity sensor without an analyzer was then plugged into an International Light IL 700 Research Radiometer. For this particular set-up, the sensitivity of the radiometer was set to $1.367*10^{-1}$. The incident light was then diverted away from the light sensors and the radiometer was adjusted to obtain a "dark reading" of $-0.1*10^{-9}$ W/cm^2/nm. The light source was then diverted back to the light sensor and the light source voltage was adjusted to obtain a reading of $2.5*10^{-5}$ W/cm^2/nm.

Next, the light sensor with the analyzer was connected to the radiometer and the sensitivity changed to $1.415*10^{-1}$. The light sensor binocular itself was then slowly rotated until a minimum intensity reading was obtained on the radiometer. This sensor was then secured in place ensuring that it could not rotate out of position during testing. The polarizer on the optical microscope was then rotated until a minimum value was

obtained, which corresponded to a fully crossed polarizer and analyzer. Following this procedure ensures that the measurements are consistent each time they are made. Note that during this experiment, recalibration must be performed every time the system is shut down (i.e. the light source was turned off).

In this experiment, all samples were heated to above 290°C and rapidly cooled to below 100°C using the modified light depolarizing technique described above. Several samples of each copolymer were prepared and tested using this technique at a variety of cooling rates. Also, the approximate cooling rate required to quench each copolymer sample was estimated in this experiment by visual inspection of quenched samples.

CHAPTER 4: RESULTS AND DISCUSSION

4.1. Characterization of Copolymers

4.1.1. Thermal Characterization

4.1.1.1. Examination of Experimental Data

The thermal behavior of copolyesters of Poly(ethylene terephthalate) (PET) containing 0, 4, 7, and 10 mol% 2-methyl-1,3-propanediol (MPDiol) were investigated using Differential Scanning Calorimetery (DSC). In particular, the glass transition temperature, cold crystallization temperature, and melting peak temperature of partially quenched samples, prepared according to that described in section 3.2.2.1.2., was determined.

Figure 4.1 shows a typical DSC curve observed during this study, in this case for PET homopolymer. As mentioned in the previous chapter, this experiment was conducted using a Mettler-Toledo DSC820 DSC. The thermodynamic sign convention utilized by this DSC is that all endothermic transition peaks point in a downward direction, while all exothermic transition peaks point in an upward direction. Therefore in this figure the cold crystallization peaks point upward while melting peaks point downward.

4.1.1.2. Glass Transition Temperature

As would be expected, an increase in the more flexible MPDiol units results in a decrease in the glass transition temperature (T_g) (see Table 4.1). Note that all data is

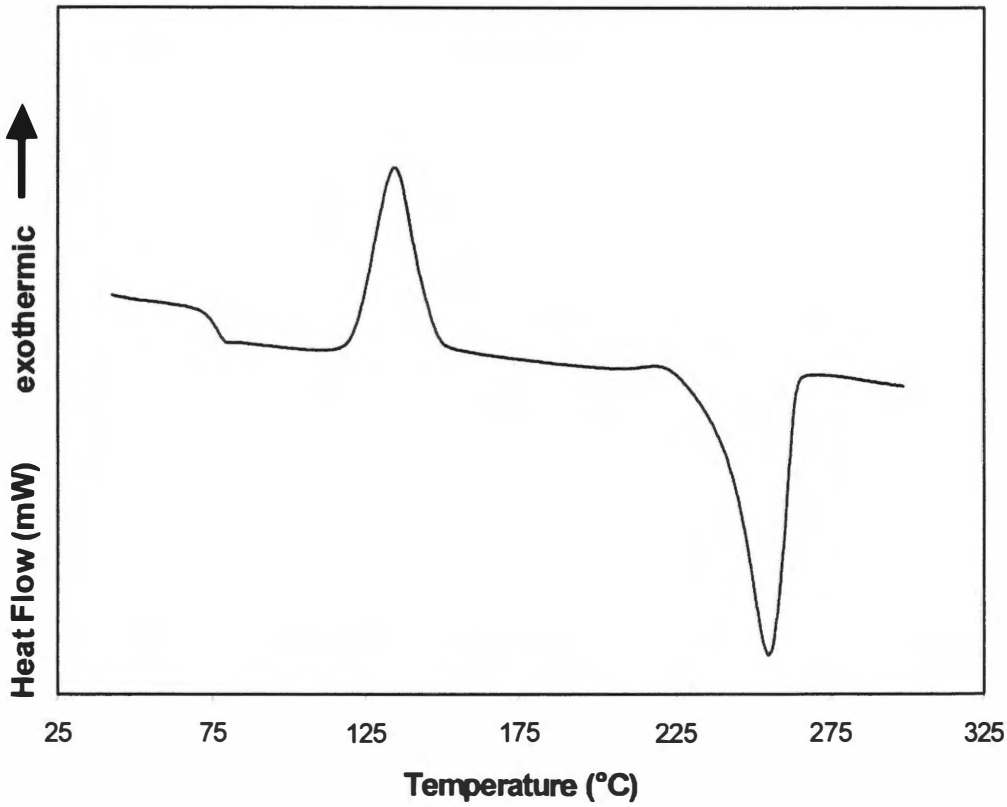

Figure 4.1: Typical DSC Curve for PET Homopolymer

Table 4.1: Summary of Glass Transition Data for PET Copolymers

Sample I.D.	Mol% Comonomer	Onset Temp. (°C)	T_g (°C)
PET	0	70.3±2.1	73.6±1.9
PET-4	4	67.2±1.6	70.5±1.4
PET-7	7	66.6±1.1	69.8±0.6
PET-10	10	66.8±0.5	69.2±0.4

NOTE: Limits based on +/-1 standard deviation

reported as the mean of three tested samples plus or minus one standard deviation unless otherwise specified. For PET homopolymer, T_g was determined to be 73.6±1.9°C, which is in good agreement with that reported by others (Kiyotsukuri et al 1994, Ulrich 1993). In comparison, the glass transition temperature of the 10mol% MPDiol samples was found to be 69.2±0.4°C, suggesting that the inclusion of the comonomer units increase the flexibility of the polymer. Although the average T_g decreases with increasing comonomer content, it is important to notice that the standard deviation suggests that there is not a significant difference between the glass transition temperatures of the three copolymers tested.

The reduction in the glass transition temperature can be attributed to the following effects: 1.) an increase in the length of the flexible group in the main polymer chain (i.e. the presence of an additional methyl group promotes main chain bond rotation); and 2.) an increase in free volume associated with the vinyl methyl group (i.e. an increase in the number of flexible side groups) (Ward and Hadley 1993). Bond rotation is more easily achieved with increasing number of flexible groups in the main chain of the polymer and therefore less thermal energy is required for molecular motion and rearrangement. Secondly, the vinyl methyl group acts like an additional chain end and therefore more

free volume is achieved at a given temperature. This allows for molecular rearrangements to occur more readily at a given temperature.

Suh (2001) found a very similar trend in his analysis of fibers made of PET copolymers containing MPDiol. As with this experiment, it was found that there was a decrease in Tg with increased MPDiol. In his experiments, the glass transition temperatures of PET MPDiol copolyester fibers spun at low speeds (≈1400m/min) were determined using DSC. His results were quite comparable to those found in this experiment.

Kiyotsukuri et al (1994) also witnessed similar results when examining the thermal properties of copolymers of PET and 2,2-dialkyl-1,3-propanediols. As with this study, they found only slight changes in the glass transition temperatures for copolymers containing up to 30mol% comonomer. Likewise, other investigators have found similiar decreases in T_g with increasing content of flexible comonomers (Varma et al 1986, Bouma et al 2001).

4.1.1.3. Cold Crystallization

The cold crystallization behavior of the copolymers reveals that as the concentration of MPDiol is increased there is a slight increase in the cold crystallization temperature (see Table 4.2). This suggests that more thermal energy (and or time) is required for the molecular rearrangement that is required for nucleation and crystal growth. This has been reported for other PET copolymers as well (Kiyotsukuri et al 1994, Park and Lee 1995).

Table 4.2: Summary of Cold Crystallization Data of PET copolymers

Sample I.D.	Onset Temp. (°C)	T_{cc} (°C)	ΔH_{cc} (J/g)
PET	118.6±2.4	129.8±4.2	40.8±0.2
PET-4	120.8±3.3	131.1±3.1	41.8±0.8
PET-7	120.5±0.5	130.6±0.4	40.1±0.5
PET-10	124.3±0.3	135.0±0.5	39.6±0.5

NOTE: Limits based on +/-1 standard deviation

What is interesting about these peaks also is the fact that, although they occur at different temperatures, there is no significant difference in the heat released during the exothermic crystallization process for all of the samples tested.

4.1.1.4. Melting Behavior

The melting behavior for each of the copolymers tested is listed in Table 4.3. Here it is quite evident that as comonomer content is increased the melt temperature decreases. This can be explained by the notion of comonomer exclusion. As the percentage of comonomer increases, the likelihood of forming lamellae with the same thickness as PET homopolymer decreases. Therefore, as crystal thickness decreases, the surface energy of the crystal becomes more influential, resulting in a depression of the melt temperature. Again, this has been witnessed for many other PET copolymers (Park and Lee 1995, Karayannidis 2000, Sakaguchi et al 1995, Sakaguchi 1997), and in particular for those containing short diols (Kiyotsukuri et al 1994, Ward and Hadley 1993, Varma et al 1986).

As suggested by a similar study conducted by Park and Lee (1995) on the thermal properties of Copoly(Ethylene Terephthalate/Imide)s, Flory's equation (Equation 2.41)

Table 4.3: Summary of Melting Data for PET copolymers

Sample I.D.	Onset Temp. (°C)	T_m (°C)	ΔH_m (J/g)	X_c (%)
PET	238.5±0.6	253.6±0.6	66.1±1.4	18.0±1.1
PET-4	225.8±1.3	243.3±1.1	64.3±4.0	16.1±2.4
PET-7	218.1±0.1	237.4±0.1	56.8±0.5	11.9±0.3
PET-10	212.5±1.6	231.0±0.4	50.8±1.0	8.0±0.3

NOTE: Limits based on +/-1 standard deviation

was used to examine the melting behavior of these copolyesters. According to equation 2.41, a plot of Tm^{-1} as a function of $-\ln(1-x_B)$ should yield a straight line with y-intercept equal to the reciprocal of the equilibrium melting temperature for PET homopolymer. Note that because this equation is applied to the experimentally determined melting temperatures (as opposed to equilibrium melting temperatures) the y-intercept in this particular application should yield an approximated value for the experimentally observed melting temperature of PET homopolymer. This plot was found to show good linearity with an R^2 value of approximately unity (see Figure 4.2). The intercept in Figure 4.2 yielded a value for Tm^0 of 251.5°C, close to the experimental value of 253.6°C found for PET homopolymer. The fact that this data appears to fit Flory's equation so well seems to support the claim that MPDiol comonomer units are excluded from the parent PET homopolymer crystal.

It should be noted that an effort was maintained to prepare all samples in the exact same manner. It is well established that the crystallinity of a sample can be roughly determined by DSC as the difference between the normalized area under the cold crystallization and the melting endotherm divided by the heat of fusion of a perfect

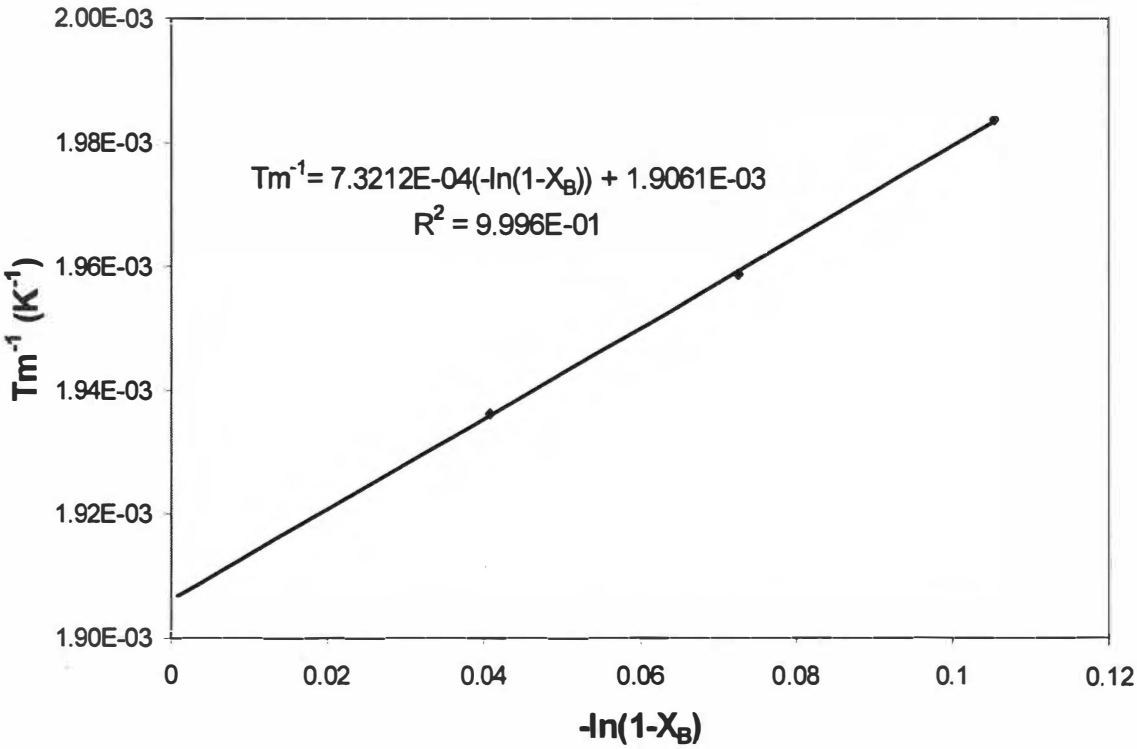

Figure 4.2: Plot of Flory's Equation for PET-MPDiol Copolymers

crystal of that sample (Equation 2.3). The exact value of the heat of fusion for a perfect PET homopolymer crystal is still somewhat in question, but is reported by Wunderlich (1980) as being 140±20 J/g. In this analysis the average value of 140 J/g was used to determine the crystallinity of the quenched samples. The initial crystallinity of the samples suggests that the crystallization kinetics during the non-isothermal quenching in liquid Nitrogen is also affected by increasing comonomer content. PET homopolymer samples showed the highest percent crystallinity (18.0 ±1.1%), while the 10% MPDiol samples displayed the lowest (8.0 ±0.3%). The data suggests that the incorporation of MPDiol, at least at concentrations greater than 7mol%, has an adverse effect on the crystallization kinetics under the high cooling rates associated with quenching in liquid nitrogen.

Suh (2001) found very similar results. In his experiments, it was shown that resins containing 10mol% MPDiol or less exhibited appreciable crystallization in the spinline, although the presence of MPDiol reduced the crystallinity compared to filaments prepared from PET homopolymer. At the same take-up velocity it was shown that increasing MPDiol content resulted in a decrease in crystallinity, birefringence, and tenacity.

As was illustrated in Figure 2.6, the region where crystallization may occur is defined, theoretically by the glass transition at the lower limit and the melting temperature as the upper limit (although it has already been explained that crystallization at the melting temperature is not possible). Thus because the glass transition temperature decreases only slightly with increasing MPDiol content, but the melting temperature decreases significantly, the region whereby crystallization is possible decreases with

increasing comonomer content. This in itself is a significant result and suggests that the incorporation of MPDiol impedes the crystallizability of these materials.

It should be noted that an additional method of sample preparation was attempted to examine the thermal characteristics of these copolymers. In this experiment, dried, sliced pellets were placed between Teflon sheets containing a 0.003 in. spacer and sandwiched between two 0.018 in. metal plates, which were in turn placed between two 0.260 in. preheated metal plates. The samples were then placed in the Wabash compression-molding machine with platen temperatures set at 550°F and allowed to "soak" with no applied pressure for two minutes. The samples were then melt pressed for 1 minute at 5 tons/in^2. The pressure was then removed and the samples were allowed to remain in the press for an additional minute to allow for the partial removal of residual stresses imposed during melt pressing. The two thinner metal sheets, containing the molten sample, were then quickly transferred to a bath of ice cold water and quenched, ensuring that the samples remained in the water bath for 1 minute. Samples were then immediately transferred to a dessicator, which was then placed under 23 in. Hg vacuum for more than 48 hours. DSC samples were then trimmed from the quenched films, placed in the DSC and tested using the same temperature program as described earlier. Unfortunately, samples prepared in this manner showed a rapid change in the DSC baseline upon melting as illustrated in Figure 4.3 for a 4% MPDiol sample.

It is unclear as to the cause of this change in baseline, but it is speculated that these samples absorbed a sufficient amount of water during melt quenching that was not able to be removed with the current vacuum system. As a result the rapid change in

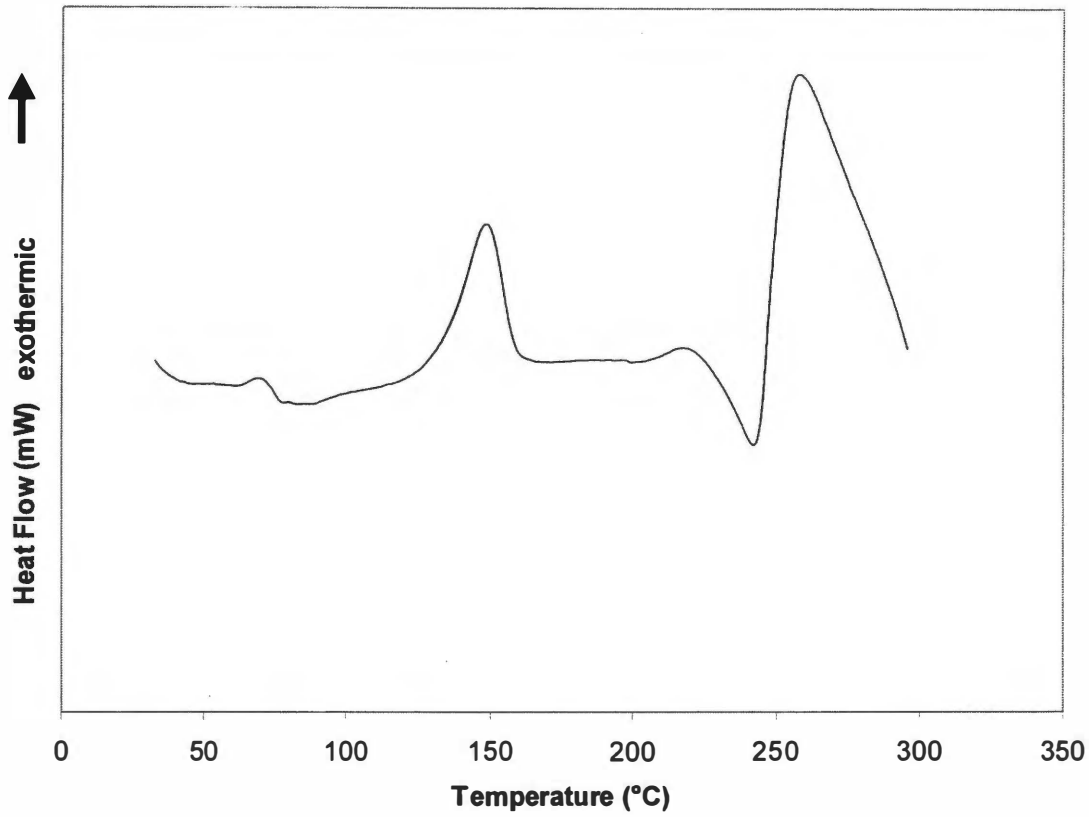

Figure 4.3: DSC Curve for PET-4 Sample Made Using Alternative Sample Preparation Technique Illustrating Severe Baseline Change Upon Melting

baseline is most likely due to thermal degradation. Since water absorption could also potentially affect the values obtained for T_g, submersion in liquid nitrogen was chosen as the preferred quenching method.

4.1.2. Determination of Contaminants – WAXD

Early optical microscopic observation revealed that the PET homopolymer appeared to show a significant amount of small particles contained within the polymer that remained, even upon melting of the polymer. As a result, Wide Angle X-ray Diffraction (WAXD) was used to determine the unknown substance contained in the PET homopolymer sample.

A PET homopolymer WAXD sample was prepared by melt pressing several dried pellets in a Wabash compression-molding machine. The pellets were placed in a 2.44 x 2.44 x 0.13 in. spacer die, which was placed between two sheets of Teflon film, and then sandwiched between two preheated metal plates. The plates were placed on the platens of the Wabash compression-molding machine and allowed to remain at 290°C for 6 minutes to ensure complete melting of the pellets. The sample was then melt pressed at 10tons/in^2 for seven minutes. The plates were then immediately taken from the machine, placed on a wooden table, and allowed to cool to room temperature. Once the sample had cooled, it was then sanded flat until it had a smooth, blemish-free surface. The final thickness of the specimen measured approximately 0.09 in. after polishing.

In this experiment a powder pattern of PET homopolymer was produced in the range $10° \leq 2\theta \leq 90°$ using a Philips X-Pert MRD X-ray diffractometer with a step size of

0.03° and a dwell time of 3.00 sec. A PW3123/10 monochromator was used in this experiment, oriented at a specific Bragg angle so as to pass Cu-K_α radiation only.

Figure 4.4 shows the resulting powder pattern obtained for the PET homopolymer sample. A computer search phase identification algorithm was performed on the powder pattern to determine the phases present where it was determined that the PET homopolymer sample contained a detectable amount of titanium dioxide, $Ti0_2$ in the form of Anatase and possibly another polymorph, Brookite.

4.2. Isothermal Crystallization of PET Copolymers

4.2.1. Examination of Experimental Data

This experiment examined the isothermal crystallization kinetics of copolymers of Poly(ethylene terephthalate) (PET) containing the comonomer 2-methyl-1,3-propanediol substituted for a fraction of the ethylene glycol normally present in PET. The objective was to determine the effect that increasing copolymer content has on the overall isothermal crystallization kinetics. A Perkin Elmer DSC7 differential scanning calorimeter was used in this experiment, with the resulting data analyzed using the Avrami equation. The activation energy of crystallization was also determined from the DSC data to examine the "ease" with which crystals form in each sample.

A typical DSC scan is shown in Figure 4.5, here for PET homopolymer isothermally crystallized at 210°C. Note that the Perkin Elmer DSC7 utilizes the opposite thermodynamic sign convention as the Mettler-Toledo DSC820 with regard to the direction of heat-flow. As is marked in this figure a peak pointing in an upward

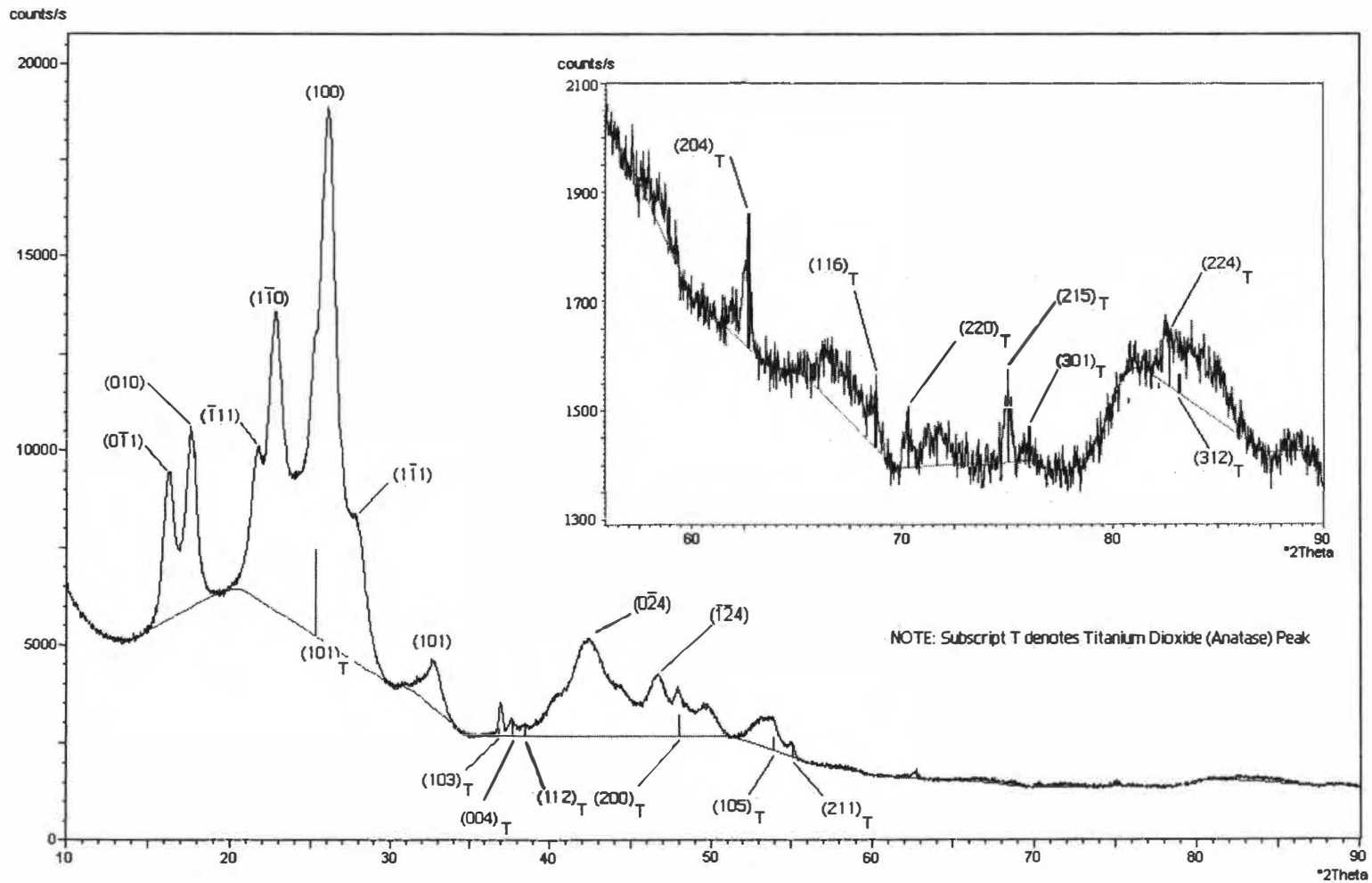

Figure 4.4: WAXD Powder Pattern of PET Homopolymer Sample Containing $Ti0_2$. Black Tick Marks Show Location of TiO_2 Peaks

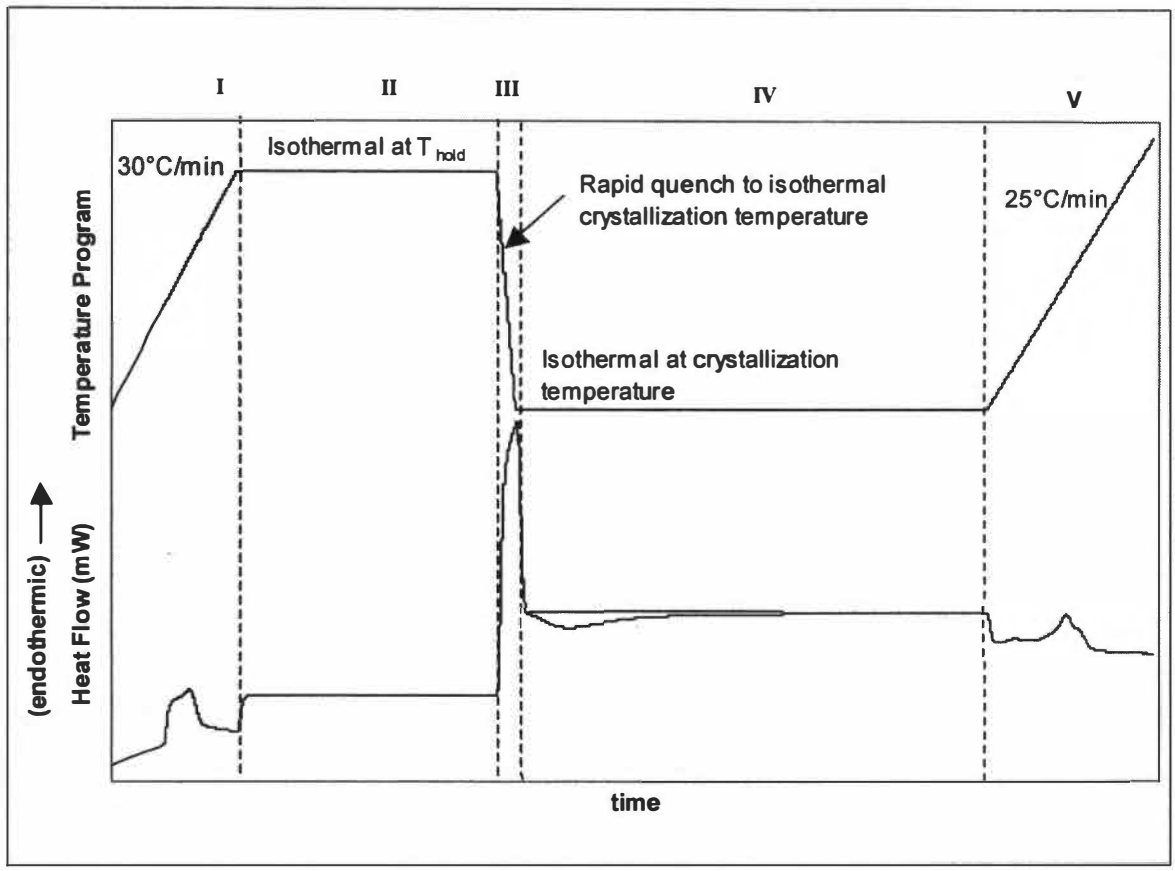

Figure 4.5: Representative DSC Scan Showing Temperature Program and Corresponding DSC Heat Flow Curve (Sample: PET Homopolymer Crystallized at 210°C)

direction signifies melting (i.e. endothermic transition) while a peak that points downward represents crystallization (i.e. exothermic transition).

Note from this figure that the polymer was first heated to above its melt temperature (section I), where it was allowed to remain at that temperature (T_{hold}) for 5 minutes (section II). As described earlier, the purpose of this step was to "erase" the previous thermal and mechanical histories imparted to the polymer during sample preparation. At the completion of this isotherm the DSC was then cooled rapidly (section III) to the isothermal crystallization temperature (section IV). The temperature was held at the isothermal crystallization temperature until a return to a horizontal baseline was achieved, where the temperature was then increased to examine the melting behavior (section V).

Figure 4.6 shows a zoomed in view of sections III and IV and illustrates how the DSC responds during the cooling from the hold temperature to the isothermal crystallization temperature. For convenience, the temperature-time program curve is also shown in this figure. Note that a large transient spike occurs in the heat-flow versus time curve during quenching. This transient region suggests that the DSC has not yet reached thermal equilibrium and is attempting to compensate for the temperature difference between the sample and reference. Thus in this region the DSC is not capable of accurately measuring any real phenomena until the onset of a stable baseline occurs prior to crystallization. This is discussed by Urbanovici et al (1997) where it is suggested that some nonisothermal crystallization may be occurring while the DSC is attempting to equilibrate at the isothermal crystallization temperature. For this reason, no curves were used in this analysis that did not show the presence of an emerging baseline prior to

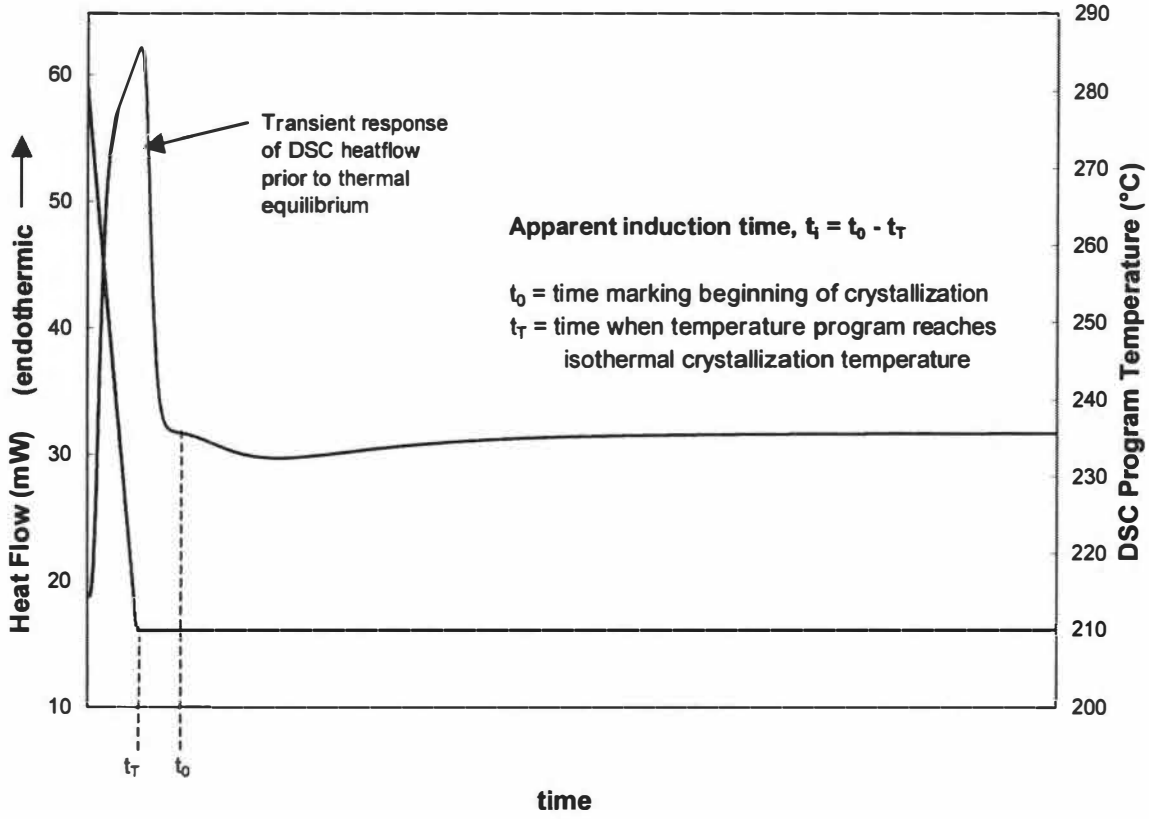

Figure 4.6: Zoomed In View of Heat Flow and Program Temperature Curves in Figure 4.5 Illustrating Technique to Determine the Induction Time

crystallization. Nevertheless, it is still quite possible, particularly at the lower isothermal crystallization temperatures, that crystallization had begun prior to reaching thermal equilibrium leading to one source of error in these experimental results. However, review of the current literature suggests that this method for examining the isothermal crystallization kinetics of polymers is typical and therefore it was used in this experiment.

Figure 4.6 illustrates how the induction time, t_i, was determined in this experiment. In practice, the time, t, is determined as the time to reach a particular reduced crystallinity, $\theta(t)$, excluding the time taken to begin the crystallization process, t_0. In this experiment, the induction time was taken as the time of the start of crystallization minus the time where the DSC program first reached the isothermal crystallization temperature, t_T, as is shown in Figure 4.6. Note that while the sample may not actually be at the isothermal crystallization temperature predicted by the program temperature, this provides for a consistent method for evaluating the induction time. Thus the induction time reported here is not actually the true induction time but rather an apparent induction time and will not necessarily be the same as that measured by some other technique. However, it is believed that the true induction time of crystallization should follow the same general trend of that reported here.

Figure 4.6 is representative of polymers crystallized at lower temperatures (i.e. higher undercoolings). Notice in Figures 4.5 and 4.6 that it appears that the DSC baseline stabilizes prior to the onset of crystallization suggesting the achievement of thermal equilibrium. However, under further magnification, Figures 4.7 and 4.8 show that the baseline is not completely flat but rather there is a slope to this curve implying that the DSC still might be attempting to compensate for a slight difference in temperature

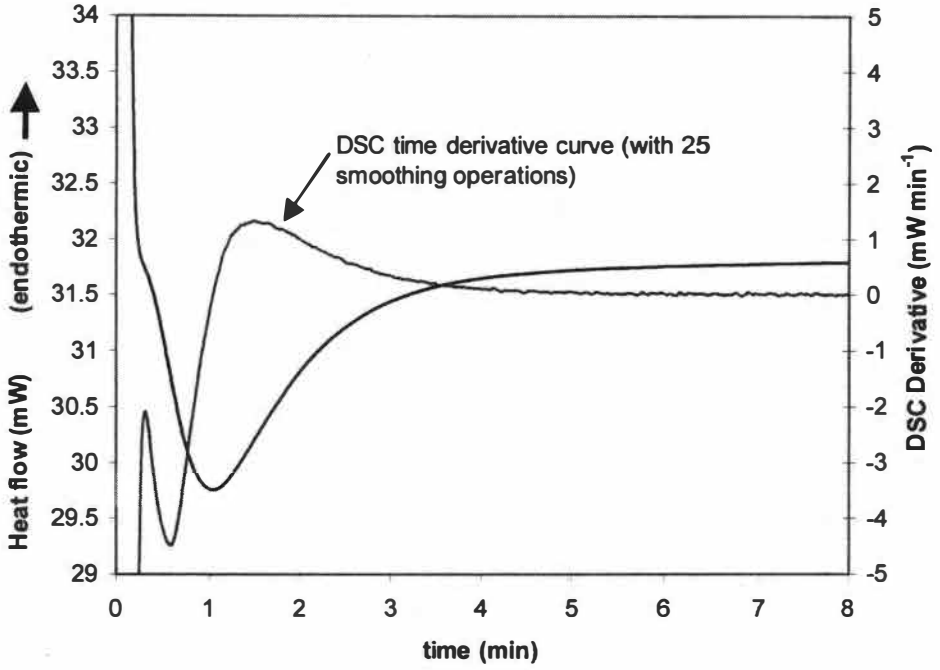

Figure 4.7: Figure Illustrating DSC Derivative Curve

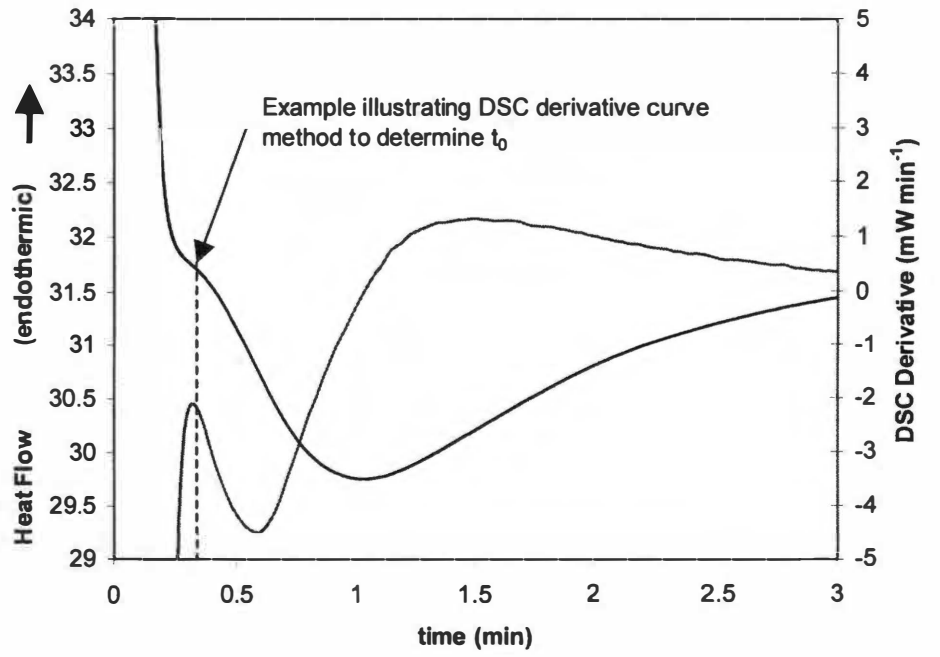

Figure 4.8: Zoomed In View of Figure 4.7 Illustrating Technique to Find t_0

between the reference and sample.

What is important to note from Figure 4.7 is that it is difficult to accurately predict exactly where crystallization begins and where it ends. To aid in this effort, the derivative of the DSC curve (i.e. d^2H/dt^2) was approximated and utilized in this experiment as is also shown in Figure 4.7 (note that all derivate curves were subjected to 25 smoothing operations to eliminate excessive noise). Figure 4.8 shows a zoomed in view of Figure 4.7 illustrating how the DSC derivative curve can be used to better determine the time, t_0. As is shown, there appears to be a sharp peak around 0.32 minutes, suggesting the existence of an otherwise undetectable inflection point in the heat-flow curve. The time when this inflection point occurs is taken to be t_0 since it appears to correspond to a thermodynamic process not associated with the transient portion of the DSC curve, and because it appears to be coincident with the approximated position of the onset of crystallization. Thus the rapid change in the DSC derivative curve allows for a less subjective interpretation of the results and ensures that experimenter bias is kept to a minimum.

Figure 4.9 also illustrates how the DSC derivative can be used to determine the time when primary crystallization has completed, t_f. While the precise value of t_f is, in most cases, not as critical as t_0, it is still important to approximate this value consistently. As is shown, t_f can be approximated as the time when the DSC derivative curve approaches zero. While this is, in itself, a somewhat subjective operation, it still helps to ensure that the majority of the primary crystallization process has been included in the analysis. As a result the derivate of the DSC curve was utilized to allow for a more

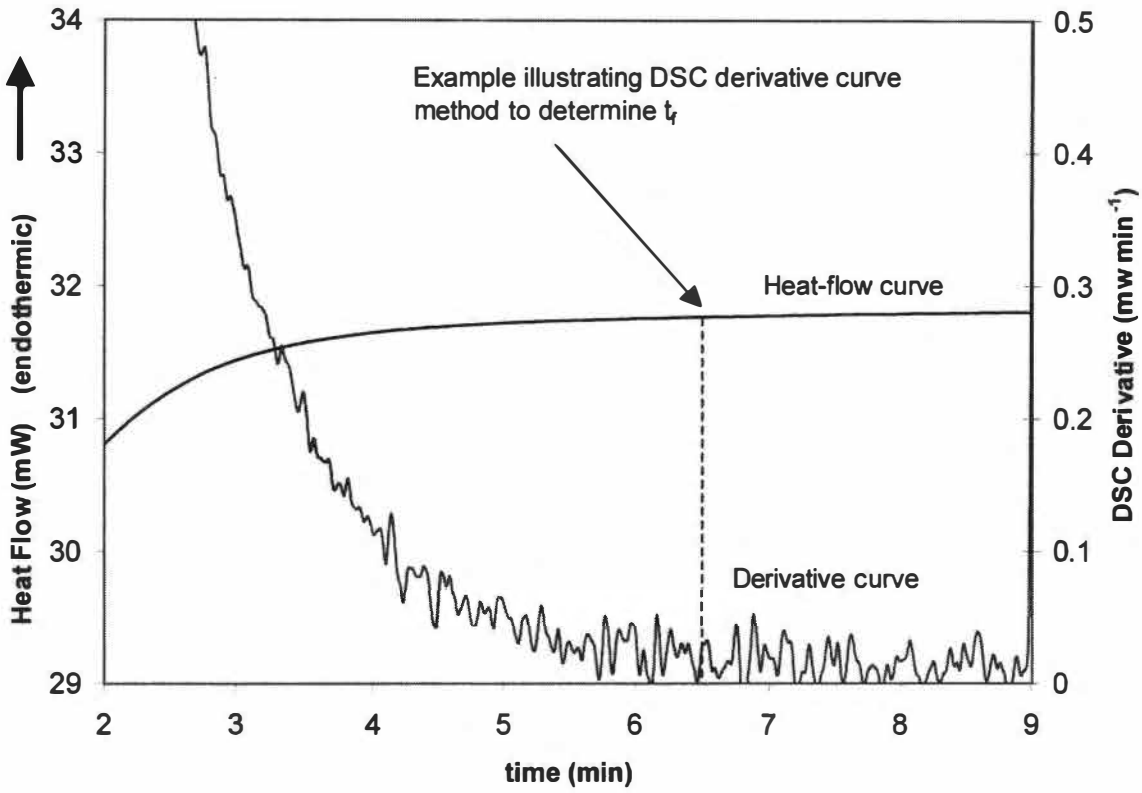

Figure 4.9: Zoomed In View of Figure 4.8 Illustrating Technique to Find t_f

consistent method for determining the beginning and ending crystallization times.

Although not easily seen at this scale, it should be noted that there was a slight increase in the slope of the DSC baseline after primary crystallization had completed. It is believed that this slope is likely due to secondary crystallization.

As was mentioned, Figures 4.5-4.9 are representative of those curves taken at high undercoolings. Figure 4.10 shows a typical DSC curve encountered at higher isothermal crystallization temperatures (i.e. lower undercoolings). Notice in this figure that the DSC baseline completely stabilizes prior to the onset of crystallization, thus ensuring thermal equilibrium is achieved prior to the beginning of crystallization.

Figure 4.11 illustrates a third type of curve encountered in this experiment. With this curve there is a second transient response of the DSC after the initial endothermic transient response associated with quenching to the isothermal crystallization temperature. What is important to note about this curve is that, again, there appears to be a stabilization of the heat-flow baseline prior to the onset of crystallization. Also note that the beginning and ending points of crystallization appear to share, more or less, the same ordinate (heat-flow) further suggesting that the DSC was in control prior to the onset of crystallization.

The crystallization kinetics in this analysis was followed by assuming that the weight fraction of a crystalline polymer is directly proportional to the amount of heat given off during the experiment. The weight fraction of crystalline material, $\theta(t)$, at a time t can then be expressed as (Vilanova et al 1985):

$$\theta(t) = \int_0^t (dH/dt)dt \Big/ \int_0^\infty (dH/dt)dt \qquad (4.1)$$

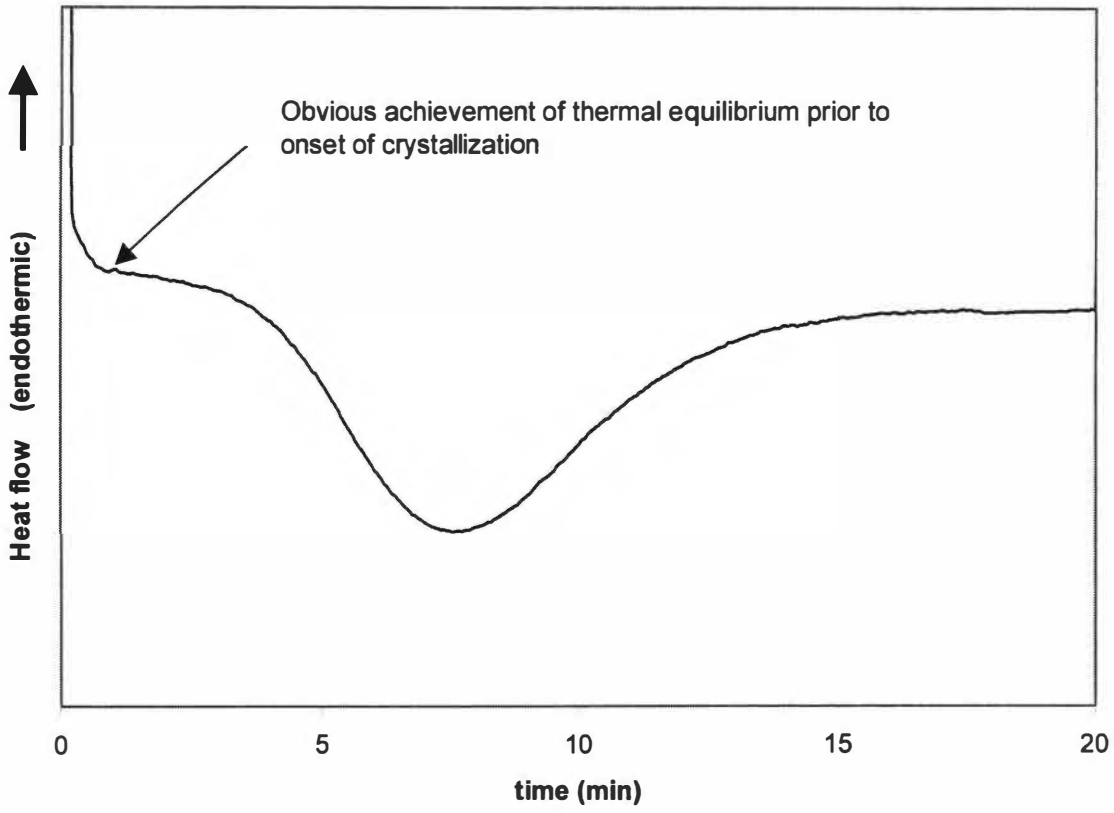

Figure 4.10: Typical DSC Curve Encountered at Low Undercoolings. The DSC Curve Shown Here For a 7mol% Copolyester Crystallized at 210°C

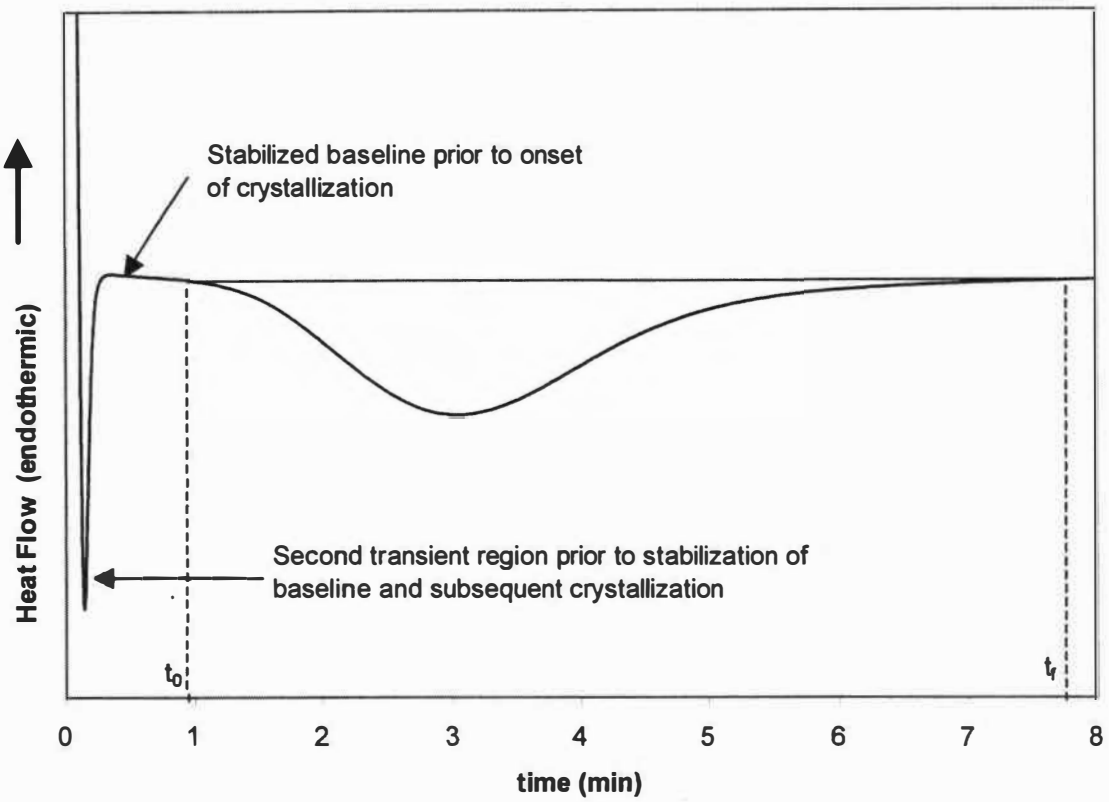

Figure 4.11: DSC Curve Showing Exothermic Transient Response Prior to Baseline Stabilization. The DSC Curve Shown here is for a 4mol% Copolyester Crystallized at 210°C

Experimentally, this fraction can be determined by DSC using the following relation:

$$\theta(t) = \frac{A_t}{A_\infty} \qquad (4.2)$$

where A_t is the area under the DSC curve at time t and A_∞ is the total area under the DSC curve. Therefore $\theta(t)$ can be viewed as a reduced or relative crystallinity, with values ranging between 0 and 1.

The bulk isothermal crystallization kinetics can be examined using an Avrami analysis by experimentally measuring the crystallization isotherm using DSC, determining the partial area under the DSC curve at different time intervals and plotting the data according to Equation 2.32. By this equation a plot of $\ln[-\ln(1-\theta(t))]$ as a function of $\ln(t-t_0)$ is predicted to yield a straight line with slope equal to n, and y-intercept equal to ln(k). It is important to note that the Avrami analysis was applied over the range $0.10 \leq \theta(t) \leq 0.80$.

The activation energy for the isothermal crystallization process can be determined by assuming that the Avrami crystallization rate constant can be described by an Arrhenius type equation:

$$k^{1/n} = k_0 \exp(-\Delta E / RT) \qquad (4.3)$$

where ΔE is the activation energy, R is the gas constant, and k_0 is a temperature-independent factor (Supaphol 2000). Equation 4.3 provides a theoretical basis for the determination of the crystallization activation energy. Taking logarithms of this equation leads to the following relation:

$$\left(\frac{1}{n}\right)\ln k = \ln(k_0) - (\Delta E / RT) \qquad (4.4)$$

Equation 4.4. suggests that a plot of (1/n)ln(k) as a function of 1/T should yield a straight line with slope = (-ΔE/R) and y-intercept = ln(k).

An alternative approach to estimate the activation energy of isothermal crystallization is to approximate the rate of crystallization (V_c) from the linear portion of the slope of θ(t) vs. t. The rate of crystallization can then be related to the activation energy of crystallization, ΔE, by the following Arrhenius type equation (Vilanova et al 1985):

$$V_c = Q\exp(-\Delta E / RT) \qquad (4.5)$$

Where Q is a constant, R is the gas constant, and T is the crystallization temperature. Taking the logarithm of Equation 4.5 results in the following equation:

$$\ln(V_c) = \ln Q - (\Delta E / RT) \qquad (4.6)$$

Equation 4.6 suggests that a plot of $\ln V_c$ vs. 1/T should yield a straight line with slope = (-ΔE/R) and y-intercept = lnQ, thus providing an alternate method to estimate the activation energy of crystallization for each copolymer.

This method for determining the activation energy is based strongly on a more phenomenological approach to describing the experimental data. However, both methods will be utilized in the analysis of these data and compared. It is important to note that, in this experiment, V_c was determined by finding the best-fit line over the range $0.10 \leq \theta(t) \leq 0.70$.

4.2.2. Avrami Analysis

Figures 4.12-4.15 show the conversion plots for the four materials tested. Figure 4.12 also illustrates how Vc (see equations 4.5 and 4.6) was estimated. These figures illustrate that increasing the isothermal crystallization temperature resulted in an increase in the crystallization half time. This is more clearly shown in Figure 4.16 where the half time of crystallization is plotted as a function of isothermal crystallization temperature. This plot shows that not only does the crystallization half time increase with increasing crystallization temperature, but also that the crystallization half time at a given temperature increases with increasing comonomer concentration.

Figure 4.17 is a plot of the apparent induction time as a function of isothermal crystallization temperature where it is shown that, as with the crystallization half times, the induction time increases with increasing crystallization temperature. Again, this plot also illustrates the effect of the comonomer on the induction time. For a given crystallization temperature, the induction time appears to increase with increasing comonomer concentration, thus signifying that at a given temperature not only do the comonomers appear to impede the crystallization process once it has started, but also that the formation of primary nuclei is inhibited by the presence of this comonomer.

These results are quantified by the use of an Avrami analysis. The Avrami plots for each copolymer are shown in Figures 4.18-4.21, which were used to determine the Avrami exponent, n, and the crystallization rate constant, k. All of the plots of $\ln[-\ln(1-\theta(t))]$ vs. $\ln(t-t_0)$ showed good linearity when performing a linear curve-fit. This was suggested not only by an R^2 value close to 1, but also when comparing the values of k and $k_{0.5}$ (evaluated using Equation 2.33).

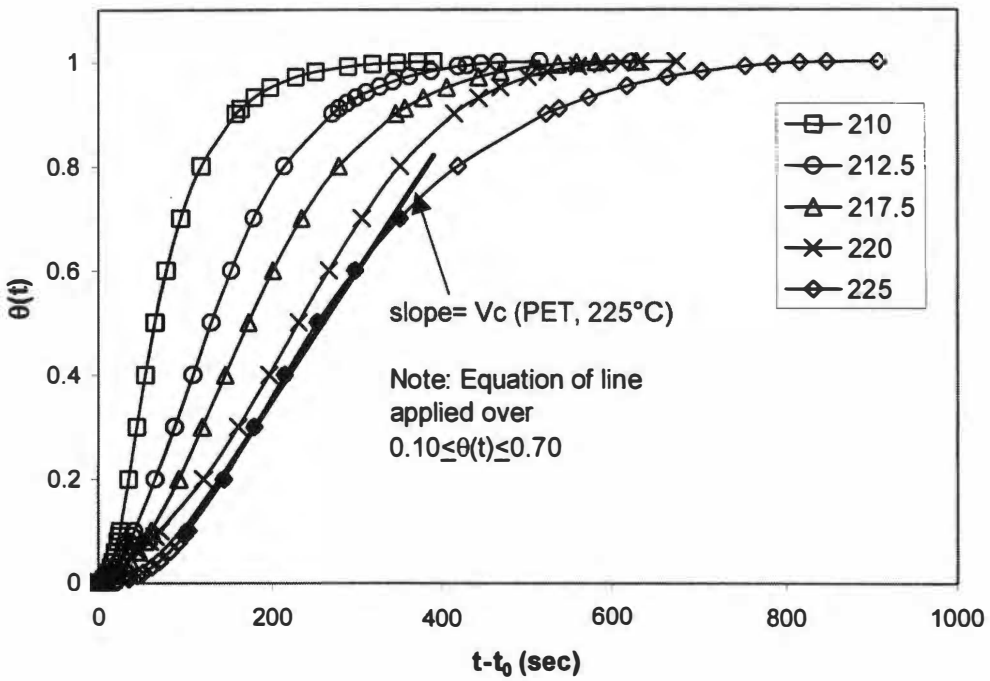

Figure 4.12: Conversion Plot for PET Homopolymer

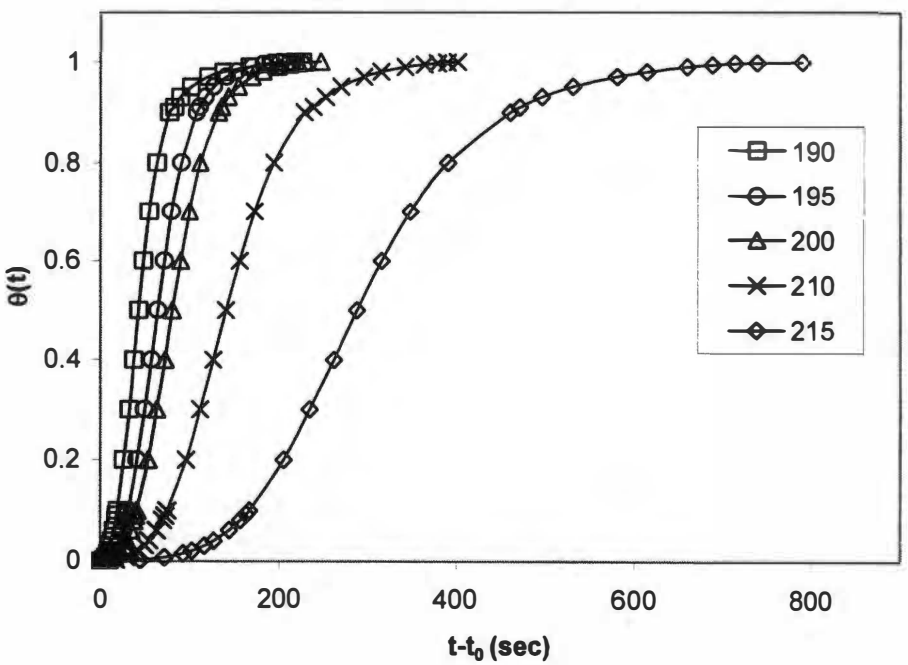

Figure 4.13: Conversion Plot for PET-4 Copolymer

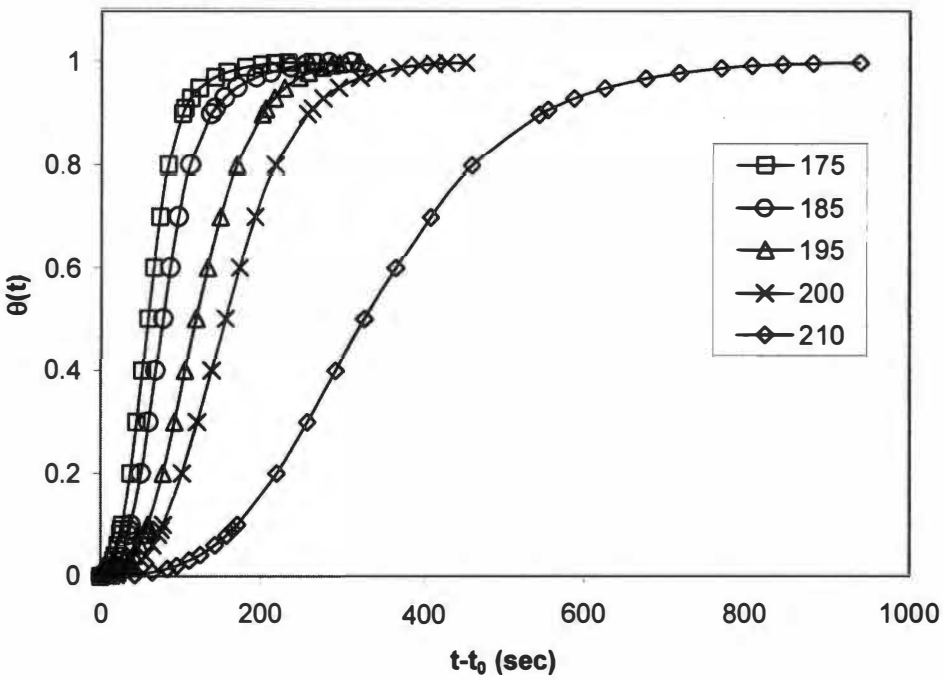

Figure 4.14: Conversion Plot for PET-7 Copolymer

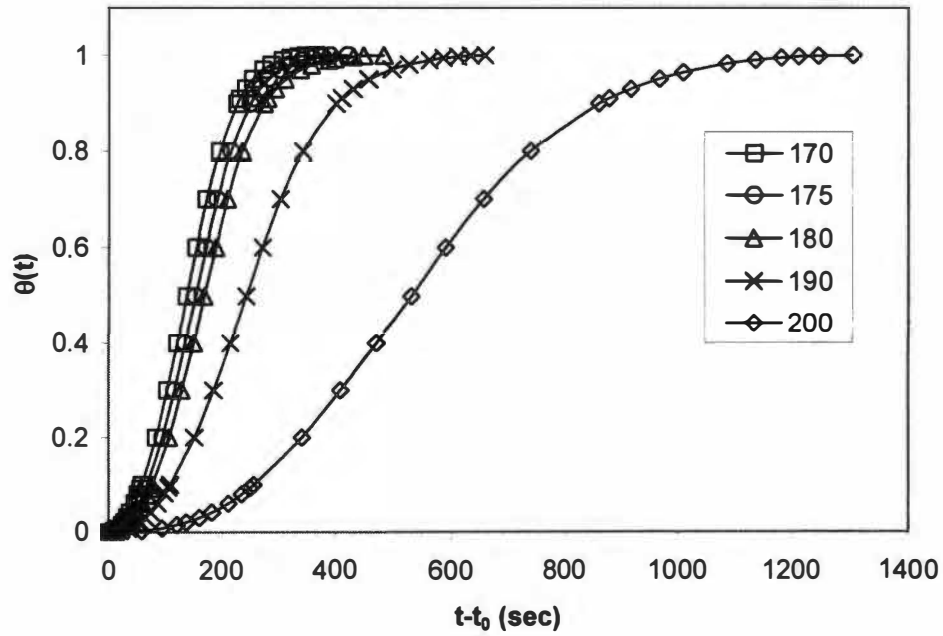

Figure 4.15: Conversion Plot for PET-10 Copolymer

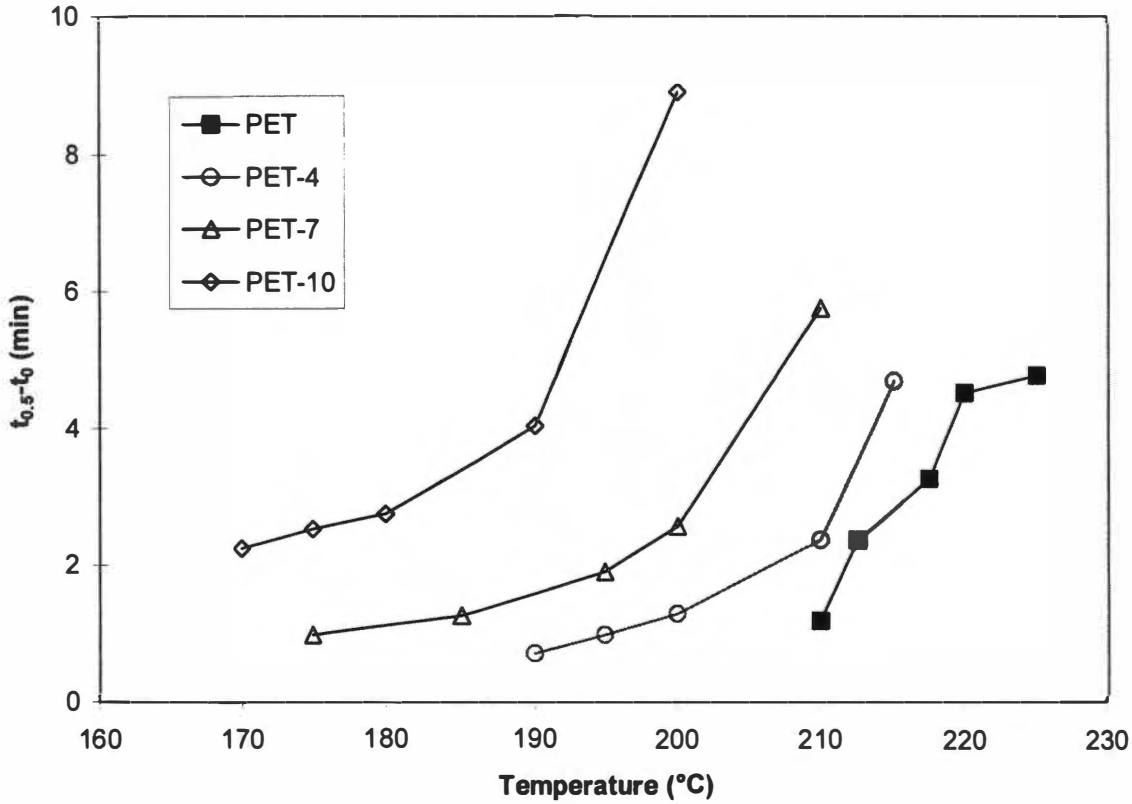

Figure 4.16: Plot of Crystallization Half Times of PET Copolymers as a Function of Isothermal Crystallization Temperature

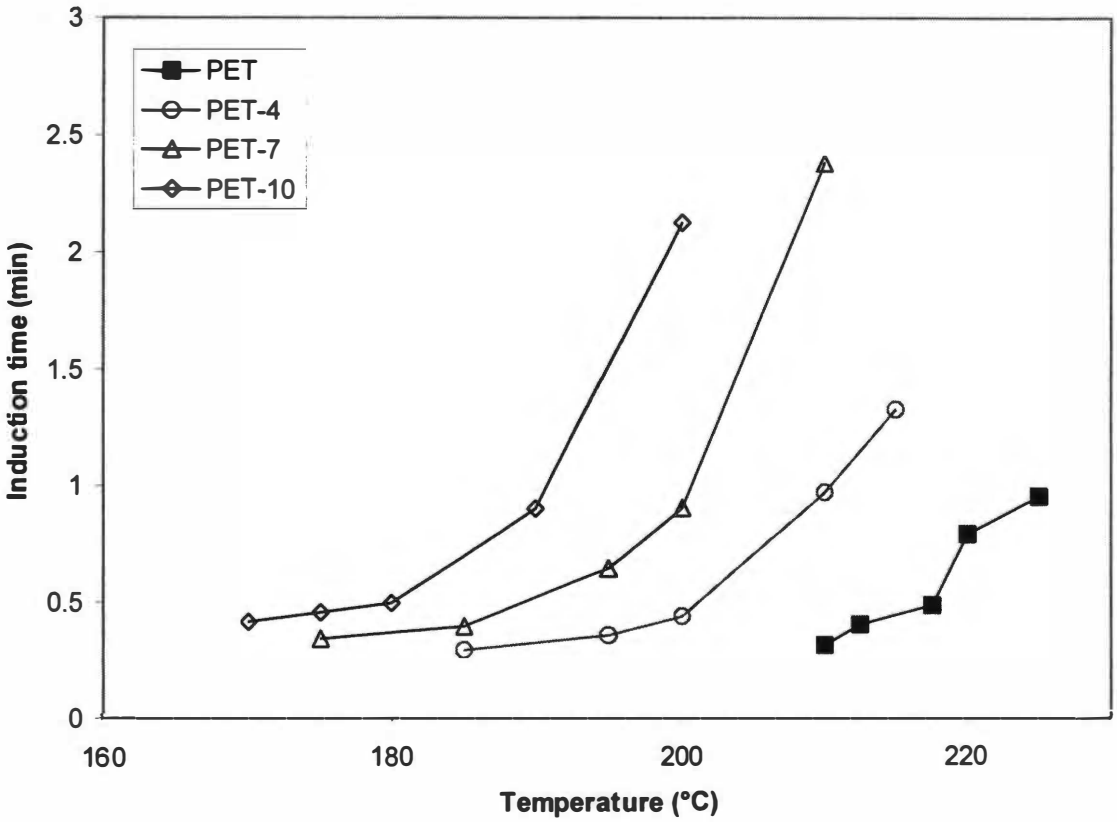

Figure 4.17: Plot of Apparent Induction Time as a Function of Isothermal Crystallization Temperature for Four Copolymers

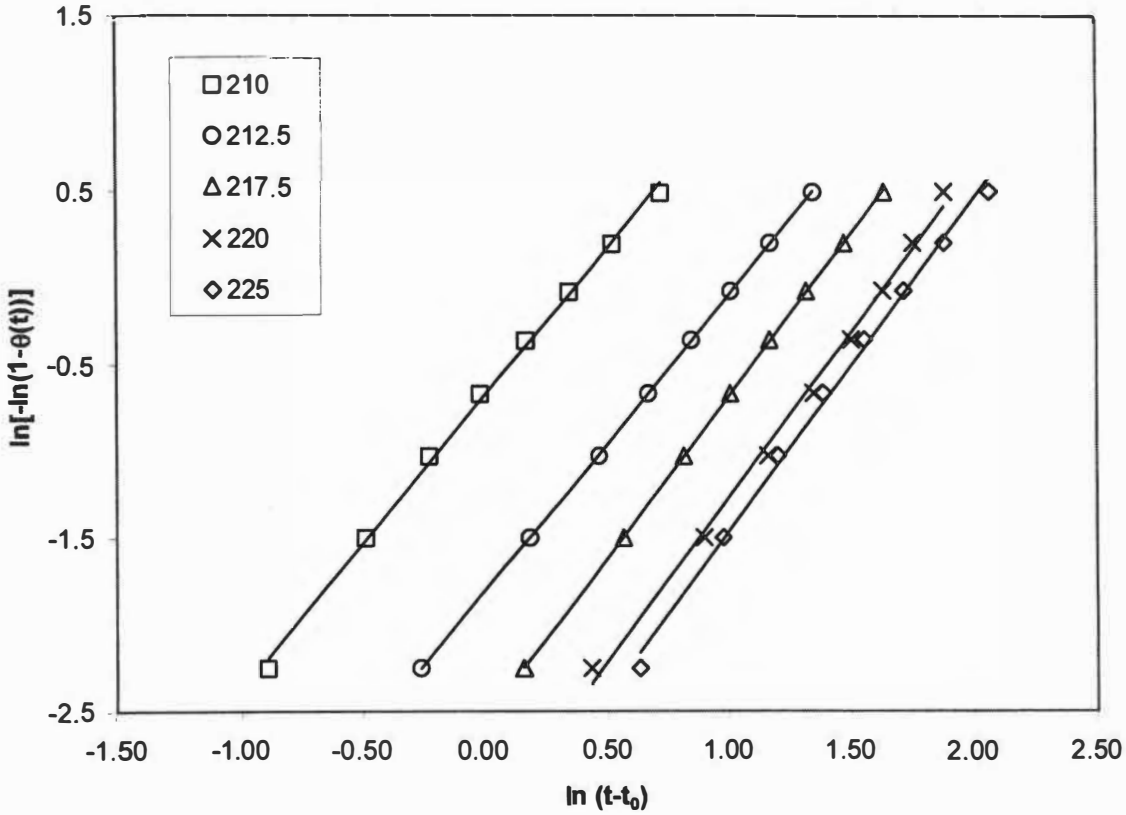

210°C:	y = 1.6935x - 0.6935	R^2 = 0.9981
212.5°C:	y = 1.6987x - 1.8185	R^2 = 1.0000
217.5°C:	y = 1.8522x - 2.5508	R^2 = 0.9999
220°C:	y = 1.8783x - 3.1568	R^2 = 0.9954
225°C:	y = 1.8943x - 3.3689	R^2 = 0.9959

Figure 4.18: Avrami Plot for PET Homopolymer

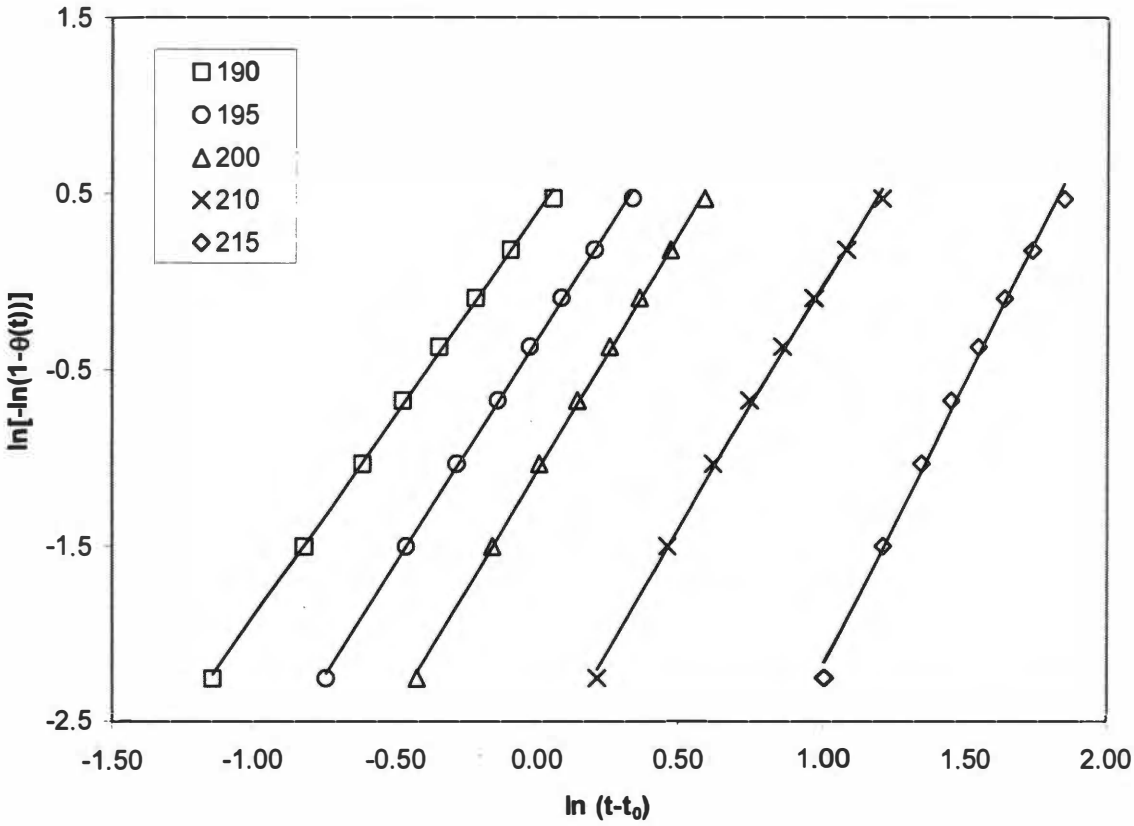

190°C:	y = 2.2956x + 0.3902	R^2 = 0.9991
195°C:	y = 2.5245x - 0.3361	R^2 = 0.9992
200°C:	y = 2.6787x - 1.0817	R^2 = 0.9992
210°C:	y = 2.7683x - 2.7914	R^2 = 0.9985
215°C:	y = 3.2355x - 5.4106	R^2 = 0.9957

Figure 4.19: Avrami Plot for PET-4 Copolymer

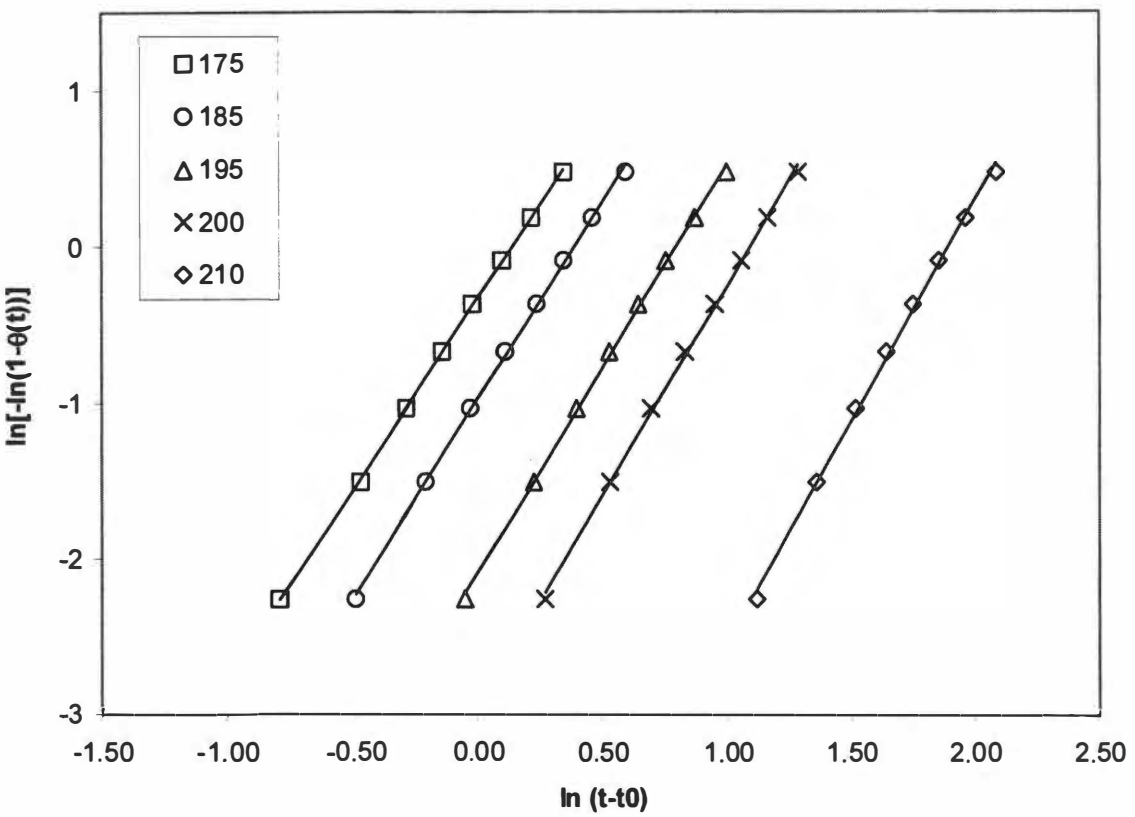

175°C:	y = 2.4108x - 0.3234	R^2 = 0.9998
185°C:	y = 2.5133x - 0.9644	R^2 = 0.9992
195°C:	y = 2.6204x - 2.0778	R^2 = 0.9991
200°C:	y = 2.678x - 2.9191	R^2 = 0.9989
210°C:	y = 2.8277x - 5.3473	R^2 = 0.9980

Figure 4.20: Avrami Plot for PET-7 Copolymer

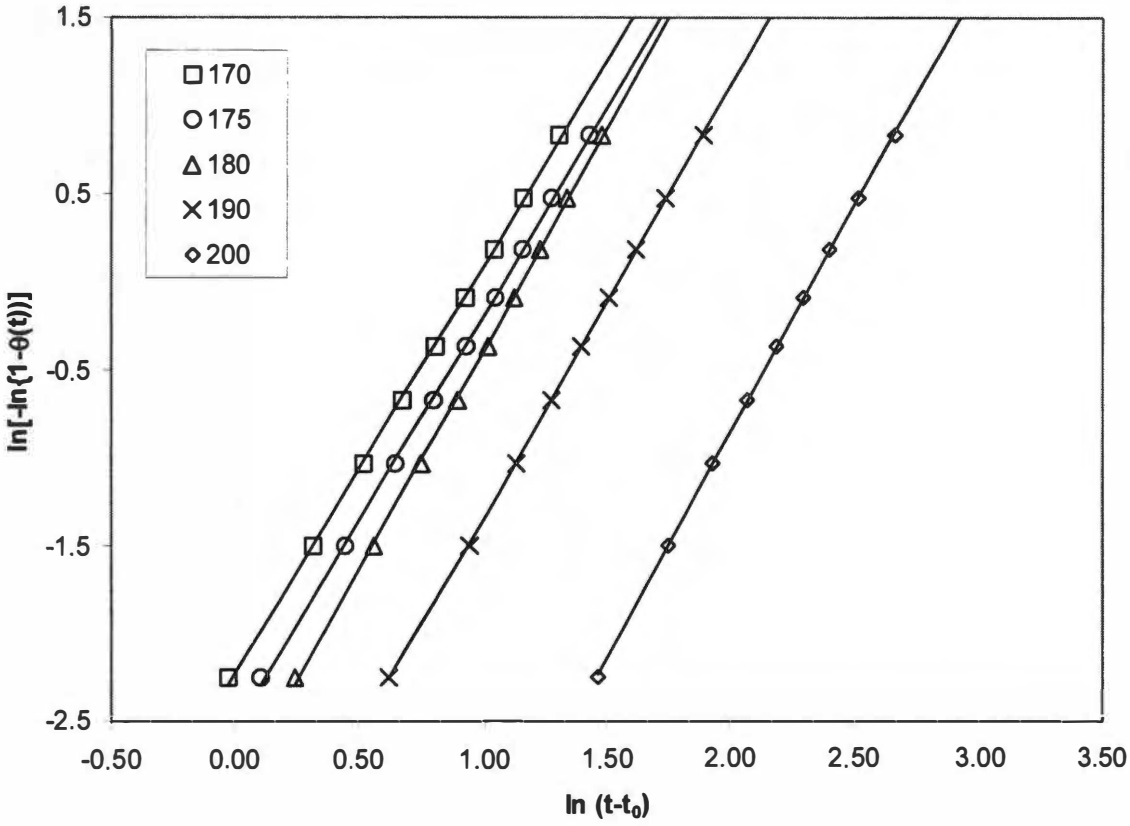

170°C:	y = 2.3297x - 2.2323	R^2 = 0.9995
175°C:	y = 2.3551x - 2.5416	R^2 = 0.9995
180°C:	y = 2.5177x - 2.9045	R^2 = 0.9995
190°C:	y = 2.4557x - 3.7949	R^2 = 0.9999
200°C:	y = 2.5729x - 5.9981	R^2 = 0.9999

Figure 4.21: Avrami Plot for PET-10 Copolymer

Table 4.4. summarizes the results of this experiment. As would be expected, the introduction of 2-methyl-1,3-propanediol does appear to have an effect on the overall isothermal crystallization kinetics of PET copolymer. The experimental results suggest that under the same operating conditions a 7mol% copolymer, for example, will crystallize much more slowly, and start crystallizing much later, than PET homopolymer. This is reflected numerically in the value of the rate constant, k.

The rate constant, determined by using both the Avrami analysis and Equation 2.33 strongly agree and quantify this phenomena. Figure 4.22 further illustrates this point, by displaying the relationship between k (or $k_{0.5}$) and the isothermal crystallization temperature for each copolymer. From Figure 4.22 it is evident that k decreases with increasing copolymer content and with increasing crystallization temperature.

As explained earlier, one of the main difficulties with the Avrami equation is in the interpretation of the Avrami exponent, n. In this experiment, the Avrami exponent appears to increase with crystallization temperature. Also, it appears that the values of n for PET homopolymer are significantly lower than that of the other copolyesters. Microscopic observation of the crystallization process for these copolyesters showed the formation of a birefringent mass such as is shown in Figure 2.5.b. The value of n for PET homopolymer is witnessed to range from 1.69 – 1.89, which may suggest that the enhanced nucleation effect of the $Ti0_2$ may have influenced the results of the Avrami analysis. A spherical, diffusion-controlled crystallization assuming athermal (i.e. predetermined) nucleation is predicted to yield an Avrami exponent of 3/2 (Wunderlich 1976). In such a case, the radial growth rates are assumed to be modeled using Equation 2.31 where the growth rates are proportional to $t^{1/2}$ instead of t.

Table 4.4: Isothermal Crystallization Data Summary for Copolyester at Various Crystallization Temperatures.

Sample	Temperature, T (°C)	$\Delta T = T_m^0 - T$ (°C)	t_i (min)	$t_{0.5} - t_0$ (min)	n	k (min^{-n})	$k_{t_{0.5}}$ (min^{-n})
PET	210	70.02	0.32	1.19	1.69	5.00E-01	5.14E-01
	212.5	67.52	0.41	2.38	1.70	1.62E-01	1.59E-01
	217.5	62.52	0.49	3.27	1.85	7.80E-02	7.72E-02
	220	60.02	0.79	4.52	1.88	4.26E-02	4.08E-02
	225	55.02	0.95	4.77	1.89	3.44E-02	3.59E-02
PET-4	190	75.24	0.33	0.71	2.30	1.48	1.52
	195	70.24	0.36	0.98	2.52	7.15E-01	7.28E-01
	200	65.24	0.44	1.30	2.68	3.39E-01	3.47E-01
	210	55.24	0.97	2.38	2.77	6.13E-02	6.32E-02
	215	50.24	1.33	4.69	3.24	4.47E-03	4.67E-03
PET-7	175	83.23	0.35	0.98	2.41	7.24E-01	7.22E-01
	185	73.23	0.40	1.26	2.51	3.81E-01	3.88E-01
	195	63.23	0.65	1.91	2.62	1.25E-01	1.28E-01
	200	58.23	0.91	2.57	2.68	5.40E-02	5.51E-02
	210	48.23	2.38	5.75	2.83	4.76E-03	4.93E-03
PET-10	170	83.63	0.42	2.25	2.33	1.07E-01	1.05E-01
	175	78.63	0.46	2.53	2.36	7.87E-02	7.79E-02
	180	73.63	0.50	2.75	2.52	5.48E-02	5.41E-02
	190	63.63	0.90	4.03	2.46	2.25E-02	2.26E-02
	200	53.63	2.13	8.89	2.57	2.48E-03	2.51E-03

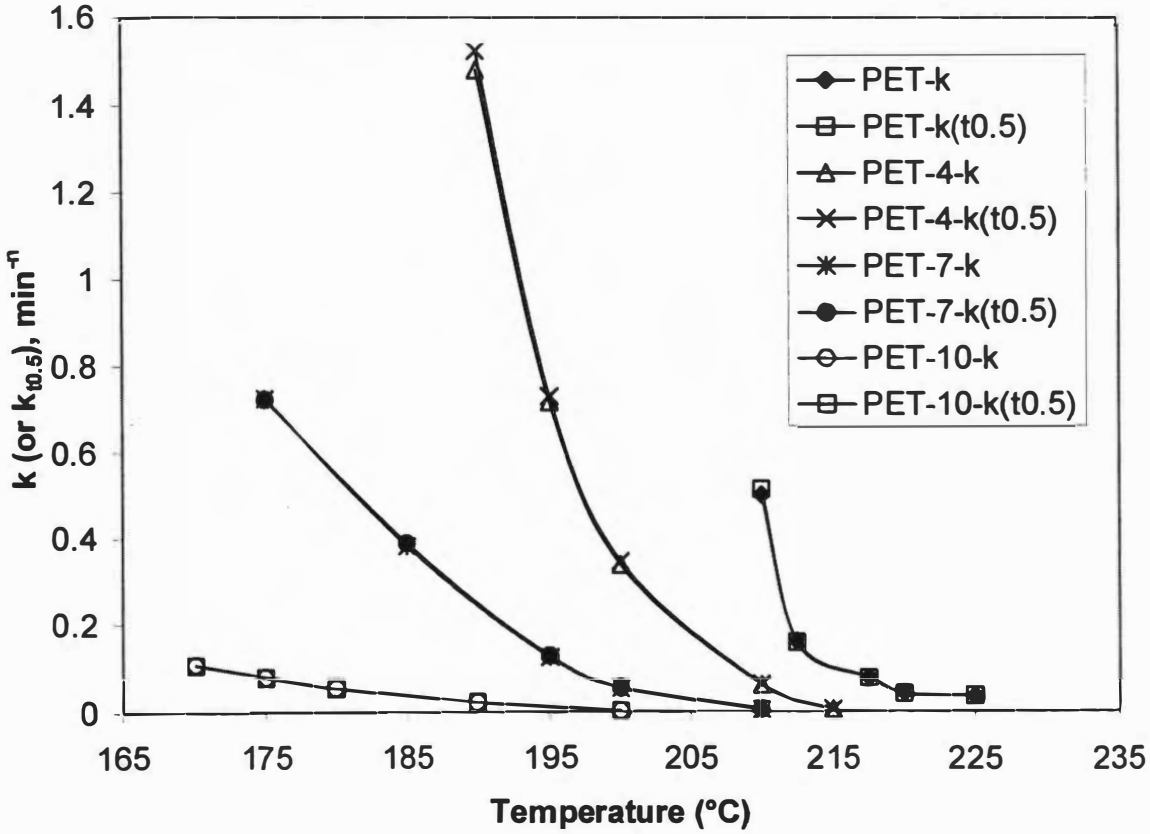

Figure 4.22: Plot of Avrami Rate Constants as a Function of Isothermal Crystallization Temperature for PET Copolymers

With regard to the PET-MPDiol copolymers in this study, the half-values of the Avrami exponent might be explained as being due to the high concentration of noncrystallizable impurities, which result again in a diffusion-controlled crystallization process. This explanation is further supported by noting that the values of n for PET-4 shift significantly from 2.30 at high undercoolings to 3.24 at high temperature while PET-10 shifts from 2.33 at low temperature to 2.57. Thus as the comonomer concentration increases it appears that the Avrami exponent approaches a value of approximately 2.5, predicted for spherical, diffusion controlled crystallization with thermal (i.e. spontaneous) nucleation (Wunderlich 1976).

The results of the estimation of activation energy of isothermal crystallization are summarized in Table 4.5. Figures 4.23 and 4.24 show how neither Equation 4.3. or Equation 4.5. appear to fit the experimental data very well. It is interesting to note however that both techniques appeared to predict very similar values for the crystallization activation energy under isothermal conditions. What is probably most important to note are not the actual values themselves but rather the general trend of the data. These results, as plotted in Figure 4.25, seem to indicate that the activation energy of bulk, isothermal crystallization increases as a function of copolymer composition. This seems to imply that increasing commoner content results in a less kinetically favorable situation. Thus the energy barrier impeding crystallization appears to increase with increasing comonomer composition.

For most simple chemical reactions the value of the activation energy is positive and thus a higher value of the activation energy represents an increased energy barrier in

Table 4.5: Activation Energy for Bulk Crystallization of PET and PET Copolymers Determined Using Equations 4.3 and 4.5

Sample	Temperature (°C)	V_c	Ea (Equ. 4.3)	Ea (Equ. 4.5)
PET	210	7.97E-03	-172.8	-162.4
	212.5	4.08E-03		
	217.5	3.17E-03		
	220	2.38E-03		
	225	2.15E-03		
PET-4	190	1.74E-02	-131.5	-116.4
	195	1.37E-02		
	200	1.08E-02		
	210	6.03E-03		
	215	3.49E-03		
PET-7	175	1.31E-02	-87.8	-82.3
	185	1.06E-02		
	195	7.19E-03		
	200	5.43E-03		
	210	2.54E-03		
PET-10	170	5.541E-03	-77.5	-73.0
	175	4.985E-03		
	180	4.819E-03		
	190	3.244E-03		
	200	1.526E-03		

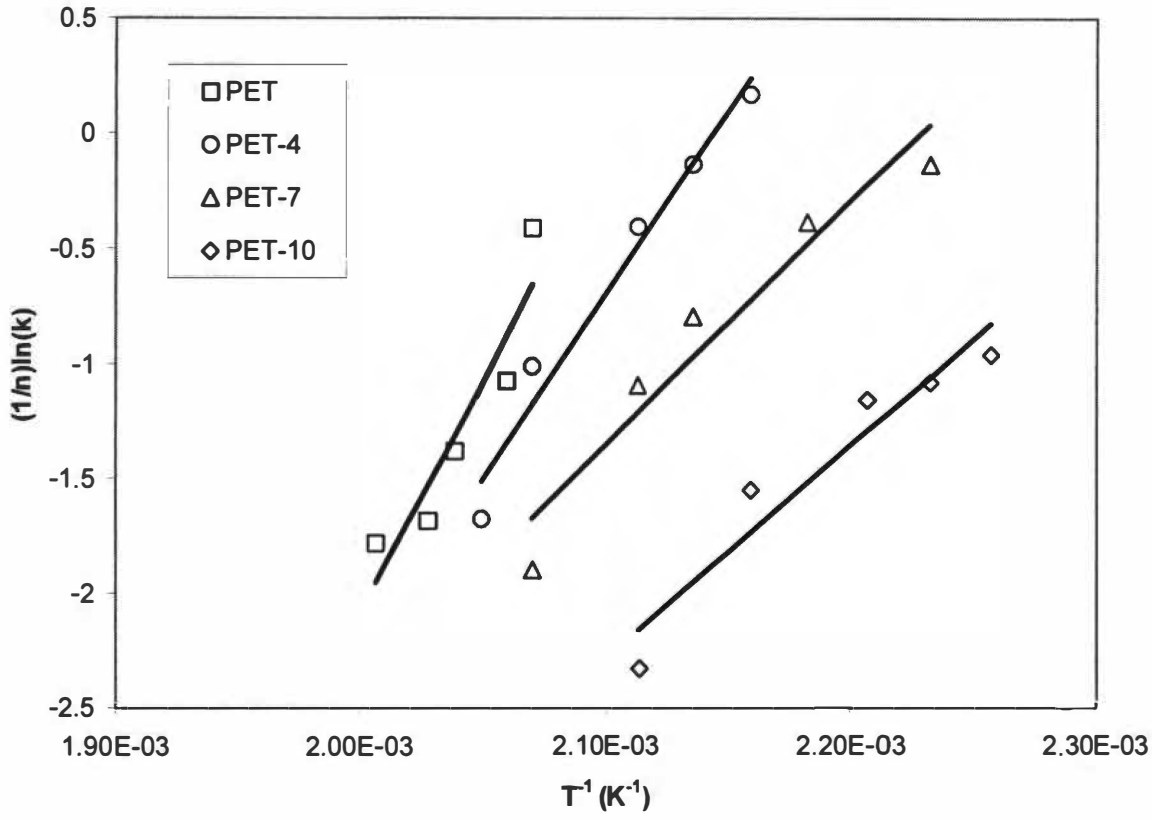

PET:	y = 20781x - 43.665	R^2 = 0.87
PET-4:	y = 15817x - 33.91	R^2 = 0.97
PET-7:	y = 10566x - 23.54	R^2 = 0.93
PET-10:	y = 9321.7x - 21.86	R^2 = 0.92

Figure 4.23: Plot of Equation 4.4 for PET Copolymers to Determine the Activation Energy of Isothermal, Bulk Crystallization

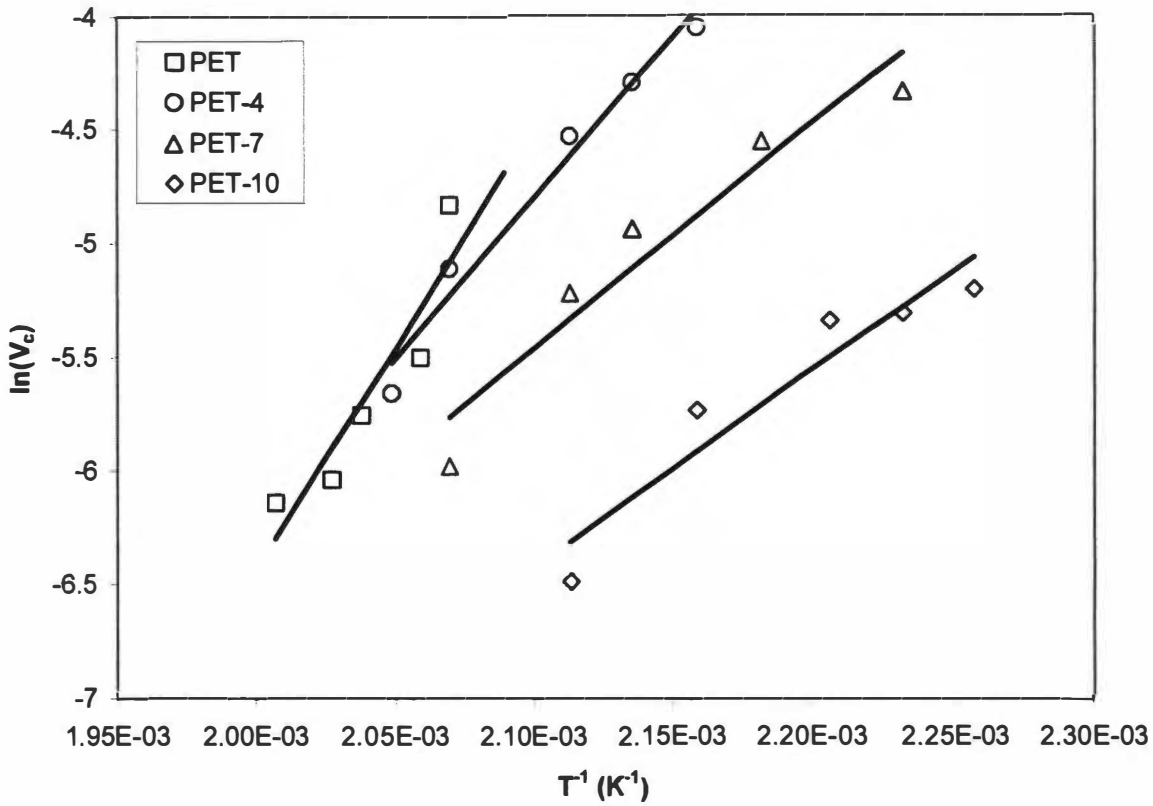

PET:	y = 19532x - 45.507	$R^2 = 0.86$
PET-4:	y = 14002x - 34.208	$R^2 = 0.97$
PET-7:	y = 9894.2x - 26.242	$R^2 = 0.92$
PET-10:	y = 8781.5x - 24.872	$R^2 = 0.90$

Figure 4.24: Plot of Equation 4.6 for PET Copolymers to Determine the Activation Energy of Isothermal, Bulk Crystallization

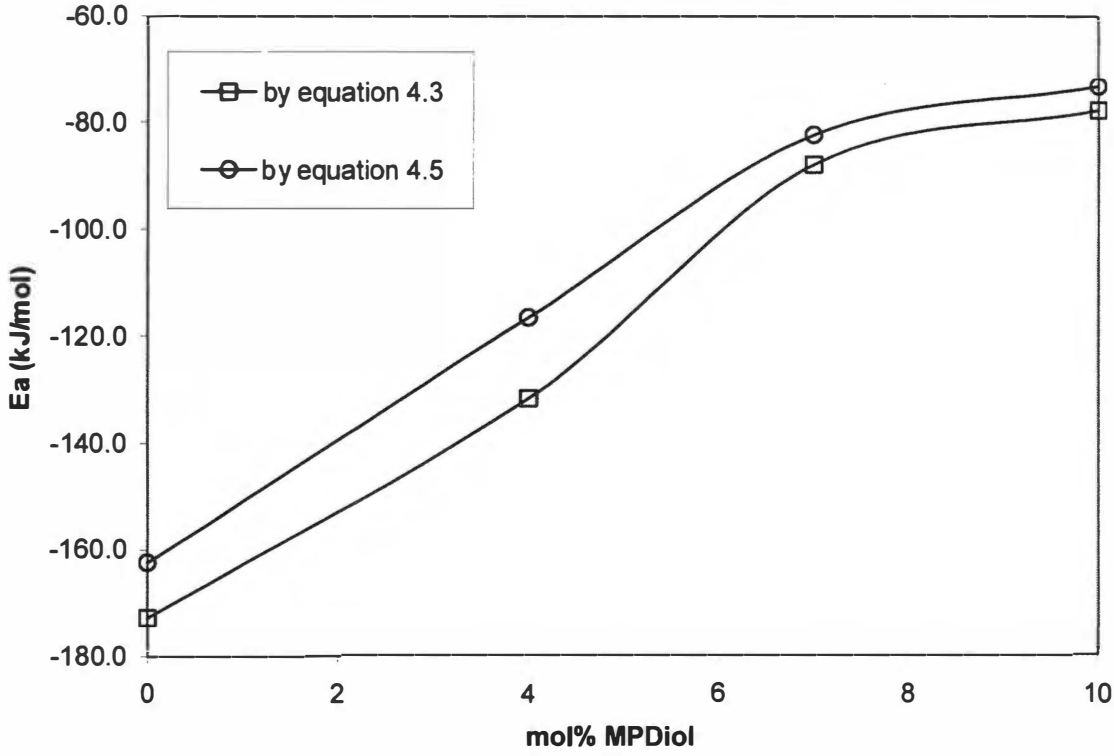

Figure 4.25: Plot of Activation Energy for Isothermal Crystallization as a Function of Comonomer Concentration

the formation of a reaction complex. For these simple types of reactions a positive value for the activation energy signifies that the reaction proceeds more rapidly with increasing temperature. This is just the opposite of the case for more complex reactions where reaction rates decrease with increasing temperature. In these cases the sign of the activation energy is negative (Atkins 1990). This is obviously the case for polymer crystallization in the temperature range investigated and therefore by Equations 4.3 and 4.5 a decrease in the value of the activation energy signifies an increase in the rate constant. Thus because PET has the lowest activation energy it is more kinetically favorable.

It should be noted that in their study on the isothermal and cold crystallization kinetics of syndiotactic polypropylenes, Supaphol and Spruiell (2001) evaluated the Arrhenius temperature dependence in describing the temperature dependence of the Avrami rate constant. In their study it was shown that, over a wider range of temperatures, that the dependence of the Avrami rate constant as a function of temperature resembled the same general shape as a plot of $t_{0.5}$ as a function of temperature, and therefore was anything but linear. This same apparent curvature in the data is found in the data in this experiment, particularly for the copolymer samples, as can be seen by careful examination of Figures 4.23 and 4.24. It is apparent in both the Avrami approach and the phenomenological approach, that even over this small temperature range, the data does appear to show some curvature. As is explained by Supaphol and Spruiell (2001) this nonlinear dependence should be expected since the Avrami rate constant is known to be related to the halftime by Equation 2.33. As is suggested by these authors, over a small temperature range the apparent linearity in the

data might lead to a false evaluation of the activation energy. Nevertheless, this analysis has been included because of its widespread use and common acceptance in the literature and because it does appear to provide for a reasonable way to compare the activation energies of these materials in a semi-quantitative fashion.

4.2.3. Isothermal Crystallization - Melting Behavior

Upon completion of isothermal crystallization the samples were subsequently reheated to 280°C at a scan rate of 25°C/min to observe the melting behavior (see Figure 4.5). It is commonly accepted that PET homopolymer, over a given range of isothermal crystallization temperatures, will often exhibit a multiple peak melting behavior upon subsequent reheating from the isothermal crystallization temperature. It is evident that at the lower isothermal crystallization temperatures each of the four copolymers exhibited the multiple melting peaks commonly witnessed for PET homopolymer, as is shown in Figures 4.26-4.29.

The results of this experiment are summarized in Table 4.6 where it is shown that the third melting peaks appear not to shift significantly with increasing crystallization temperature. However, it does appear that the first and second melting peaks both shift to higher temperatures with increasing isothermal crystallization temperature. Additionally, Figures 4.26-4.29 illustrate that the second melting endotherm appears to increase in magnitude with increasing crystallization temperature at the expense of the third melting peak.

Many investigators attribute the first melting peak as the melting of subsidiary lamellae (from secondary crystallization), the second melting endotherm to the melting of

Table 4.6: Summary of Observed Melting Behavior Following Isothermal Crystallization

Sample	T_c (°C)	T_m^I (°C)	T_m^{II} (°C)	T_m^{III} (°C)	T_m^0 (°C)
PET	210	223.1±0.05	248.1±0.40	254.3±0.04	280.0
	212.5	229.6±1.10	249.3±0.10	----	
	217.5	235.6±0.26	251.4±0.19	----	
	220	238.5±0.14	252.6±0.08	----	
	225	246.4±0.96	255.0±0.21	----	
PET-4	190	200.6±.05	235.0±0.05	244.2±0.44	265.2
	195	207.0±0.78	238.5±0.16	246.0+1.30	
	200	212.1±0.75	240.3±0.05	----	
	210	220.8±0.06	244.1±0.18	----	
	215	233.0±1.41	245.0±0.29	----	
PET-7	175	186.7±0.05	227.3±0.17	238.6±0.05	258.2
	185	196.5±0.03	230.5±0.24	238.6±0.06	
	195	206.0±0.01	234.5±0.10	----	
	200	212.5±0.17	236.7±0.17	----	
	210	224.6±0.25	240.1±0.10	----	
PET-10	170	181.4±0.05	220.6±.05	232.5±.05	253.6
	175	186.8±0.10	223.1±0.05	232.6±0.05	
	180	191.2±0.08	225.1±0.10	232.5±0.08	
	190	202.4±0.10	229.2±0.10	----	
	200	216.6±0.28	232.4±0.24	----	

NOTE: Limits based on +/- 1 standard deviation unless otherwise specified

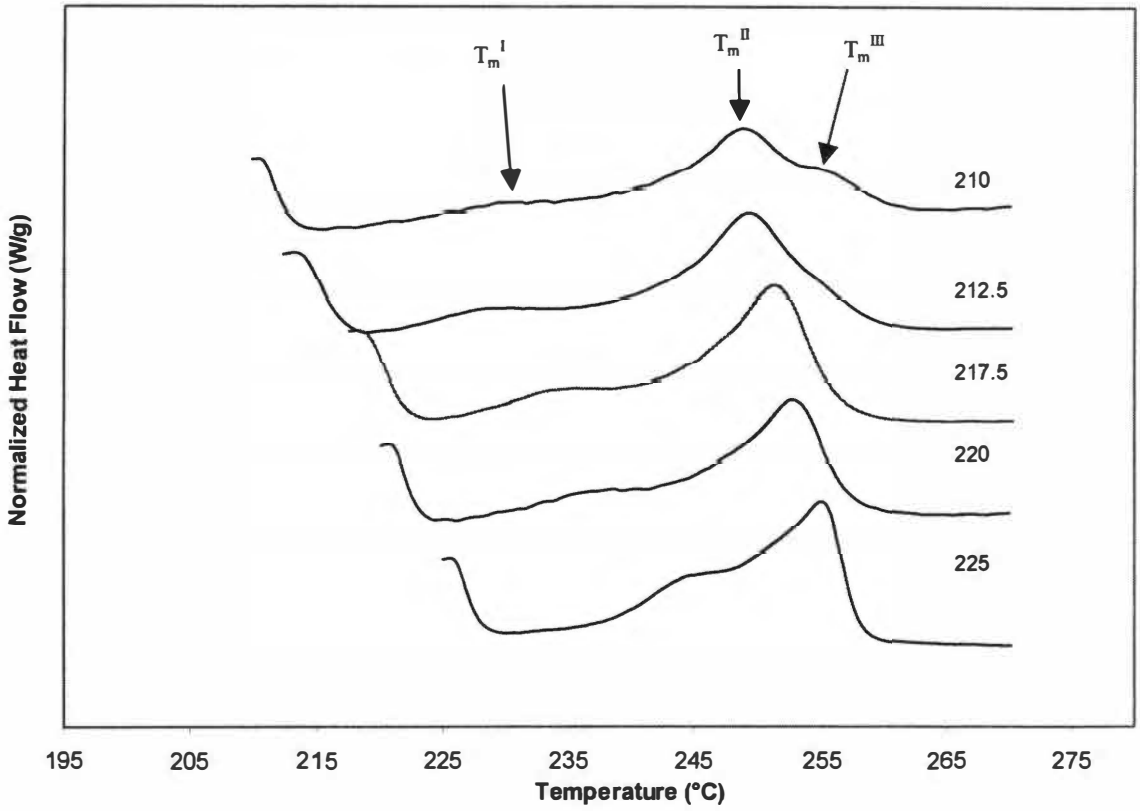

Figure 4.26: Representative DSC Melting Curves Following Isothermal Crystallization at the Specified Temperatures for PET Homopolymer

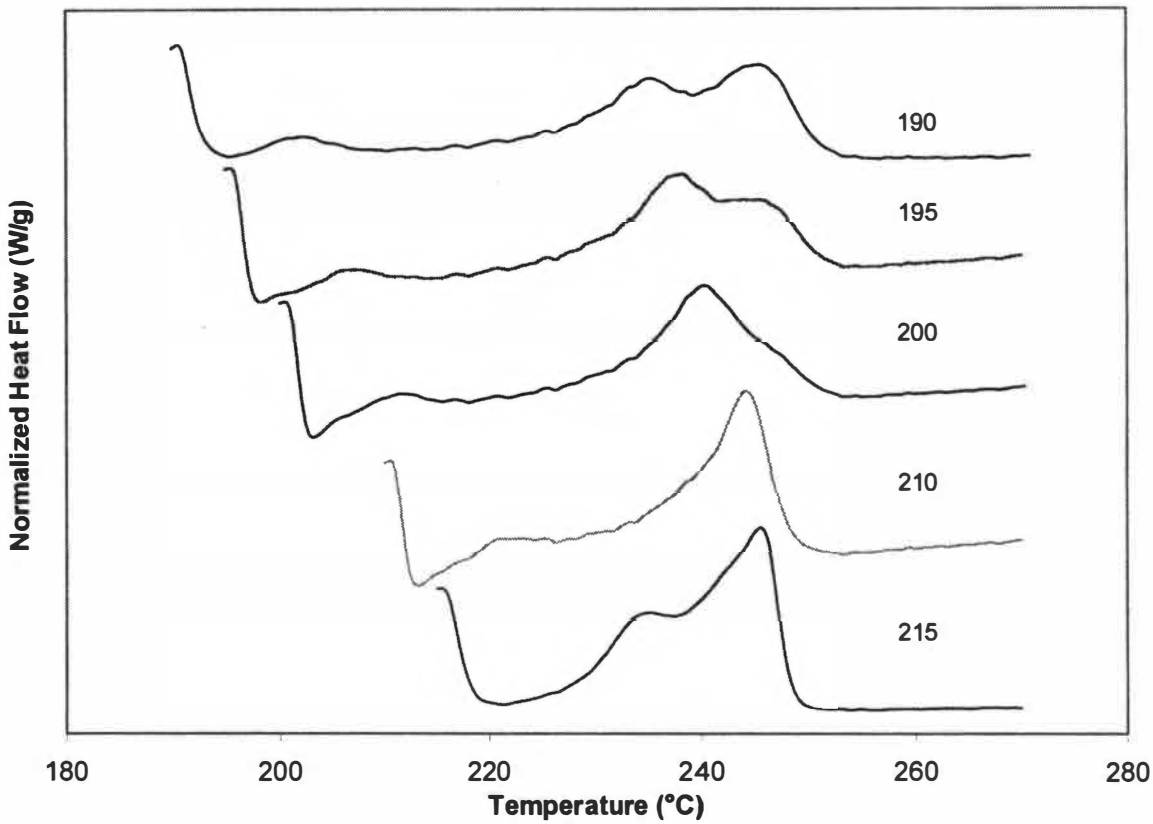

Figure 4.27: Representative DSC Melting Curves Following Isothermal Crystallization at the Specified Temperatures for PET-4 Copolymer

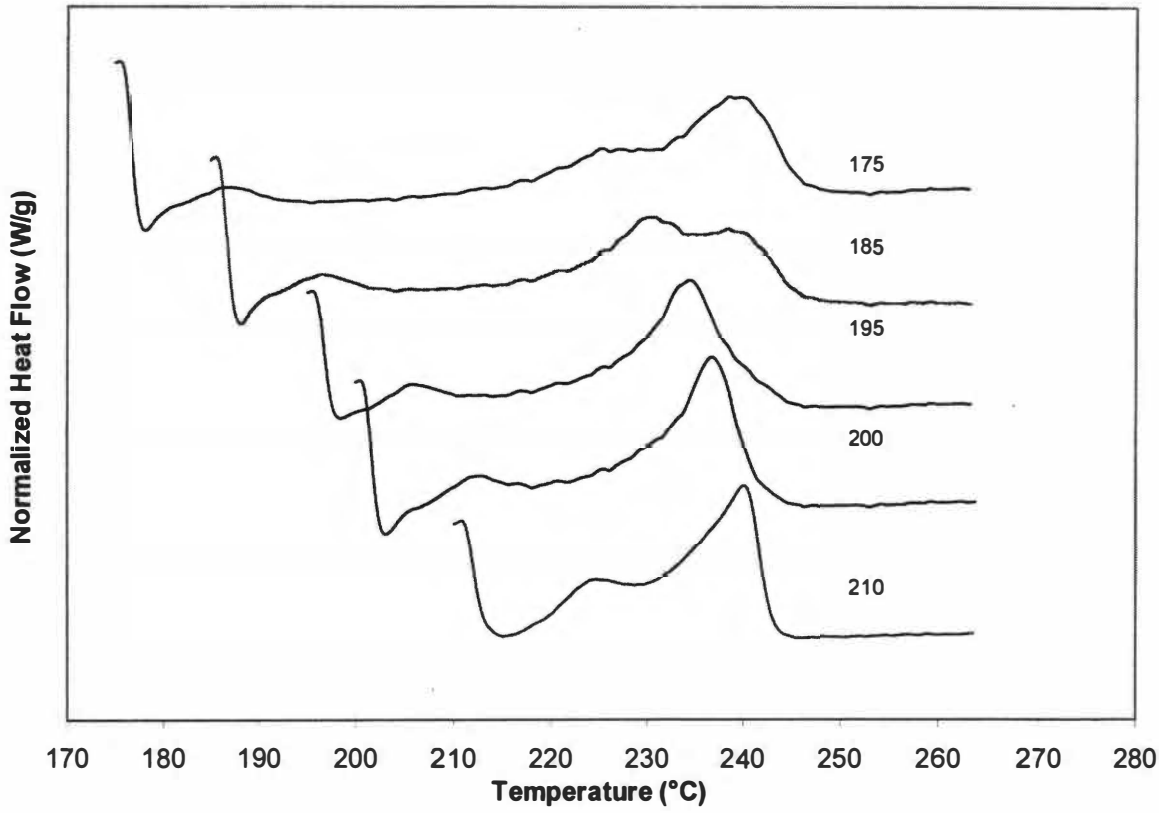

Figure 4.28: Representative DSC Melting Curves Following Isothermal Crystallization at the Specified Temperatures for PET-7 Copolymer

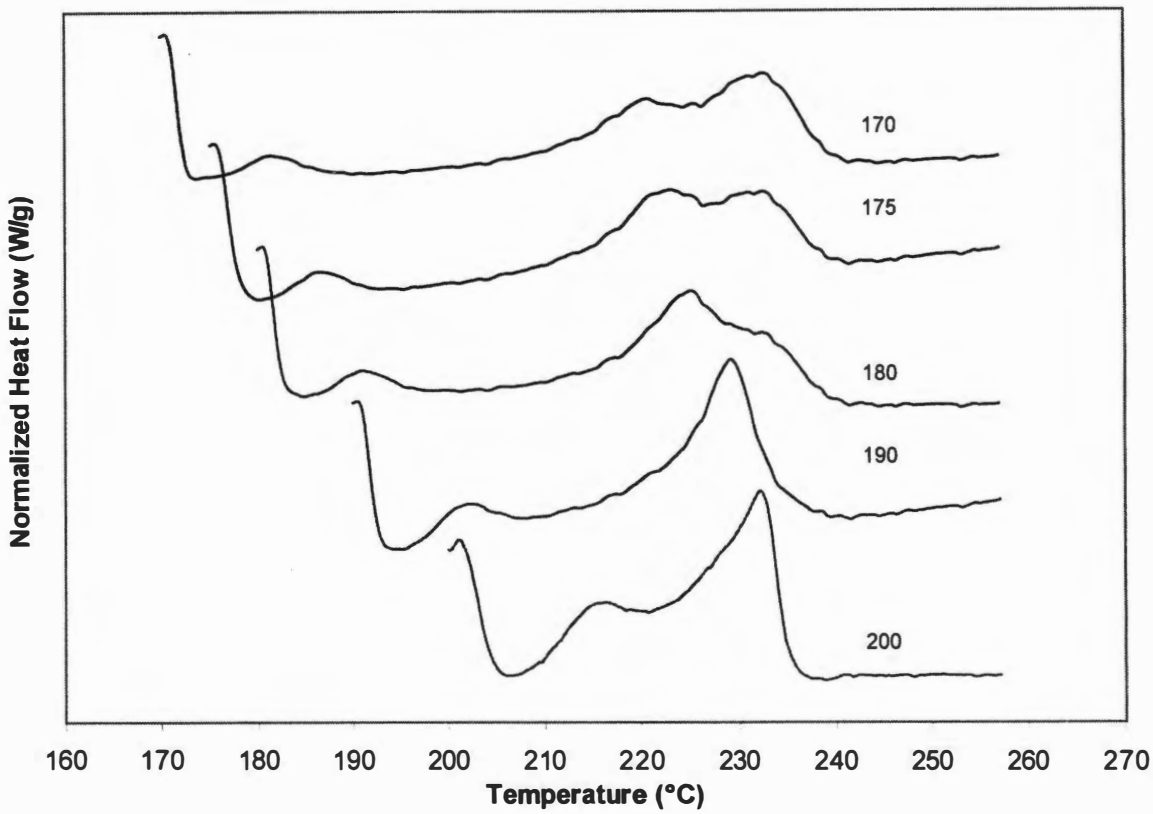

Figure 4.29: Representative DSC Melting Curves Following Isothermal Crystallization at the Specified Temperatures for PET-10 Copolymer

the dominant lamellae, and the third endotherm to recrystallization (Zhou and Clough 1988, Wang et al 1999, Lu and Hay 2001). Thus the equilibrium melting temperature was estimated by the Hoffman-Weeks method using the peak temperature value of the second melting peak. From Figure 4.30 it is evident that the Hoffman-Weeks plot showed good linearity. Additionally, the equilibrium melting temperature for PET homopolymer, which was found to be 280.0°C, agreed with that found by other investigators (Myagi and Wunderlich 1972, Taylor 1962, Wlochowicz and Przygocki 1973).

As is mentioned earlier, there is some controversy as to the actual morphological explanation of these three melting endotherms. Medellin-Rodrigez et al (1997, 1998) recently proposed a somewhat different explanation for the multiple melting endotherms observed in the melting of isothermally crystallized PET samples. In their study the authors suggested that the first melting endotherm was associated with the final stage of secondary crystallization (small branches of metastable crystalline material), the second endotherm was associated with the secondary crystallization (mainly metastable secondary branches), and the third endotherm with the primary crystals having undergone some degrees of recrystallization during the heating scan.

Since the physics of this process are still in question, the equilibrium melting point values determined by the Hoffman-Weeks method in this study should be approached with some caution. The values listed in Table 4.6 should be viewed as estimates determined with the assumption that the peak melting temperatures of the second melting endotherm are attributed solely to the crystals formed during the isothermal crystallization process. The equilibrium melting point temperatures for the

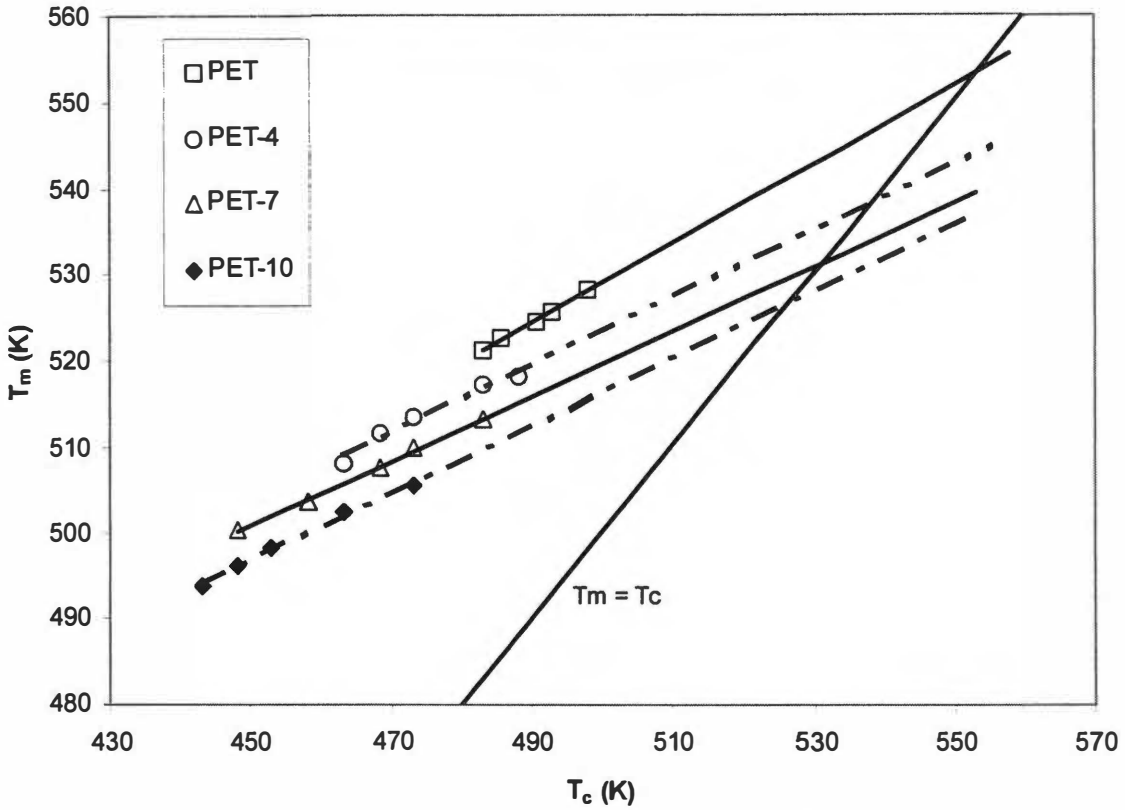

PET:	y = 0.456x + 300.902	$R^2 = 0.998$
PET-4:	y = 0.390x + 328.289	$R^2 = 0.969$
PET-7:	y = 0.3744x + 332.44	$R^2 = 0.998$
PET-10:	y = 0.390x + 321.197	$R^2 = 0.995$

Figure 4.30: Hoffman-Weeks Plot for Four Materials

PET copolymers were examined again using the Flory melting point equation (Equation 2.41) resulting in Figure 4.31.

The Flory equation appeared to fit the experimental data reasonably well (R^2=0.985), predicting a value of 545.6K (272.4°C) for the equilibrium melting point of PET homopolymer. Although there is nearly an 8 degree difference between these two values, the resulting percent difference between T_m^0 found by the Flory equation and that determined using the Hoffman-Weeks method was found to be 1.38%, well within the limits of acceptable experimental error.

This experimental piece of evidence appears to further support the claim that MPDiol units are rejected from the parent PET homopolymer crystal, thus resulting in a depression of the melting temperature as the MPDiol content is increased.

4.2.4. Further Discussion of Isothermal Crystallization Results

Determination of the equilibrium melting temperatures for the four materials allows for the isothermal crystallization kinetics to be examined on the basis of the degree of undercooling (i.e. $\Delta T=T_m^0-T_m$). For convenience, the values of ΔT for each copolymer and crystallization temperature have been included in Table 4.4 (see the previous section dealing with the Avrami analysis of these copolyesters).

Figure 4.32 is a plot of the apparent induction time as a function of undercooling. Here it is evident that, at concentrations up to 4mol% MPDiol, there appears to be little to no effect on the induction time. However the 7 and 10mol% copolyesters appear to exhibit an increase in apparent induction time as a function of undercooling. An increase

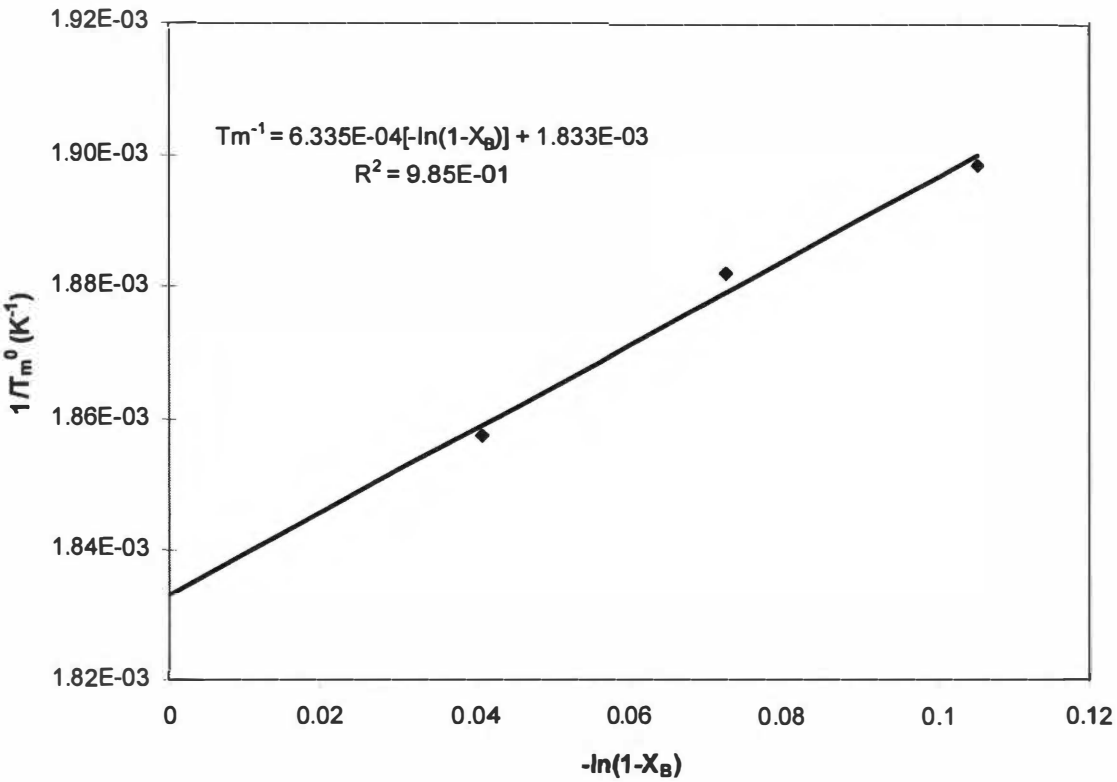

Figure 4.31: Plot of Flory's Melting Equation to Predict the Equilibrium Melting Temperature of PET Homopolymer

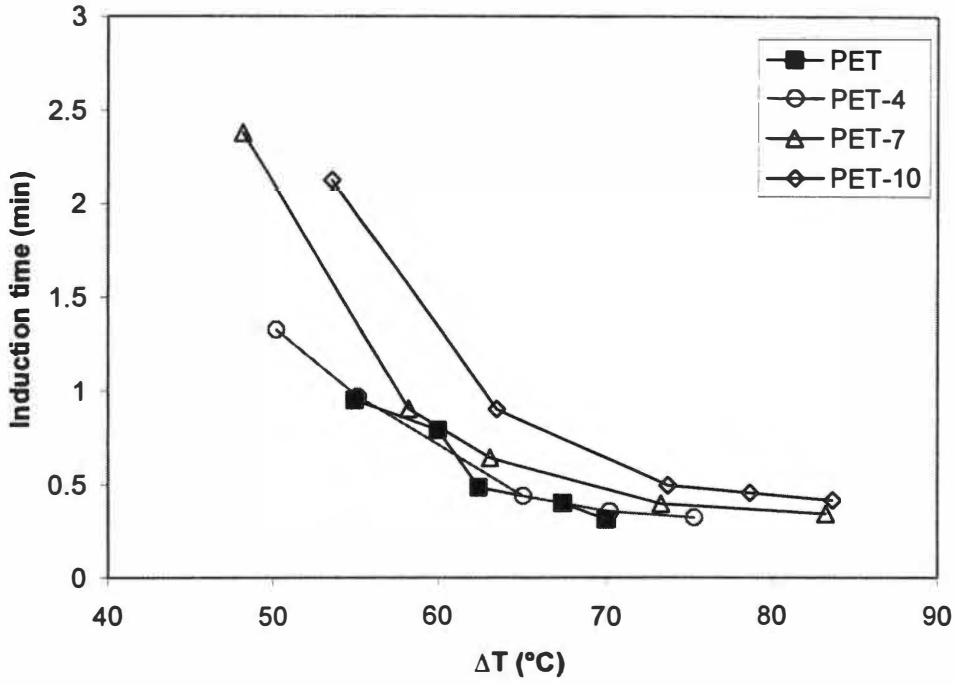

Figure 4.32: Plot of Apparent Induction Time as a Function of Undercooling

in induction time would seem to imply that the presence of this comonomer, at concentrations above 7mol%, appears to impede primary nucleation.

A plot of the crystallization half time as a function of undercooling is shown in Figure 4.33. Here the data suggests that the 4 and 7 mol% copolymers crystallize more rapidly than PET homopolymer at a given undercooling. This would imply that MPDiol at concentrations less than or equal to 7mol% appear to actually enhance crystallization at a given undercooling.

Figure 4.34 shows the influence of copolymer concentration on the Avrami rate constant as a function of ΔT. As before, the order of crystallization rate as a function of undercooling would appear to be: PET-4>PET-7$\geq$PET>PET-10.

It would appear that, by this type of examination, copolymer concentrations up to 7mol% MPDiol appear to actually enhance crystallization at a given degree of supercooling. It is important to note that this does not change the reality that PET crystallizes more rapidly than the other copolymers at a given temperature, but that at the same undercooling, the presence of the comonomer is shown to actually improve the crystallization kinetics with low MPDiol concentration (i.e. less than or equal to 4mol%). In particular it would seem that the MPDiol units do not appear to enhance primary nucleation as implied by the induction time results illustrated in Figure 4.32. However, the results shown in Figures 4.33 and 4.34 do seem to suggest that, at a particular undercooling, that crystal growth is enhanced by low concentrations of MPDiol.

Experimental evidence seems to suggest that the 4mol% copolymer shows the highest crystallization rate at a given undercooling. This is in good agreement with that

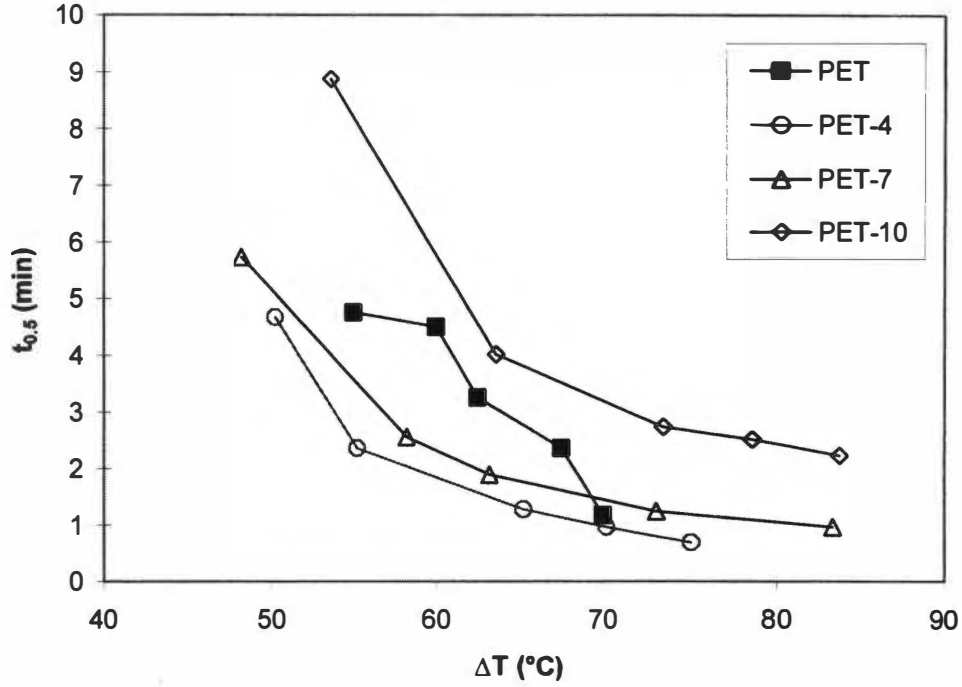

Figure 4.33: Plot of Isothermal Crystallization Half Time as a Function of Undercooling

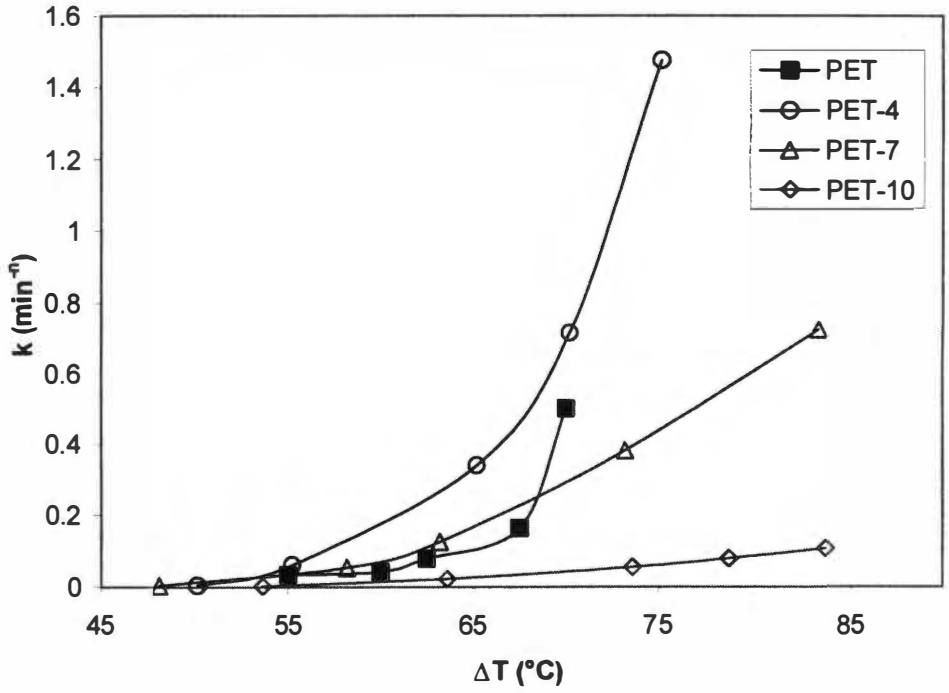

Figure 4.34 Plot of Avrami Rate Constant as a Function of Undercooling

argued by others (Bouma et al 2001, Bier et al 1977) who have suggested that PET copolymers containing short codiols exhibit enhanced crystallization rates when comonomer concentration is less than or equal to 5mol%. This has been explained as being due to increased chain flexibility compared to the more rigid PET molecule thus allowing for enhanced chain folding during crystallization. However, it appears that too high of a concentration of comonomer negates this kinetically favorable situation due to comonomer exclusion from the parent PET crystal. In the case of MPDiol, it appears that, with regard to undercooling, concentrations less than approximately 7-8mol% comonomer appear to show improved crystallizability, with the optimum concentration appearing to be less than or equal to about 4-5 mol% MPDiol.

Note however that there are a few sources of error in this particular experiment. As is described earlier, the values of Tm^0 are somewhat in question. While it does appear that the equilibrium melting temperature determined for PET homopolymer does agree well with that found by other investigators, the assignment of the melting peaks observed in this experiment are still in question and, as stated earlier, the equilibrium melting temperatures should therefore be approached with some caution.

Secondly, since the PET homopolymer in this experiment is known to contain $Ti0_2$, a potential nucleating agent, it is possible that even the 10% comonomer might exhibit improved crystallizability over pure PET homopolymer. In the literature it does appear that some investigators have been able to measure the isothermal crystallization kinetics of PET at lower isothermal crystallization temperatures using DSC. Their data seems to suggest that the PET homopolymer in this experiment does crystallize much faster at a given temperature. This is illustrated in Figures 4.35 and 4.36 where the half

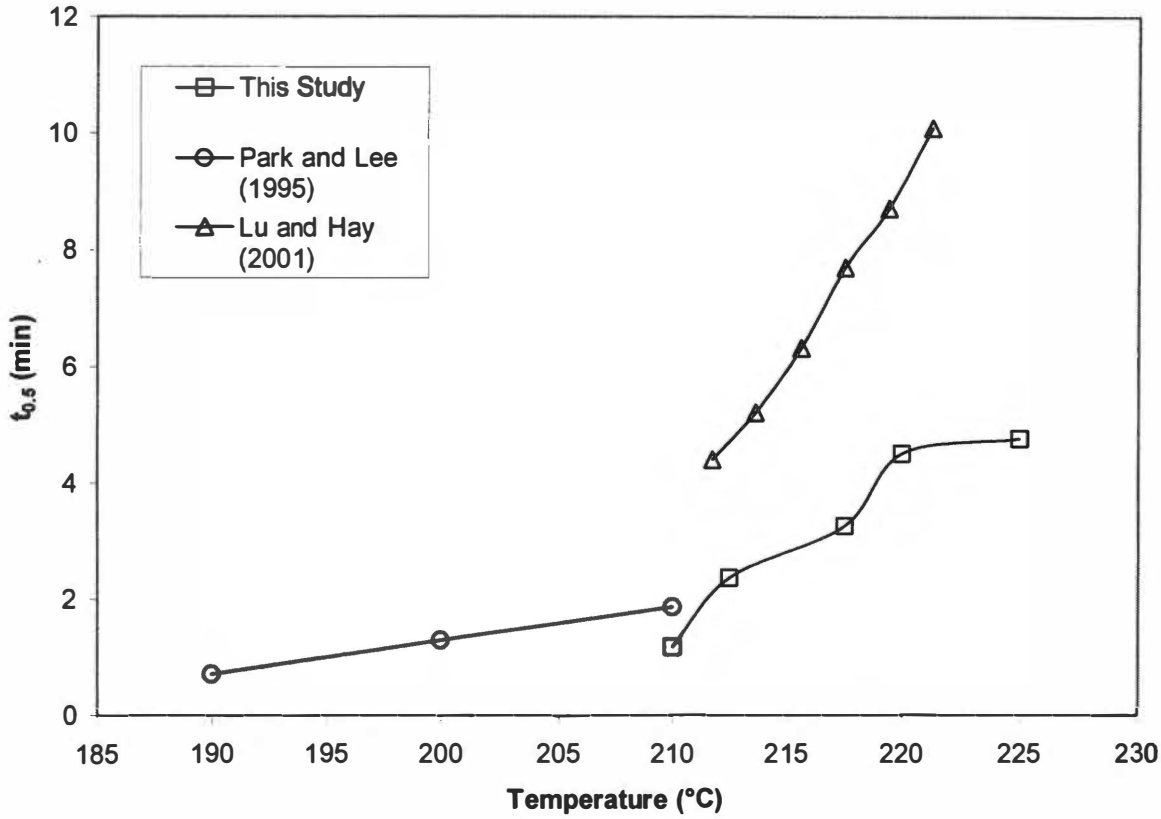

Figure 4.35: Comparison of Crystallization Half Time as a Function of Isothermal Crystallization Temperature for Three Studies

Source: Park, L. and Lee, D., Poly. Eng. Sci., 35, 1629 (1995).; Lu, X. and Hay, J., Polymer, 42, 9423 (2001).

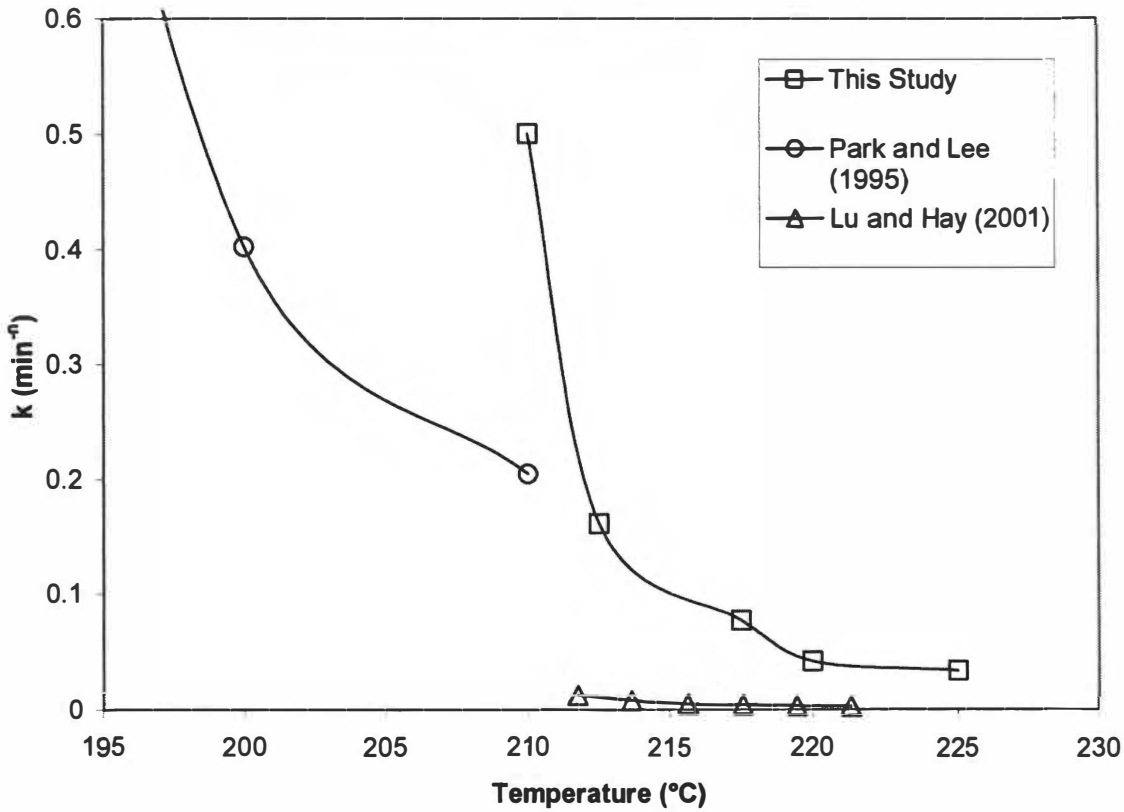

Figure 4.36: Comparison of Avrami Rate Constant, k, as a Function of Isothermal Crystallization Temperature for Three Studies

Source: Park, L. and Lee, D., Poly. Eng. Sci., 35, 1629 (1995).; Lu, X. and Hay, J., Polymer, 42, 9423 (2001).

times and Avrami rate constants taken from studies by Park and Lee (1995), Lu and Hay (2001), and this study are plotted as functions of isothermal crystallization temperature and compared. It appears that in both cases, the PET homopolymer examined in this experiment crystallizes much more rapidly than that found by these authors. However, it is important to note that the crystallization of PET is very complex and has been shown to be a function of many variables including molecular weight, diethylene glycol content, and amount and type of contamination.

4.3. Nonisothermal Crystallization

4.3.1. Differential Scanning Calorimetry- Low Cooling Rates

4.3.1.1. Examination of Experimental Data

This experiment examined the nonisothermal crystallization kinetics of copolymers of Polyethylene Terephthalate (PET) containing the comonomer 2-methyl-1,3-propanediol (MPDiol) with PET homopolymer to determine the effect that increasing copolymer content has on the overall nonisothermal crystallization kinetics under moderate cooling conditions. A Mettler-Toledo DSC820 Differential Scanning Calorimeter was used in this experiment, with the resulting data analyzed using the Avrami and Ozawa equations. As explained earlier, the sign convention utilized by this particular DSC is that crystallization peaks (i.e. exothermic transitions) point in an upward direction while melting peaks (i.e. endothermic transitions) point in a downward direction; just the opposite of that for the Perkin-Elmer DSC7.

Figure 4.37 shows a typical nonisothermal DSC scan, in this case for PET homopolymer with a cooling rate of 7.5°C/min. As previously discussed, all samples were first heated to 290°C and allowed to remain at that temperature for 10 minutes to ensure that the previous melt history of the polymer had been erased as well as to guarantee that the DSC had achieved thermal equilibrium prior to cooling. Upon completion of the initial isothermal at 290°C the DSC was then programmed to cool at a linear rate, ranging from 1-12.5°C/min, to a temperature of 30°C so as to observe the nonisothermal crystallization. The DSC was then held isothermally at 30°C for 10 minutes, again to ensure the achievement of thermal equilibrium. Upon completion of this isothermal the DSC was then heated at 10°C/min to 290°C so as to observe the melting behavior.

The DSC derivative curve was used to estimate the beginning and ending points of crystallization. This ensured that the majority of the heat evolved during crystallization was included in the data analysis. This is illustrated in Figure 4.38 for PET homopolymer cooled at 7.5°C/min. From examination of the first derivative it is more evident that the rate of change of the DSC endotherm (i.e. the beginning of crystallization) for this particular curve occurs at approximately 230°C and ends at approximately 198°C.

Since a heat flux DSC was used, it is expected that during the cooling scan the temperature of the reference and sample pans will most likely be different, especially during a thermodynamic transition. As a result, the analysis of this data was examined in

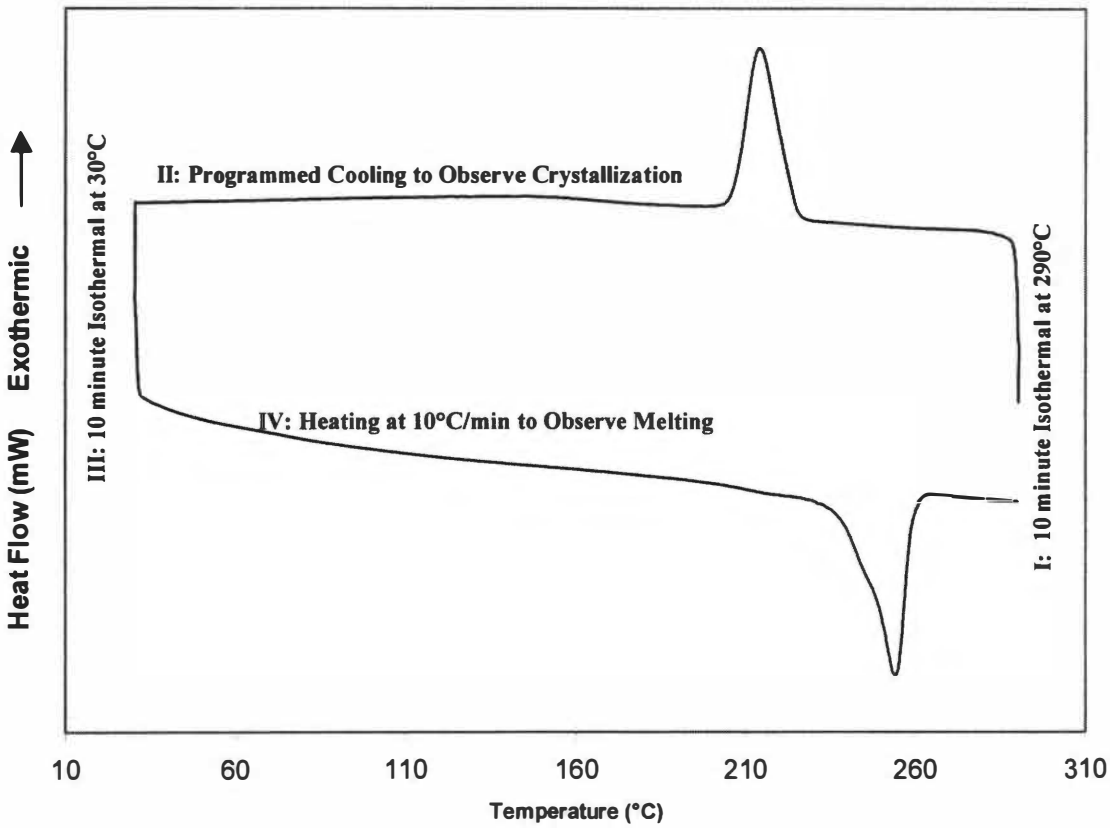

Figure 4.37: Typical Nonisothermal DSC Scan (shown here for PET homopolymer at a cooling rate of 7.5°C/min)

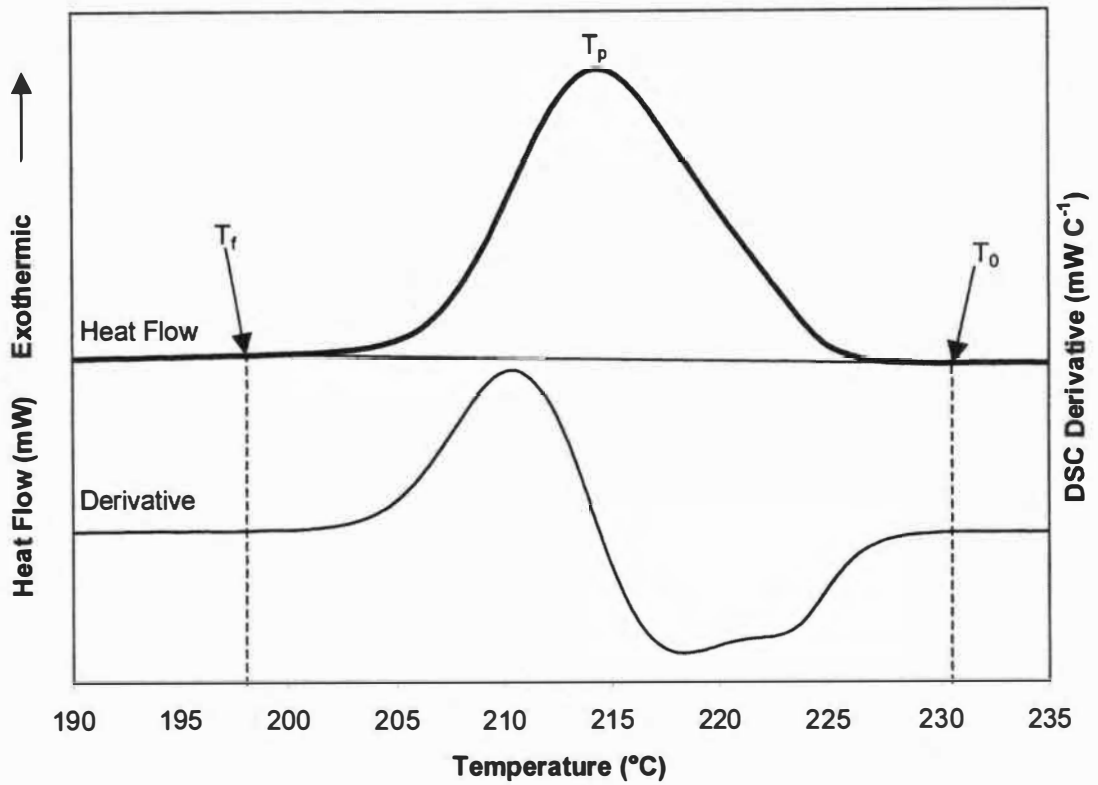

Figure 4.38: Heat Flow Curve and Corresponding DSC Derivative Curve for PET Homopolymer Cooled at 7.5°C/min

terms of the experimentally measured sample temperature, as opposed to the reference temperature.

Typical DSC scans for the four copolyesters are shown in Figures 4.39-4.42 along with their corresponding conversion curves as a function of temperature. There are two important points to notice in these raw data scans. First, it is evident that as the cooling rate is increased the normalized heat flow increases. Secondly, it is evident that the peak temperature, T_p, as well as the onset of crystallization, is shifted to lower temperatures with increasing cooling rate. This is further illustrated by the temperature based conversion curves shown in Figures 4.43-4.46. These figures suggest that the half-times of crystallization are shifted to lower temperatures with increasing cooling rate. From these plots it is also clear that crystallization occurs over a wider temperature range as the cooling rate is increased. Additionally, these plots clearly illustrate how the onset of crystallization is shifted to lower temperatures with increasing cooling rate. This suggests that nuclei formation is hindered with increasing cooling rate, even under these moderate cooling conditions.

Assuming that thermal lag is kept to a minimum, then under linear cooling conditions the time, t, the temperature at any time, T, the initial temperature, T_0, and the cooling rate, ϕ, are related by the simple equation:

$$t = \frac{T_0 - T}{\phi} \qquad (4.7.)$$

Thus equation 4.7 allows for the conversion from one coordinate system to the other. Conversion curves, plotted as a function of time, are shown in Figures 4.47-4.50 for the

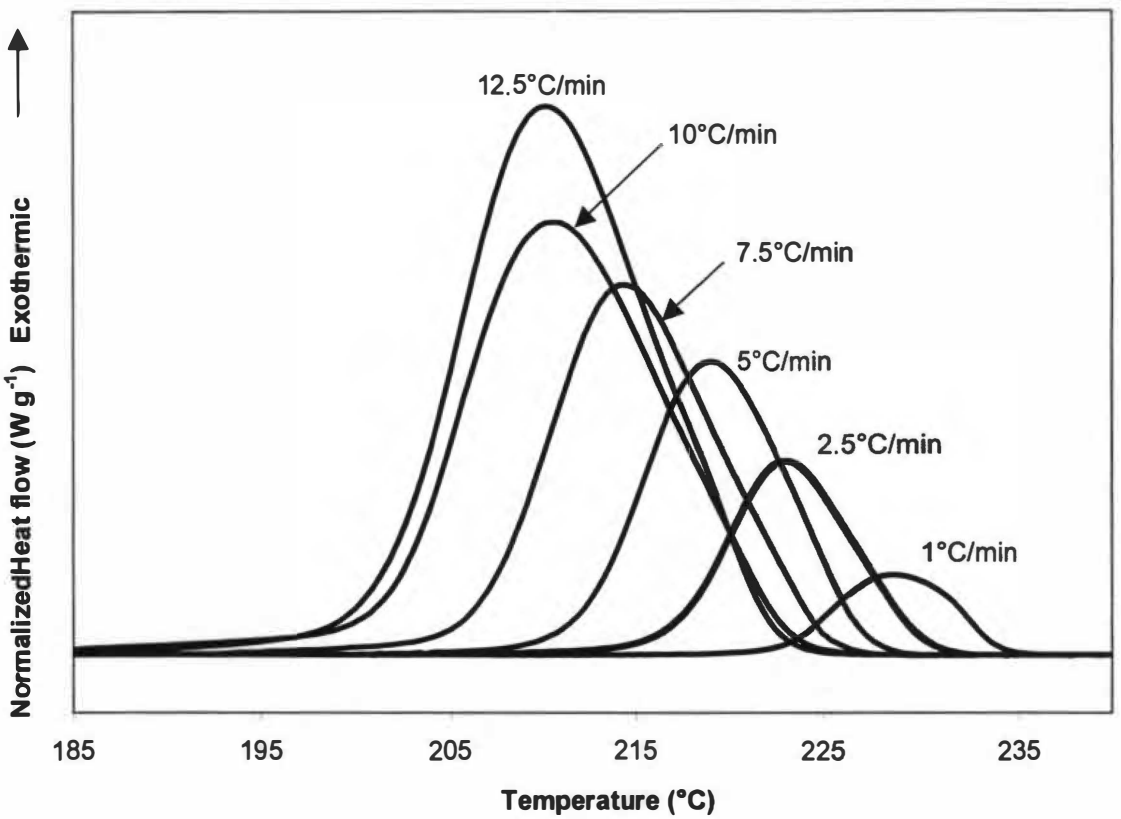

Figure 4.39: Typical Nonisothermal Crystallization Exotherms for PET Homopolymer at a Variety of Cooling Rates

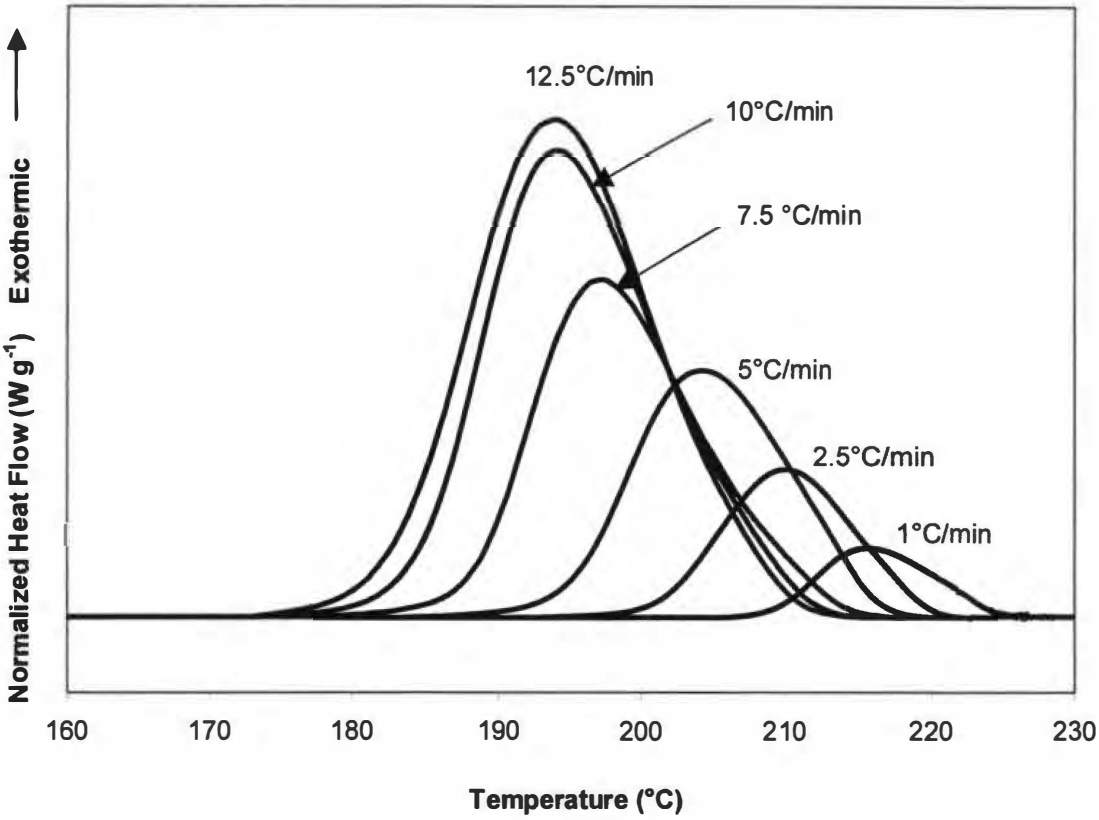

Figure 4.40: Typical Nonisothermal Crystallization Exotherms for PET-4 Copolymer at a Variety of Cooling Rates

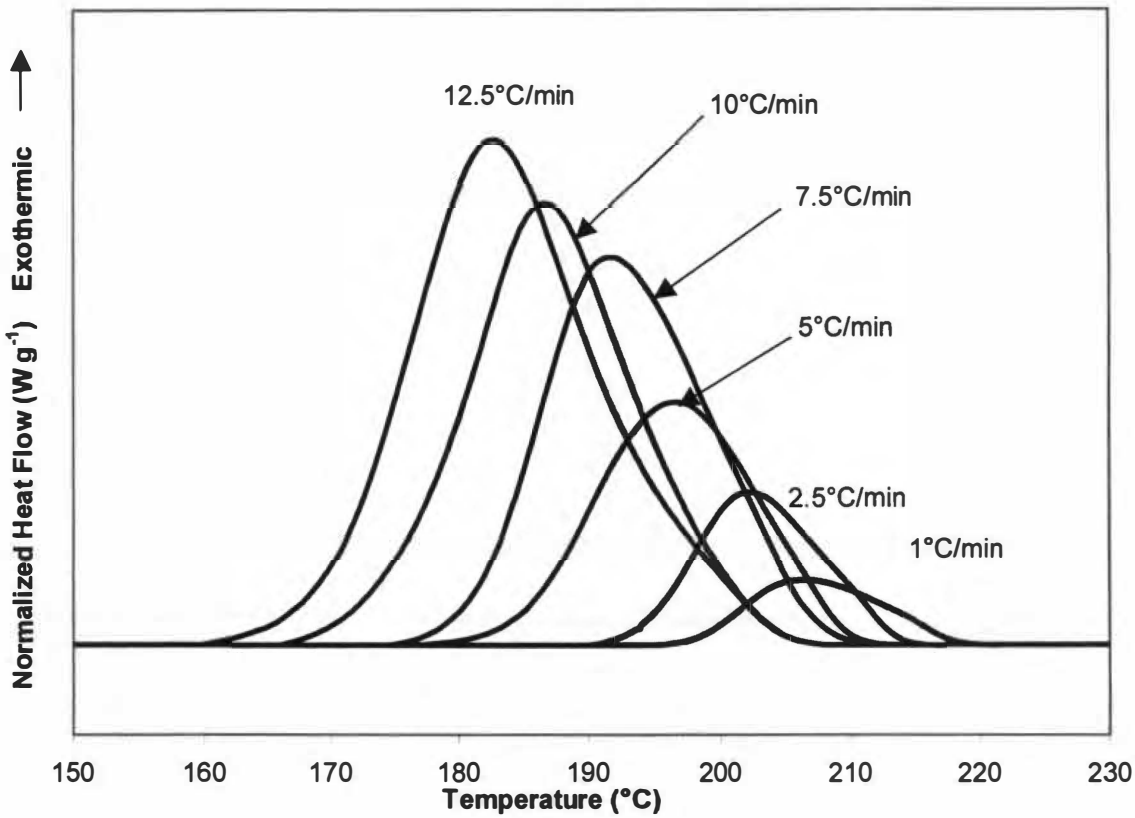

Figure 4.41: Typical Nonisothermal Crystallization Exotherms for PET-7 Copolymer at a Variety of Cooling Rates

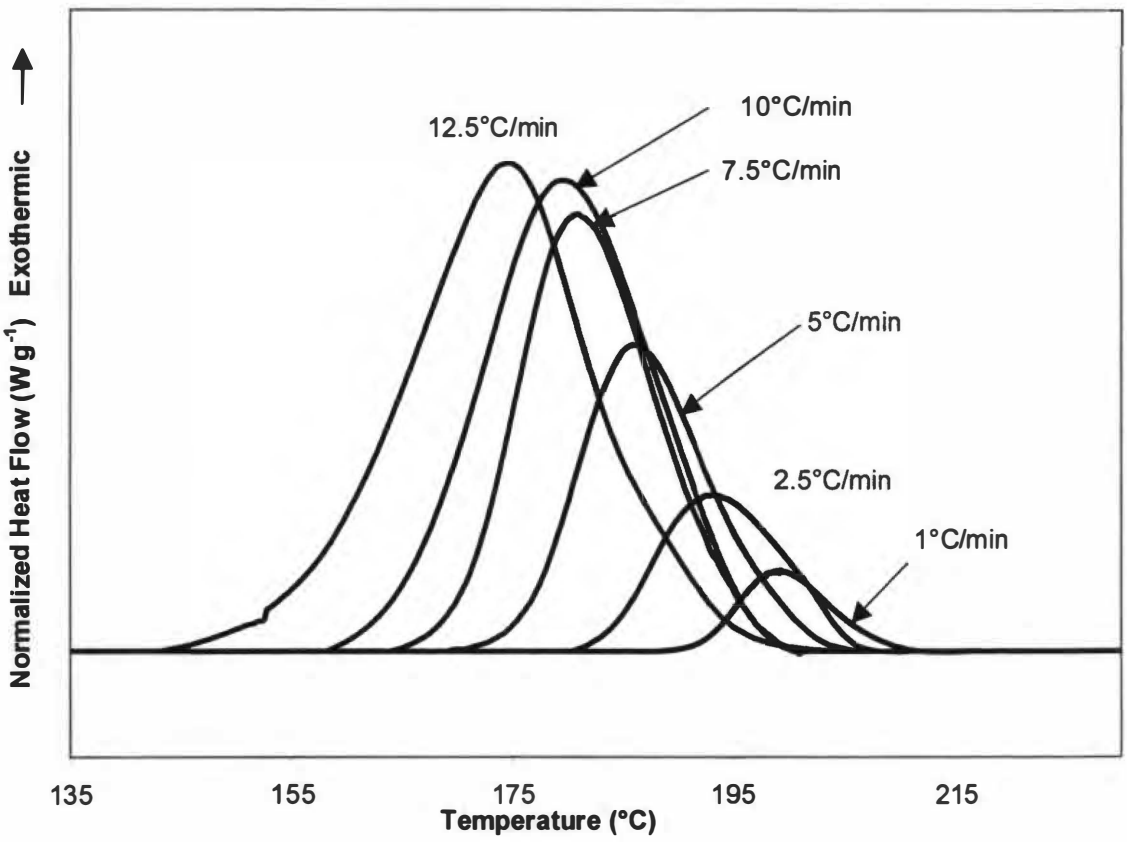

Figure 4.42: Typical Nonisothermal Crystallization Exotherms for PET-10 Copolymer at a Variety of Cooling Rates

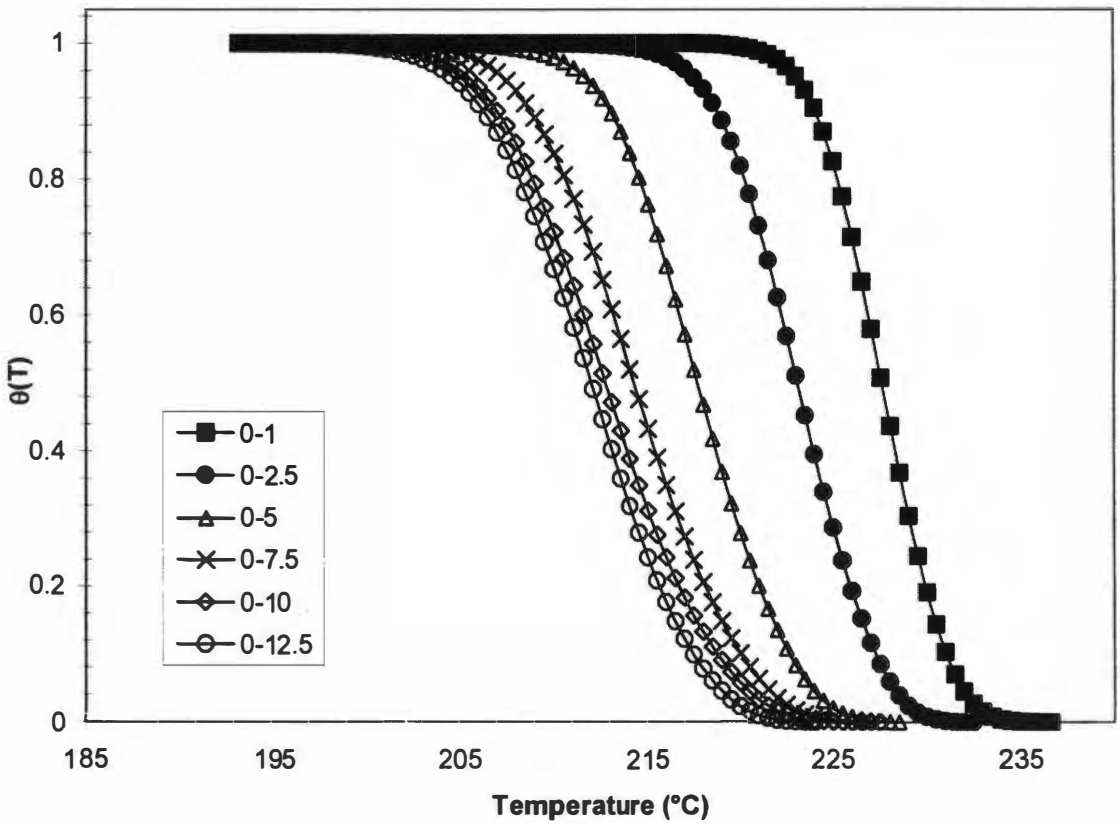

Figure 4.43: Nonisothermal DSC Crystallization Conversion Curves for PET Homopolymer

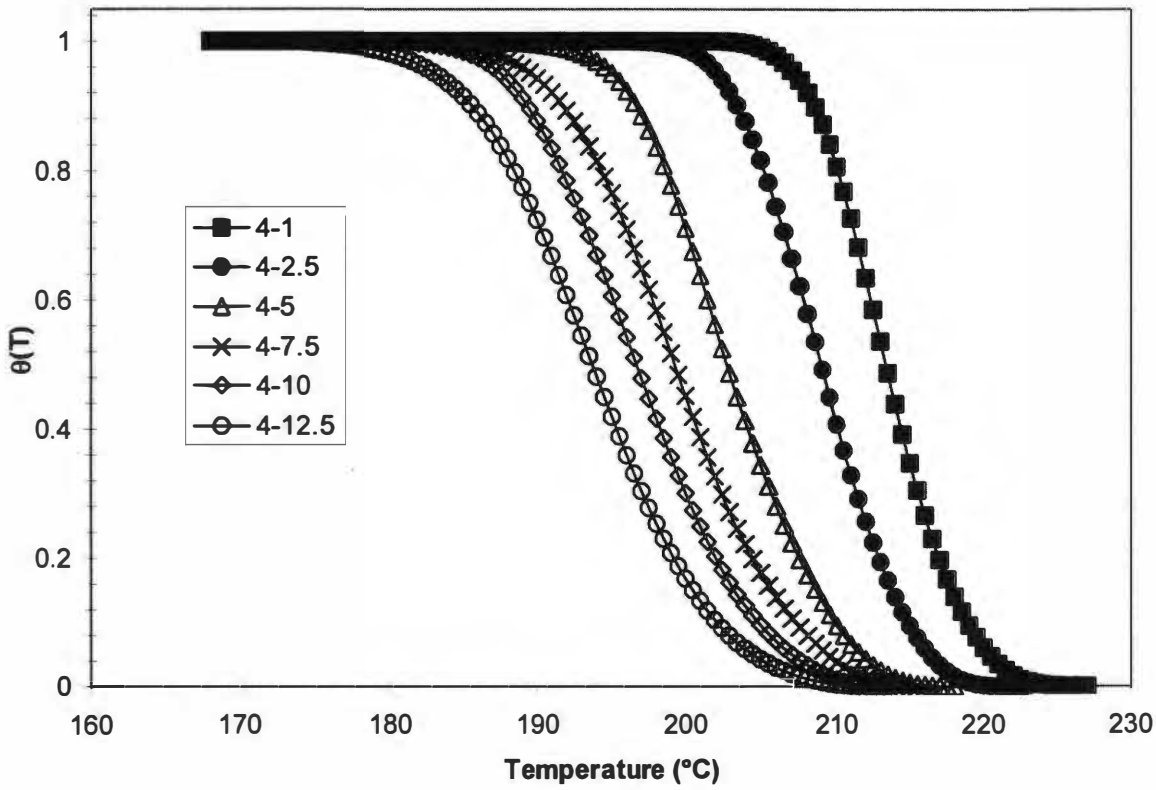

Figure 4.44: Nonisothermal DSC Crystallization Conversion Curves for PET-4 Copolymer

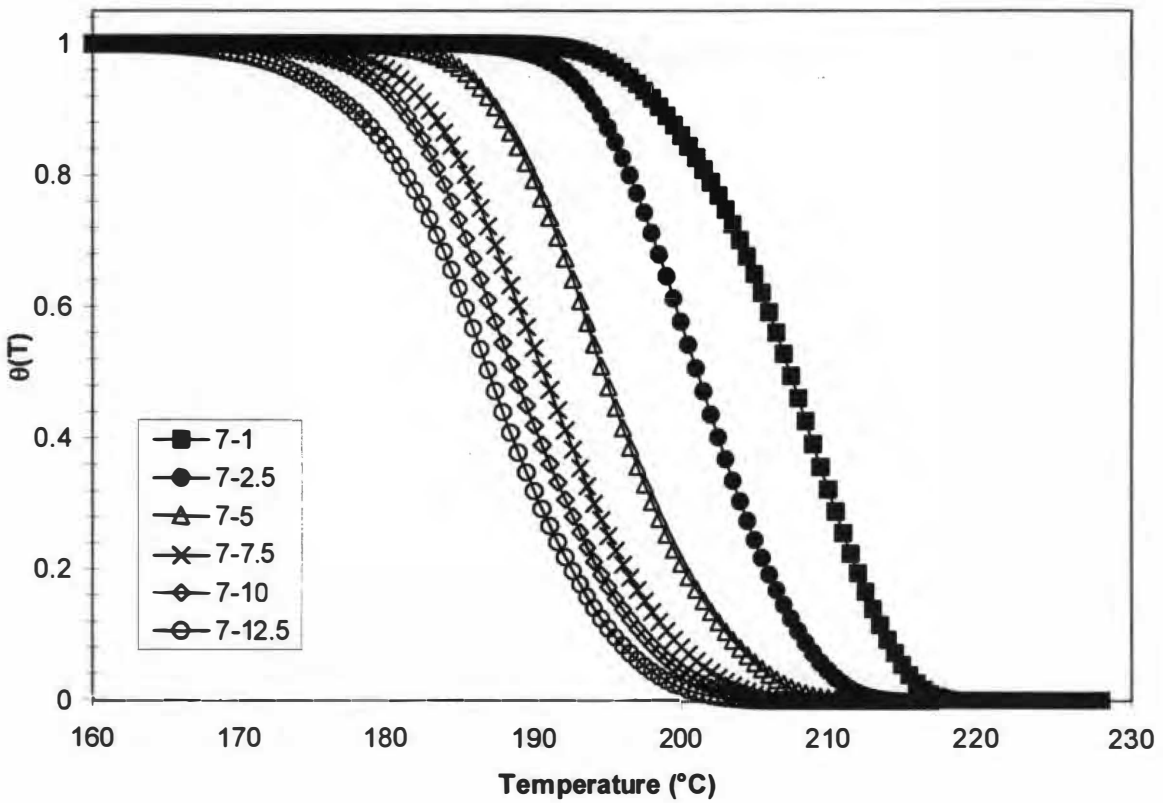

Figure 4.45: Nonisothermal DSC Crystallization Conversion Curves as a Function of Temperature for PET-7 Copolymer

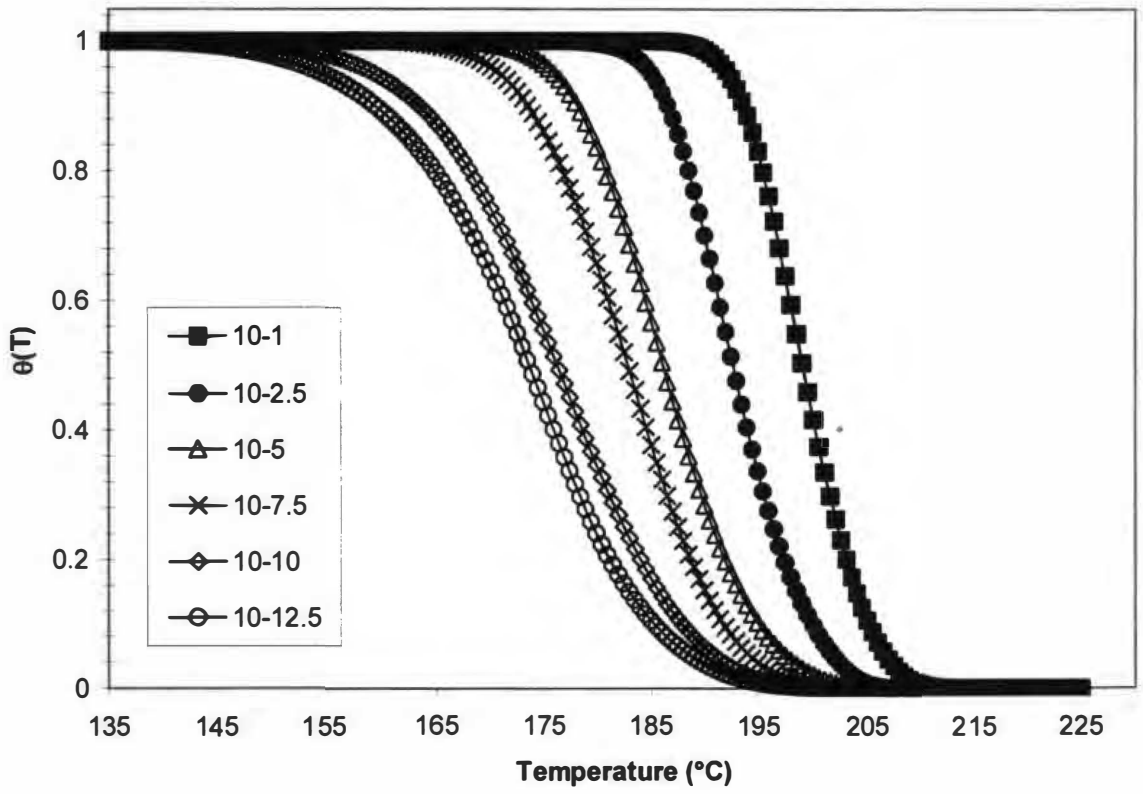

Figure 4.46: Nonisothermal DSC Crystallization Conversion Curves as a Function of Temperature for PET-10 Copolymer

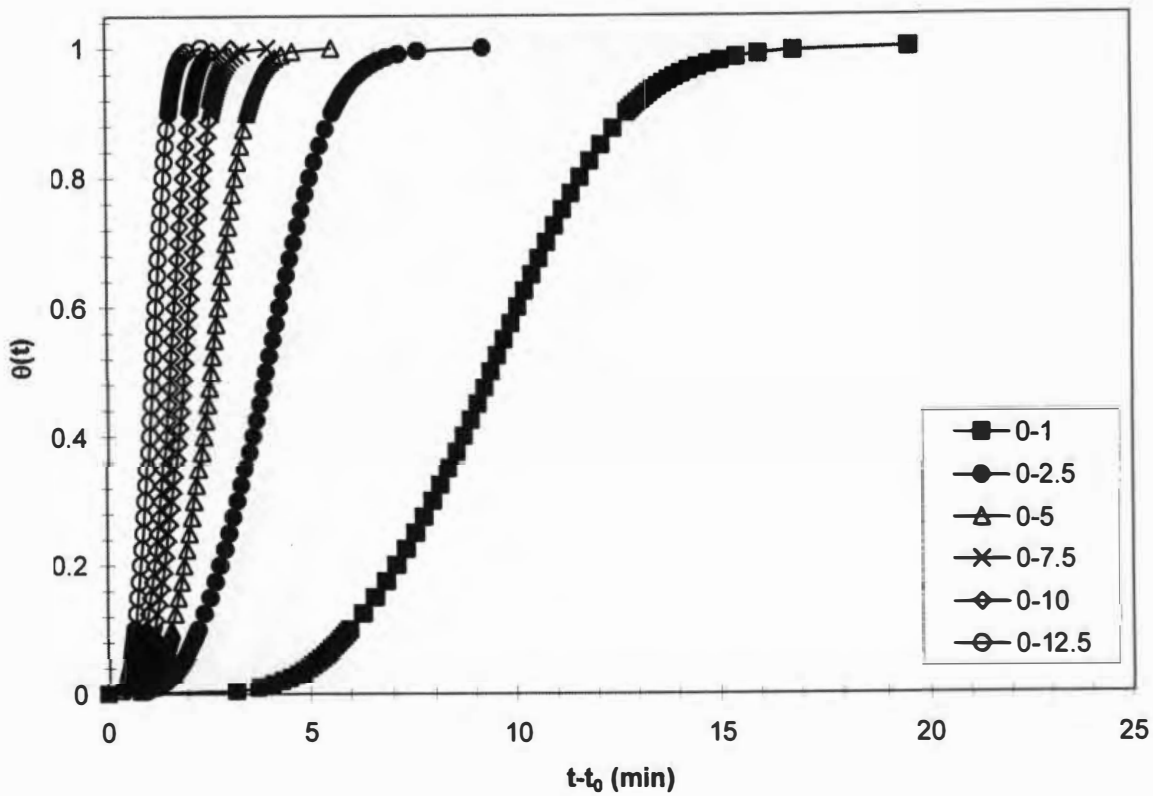

Figure 4.47: Nonisothermal DSC Crystallization Conversion Curves as a Function of Time for PET Homopolymer

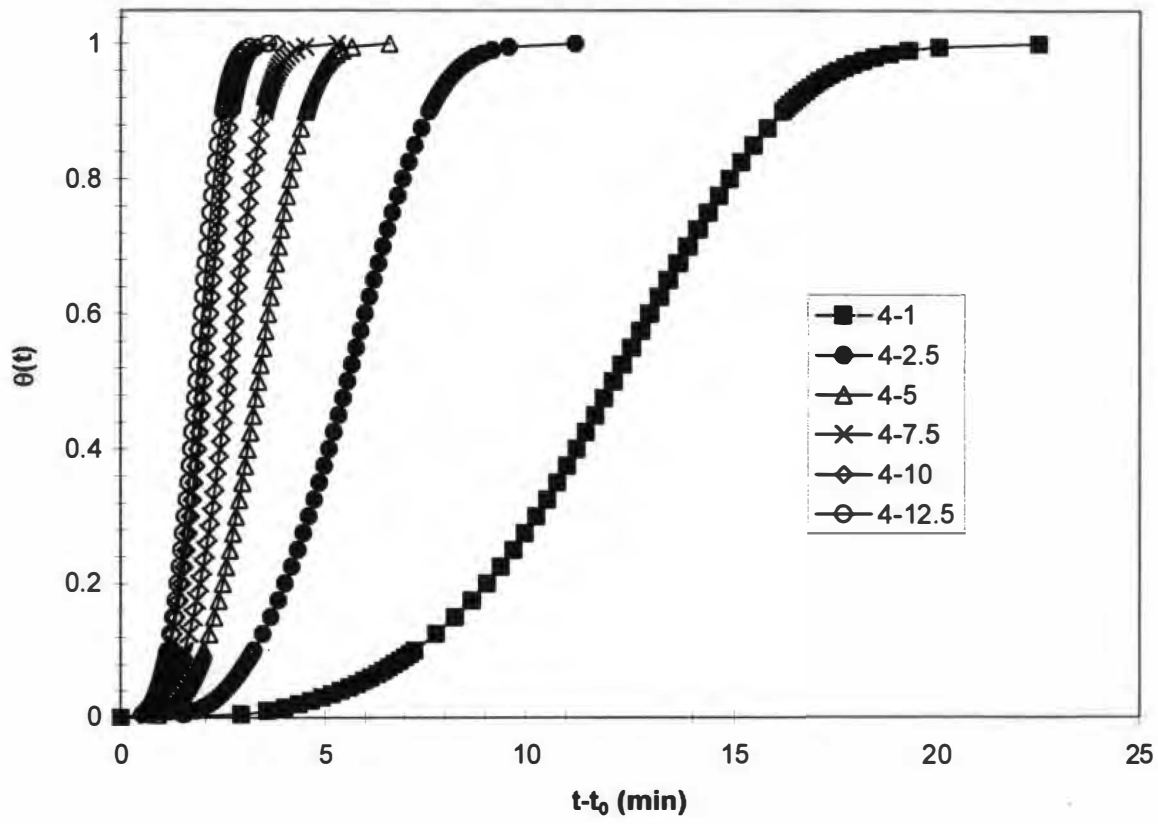

Figure 4.48: Nonisothermal DSC Crystallization Conversion Curves as a Function of Time for PET-4 Copolymer

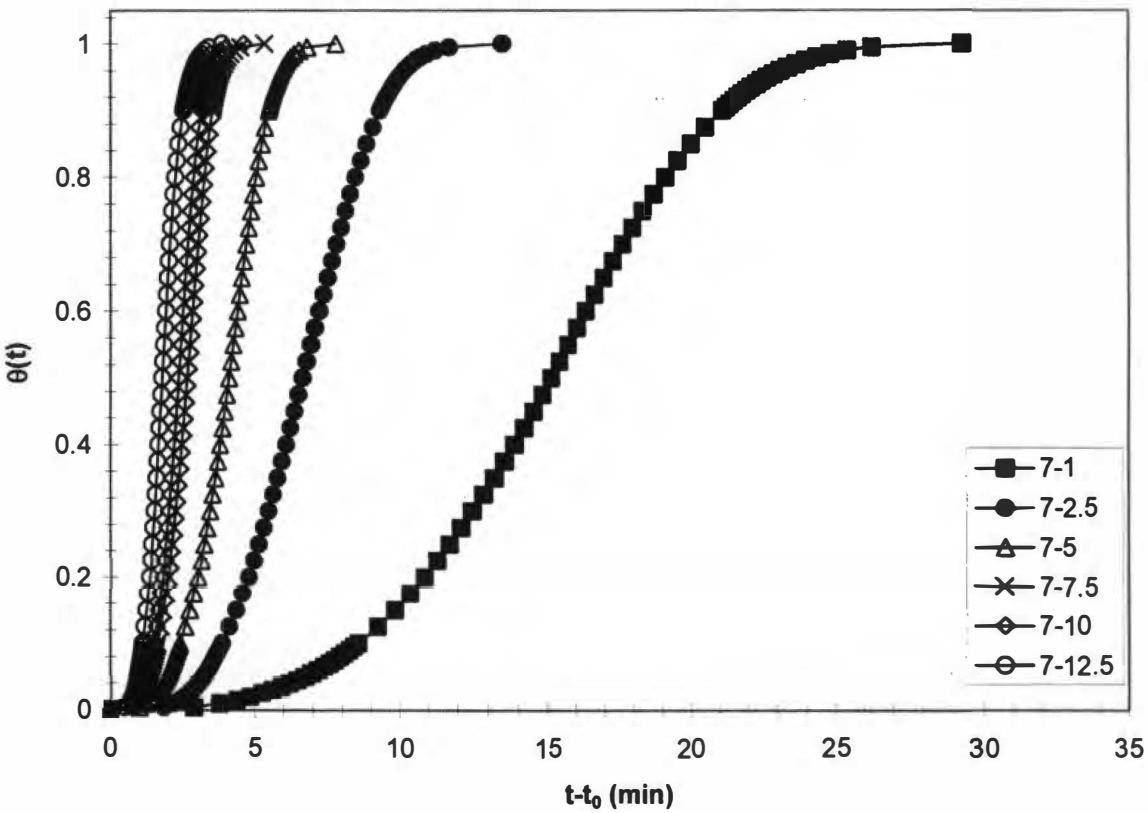

Figure 4.49: Nonisothermal DSC Crystallization Conversion Curves as a Function of Time for PET-7 Copolymer

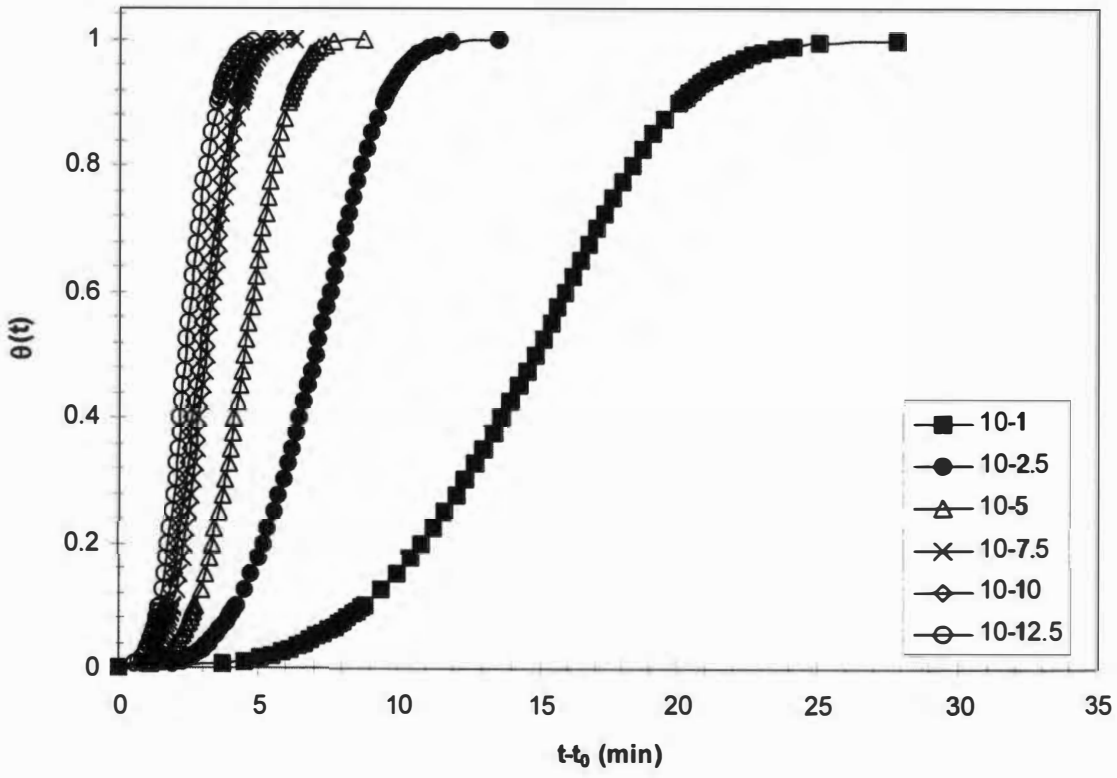

Figure 4.50: Nonisothermal DSC Crystallization Conversion Curves as a Function of Time for PET-10 Copolymer

four copolyesters and reveal the relationship between crystallization conversion rate and cooling rate. As would be expected, these plots suggest that the rate of crystallization increases with increasing cooling rate, likely due to the enhanced driving force for crystallization as the curves are shifted to lower temperatures.

In this analysis the Avrami equation (Equation 2.30) and the Ozawa equation (Equation 2.37) were used to analyze the experimental data, with the weight fraction of crystalline material at any time determined by the use of equation 4.2. It is important to note that neither the Ozawa equation nor the Avrami equation account for secondary crystallization. As a result, the Avrami equation was applied over the range $0.10 \leq \theta(t) \leq 0.80$, while the Ozawa equation was applied over the entire data. As suggested by Hillier (1965), a false value of the Avrami exponent, n, might be obtained if secondary crystallization is ignored in an isothermal experiment, but Ozawa argued that this effect is not serious in nonisothermal experiments since the slower secondary crystallization following the primary one becomes less significant at the lower temperature (Ozawa 1971). Even still, Ozawa's technique appears to be very sensitive as to where the beginning and endpoints are chosen. While the use of the DSC derivative is believed to aid in this effort, it should be noted that surely some experimental error is expected to occur near the limits of the crystallization process (i.e. when $\theta(T)$ is very near 0 and 1).

As before, the activation energy of crystallization was determined in this experiment. For the case of nonisothermal crystallization, this can be accomplished by using the Kissinger equation given by:

$$\ln\left(\frac{\phi}{T_p^{\,2}}\right) = \ln C + \frac{E_a}{RT_p} \qquad (4.8.)$$

where T_p is the peak crystallization temperature, R is the gas constant, and E_a is the activation energy. Equation 4.8 suggests that a plot of ln (ϕ/T_p^2) as a function of T_p^{-1} is predicted to yield a straight line with slope equal to the activation energy and y-intercept equal to a constant.

4.3.1.2. Analysis of Nonisothermal DSC Data

The results of this experiment are summarized in Table 4.7. One method of describing the nonisothermal crystallization kinetics of a polymer is to examine how the peak crystallization temperature is influenced by the cooling rate (CR). This is commonly examined by defining a time, t_p, which is the time that a sample spends in order to drop from a standard temperature in the melt (ca. 290°C) to the peak crystallization temperature, T_p. A plot of the reciprocal of t_p as a function of cooling rate is commonly used to describe the rate of nonisothermal crystallization. This is illustrated in Figure 4.51 where it is shown that a strong linear relationship exists between the reciprocal of t_p and the cooling rate. From this plot it is evident that the time to reach the peak temperature, at a given cooling rate, increases with increasing comonomer composition. These results would seem to indicate that, as with isothermal crystallization, the comonomer serves to impede crystallization under moderate nonisothermal crystallization conditions and that a stronger thermodynamic driving force is required with increasing MPDiol content.

The temperatures, $T_{0.01}$ and $T_{0.99}$, corresponding to the average temperatures at $\theta(T) = 0.01$ and 0.99 respectively have also been included in Table 4.7. Examination of

Table 4.7: Summary of Results for DSC Nonisothermal Crystallization Experiment

Sample	Cooling Rate (°C min^{-1})	$T_{0.1}$* (°C)	$T_{0.99}$* (°C)	ΔH_c (J/g)	t_p (min)*	T_p (°C)
PET	1	233.2	221.0	59.3±1.0	62.53	227.5±0.9
	2.5	229.8	214.9	57.7±0.5	26.85	222.9±0.7
	5	225.7	208.8	57.5±1.1	14.54	217.3±1.1
	7.5	223.4	204.6	56.7±1.8	10.15	213.9±1.7
	10	222.5	202.8	56.9±0.5	7.81	211.9±1.5
	12.5	220.9	201.5	56.8±1.5	6.28	211.5±0.5
PET-4	1	221.7	205.4	46.3±4.9	77.7	212.3±2.4
	2.5	218.4	199.9	52.6±0.6	32.77	208.1±1.6
	5	215.1	192.2	50.7±1.7	17.60	202.0±1.4
	7.5	212.4	186.1	50.3±0.4	12.20	198.5±1.7
	10	210.1	184.2	51.1±0.1	9.42	195.8±1.5
	12.5	208.1	176.9	49.8±0.9	7.74	193.3±0.9
PET-7	1	212.7	191.1	45.4±4.1	83.24	206.8±5.1
	2.5	212.2	189.6	48.1±4.3	35.77	200.6±1.2
	5	208.8	182.4	48.5±1.0	19.32	193.4±1.3
	7.5	203.8	178.0	48.2±1.1	13.37	189.7±1.5
	10	203.2	174.2	49.1±0.5	10.22	187.8±1.1
	12.5	201.5	168.8	48.3±0.5	8.23	187.1±0.1
PET-10	1	209.3	189.8	44.9±0.5	91.63	198.4±1.0
	2.5	204.7	181.9	46.1±0.7	39.33	191.7±1.8
	5	201.5	171.9	45.7±0.1	20.97	185.2±0.5
	7.5	198.3	166.0	45.9±0.5	14.24	183.2±0.3
	10	196.0	152.2	46.8±1.9	11.24	177.6±2.1
	12.5	194.5	146.3	48.6±0.5	9.18	175.3±0.8

* Calculated using equation 4.7.

NOTE: Limits based on +/-1 standard deviation

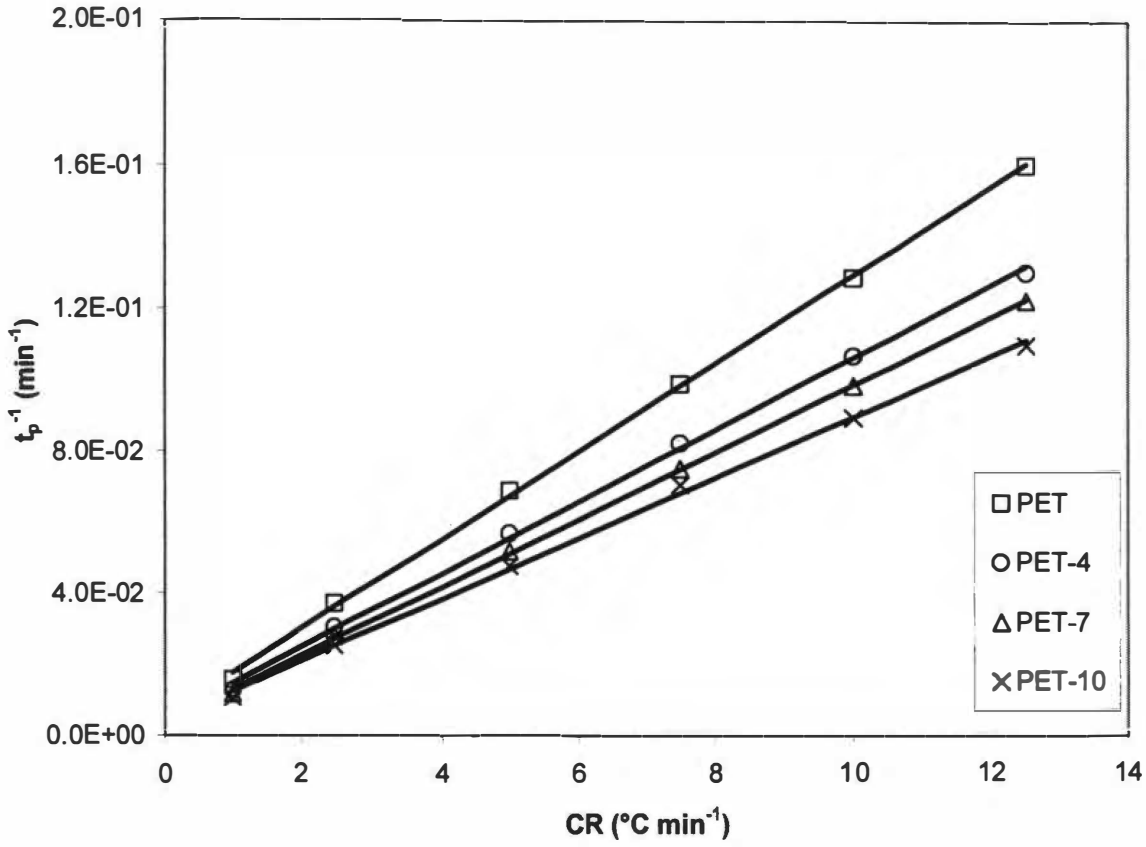

PET:	y = 1.23E-02x + 5.53E-03	R^2 = 0.9995
PET-4:	y = 1.01E-02x + 4.86E-03	R^2 = 0.9988
PET-7:	y = 9.44E-03x + 3.72E-03	R^2 = 0.9997
PET-10:	y = 8.51E-03x + 4.10E-03	R^2 = 0.9984

Figure 4.51: Plot of t_p^{-1} as a Function of Cooling Rate for Four Copolyesters

these quantities further suggests that the crystallization temperature range is shifted to lower temperatures with increasing cooling rate and comonomer concentration.

Figure 4.52 further demonstrates the effect of MPDiol on the nonisothermal crystallization kinetics by showing the relationship between the half time of crystallization ($t_{0.5}$-t_0) and the cooling rate for the four copolyesters. Again, it is evident that the comonomer serves to increase the half time of crystallization suggesting that once crystallization has started, the MPDiol comonomer again negatively influences the rate of crystallization. It should also be noted that the half time data in this figure appears to fit an exponential type curve reasonably well. As discussed earlier, this is to be expected since $t_{0.5}$ and the radial growth rate, G, are expected to be roughly proportional. This relationship is further illustrated in Figure 4.53 where the logarithm of the half time is plotted as a function of Cooling Rate for the four copolyesters. In this figure it is evident that the experimental data fits this logarithmic relationship quite well ($R^2 \approx 1$).

The peak temperatures for each of the four copolymers were also plotted as a function of the cube root of the cooling rate in accordance to that suggested by Lawton (1985). As is shown in Figure 4.54 the experimental data appeared to fit this model reasonably well. The intercept of the Lawton plot, which is related to the crystallization rate of the sample, showed a decrease with increasing MPDiol content, thus again suggesting that MPDiol impedes crystallization under nonisothermal conditions. This same effect was witnessed by Park and Lee (1995) for PET copolyesters containing 4,4'-bis[(4-carbo-2-hydroxyethoxy) phthalimido] diphenylmethane (BHEI).

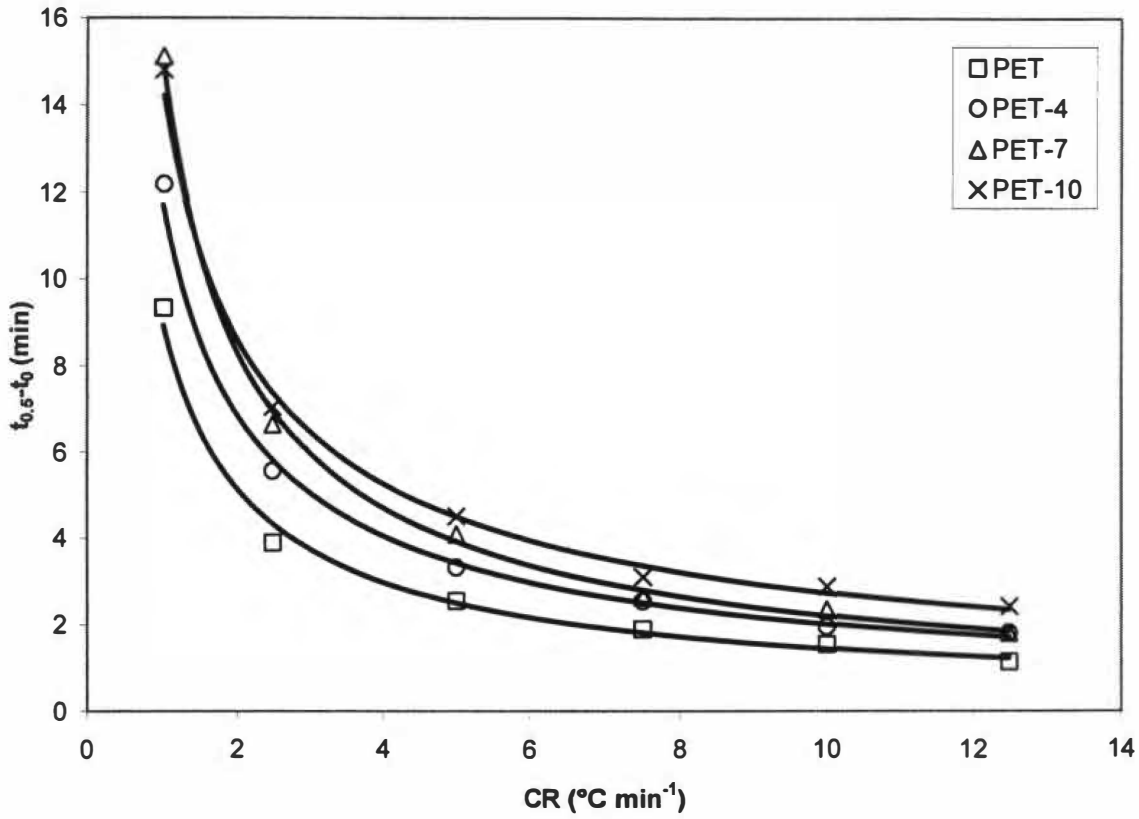

Figure 4.52: Plot of Half-time of Crystallization ($t_{0.5}$-t_0) as a Function of Cooling Rate for Four Copolyesters

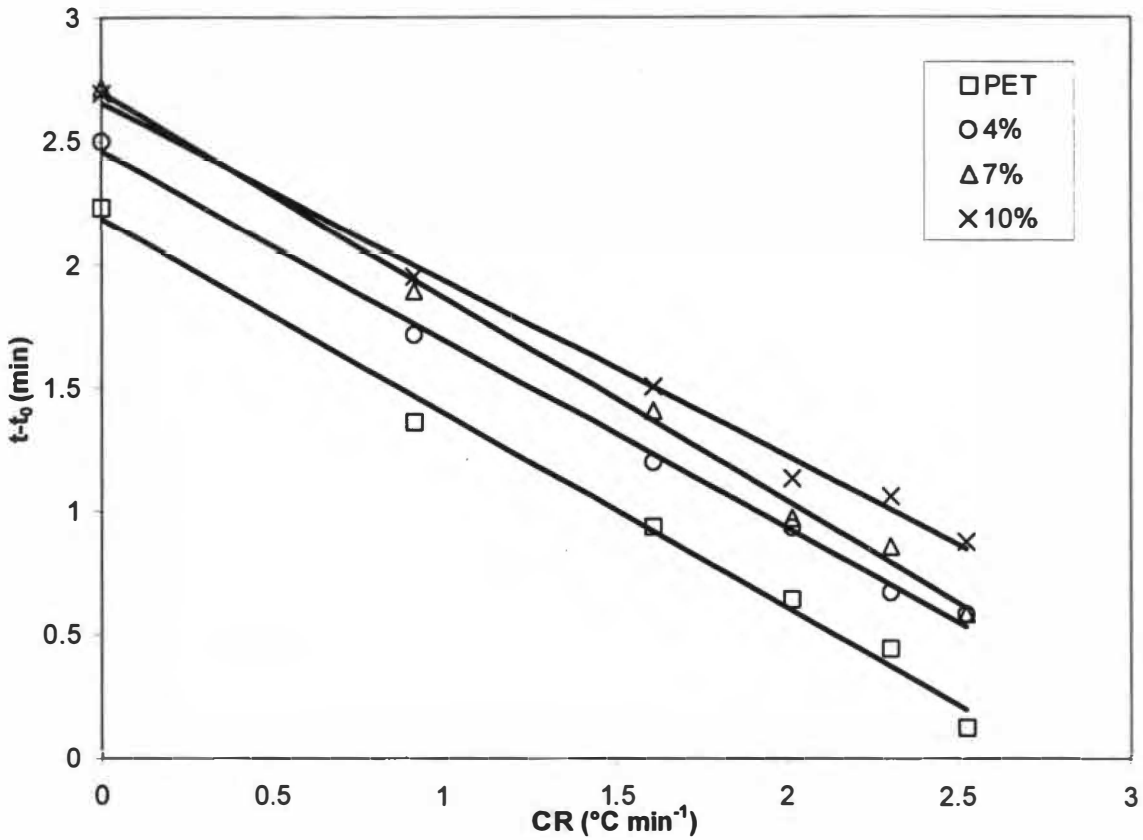

PET:	y = -0.7876x + 2.1909	R^2 = 0.991
PET-4:	y = -0.7612x + 2.4602	R^2 = 0.997
PET-7:	y = -0.8242x + 2.6965	R^2 = 0.996
PET-10:	y = -0.7131x + 2.6544	R^2 = 0.994

Figure 4.53: Logarithmic Plot of Half-time of Crystallization ($t_{0.5}$-t_0) as a Function of Cooling Rate for Four Copolyesters

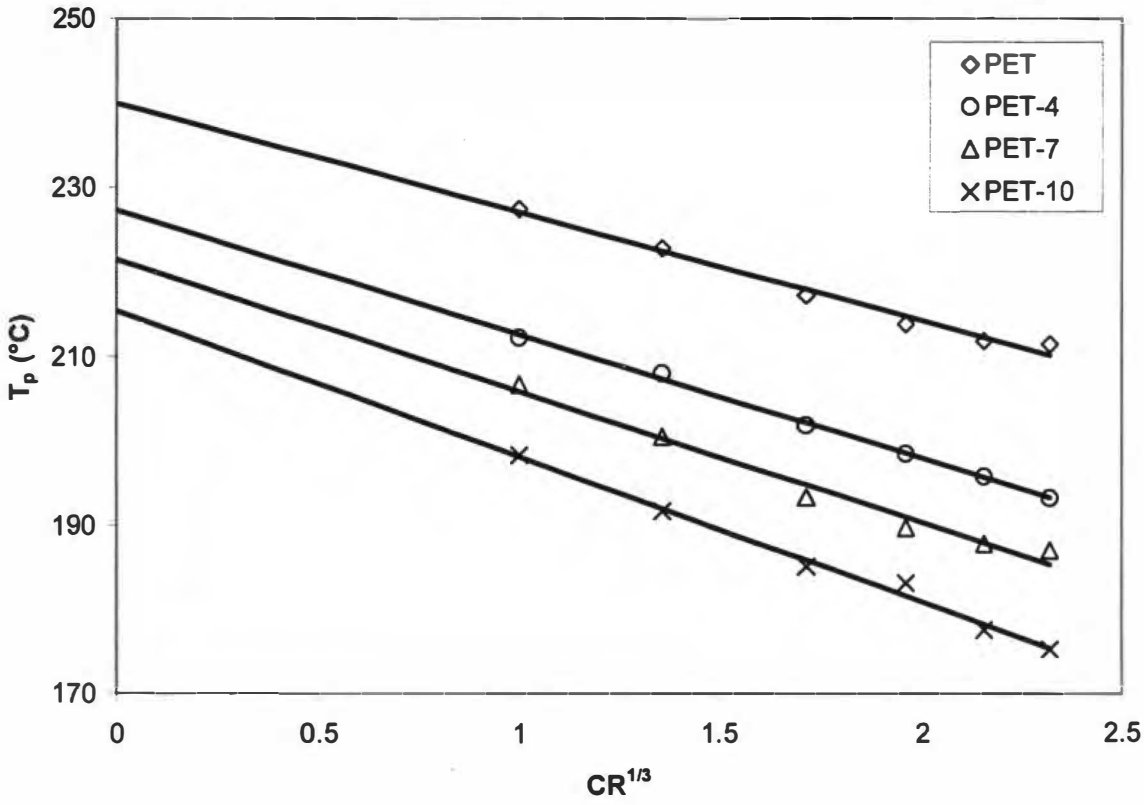

PET:	y = -12.788x + 239.87	R^2 = 0.983
PET-4:	y = -14.638x + 227.27	R^2 = 0.998
PET-7:	y = -15.558x + 221.46	R^2 = 0.976
PET-10:	y = -17.256x + 215.42	R^2 = 0.991

Figure 4.54: Lawton Plot for Four Materials

4.3.1.3. Avrami Analysis of Nonisothermal DSC Data

The results of the Avrami analysis for the nonisothermal crystallization were determined according to equations 2.30 and 2.32 and are listed in Table 4.8. The Avrami plots for the four copolymers are shown in Figures 4.55-4.58. All Avrami plots showed exceptional linearity ($R^2 \geq 0.99$) suggesting the predominance of primary crystallization over the specified range. These plots also quantitatively describe how the rate of crystallization increases with increasing cooling rate. This is more easily seen by examining Figure 4.59 where the Avrami rate constant, k, is plotted as a function of cooling rate. Here it is shown that the Avrami rate constant appears to be nearly equal for all four copolymers at the lowest cooling rate (1°C/min). However, as the cooling rate is increased it appears that the presence of MPDiol serves to reduce the rate of crystallization. This is to be somewhat expected in that at very low cooling rates there would be a sufficient amount of time for the necessary molecular rearrangement required for crystal formation while at higher cooling rates there is less time allowed for the macromolecules to form crystals.

As is illustrated in Figures 4.39-4.47, as the cooling rate is increased the crystallization process is shifted to lower temperatures. Additionally, because these materials were predicted to have different equilibrium melting temperatures, comparing them on the basis of cooling rate alone may not sufficiently describe the experimental data. This is illustrated in Figure 4.60 where the Avrami rate constant data is plotted as a function of peak crystallization temperature. This figure, unlike Figure 4.59 suggests that the incorporation of MPDiol has a significant impact on the rate of crystallization at a given temperature and that the trend is clearly that as MPDiol content increases, the rate

Table 4.8: Summary of Avrami Analysis for Nonisothermal Crystallization Using DSC for PET Copolymers

Sample	Cooling Rate (°C min^{-1})	n	k (min^{-n})	$t_{0.5} - t_0$ (min)	$k_{t_{0.5}}$ (min^{-n})
PET	1	4.06	7.82E-05	9.35	7.87E-05
	2.5	3.36	7.09E-03	3.91	7.08E-03
	5	3.90	1.78E-02	2.57	1.76E-02
	7.7	3.84	5.81E-02	1.91	5.76E-02
	10	3.92	1.21E-01	1.57	1.19E-01
	12.5	3.68	4.38E-01	1.14	4.35E-01
PET-4	1	3.84	4.79E-05	12.18	4.69E-05
	2.5	3.52	1.68E-03	5.57	1.65E-03
	5	3.62	9.03E-03	3.33	8.91E-03
	7.7	3.64	2.30E-02	2.56	2.28E-02
	10	3.60	6.14E-02	1.97	6.02E-02
	12.5	4.08	6.25E-02	1.80	6.24E-02
PET-7	1	3.43	6.33E-05	15.12	6.25E-05
	2.5	3.44	1.03E-03	6.66	1.03E-03
	5	3.68	3.91E-03	4.10	3.82E-03
	7.7	4.03	1.36E-02	2.66	1.35E-02
	10	4.28	1.73E-02	2.37	1.72E-02
	12.5	4.03	6.31E-02	1.81	6.40E-02
PET-10	1	3.73	3.03E-05	14.80	2.99E-05
	2.5	3.76	4.59E-04	7.06	4.51E-04
	5	3.81	2.23E-03	4.52	2.20E-03
	7.7	3.88	8.28E-03	3.12	8.39E-03
	10	3.63	1.41E-02	2.91	1.44E-02
	12.5	3.75	2.44E-02	2.42	2.53E-02

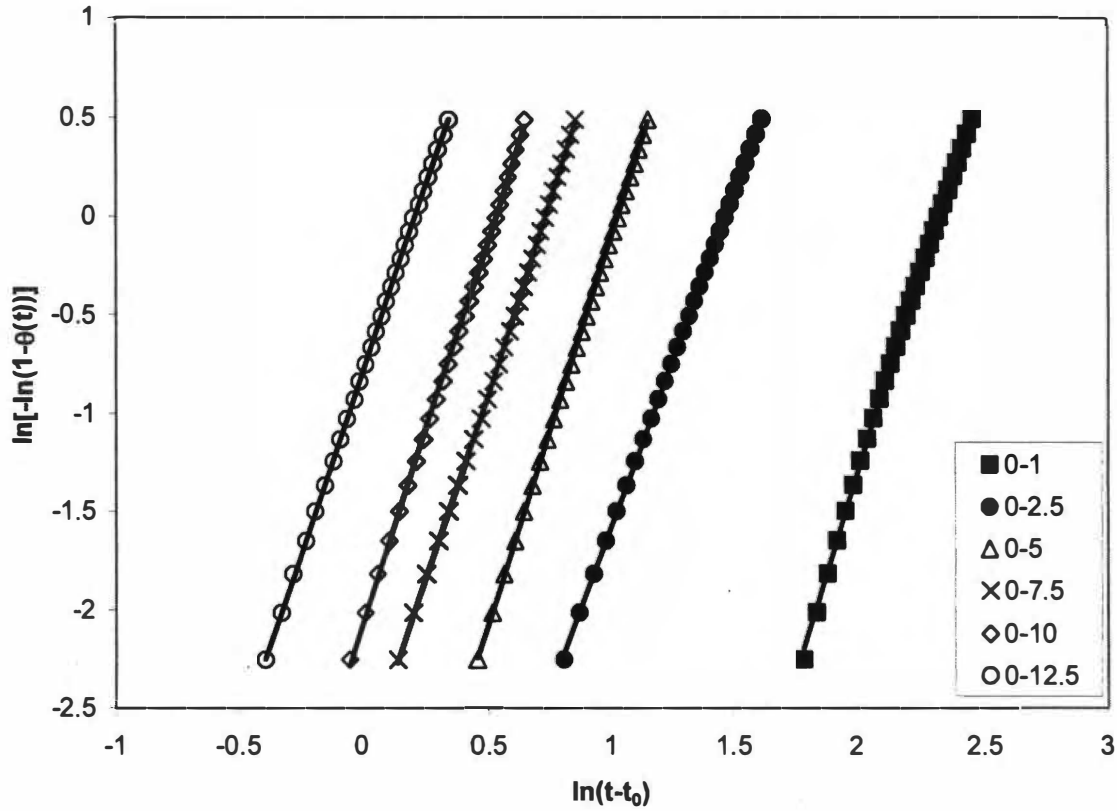

1°C/min:	y = 4.0635x - 9.4566	R^2 = 0.9995
2.5°C/min:	y = 3.3604x - 4.9489	R^2 = 0.9999
5°C/min:	y = 3.8968x - 4.0312	R^2 = 0.9999
7.5°C/min:	y = 3.8357x - 2.8452	R^2 = 0.9998
10°C/min:	y = 3.9187x - 2.1109	R^2 = 0.9994
12.5°C/min:	y = 3.6844x - 0.8261	R^2 = 0.9999

Figure 4.55: Avrami Plot for Nonisothermal Crystallization of PET Homopolymer Under Moderate Cooling Conditions

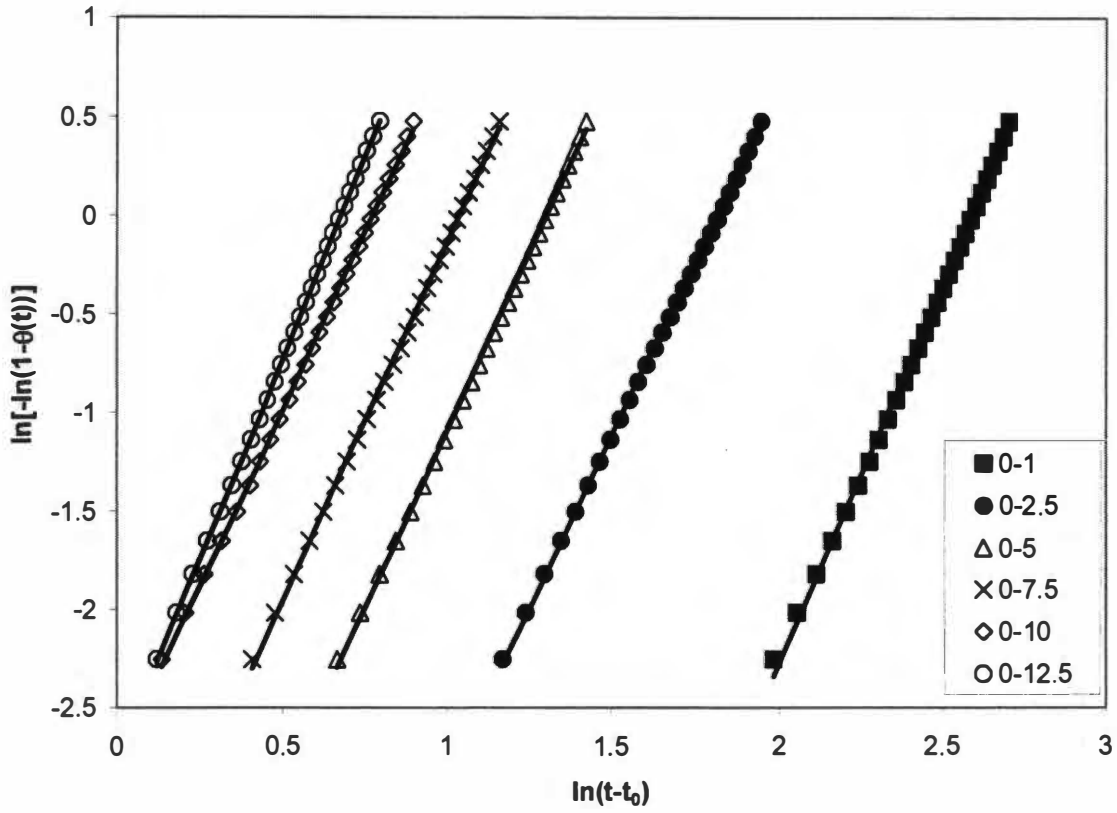

1°C/min:	y = 3.8405x - 9.9462	R^2 = 0.9982
2.5°C/min:	y = 3.5154x - 6.3904	R^2 = 0.9995
5°C/min:	y = 3.6172x - 4.7069	R^2 = 0.9994
7.5°C/min:	y = 3.6374x - 3.771	R^2 = 0.9995
10°C/min:	y = 3.6032x - 2.791	R^2 = 0.9995
12.5°C/min:	y = 4.0814x - 2.7723	R^2 = 0.9999

Figure 4.56: Avrami Plot for Nonisothermal Crystallization of PET-4 Copolymer Under Moderate Cooling Conditions

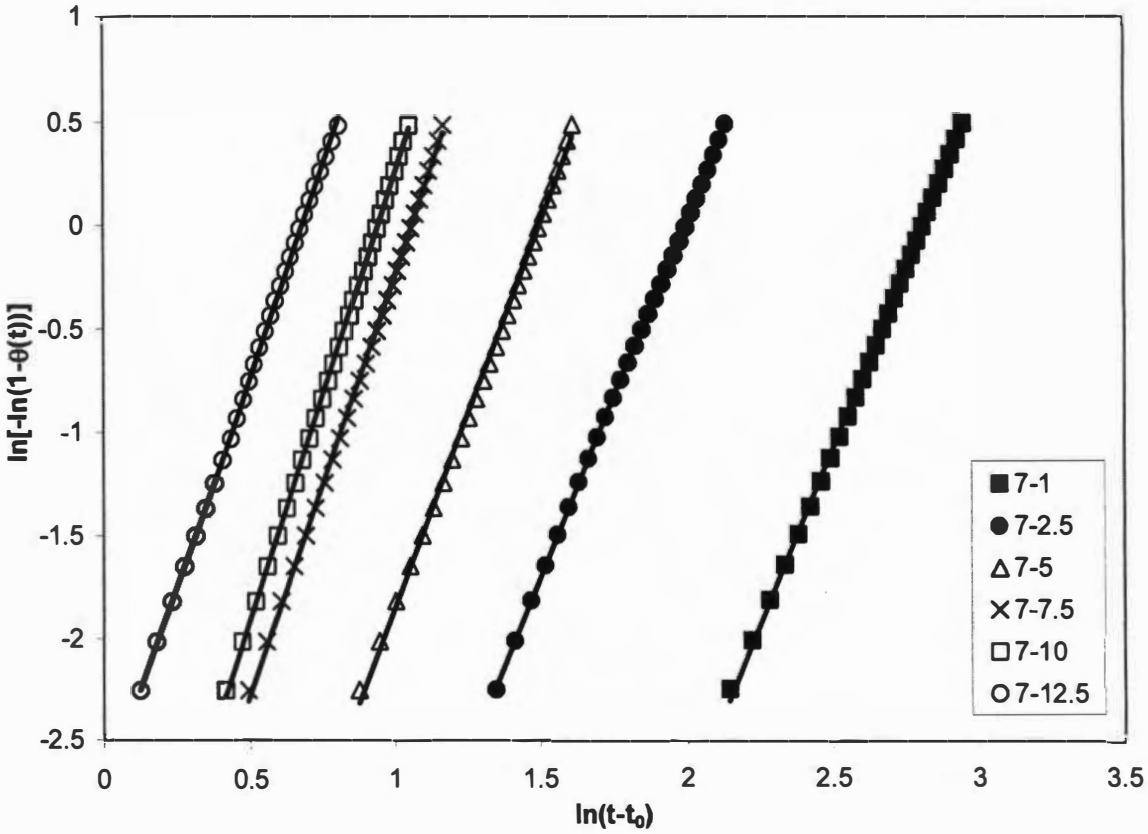

1°C/min:	y = 3.4292x - 9.6683	R^2 = 0.9993
2.5°C/min:	y = 3.4365x - 6.8755	R^2 = 0.9999
5°C/min:	y = 3.6845x - 5.5436	R^2 = 0.9985
7.5°C/min:	y = 4.0274x - 4.2944	R^2 = 0.9993
10°C/min:	y = 4.2798x - 4.0544	R^2 = 0.9997
12.5°C/min:	y = 4.0289x - 2.7635	R^2 = 0.9997

Figure 4.57: Avrami Plot for Nonisothermal Crystallization of PET-7 Copolymer Under Moderate Cooling Conditions

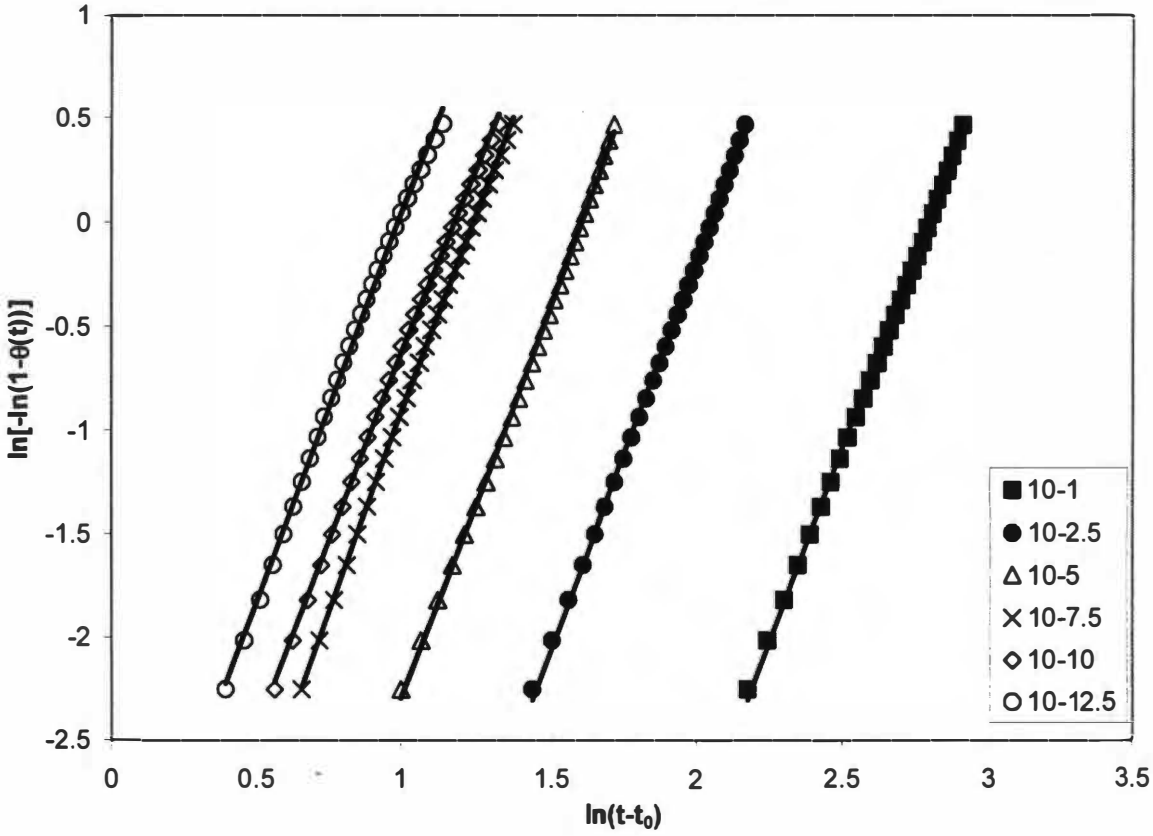

1°C/min: $y = 3.7303x - 10.404$ $R^2 = 0.9992$

2.5°C/min: $y = 3.7551x - 7.6856$ $R^2 = 0.9990$

5°C/min: $y = 3.8144x - 6.1057$ $R^2 = 0.9993$

7.5°C/min: $y = 3.8793x - 4.7941$ $R^2 = 0.9998$

10°C/min: $y = 3.6289x - 4.259$ $R^2 = 0.9992$

12.5°C/min: $y = 3.7519x - 3.7125$ $R^2 = 0.9984$

Figure 4.58: Avrami Plot for Nonisothermal Crystallization of PET-10 Copolymer Under Moderate Cooling Conditions

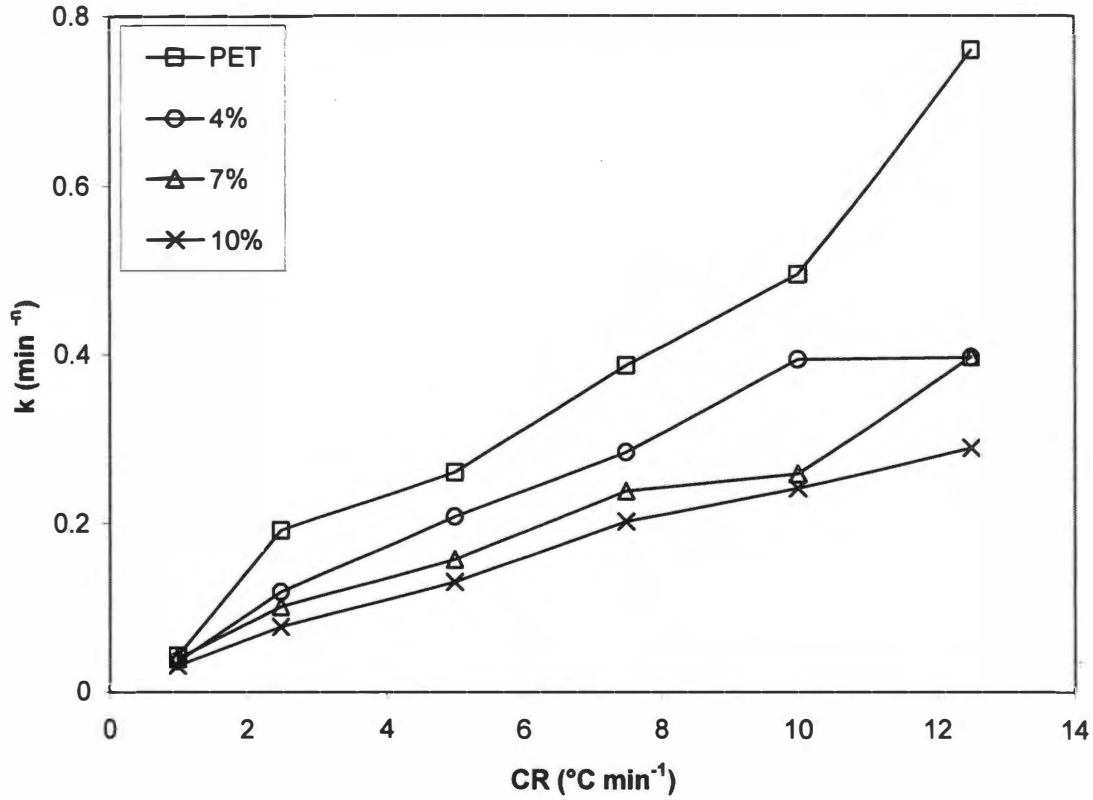

Figure 4.59: Plot of Avrami Rate Constant as a Function of Cooling Rate for Four Copolymers Under Moderate Cooling Conditions

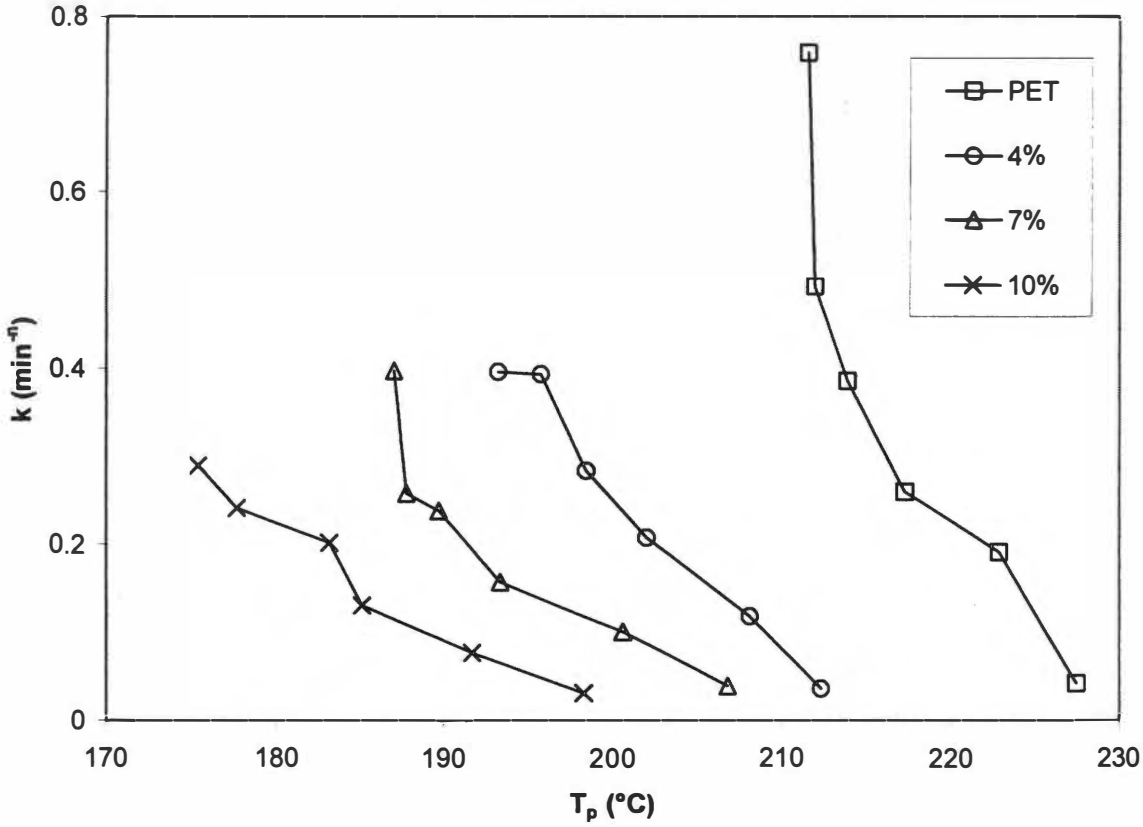

Figure 4.60: Plot of Avrami Rate Constant as a Function of Peak Crystallization Temperature, T_p, for Four Copolymers Under Moderate Cooling Conditions

of crystallization at a particular temperature decreases. As is shown in Figure 4.61 even as a function of undercooling (defined in this case as $\Delta T=T_p-T_m^0$) these data would suggest that an increase in MPDiol concentration results in a decrease in the rate of crystallization. Note also the strong similarity between Figures 4.59 and 4.60 implying that the undercooling and cooling rate are both related to the Avrami rate constant in a very similar manner.

The Avrami exponents in this experiment appear to range from about 3.4 -4.3 for the materials tested. Assuming spherical, three-dimensional growth this suggests the existence of homogeneous nucleation and interface growth control. This is to be completely expected for the three copolyesters tested. However, the fact that n is nearly equal to 4 for PET homopolymer is somewhat unexpected since this material is known to contain $Ti0_2$, which is believed to enhance the rate of nucleation of PET. The fact that n is not equal to 3 (expected for three dimensional spherical growth with heterogeneous nucleation) might suggest that under nonisothermal conditions the nucleation effect of $Ti0_2$ is minimal, even under these moderate cooling conditions.

The Avrami index also appears to decrease with increasing temperature. This might be explained in that as the temperature of crystallization is lowered (a consequence of increasing cooling rate) the position on the growth rate curve, such as that shown in Figure 2.6, is shifted to the left. Thus with decreasing temperature it is expected that the rate of diffusion may become more of a factor thus causing n to be shifted from 4.0 to 3.0 when diffusion control becomes dominant. Additionally, Equations 2.5 and 2.30 are really most appropriately applied under isothermal conditions. Under even moderate

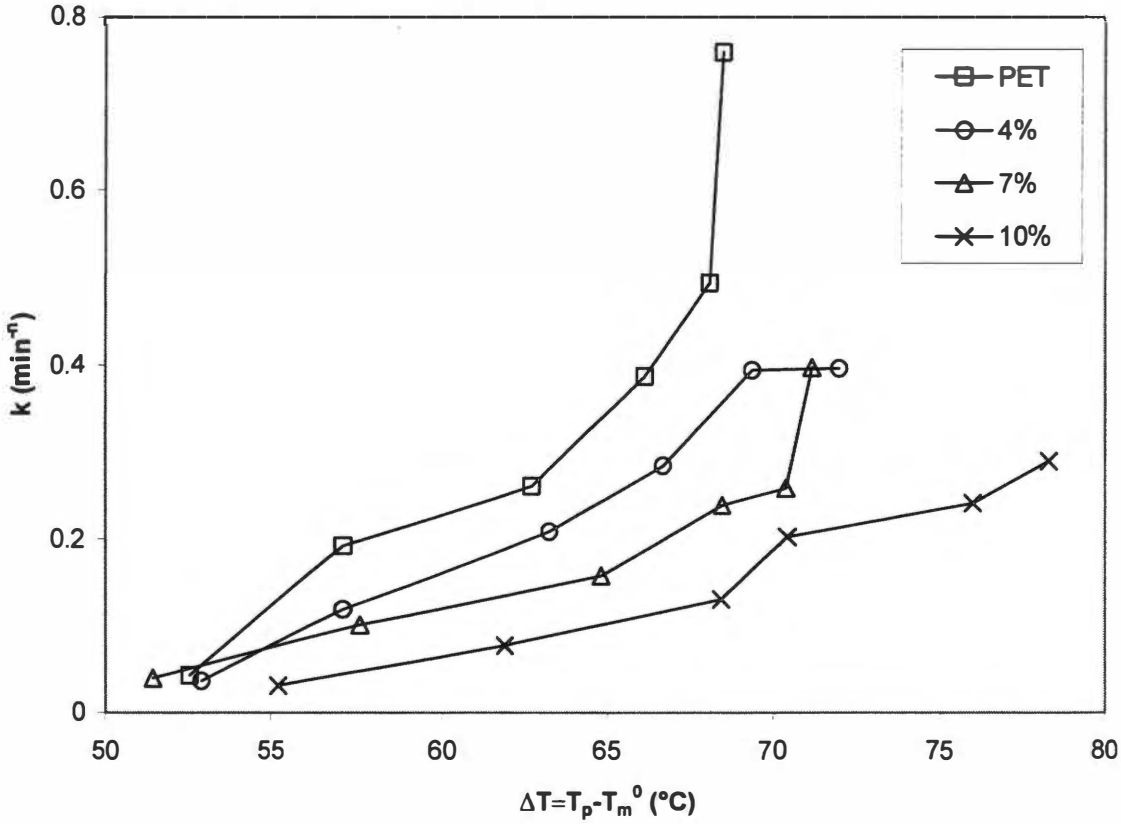

Figure 4.61: Plot of Avrami Rate Constant as a Function of Undercooling ($\Delta T=T_p-T_m^0$) for Four Copolymers Under Moderate Cooling Conditions

conditions it is not necessarily expected that the growth rates would strictly follow the linear relationship predicted by these equations. As a result, some error in the determination of the value of the Avrami exponent might be expected. This may have something to do with the fact that the polymers are being crystallized nonisothermally and therefore the possibility of forming spherulites, and consequently lamellae, of different sizes is more likely than during isothermal experiments. Nevertheless, it should be noted that the values obtained in this experiment seem to better predict what is believed to be the actual morphology of these polymers than that obtained in the isothermal experiment described earlier.

As mentioned earlier, the activation energy was determined by the use of the Kissinger equation (Equation 4.8.). The plot used to determine the activation energies of crystallization for the four materials is shown in Figure 4.62. Here it is evident that the experimental data fit the Kissinger equation reasonably well with a correlation coefficient ranging from 0.97 – 0.99. What is interesting to note from these data is that, although these values are significantly lower in magnitude than that determined from the isothermal crystallization data, they appear to follow much the same trend. This is illustrated in Figure 4.63 where again it is shown that PET homopolymer has the lowest (i.e. most negative) activation energy and therefore is predicted to be the most kinetically favorable at a given temperature (or cooling rate). These data appears to support the claim that the presence of MPDiol results in a less kinetically favorable situation. These data also seem to suggest that there is nearly a linear relationship between MPDiol concentration and activation energy.

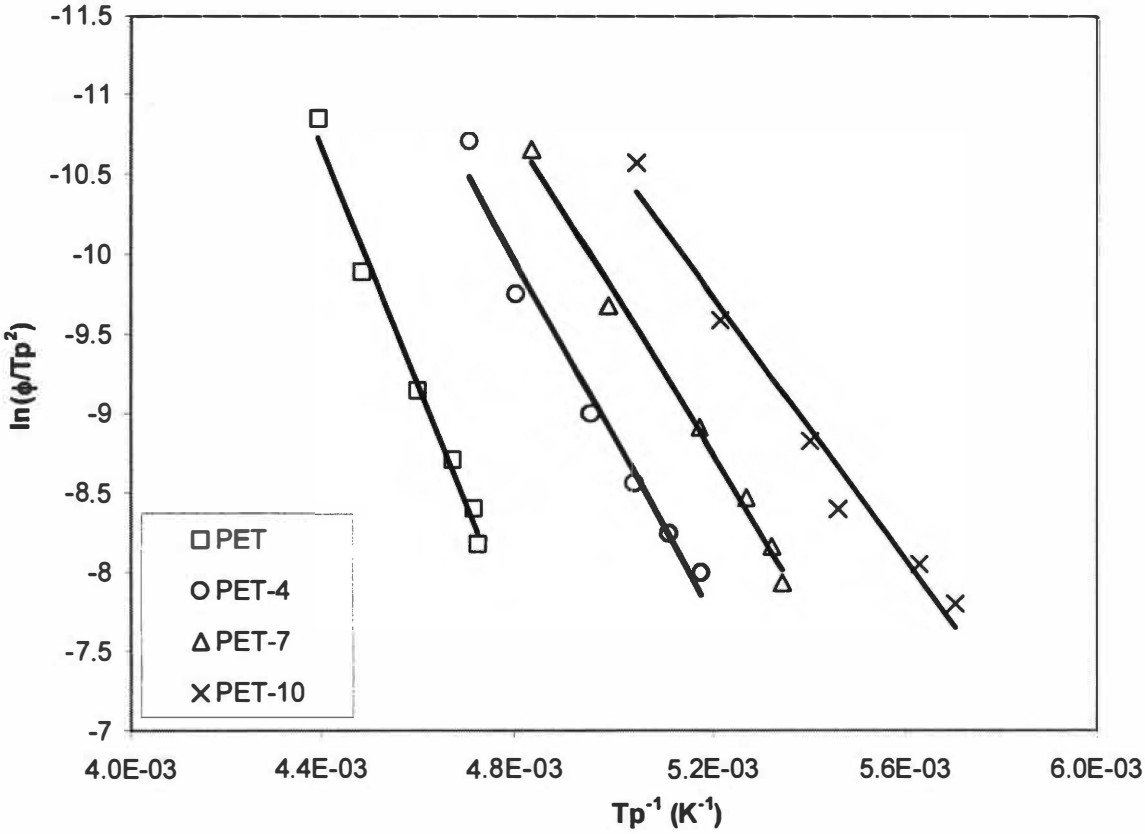

PET:	y = 7481.2x - 43.624	$R^2 = 0.989$
PET-4:	y = 5671.6x - 37.206	$R^2 = 0.976$
PET-7:	y = 5037.7x - 34.947	$R^2 = 0.992$
PET-10:	y = 4127.7x - 31.205	$R^2 = 0.973$

Figure 4.62: Plot of Nonisothermal DSC Data According to the Kissinger Equation to Determine the Activation Energy of Crystallization

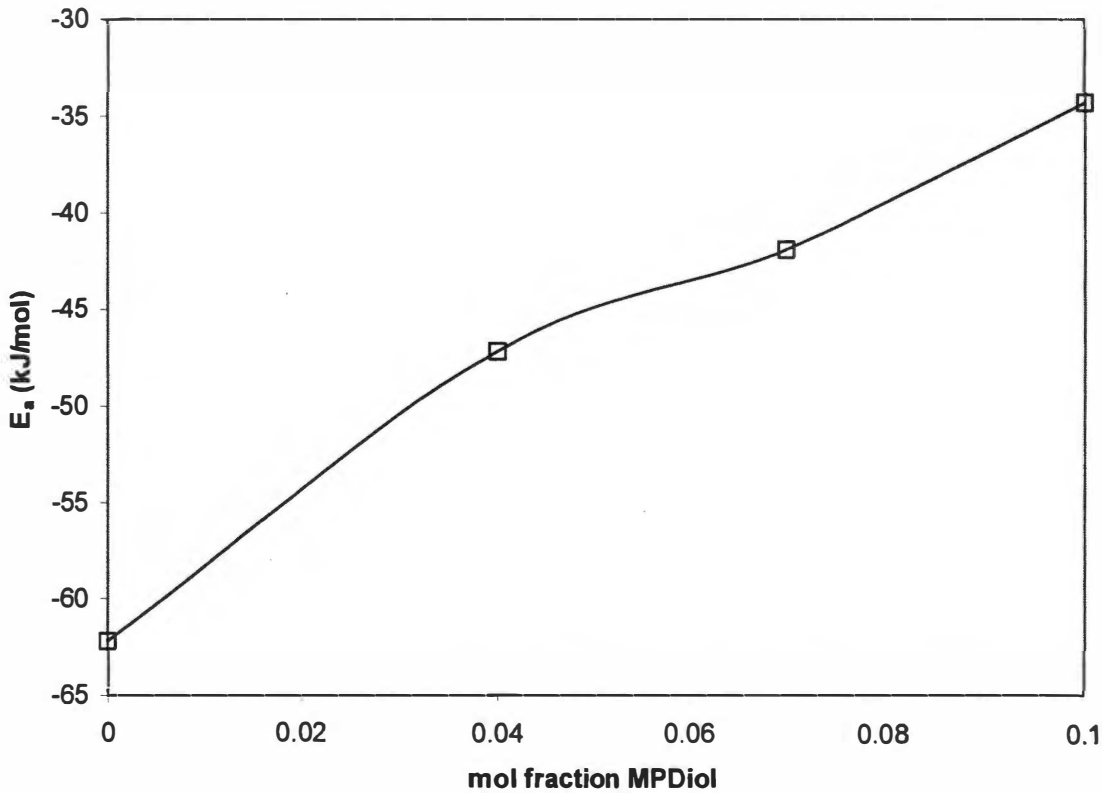

Figure 4.63: Plot of Activation Energy Determined Using the Kissinger Equation as a Function of Comonomer Concentration

4.3.1.4. Ozawa Analysis of Nonisothermal DSC Data

In addition to the Avrami analysis, an Ozawa analysis was also performed to examine the experimental data. Table 4.9 summarizes the results of this experiment, with Figures 4.64-4.67 showing the Ozawa plots for these four materials. It is important to note that the Ozawa equation was applied only over the data where three or more data points were available to generate a trend line to ensure a higher degree of data precision. In addition the data reported here was taken only over a temperature range that would allow for a direct comparison of these four materials. Even with these conditions applied the Ozawa plot did not show exceptionally good linearity. One source of this nonlinearity may be due to experimental error associated with sample variation. As would be expected, several curves were obtained for each copolyester at a particular cooling rate with the resulting data averaged and examined using equation 2.38. However, variation in the onset and endset of crystallization, as well as experimenter bias, may have introduced some error in the data analysis.

Since the Ozawa equation is really just an extension of the Avrami equation specifically derived for the case of nonisothermal crystallization it is reasonable to expect that the exponents n and n_0 should correlate somewhat well with one another. However this does not appear to be the case. It is interesting to note however that the values of n_0 obtained by the Ozawa analysis do appear to follow a similar trend to that found in isothermal crystallization experiments, particularly those obtained at the lowest undercoolings. Generally, the results of the Avrami analysis under isothermal conditions showed values of n for PET ranging from approximately 1.7-2.0, while values of 2.3-3.2

Table 4.9: Summary of Ozawa Analysis for Nonisothermal Crystallization Using DSC for PET Copolymers

Temperature (°C)	Sample							
	PET		4%		7%		10%	
	n_0	α_0 (°C min^{-1})^n	n_0	α_0 (°C min^{-1})^n	n_0	α_0 (°C min^{-1})^n	n_0	α_0 (°C min^{-1})^n
165	--------	--------	--------	--------	--------	--------	2.14	329.90
170	--------	--------	--------	--------	--------	--------	1.92	129.89
175	--------	--------	--------	--------	1.18	60.86	1.99	90.19
180	--------	--------	--------	--------	1.16	37.20	1.87	34.73
185	--------	--------	1.29	68.76	1.24	22.42	2.01	20.73
190	--------	--------	1.53	64.39	1.17	8.52	1.85	5.41
195	--------	--------	1.72	45.22	1.39	4.91	2.11	2.32
200	0.75	35.68	1.91	26.31	1.78	2.94	2.52	0.76
205	1.00	31.94	1.81	6.36	2.62	1.91	2.86	0.11
210	1.31	28.12	2.34	2.80	2.66	0.43	--------	--------
215	1.77	22.85	2.89	0.65	--------	--------	--------	--------
220	2.13	7.80	--------	--------	--------	--------	--------	--------
225	3.38	3.21	--------	--------	--------	--------	--------	--------

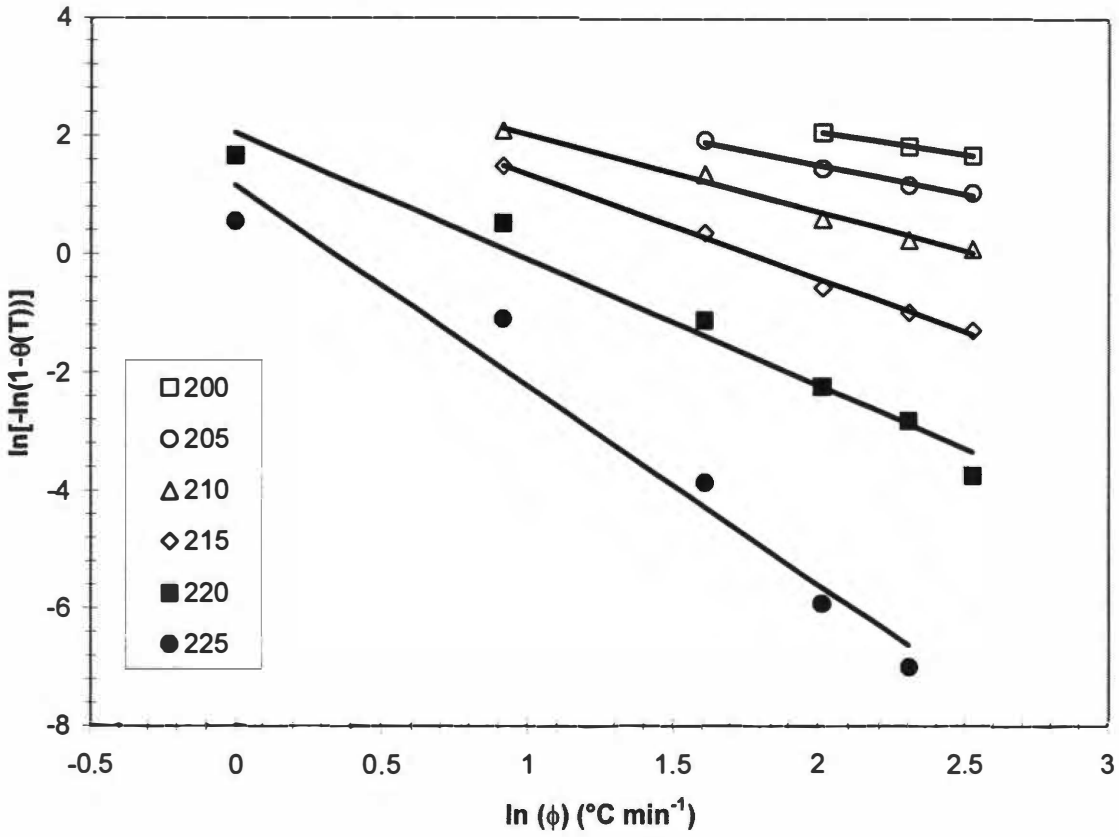

200°C:	y = -0.7522x + 3.5747	R^2 = 0.9958
205°C:	y = -0.9773x + 3.464	R^2 = 0.9842
210°C:	y = -1.3105x + 3.3366	R^2 = 0.9871
215°C:	y = -1.772x + 3.1288	R^2 = 0.9944
220°C:	y = -2.1331x + 2.0538	R^2 = 0.9731
225°C:	y = -3.379x + 1.1653	R^2 = 0.9632

Figure 4.64: Ozawa Plot for PET Homopolymer

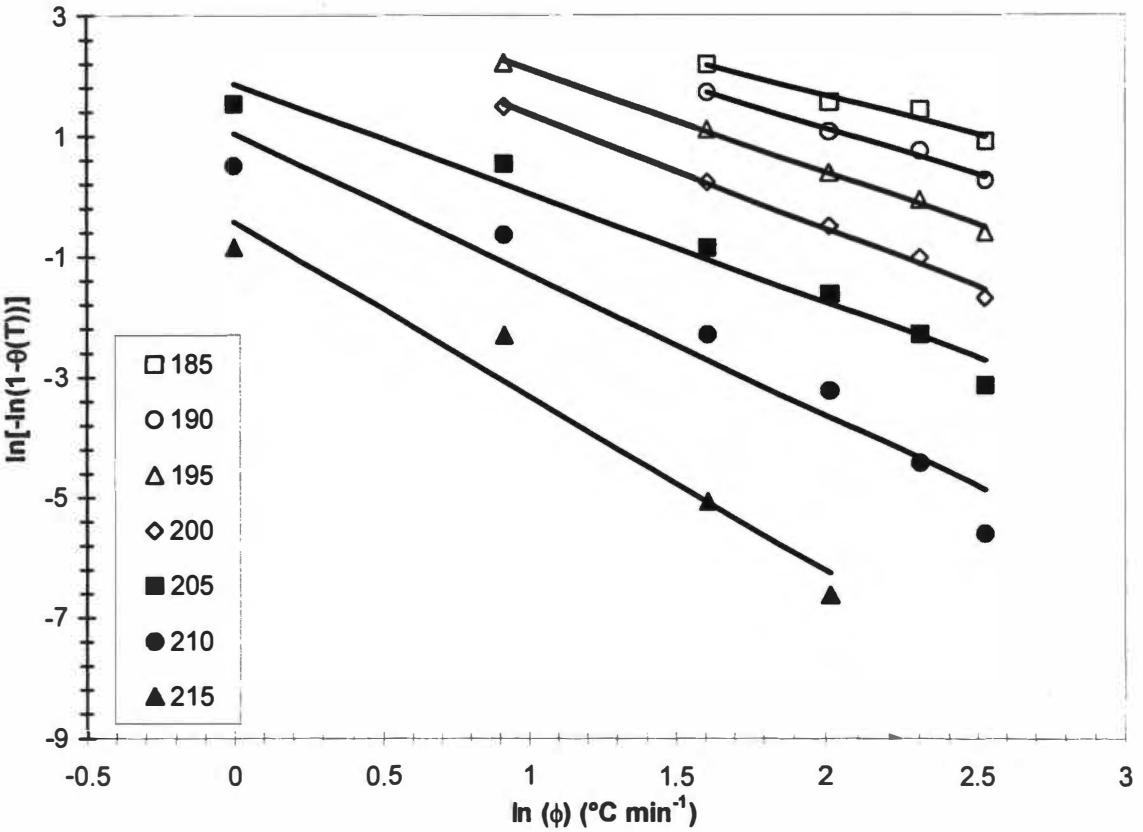

185°C:	y = -1.2892x + 4.2306	R^2 = 0.9539
190°C:	y = -1.528x + 4.165	R^2 = 0.9887
195°C:	y = -1.7156x + 3.8116	R^2 = 0.9964
200°C:	y = -1.9101x + 3.2699	R^2 = 0.9938
205°C:	y = -1.8121x + 1.8504	R^2 = 0.9703
210°C:	y = -2.337x + 1.0312	R^2 = 0.9461
215°C:	y = -2.8916x - 0.4281	R^2 = 0.9556

Figure 4.65: Ozawa Plot for PET-4 Copolymer

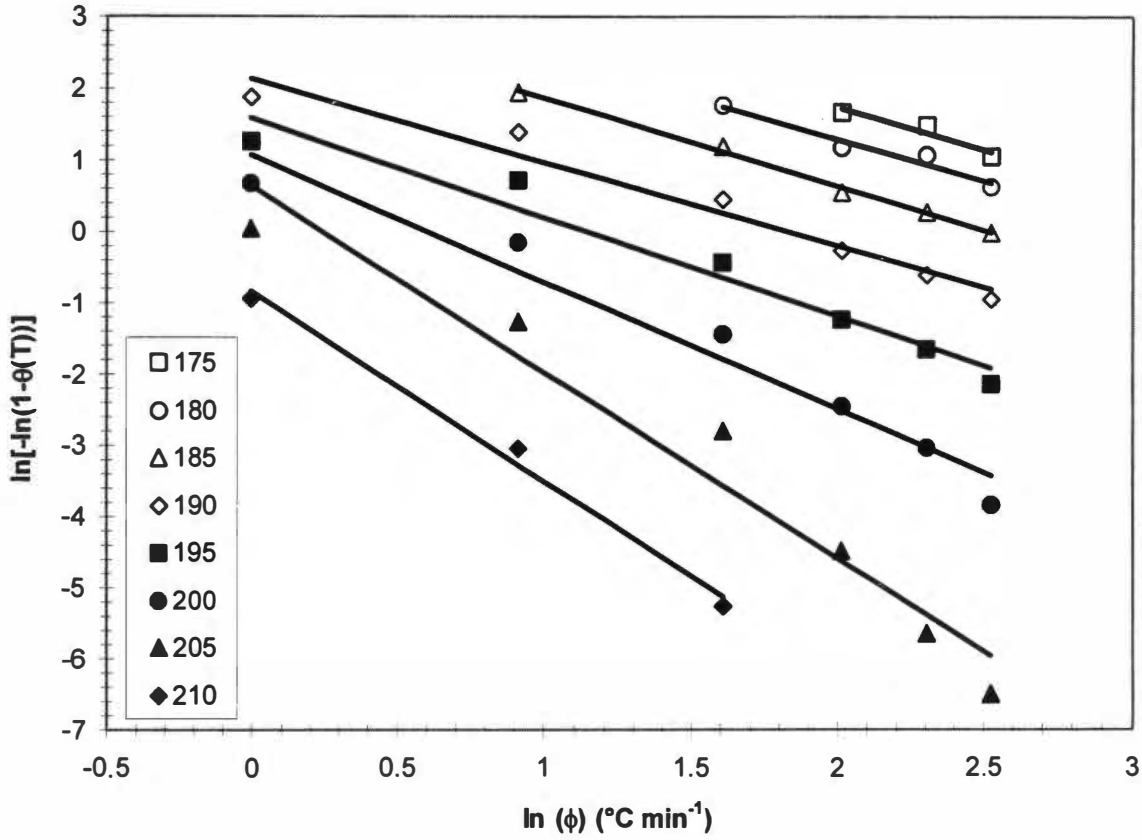

175°C:	y = -1.1839x + 4.1086	R^2 = 0.912
180°C:	y = -1.1609x + 3.6162	R^2 = 0.9546
185°C:	y = -1.2357x + 3.1098	R^2 = 0.9954
190°C:	y = -1.1667x + 2.1419	R^2 = 0.9635
195°C:	y = -1.3879x + 1.5905	R^2 = 0.9597
200°C:	y = -1.7816x + 1.0782	R^2 = 0.9586
205°C:	y = -2.6153x + 0.6461	R^2 = 0.9518
210°C:	y = -2.6624x - 0.836	R^2 = 0.9908

Figure 4.66: Ozawa Plot for PET-7 Copolymer

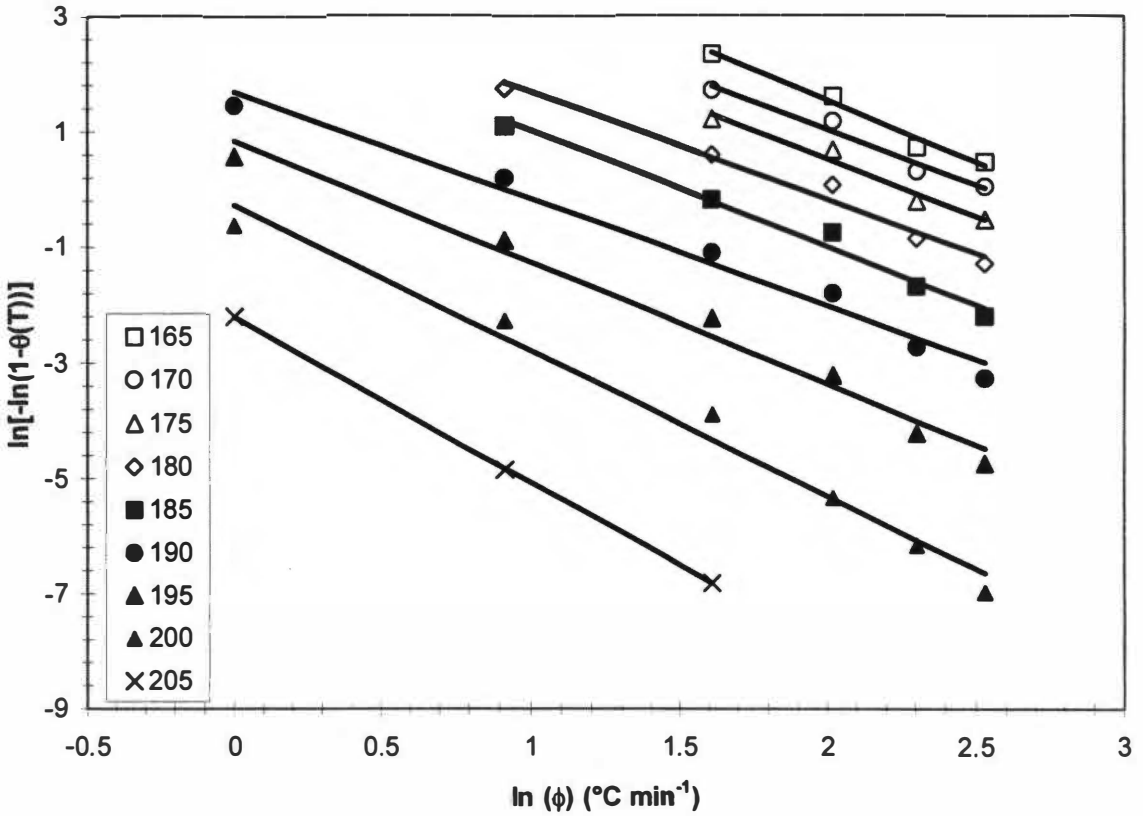

165°C:	y = -2.1382x + 5.7988	R^2 = 0.9812
170°C:	y = -1.9226x + 4.8667	R^2 = 0.9687
175°C:	y = -1.9946x + 4.5019	R^2 = 0.9692
180°C:	y = -1.8662x + 3.5477	R^2 = 0.9793
185°C:	y = -2.0143x + 3.0317	R^2 = 0.9829
190°C:	y = -1.8531x + 1.6877	R^2 = 0.982
195°C:	y = -2.1062x + 0.8407	R^2 = 0.9825
200°C:	y = -2.5188x - 0.2685	R^2 = 0.9821
205°C:	y = -2.8619x - 2.2015	R^2 = 1.0000

Figure 4.67: Ozawa Plot for PET-10 Copolymer

were found for the three copolyester samples (see Table 4.4). Over the same temperature range, the Ozawa analysis predicted values of n_0 ranging from 1.3-3.4 for PET homopolymer, and 1.2-2.9 for the three copolyester samples. Thus it would appear that the Ozawa equation, in this particular case, fails to provide experimental evidence substantiated with other experimental results, except at the lowest undercoolings. This may be partially due to the fact that, at the highest undercoolings fewer points can be included in the best-fit trend line used to determine n_0 and α_0 and may lead to some experimental error. In most of these plots it appears that the correlation coefficient approaches 1 as the temperature is increased (i.e. the undercooling is decreased). This may be partially attributed to the increased number of points included in the trend line. From a physical perspective, this might also be explained as being due to the fact that the crystallization rates at the higher temperatures are likely to be more reproducible than near the end of the crystallization process, where crystallization rates are likely the highest (provided that the undercooling is not so great that diffusion control has become dominant).

Nevertheless, the trends of the Ozawa data appear to qualitatively agree with that found by the Avrami analysis. Figure 4.68 is a plot of the Ozawa cooling crystallization function as it relates to the sample temperature. From this plot it is evident that the rate of nonisothermal crystallization at a particular temperature follows the order: PET>PET-4>PET-7$\geq$PET-10.

From a qualitative standpoint the Ozawa analysis data also appears to follow the same general trend as that found during isothermal crystallization and further supports the

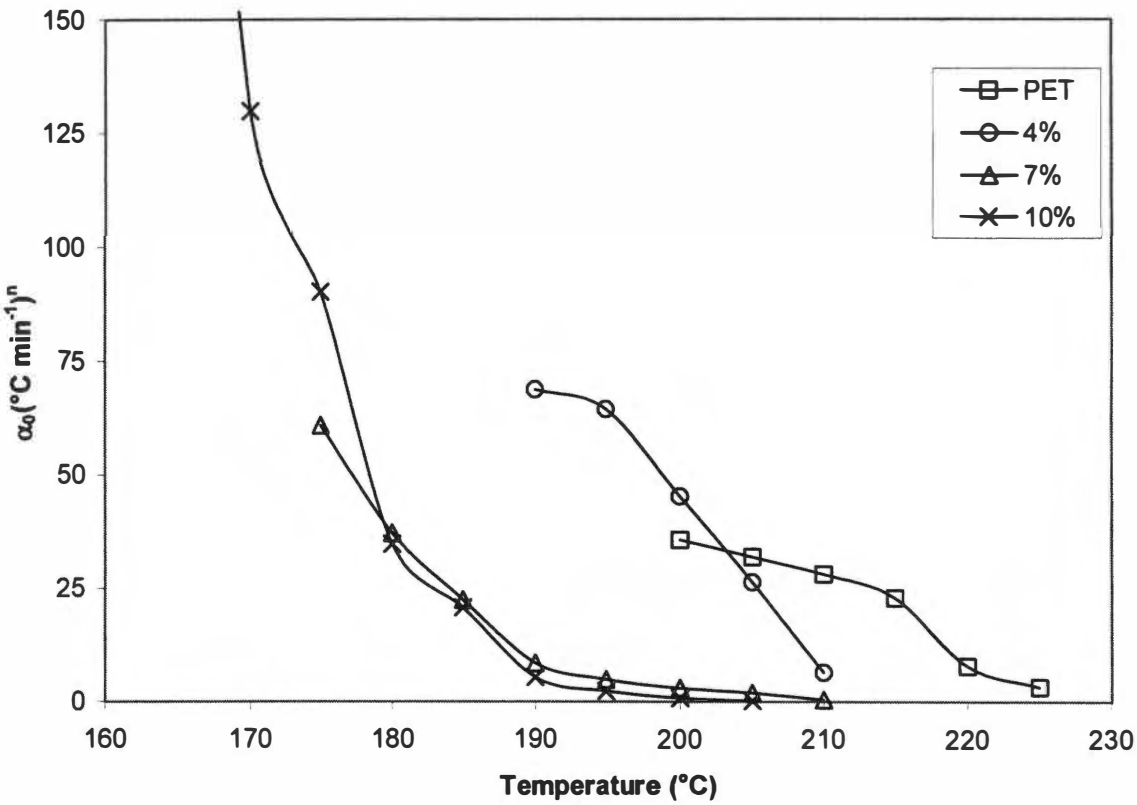

Figure 4.68: Plot of Ozawa Cooling Crystallization Rate Constant, α_0, as a Function of Temperature

claim that PET crystallizes more rapidly than any of the copolyesters, and that an increase in MPDiol concentration results in a decrease in the crystallization rate at a given temperature.

4.3.1.5. Nonisothermal DSC Melting Behavior

As mentioned previously, upon completion of the cooling to 30°C, the samples were held at the isothermal temperature for 10 minutes and then reheated at 10°C/min to observe their melting behavior. It was discovered that multiple melting peaks, similar to those witnessed during the isothermal crystallization experiment, were again witnessed for nonisothermally crystallized copolyesters. The melting behavior of the four PET copolymers is illustrated in Figures 4.69-4.72, with the results of the melting experiments summarized in Table 4.10. Figure 4.73 and 4.74 show a zoomed view of a typical melting peak and show the multiple melting phenomena. Comparing Tables 4.6 and 4.10 it is also evident that the multiple melting peaks occur over nearly the same temperature range in nonisothermal crystallization as they did during isothermal crystallization.

As before, the first melting peak appears to be shifted to lower temperatures with increasing cooling rate. This is in good agreement with that found in isothermal experiments in that the first melting peak was shown to shift to lower temperatures with decreasing crystallization temperature. Also, the second melting peak appears to grow in area at the expense of the third melting peak, and likewise appears to shift to lower temperatures with increasing cooling rate. Again this is similar to that witnessed during the isothermal experiment.

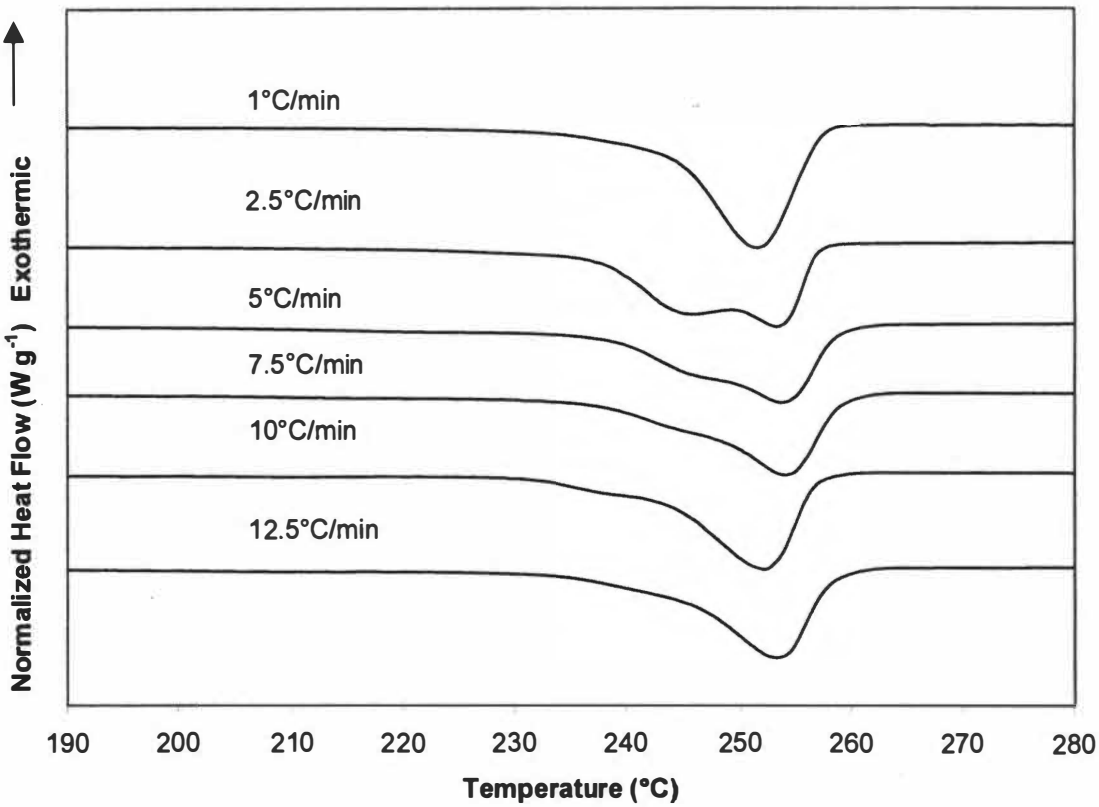

Figure 4.69: Plot of Subsequent Melting Behavior For PET Homopolymer After Nonisothermal Crystallization in DSC

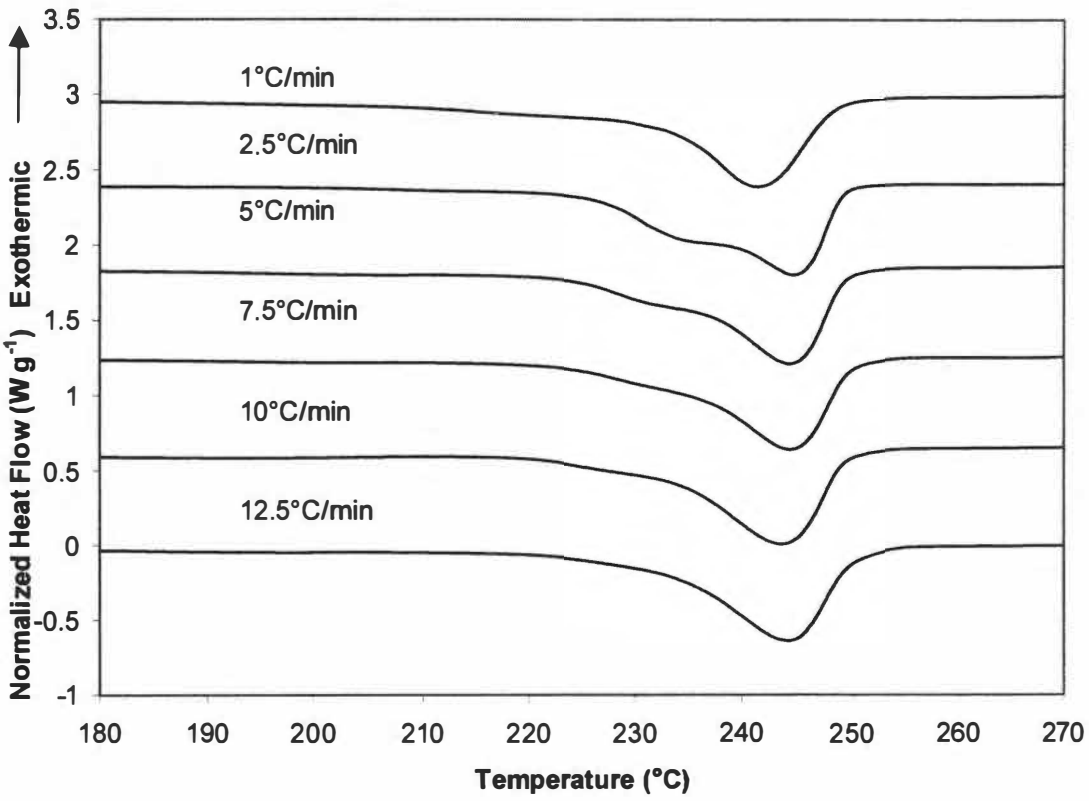

Figure 4.70: Plot of Subsequent Melting Behavior For PET-4 Copolymer After Nonisothermal Crystallization in DSC

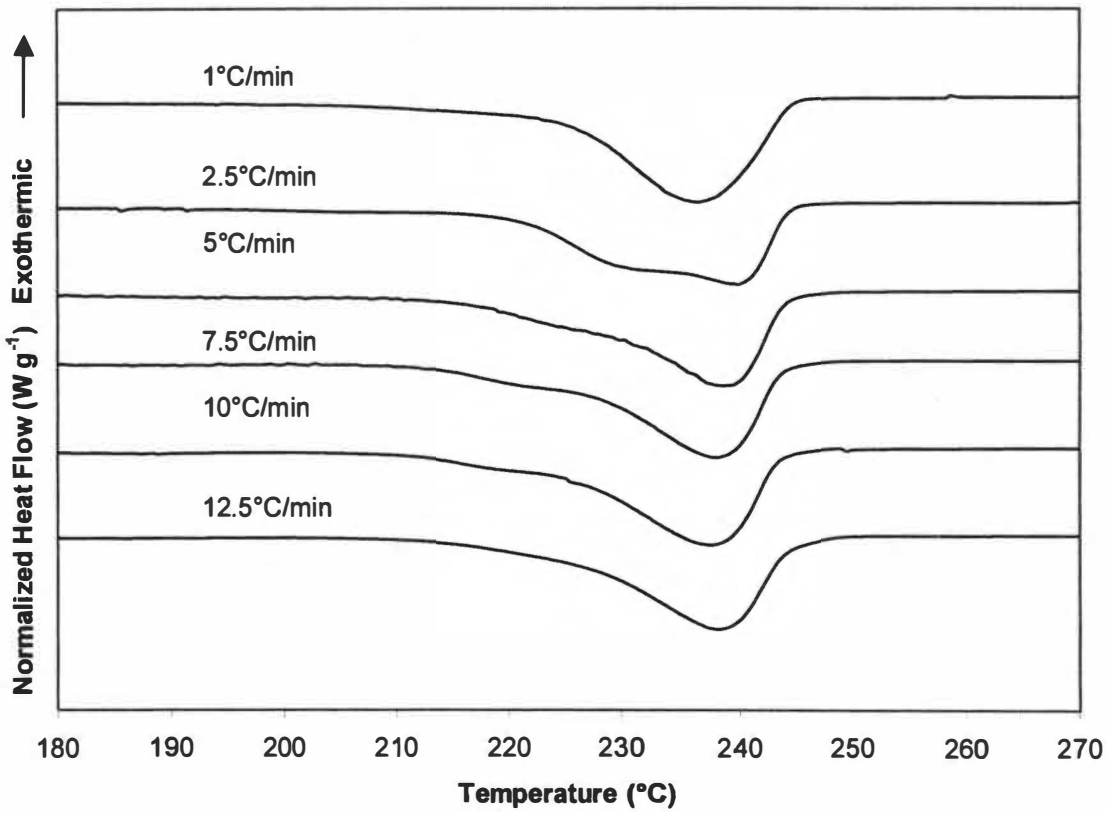

Figure 4.71: Plot of Subsequent Melting Behavior For PET-7 Copolymer After Nonisothermal Crystallization in DSC

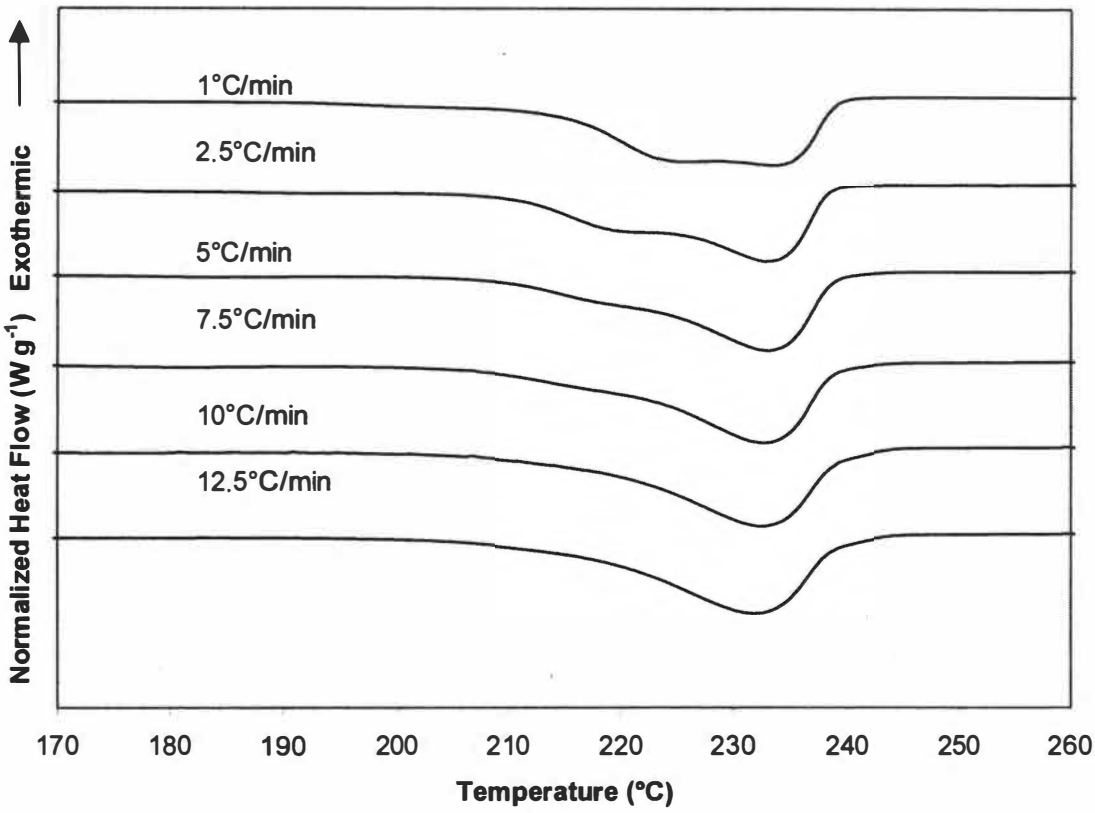

Figure 4.72: Plot of Subsequent Melting Behavior for PET-10 Copolymer After Nonisothermal Crystallization in DSC

Table 4.10: Summary of Results for Melting Behavior of Samples Crystallized Under Moderate Cooling Conditions

Sample	Cooling Rate (°C min^{-1})	$T_{0.1}$*	$T_{0.99}$*	ΔH_m (J/g)	T_m^I (°C)	T_m^{II} (°C)	T_m^{III} (°C)
PET	1	233.2	221.0	65.4±1.2	----	250.3±1.6	----
	2.5	229.8	214.9	61.3±0.6	----	247.7±1.2	253.4±0.2
	5	225.7	208.8	58.5±0.7	219.2±1.9	243.6±1.9	253.0±0.6
	7.5	223.4	204.6	57.5±0.4	213.5±1.3	239.7±2.7	252.2±1.2
	10	222.5	202.8	57.0±0.4	211.9±2.0	238.6±1.3	252.2±0.6
	12.5	220.9	201.5	56.0±0.8	208.6±1.7	238.4±0.7	252.6±0.5
PET-4	1	221.7	205.4	52.5±2.5	219.1±2.4	241.1±0.6	----
	2.5	218.4	199.9	52.8±0.1	211.6±2.3	235.0±1.2	244.9±0.2
	5	215.1	192.2	49.2±2.3	201.3±2.6	232.3±1.5	244.6±0.3
	7.5	212.4	186.1	50.4±0.7	197.6±1.8	230.0±0.4	244.6±0.3
	10	210.1	184.2	51.0±1.0	194.3±1.5	227.2±0.8	244.1±0.2
	12.5	208.1	176.9	49.5±1.1	191.5±1.5	----	244.2±0.2
PET-7	1	212.7	191.1	49.1±6.6	203.8±1.0	----	235.1±1.1
	2.5	212.2	189.6	48.5±4.2	201.6±1.3	229.3±0.4	238.7±1.1
	5	208.8	182.4	48.5±0.9	193.1±1.9	224.9±0.8	238.8±0.2
	7.5	203.8	178.0	48.9±0.9	188.2±0.8	220.2±0.4	238.3±0.5
	10	203.2	174.2	49.1±0.7	186.2±1.7	219.7±1.1	237.9±0.5
	12.5	201.5	168.8	48.3±0.9	184.9±1.2	219.6±0.6	238.1±0.1
PET-10	1	209.3	189.8	48.2±0.6	201.5±1.7	226.4±1.7	233.3±0.6
	2.5	204.7	181.9	46.8±0.2	192.4±2.3	219.6±2.2	233.0±0.5
	5	201.5	171.9	45.8±0.4	184.8±0.4	216.8±0.9	233.0±0.1
	7.5	198.3	166.0	46.0±0.8	181.4±2.0	215.7±0.4	232.6±0.1
	10	196.0	152.2	47.3±0.3	174.2±1.3	213.0±0.3	232.4±0.1
	12.5	194.5	146.3	48.6±0.5	173.0±1.3	----	232.0±0.3

NOTE: Limits Based on +/-1 standard Deviation

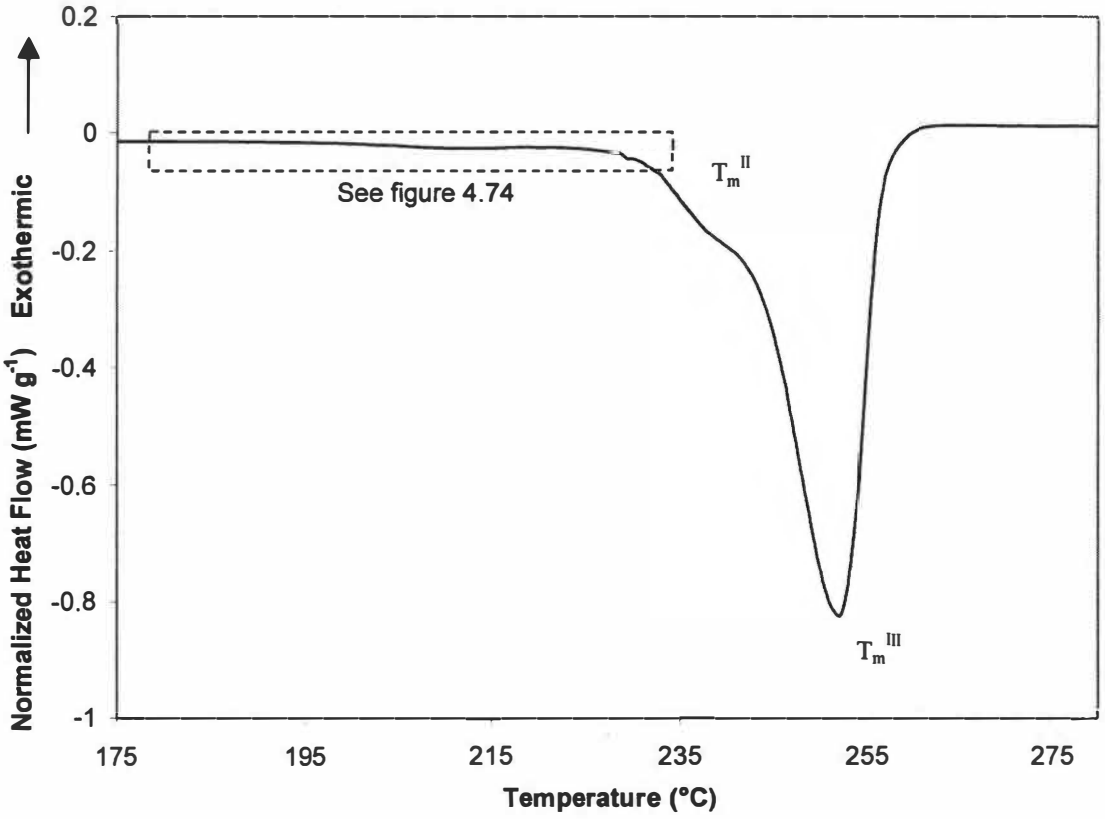

Figure 4.73: Melting Peak for PET Homopolymer Crystallized at 10°C/min Cooling Rate

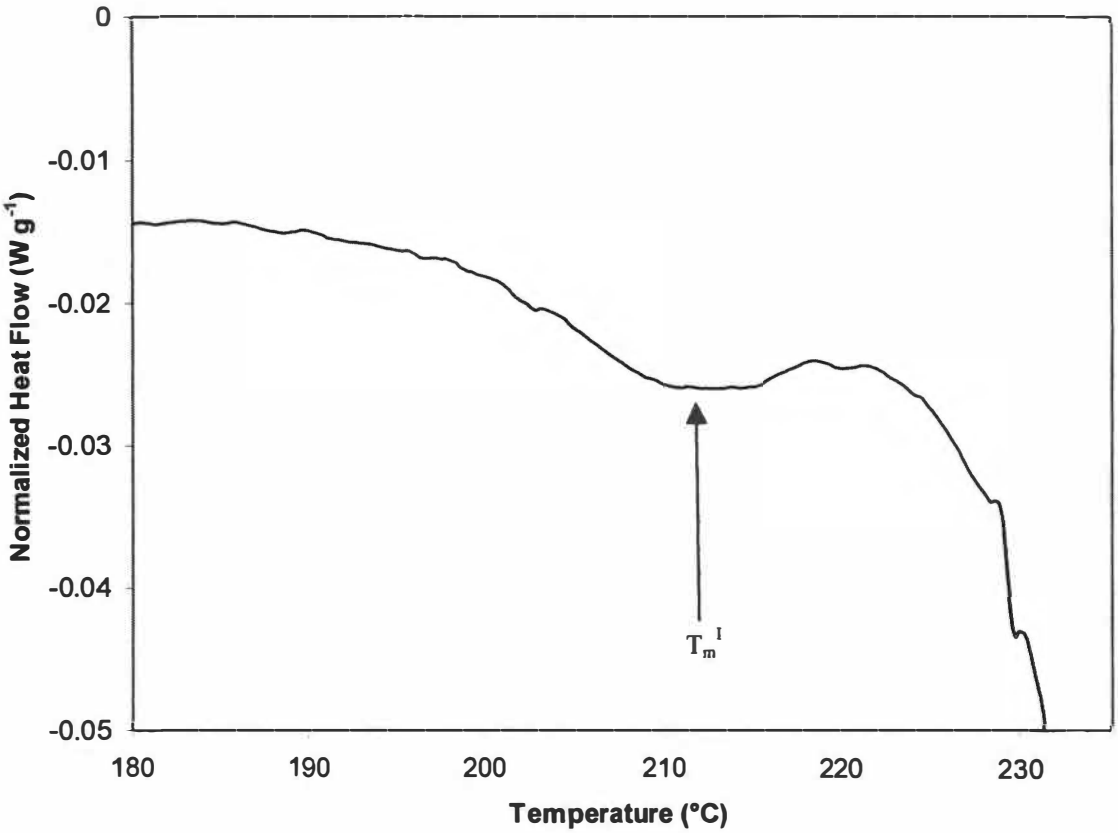

Figure 4.74: Zoomed View of Figure 4.73 Showing T_m^I

What is also important to note about the melting and crystallization behavior is that it appears that, within experimental error, the heat of crystallization and heat of fusion are nearly equal at the highest cooling rates for any one material. However as the cooling rate is decreased it appears that the discrepancy between these two values seems to increase, until at 1°C/min there is as much as a 13% difference between these two quantities. Although a portion of this discrepancy may be attributed to experimental error, as indicated by the rather large standard deviations at these lower cooling rates, it appears that a portion of this discrepancy may be related to something physical. As is shown in Figure 4.37 there appeared to be no significant cold crystallization observed during the reheating scan from 30°C. If the trend had showed a discrepancy between these values with increasing cooling rate, and if significant cold crystallization was observed during the reheating scan, then it might be suggested that at the higher cooing rates the materials were being partially quenched and that the additional heat was obtained by cold crystallization during the reheating scan. However, because the discrepancy in these two values appears to increase with decreasing cooling rate this is likely not the case. By Figures 4.39-4.42 it is evident that as cooling rate decreases the temperatures at which crystallize occurs increases. Thus it is conceivable that the additional heat might result from secondary crystallization during the cooling scan, which is likely to be more significant at the lower cooling rates where crystallization occurs at higher temperatures.

It is also evident from this data that the discrepancy between these two heats of transition appears to decrease with increasing copolymer content. If secondary crystallization is the cause of this additional heat being observed during melting then it

would appear that an increase in MPDiol content impedes the ability of these materials to continue to crystallize after the primary crystallization step has finished. Assuming comonomer exclusion from the PET homopolymer crystal, this seems somewhat intuitive in that with increasing comonomer content, the thickness of the lamellae will be primarily defined by the distance between adjacent MPDiol units in the copolymer chain. Provided that these copolymers are completely random, statistically it is expected that an increase in MPDiol concentration should result in a decrease in the distance between adjacent MPDiol units in the polymer chain. Thus it is expected that with increasing MPDiol content the lamellae will become thinner and the amount of MPDiol and uncrystallizable units rejected from the crystal will increase. This might explain why the heat released during crystallization decreases and why secondary crystallization appears to become less significant with increasing MPDiol content.

One other important point is to consider the normalized heat flow data shown in Figures 4.39-4.42 in the context of these results. These temperature based DSC curves may be falsely taken to indicate that ΔHc increases with increasing cooling rate. This is not actually the case as confirmed by Tables 4.7 and 4.10 where the heat of crystallization is shown to be approximately equal for any one given material, regardless of cooling rate. This apparent inconsistency can be explained by noting that these curves are shown as a function of temperature and not time. The area under these temperature based curves suggests that at a higher cooling rate, the heat released as a function of temperature will be greater near the peak crystallization temperature than for materials cooled at lower cooling rates. However, the total amount of time that the material spends at any given temperature will decrease as the cooling rate is increased. Thus for any

given material, if heat flow had been plotted as a function of time it is expected that the area under these curves would be approximately equal regardless of cooling rate.

4.3.1.6. Influence of Hold Temperature and Hold Time on Crystallization Kinetics

In the case of the isothermal crystallization experiment, the PET copolymers were heated to a temperature about 30°C above their observed melting temperature, held at that temperature for five minutes and then quenched to their isothermal crystallization temperature. In contrast, nonisothermal experiments were performed by heating all copolymers to the same temperature (ca. 290°C), holding at that temperature for 10 minutes, and cooling to 30°C to observe the resulting crystallization behavior.

In the case of isothermal crystallization it seems most appropriate to examine the data on the basis of undercooling, while in nonisothermal experiments it seems most practical to compare the results when cooling from the same initial temperature. While it was shown by the Hoffman-Weeks analysis that, in both experiments, the materials were held at, or above, their equilibrium melting temperatures it might be interesting to examine how these two different holding conditions influenced the crystallization kinetics of these polymers. In order to compare the results of these two experiments it seems imperative that the effects of holding temperature, T_{hold}, and holding time, t_{hold}, have on the crystallization kinetics of these polymers. While more elaborate techniques could be applied to make this comparison, the half time of crystallization and the Avrami rate constant should be sufficient in providing some insight as to the effect of these two variables on the resulting crystallization behavior.

A nonisothermal experiment was set up to examine these two variables. First, the effect of temperature was examined by heating the samples to a particular temperature, allowing it to remain at that temperature for 10 minutes, and then cooling at 10°C/min to 30°C to observe the resulting nonisothermal crystallization. For PET homopolymer, this was performed over the temperature range of 280-295°C, with the results shown in Table 4.11.

The half times as a function of hold temperature is shown in Figure 4.75. Here it is shown that the hold temperature does appear to have some influence on the crystallization half time. This plot suggests that PET crystallizes most rapidly when held at lower temperatures, which might suggest that although the temperature is held above the equilibrium melting temperature, there still may be some predetermined nuclei in the melt. This is also revealed when examining the Avrami rate constant, k, as a function of hold temperature (see Figure 4.76) where it appears that the Avrami rate constant

Table 4.11: Results of Hold Temperature Experiment for PET Homopolymer with 10°C/min Cooling Rate and 10 Minute Hold Time

T_{hold} (°C)	$t_{0.5}$-t_0 (min)	Avrami exponent, n	Avrami Rate Constant, k (min^{-n})
280	1.32	4.40	2.00E-01
285	1.46	4.20	1.42E-01
290	1.57	3.80	1.23E-01
295	1.94	3.60	3.33E-02

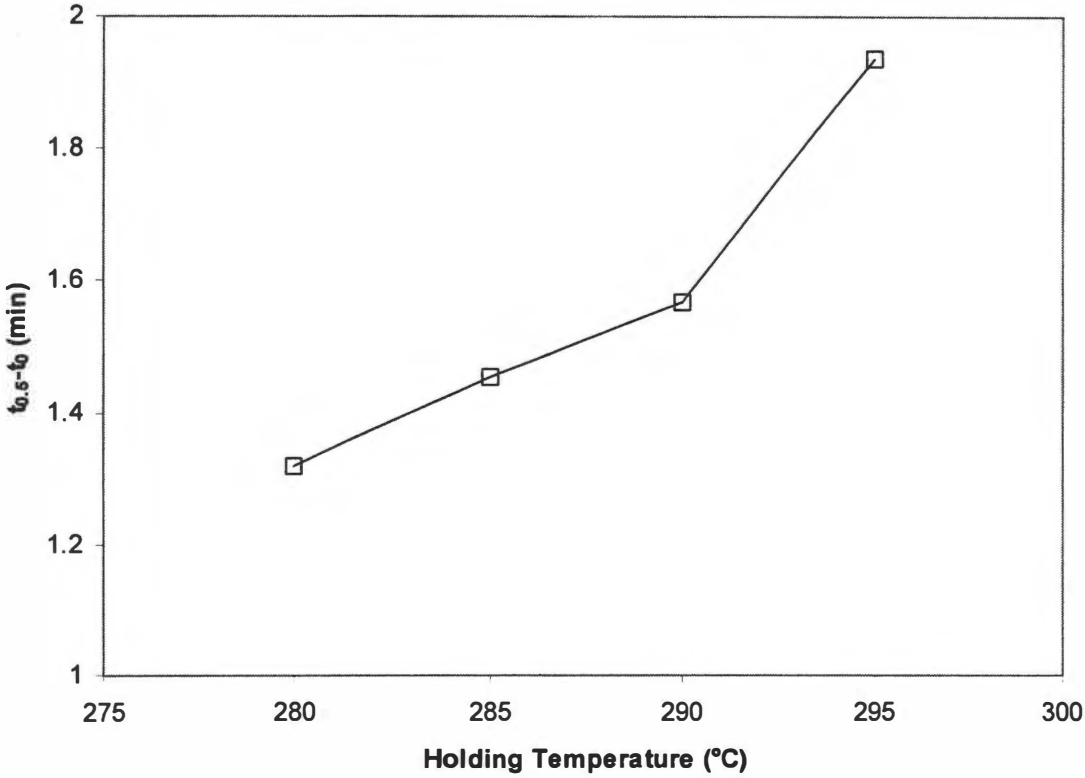

Figure 4.75: Effect of Hold Temperature on the Half Time of Crystallization for PET Homopolymer Crystallized Nonisothermally at 10°C/min

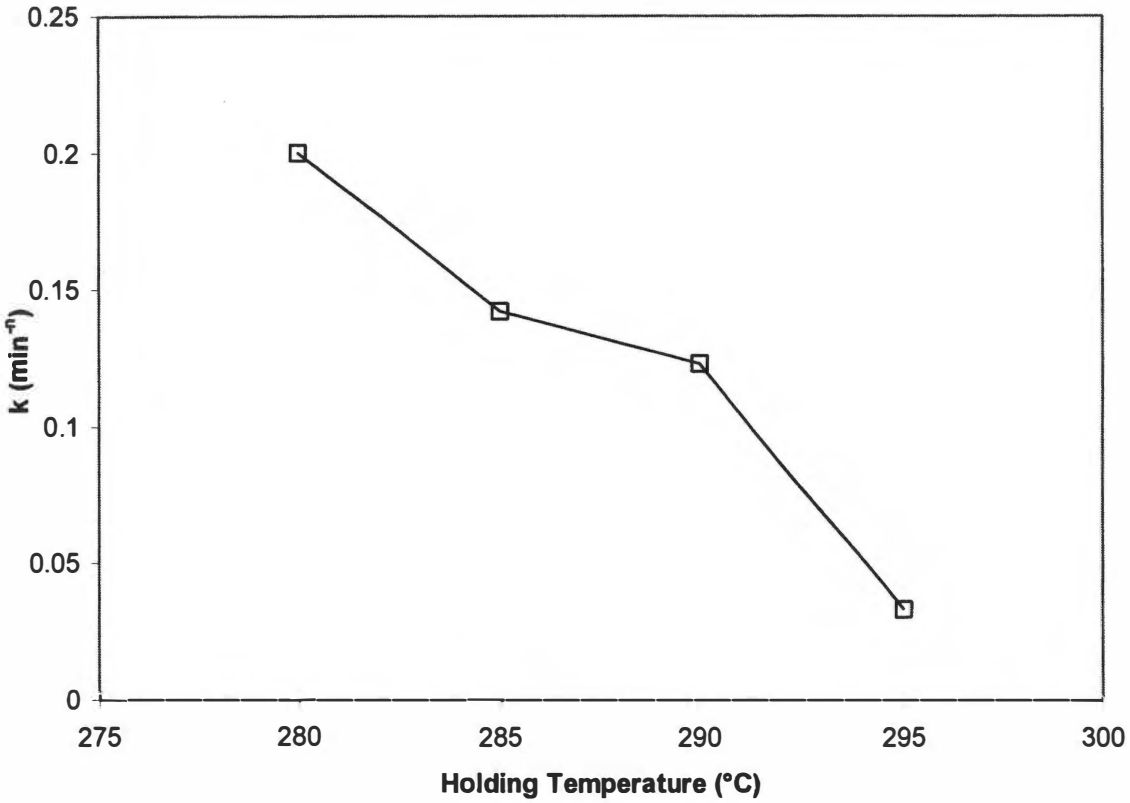

Figure 4.76: Effect of Hold Time on the Avrami Rate Constant, k, for PET Homopolymer Crystallized Nonisothermally at 10°C/min

decreases with increasing hold temperature. The Avrami exponent, n, is apparently also influenced by hold temperature. This is illustrated in Figure 4.77 where it appears that n decreases in a linear fashion with increasing holding temperature.

This same experiment was also performed by keeping the hold temperature constant and changing the time held in the melt, t_{hold}. The results of this experiment are shown in Table 4.12. This experiment was performed for PET homopolymer at the equilibrium melting temperature, 280°C, and at 290°C. Again, the halftimes of crystallization were plotted as functions of hold temperature and are shown in Figure 4.78. From this plot it is evident that the hold time does not appear to make a significant difference in the half time values for the polymers crystallized at 280°C. However, it is evident that hold time does have a significant influence on the polymers with a T_{hold}=290°C. Additionally it appears that, for both temperatures, the half times were quite comparable at the 5 minute hold time.

Table 4.12: Results of Hold Time Experiment for PET Homopolymer with 10°C/min Cooling Rate

T_{hold} (°C)	t_{hold} (min)	$t_{0.5}$-t_0 (min)	Avrami exponent, n	Avrami Rate Constant, k (min^{-n})
280	5	1.36	3.60	2.25E-01
	10	1.32	4.40	2.02E-01
	15	1.32	3.50	2.73E-01
290	5	1.39	3.52	2.21E-01
	10	1.57	3.80	1.23E-01
	15	2.06	4.62	2.57E-02

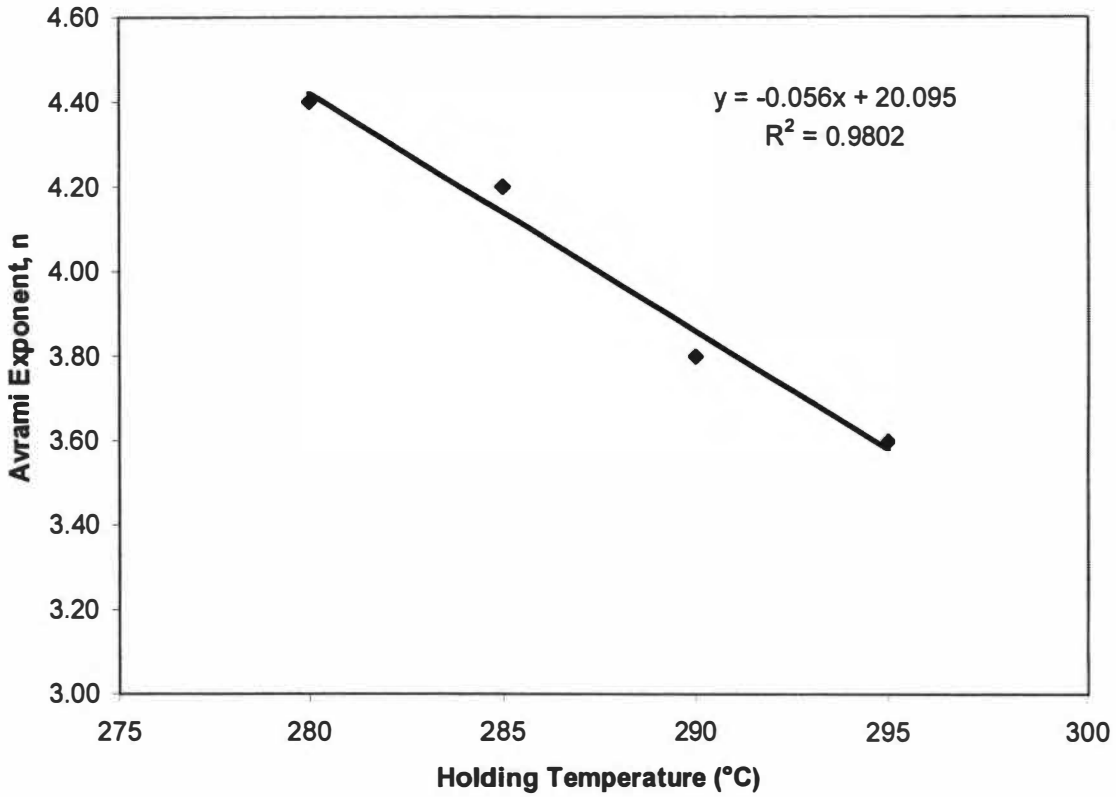

Figure 4.77: Effect of Hold Time on the Avrami Exponent, n, for PET Homopolymer Crystallized Nonisothermally at 10°C/min

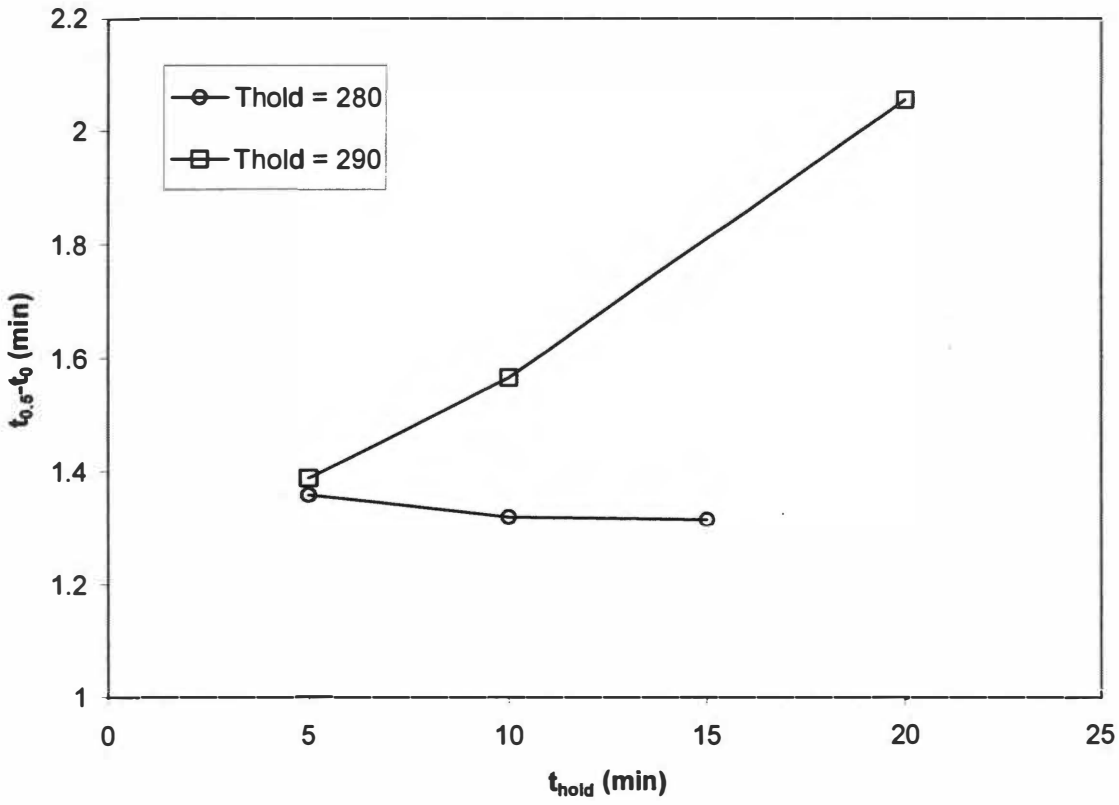

Figure 4.78: Effect of Hold Time on the Half Time of Crystallization for PET Homopolymer Crystallized Nonisothermally at 10°C/min

A similar experiment was also conducted for the copolymers examined in this study where the two temperature-time combinations used in the isothermal and nonisothermal experiments were compared for each material. The results for these studies are summarized in Table 4.13. It would appear that for the 4 and 7mol% MPDiol copolymers, that the combined effect of an increase in holding temperature and holding time influences the crystallization kinetics of these materials. The PET-7 copolyester behaved in much the same way as PET homopolymer in that the half time and Avrami exponents increased, while the Avrami rate constant decreased with an increase in holding temperature and time. In contrast, the PET-10 copolymer appeared to be largely unaffected by these two variables. In the case of the PET-4 sample, an increase in T_{hold} and t_{hold} results in a significant increase in the value of the Avrami constant and a decrease in the half time, just the opposite of that found for the PET homopolymer samples. While this is not well understood, it is evident that the hold time and

Table 4.13: Comparison of Nonisothermal Crystallization Data for PET Copolyesters at Different Hold Temperatures and Times

Sample	T_{hold} (°C)	t_{hold} (min)	$t_{0.5}$-t_0 (min)	Avrami exponent, n	Avrami Rate Constant, k (min^{-n})
PET-4	270	5	2.16	4.06	3.05E-02
	290	10	1.97	3.60	6.14E-02
PET-7	270	5	2.16	3.82	3.65E-02
	290	10	2.37	4.28	1.73E-02
PET-10	260	5	2.89	3.54	1.62E-02
	290	10	2.91	3.63	1.41E-02

temperature does have some influence on the results of these experiments, at least for PET copolyesters containing less than or equal to 7mol% MPDiol.

This experimental evidence might suggest that although both of these temperatures are equal to or greater than the equilibrium melting temperature, there is a sort of predetermined nuclei that exists in the melt, even when the temperature is held at or above the equilibrium melting temperature. The implications of these results are that, because the isothermal and nonisothermal experiments were conducted using different holding temperatures and times, making direct comparisons between these results out of context should be avoided. Nevertheless, comparing the values and trends in the data for both experiments suggests that the addition of MPDiol reduces the overall degree of crystallinity, the rate of nucleation, and the overall rate of crystallization.

4.3.2. Light Depolarizing Microscopy – High Cooling Rates

4.3.2.1. Examination of Experimental Data

The results of this experiment are summarized in Tables 4.14 - 4.17 for the four copolymers. Note that because this experimental technique does not necessarily allow for the exact replication of a particular cooling rate, and that the cooling rate is determined after the experimental run has been made, that the results reported here do not represent average values but rather each individual data point was obtained from a separate experimental run. As a result, in some cases the results from two experimental runs might show the same or nearly the same cooling conditions, but yield somewhat different values for the same cooling rate. Unless just cause could be found for the

Table 4.14: Summary Data for Nonisothermal Crystallization of PET Homopolymer Using LDM System

CRF (sec^{-1})	CR (°C/sec)	$t_{0.5}$-t_0 (sec)	$t_{0.5}$-$t_{290°C}$ (sec)	$t_{0.5}$-t_{Dm} (sec)	T{θ(t)=0.5} (°C)	t_0-t_{290} (sec)	T{θ(t)=0} (°C)	T{θ(t)=1} (°C)	t{θ(t)=1} (sec)
0.0007	0.1676	96.0	249.0	426.2	208.2	153	224.5	196.8	317.0
0.0007	0.1681	97.0	250.0	426.6	208.2	153	224.5	195.0	329.0
0.0013	0.3331	52.5	284.0	256.5	194.6	232	211.7	172.6	355.0
0.0013	0.3333	49.0	284.0	256.0	194.6	235	210.8	167.3	373.0
0.0013	0.3332	45.0	285.0	257.5	194.6	240	209.1	171.7	356.0
0.0069	1.6017	30.0	88.5	85.3	171.2	58.5	192.4	133.7	169.0
0.0077	1.7716	34.0	87.0	84.8	165.5	53	190.2	123.9	183.0
0.0079	1.8530	24.8	72.0	70.1	177.8	47	197.6	147.4	130.0
0.0085	1.9857	30.0	76.0	74.1	169.0	46	193.7	130.6	156.0
0.0088	2.0528	30.0	76.0	73.3	167.7	46	193.2	133.2	143.0
0.0103	2.3852	26.5	67.5	65.3	162.4	41	188.8	125.2	132.0
0.0127	3.0328	27.5	61.5	57.3	165.1	34	194.6	126.1	139.0
0.0139	3.2045	21.5	50.5	49.6	165.3	29	190.2	127.0	122.0
0.0150	3.4761	23.5	51.0	49.7	157.1	27.5	189.7	134.1	84.5
0.0157	3.5970	21.0	48.0	47.0	157.1	27	187.1	127.0	91.5
0.0173	3.9736	21.0	46.5	45.2	153.2	25.5	186.2	121.2	97.0
0.0175	4.0052	19.0	43.0	42.4	158.0	24	187.1	115.9	121.0
0.0185	4.2073	19.0	43.5	42.5	147.9	24.5	181.4	112.8	98.5
0.0202	4.6711	16.5	37.5	36.5	156.2	21	188.0	120.3	89.5
0.0205	4.6513	17.5	40.0	39.1	146.5	22.5	180.0	116.3	80.5
0.0206	4.8783	19.5	38.0	37.0	155.4	18.5	195.9	122.6	83.5
0.0207	4.9093	17.8	40.5	39.6	150.1	23	182.7	109.2	96.5
0.0212	4.9304	18.9	37.0	36.5	153.2	18	193.2	123.5	76.0

Table 4.15: Summary Data for Nonisothermal Crystallization of PET-4 Copolyester Using LDM System

CRF (sec^{-1})	CR (°C/sec)	$t_{0.5}-t_0$ (sec)	$t_{0.5}-t_{290°C}$ (sec)	$t_{0.5}-t_{Tm°}$ (sec)	$T\{\theta(t)=0.5\}$ (°C)	t_0-t_{290} (sec)	$T\{\theta(t)=0\}$ (°C)	$T\{\theta(t)=1\}$ (°C)	$t\{\theta(t)=1\}$ (sec)
0.0007	0.1656	55.0	317.0	466.8	202.5	472.6	211.7	177.8	465.0
0.0007	0.1658	54.0	318.0	467.6	202.5	474.8	211.3	178.3	462.0
0.0015	0.3329	37.0	172.0	246.5	194.1	251.3	206.0	143.9	351.0
0.0015	0.3343	38.0	185.5	259.7	193.2	252.9	205.6	145.2	362.0
0.0066	1.5510	22.0	82.0	72.1	179.6	60.0	195.0	149.2	139.0
0.0079	1.8119	23.7	75.7	69.0	172.8	52.0	189.3	150.5	116.0
0.0125	2.8475	17.5	54.0	49.0	165.1	36.5	183.1	140.8	93.0
0.0139	3.1913	20.0	55.0	49.0	159.8	35.0	181.8	126.1	112.0
0.0158	3.3932	21.5	56.5	52.9	140.8	35.0	164.6	111.4	109.0
0.0177	4.0422	19.5	46.5	42.3	155.0	27.0	181.4	117.2	114.0
0.0186	4.3135	21.0	44.5	40.3	149.6	23.5	187.5	110.1	104.5
0.0188	4.2600	19.3	41.3	38.9	149.8	22.5	184.0	113.7	90.5
0.0191	4.3901	19.5	43.5	39.1	147.9	24.0	184.0	114.6	86.5
0.0208	4.5185	16.5	43.0	39.8	139.0	26.5	166.4	114.5	76.0
0.0209	4.6566	17.3	41.0	37.8	143.0	24.0	174.8	111.4	82.0
0.0211	4.7588	18.3	43.3	39.2	148.3	25.0	175.6	110.1	108.0
0.0218	4.7736	16.0	40.5	37.4	139.9	24.5	169.0	113.7	73.5
0.0230	5.0485	15.0	40.0	36.3	136.8	25.0	165.5	111.0	73.5

Table 4.16: Summary Data for Nonisothermal Crystallization of PET-7 Copolyester Using LDM System

CRF (sec^{-1})	CR (°C/sec)	$t_{0.5}$-t_0 (sec)	$t_{0.5}$-$t_{290°C}$ (sec)	$t_{0.5}$-t_{Dme} (sec)	T{θ(t)=0.5} (°C)	t_0-t_{290} (sec)	T{θ(t)=0} (°C)	T{θ(t)=1} (°C)	t{θ(t)=1} (sec)
0.0007	0.1668	61.0	585.5	506.6	192.4	524.5	202.5	163.7	486.0
0.0007	0.1667	66.0	587.1	507.8	192.4	521.1	202.9	170.8	445.0
0.0007	0.1668	59.0	575.7	496.6	194.1	516.7	203.8	175.6	415.0
0.0015	0.3333	48.0	323.9	283.4	182.7	275.9	198.1	154.5	293.0
0.0015	0.3347	48.0	323.0	283.0	182.2	275.0	198.1	159.8	266.0
0.0079	1.7355	38.0	101.0	91.7	150.9	63.0	174.8	119.9	173.0
0.0095	2.0579	33.0	87.0	79.9	148.3	54.0	171.2	112.3	174.0
0.0098	2.1237	34.5	86.5	79.4	147.2	52.0	171.7	112.8	169.0
0.0098	2.1170	32.0	85.0	78.1	147.9	53.0	169.9	108.3	183.0
0.0104	2.2467	34.0	85.0	78.1	146.1	51.0	168.6	112.3	171.5
0.0107	2.2952	33.5	85.5	78.1	141.2	52.0	165.5	107.4	171.5
0.0129	2.8586	39.0	77.0	71.0	142.1	38.0	175.6	105.2	168.0
0.0131	2.8634	37.0	76.0	70.5	139.9	39.0	170.8	104.3	167.0
0.0138	2.9437	31.0	72.5	66.5	136.8	41.5	163.3	103.8	154.0
0.0141	2.9427	33.0	71.0	67.5	139.4	38.0	162.9	107.4	153.0
0.0154	3.2155	24.5	63.0	58.3	135.5	38.5	158.5	115.0	103.0
0.0155	3.3130	27.0	64.5	59.1	135.5	37.5	161.5	110.1	115.0
0.0161	3.5438	32.5	64.0	59.1	141.2	31.5	173.4	112.3	130.0
0.0162	3.6420	28.5	61.5	54.6	142.1	33.0	174.3	109.2	126.5
0.0184	3.9067	23.0	53.5	49.8	132.3	30.5	162.0	104.7	101.0
0.0200	4.3273	22.0	52.0	47.0	130.6	30.0	161.5	105.2	94.0

Table 4.17: Summary Data for Nonisothermal Crystallization of PET-10 Copolyester Using LDM System

CRF (sec^{-1})	CR (°C/sec)	$t_{0.5}-t_0$ (sec)	$t_{0.5}-t_{290-C}$ (sec)	$t_{0.5}-t_{Dm}$ (sec)	$T\{\Theta(t)=0.5\}$ (°C)	t_0-t_{290} (sec)	$T\{\Theta(t)=0\}$ (°C)	$T\{\Theta(t)=1\}$ (°C)	$t\{\Theta(t)=1\}$ (sec)
0.0008	0.1671	76.0	654.79	484.8	180.5	578.8	193.2	151.4	439.0
0.0008	0.1678	69.0	647.00	477.9	181.4	578.0	192.8	154.9	417.0
0.0014	0.3351	73.0	390.00	285.0	162.0	317.0	183.1	122.6	581.0
0.0014	0.3342	73.0	387.00	280.0	164.2	314.0	184.4	122.6	599.0
0.0053	1.1384	51.0	150.00	135.1	142.5	99.0	167.7	104.3	269.0
0.0053	1.1373	53.0	148.00	134.1	145.2	95.0	170.4	103.8	283.0
0.0054	1.1943	57.0	152.00	135.5	143.0	95.0	172.1	102.9	283.0
0.0055	1.1968	52.0	114.00	108.2	135.9	62.0	156.7	104.7	181.0
0.0056	1.2079	51.0	144.00	129.5	142.5	93.0	168.6	109.6	239.0
0.0058	1.2062	43.0	142.00	129.1	137.2	99.0	158.5	105.6	234.0
0.0059	1.328	51.0	152.00	152.0	143.0	72.0	168.2	101.6	279.0
0.0062	1.3388	50.0	134.00	121.9	141.2	85.0	166.8	105.6	245.0
0.0063	1.3495	51.0	134.00	122.0	141.2	83.0	167.3	105.6	245.0
0.0066	1.3988	42.5	127.50	115.4	138.1	80.5	161.5	114.1	192.0
0.0068	1.4295	49.0	129.50	119.0	138.1	90.0	163.3	111.4	208.5
0.0072	1.5172	43.0	116.00	107.0	139.9	73.0	164.6	112.3	182.0
0.0084	1.7793	45.0	108.00	100.0	138.1	63.0	164.6	106.9	188.0

exclusion of any data point it was included in the analysis with the expectation that a sufficient number of points should yield an acceptable average value for the data trend.

Figure 4.79 shows a typical cooling curve observed during this experiment, in this case for PET homopolymer. In this figure the determination of the average cooling rate, CR, and the cooling rate function, CRF, given by equation 3.3. are illustrated. To determine the average cooling rate a best-fit linear regression line is applied to the initial portion of the cooling curve up to the time when crystallization is first detected. Likewise, the cooling rate function, CRF, was determined by application of a best-fit exponential regression line over the same data range according to equation 3.3.

At higher cooling rates it was observed that equation 3.3. fit the data very well. However as the cooling rate was decreased, it was observed that the correlation coefficient also decreased. Thus the confidence in the precise value of CRF and CR decreases with decreasing cooling rate and is expected to introduce some experimental error into these data.

Note also that these cooling rate curves are somewhat different from those encountered for Polyethylene (PE) (Ding and Spruiell 1996, Supaphol and Spruiell 1998, Supaphol 1996) and isotactic Polypropylene (i-PP) (Ding and Spruiell 1996) in that the cooling curves for PET and the PET copolymers do not show the typical constant temperature step commonly observed for these other materials. This is illustrated in Figure 4.80 for HDPE where it is evident that, at a particular temperature, the heat released during the exothermic crystallization process is sufficient to counteract the heat removed by the cooling medium thus leading to a constant temperature region, referred to as the plateau temperature. Since PET apparently does not liberate as much heat as

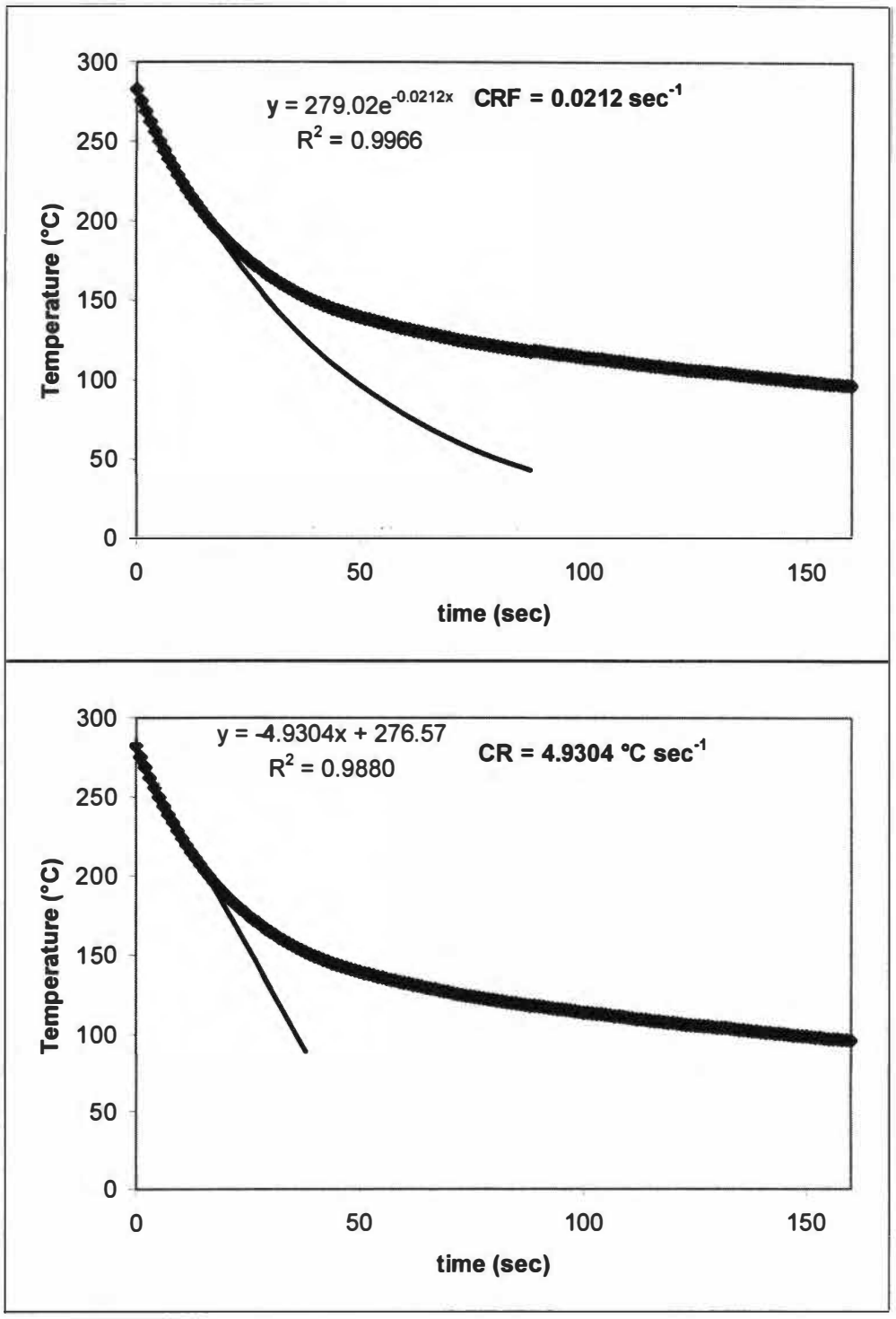

Figure 4.79: Plot of Cooling Curves for PET Homopolymer Illustrating Technique to Determine CRF and CR

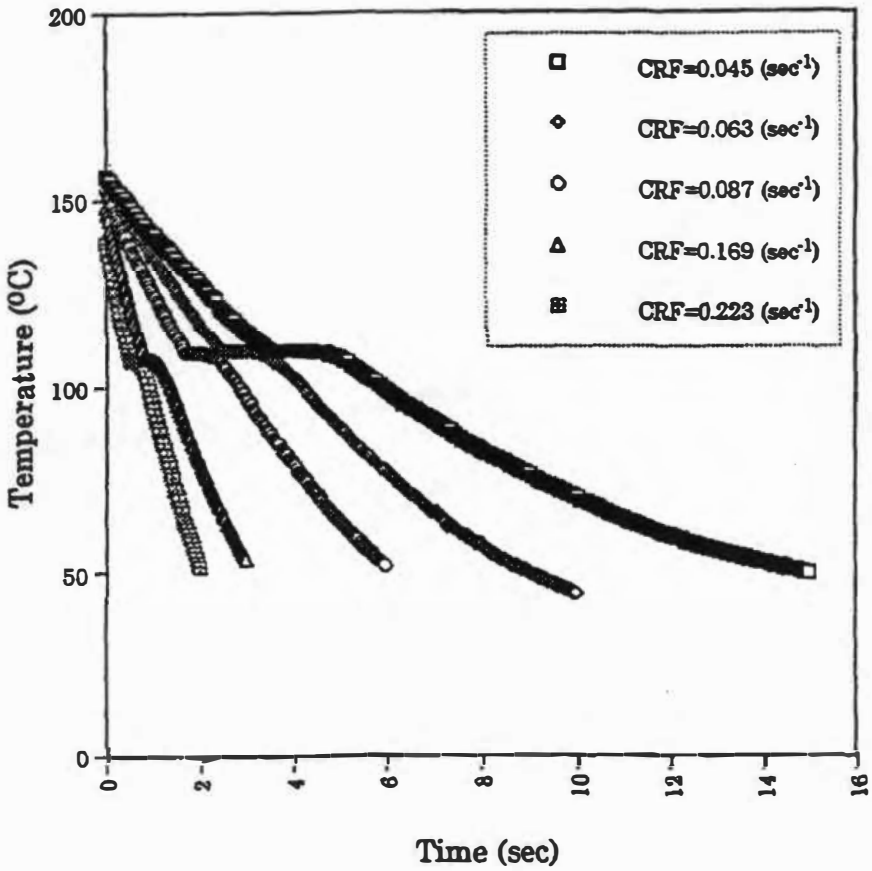

Figure 4.80: Plot of Typical Cooling Curves for HDPE Illustrating Plateau Temperature

Source: Supaphol, P., MS Thesis, University of Tenn. (1994).

quickly during crystallization as do the polyolefins previously examined by this technique, the plateau temperature is not witnessed for the materials examined in this study. Supaphol (1996) examined the thermal properties of two linear HDPE fractions at a cooling rate of 10°C/min where the heat released at this cooling rate was found to range from 188.8 - 192.9 J/g whereas the materials examined in this experiment under the same relative cooling conditions displayed heats of crystallization with average values ranging from 56.9 J/g for PET to 46.8 J/g for the PET-10 samples. Thus in this case it is evident that the total amount of heat released for these materials is significantly lower than HDPE. Likewise, PET is known to crystallize much more slowly than PE. As a result, the heat released by PET occurs over a longer span of time than in the case of PE.

When present, the plateau temperature can be used as a convenient temperature to describe this type of experimental data. However, because it is was not observed for the materials examined in this study it was decided to describe the experimental data by plotting the results as a function of the temperature when the reduced crystallinity had reached 50% (i.e. at $\theta(T) = 0.50$).

From the cooling rate curve it is evident that, at first, the initial slope of the cooling curve is very steep indicating a very rapid cooling condition. However, due to the heat liberated during crystallization, and the fact that the temperature difference between the sample and the surrounding temperature decreases, the slope begins to level off with increasing time. Unlike in DSC experiments, where the cooling rate is constant, in these experiments the cooling rate decays exponentially with time. For the lowest cooling rates (i.e. 10 and 20°C/min) a Mettler-Toledo FP82 hot-stage was used in replacement of the nitrogen gas cooling system. Thus for these two cooling rates the

cooling rate curves are nearly linear and thus should be very similar to that obtained in a DSC experiment, assuming there is negligible thermal lag in the both experiments.

Ding and Spruiell (1996) and Supaphol and Spruiell (1998) both observed that the CRF and CR were directly proportional for the materials that they examined using this LDM technique. This was also witnessed in this experiment as is illustrated in Figure 4.81.

As was described in the experimental chapter, equations 3.10. and 3.11. require that the light intensity with and without an analyzer be measured simultaneously to determine the crystallization conversion rate at any time, when a sample is subjected to high cooling rates. This is illustrated in Figures 4.82 and 4.83 where the light intensities with and without an analyzer are both plotted as functions of time. These particular curves are typical for all samples crystallized using the nitrogen gas cooling method at the lower measured cooling rates (i.e. cooling rates greater than that obtained using the hot-stage cooling method but not near the critical cooling rate for quenching the sample to the glassy state). Notice in this plot that the light intensity without an analyzer decreases with increasing time (i.e. decreasing temperature) while the light intensity with an analyzer behaves in just the opposite manner. When the material is first heated to above its equilibrium melting temperature and subsequently cooled the light intensity with an analyzer is expected to yield a somewhat lower value (theoretically this value should be zero for perfectly crossed nichols). However, as the sample begins to crystallize the spherulitic structure will begin to rotate the light such that the intensity of the light passing through the analyzer increases. As the crystallization process comes to an end the light intensity again levels off to a constant value. The light intensity without

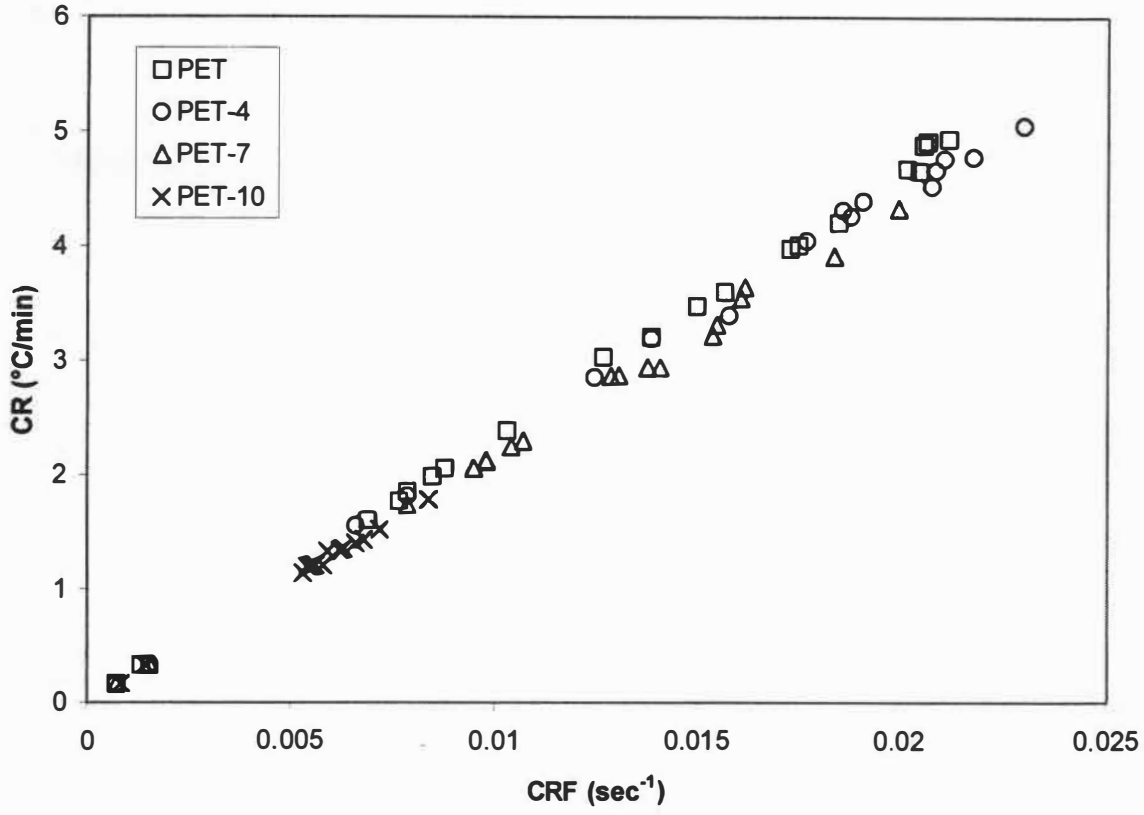

PET:	y = 230.68x + 0.0184	R^2 = 0.9991
PET-4:	y = 222.09x + 0.0339	R^2 = 0.9979
PET-7:	y = 214.75x + 0.016	R^2 = 0.9982
PET-10:	y = 210.39x + 0.0239	R^2 = 0.9974

Figure 4.81: Relationship between CRF and CR for the Four Materials

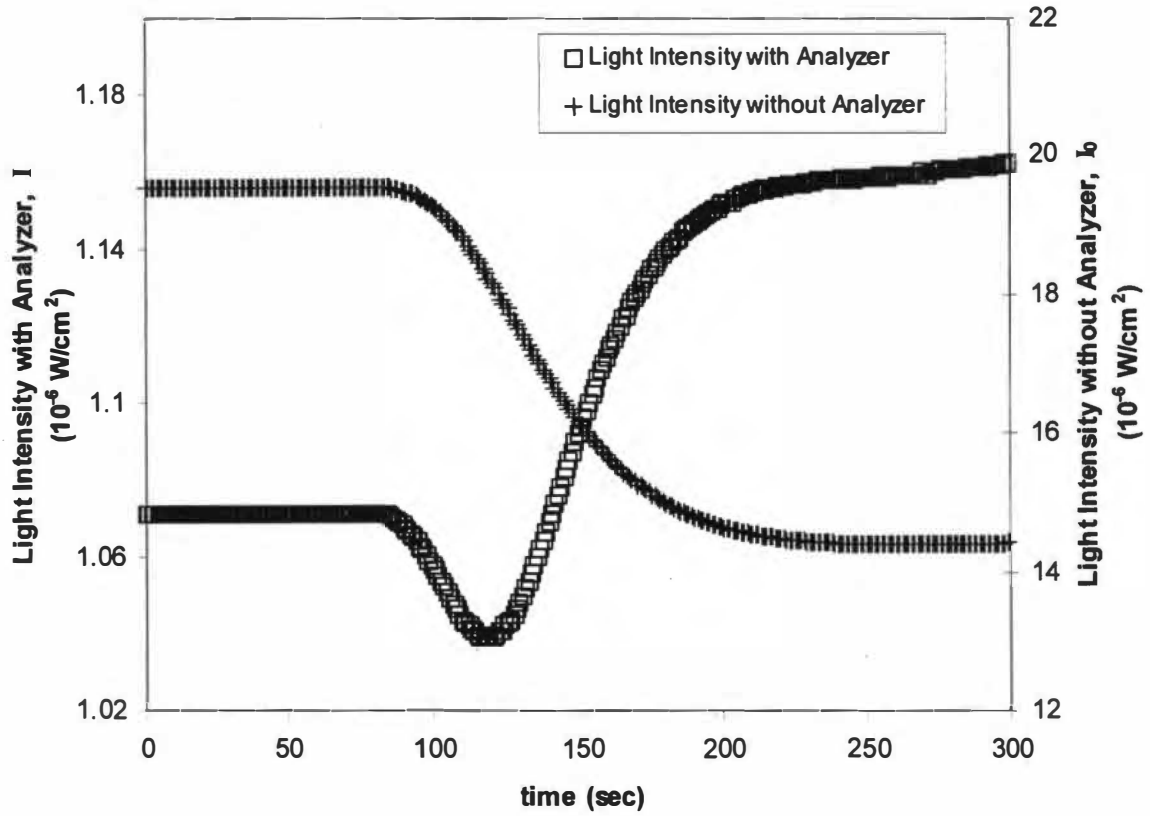

Figure 4.82: Typical Plot of I and I_0 for Copolyesters at Lower Cooling Rates Using Nitrogen Gas Cooling System. In this case the data is for PET-10 sample with CRF=0.0053 sec^{-1}.

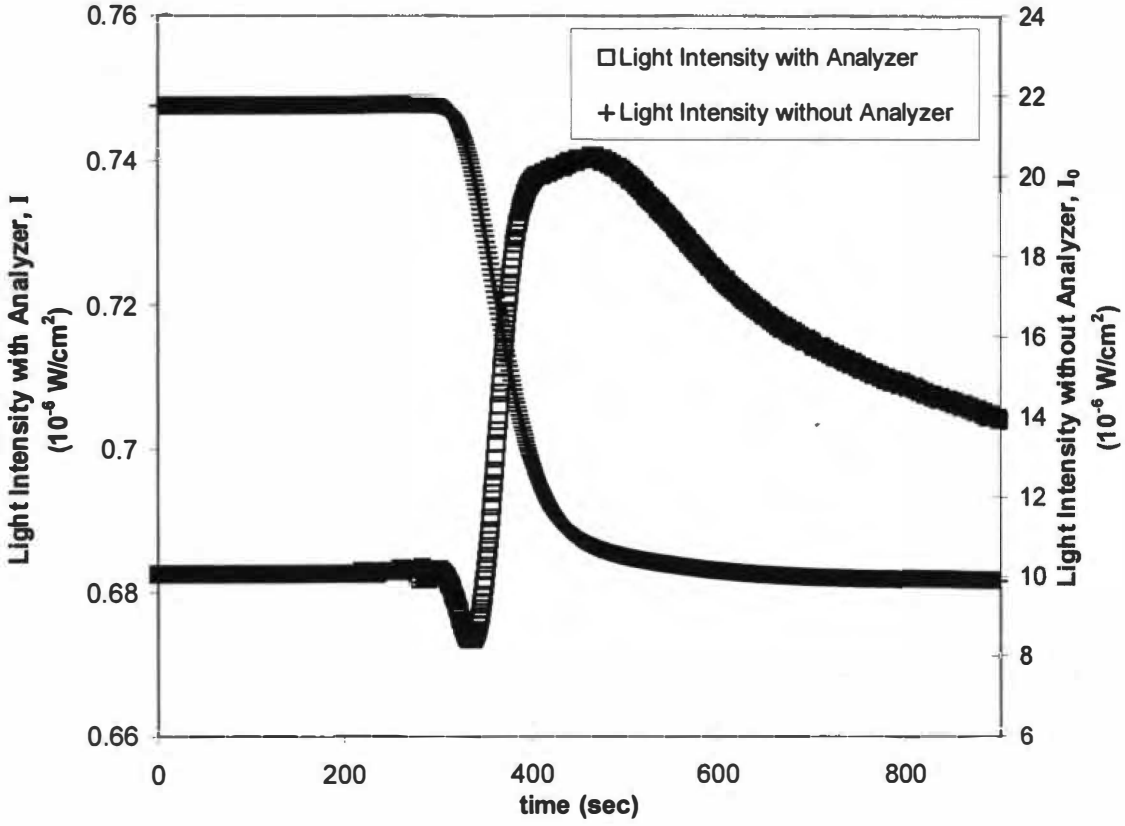

Figure 4.83: Typical Plot of I and I_0 for 10mol% Copolymer Cooled at 20°C/min Cooling Rate Using Hotstage.

an analyzer is expected to yield just the opposite result since it is expected that the spherulitic morphology of the crystallized polymer will rotate and scatter light away from the objective lens as crystallization ensues.

As is explained by Ding and Spruiell (1996), as spherulites first begin to form they have a tendency to scatter more light than they depolarize. However, as the number and size of the spherulites increase, a point is reached where the spherulites scatter less light. Experimentally this can be observed in the plot of I and/or I_0 and explains why the local minimum is observed for I in Figures 4.82 and 4.83.

Not every raw data plot resembled that shown in Figures 4.82 and 4.83. Those samples crystallized at the lowest cooling rates actually more resembled that shown in Figure 4.84, here for a PET-7 copolyester crystallized at 10°C/min. In these cases it was observed that again, the light intensity without an analyzer, I_0 decreases with increasing time and can be explained as being due to the fact that light is rotated away from the objective lens as the sample becomes more birefringent. However, the plot of the light intensity with an analyzer, I, as a function of time appears very different from that shown in Figures 4.82 and 4.83. In this case, as the polymer first begins to crystallize, the light intensity passes through a local minimum, reaches a maximum value and then slowly decreases again to a minimum value whose magnitude is lower than the initial value of I. It is likely that, as before, the local minimum in the curve is due to the initial scattering of light by small spherulites while the increase to a local maximum is due to the rotation of light by the birefringent polymer spherulites. As the polymer sample continues to reach a higher degree of crystallinity it is likely that some of the light initially leaking through the analyzer, as well as some of light rotated by the polymer sample becomes absorbed and

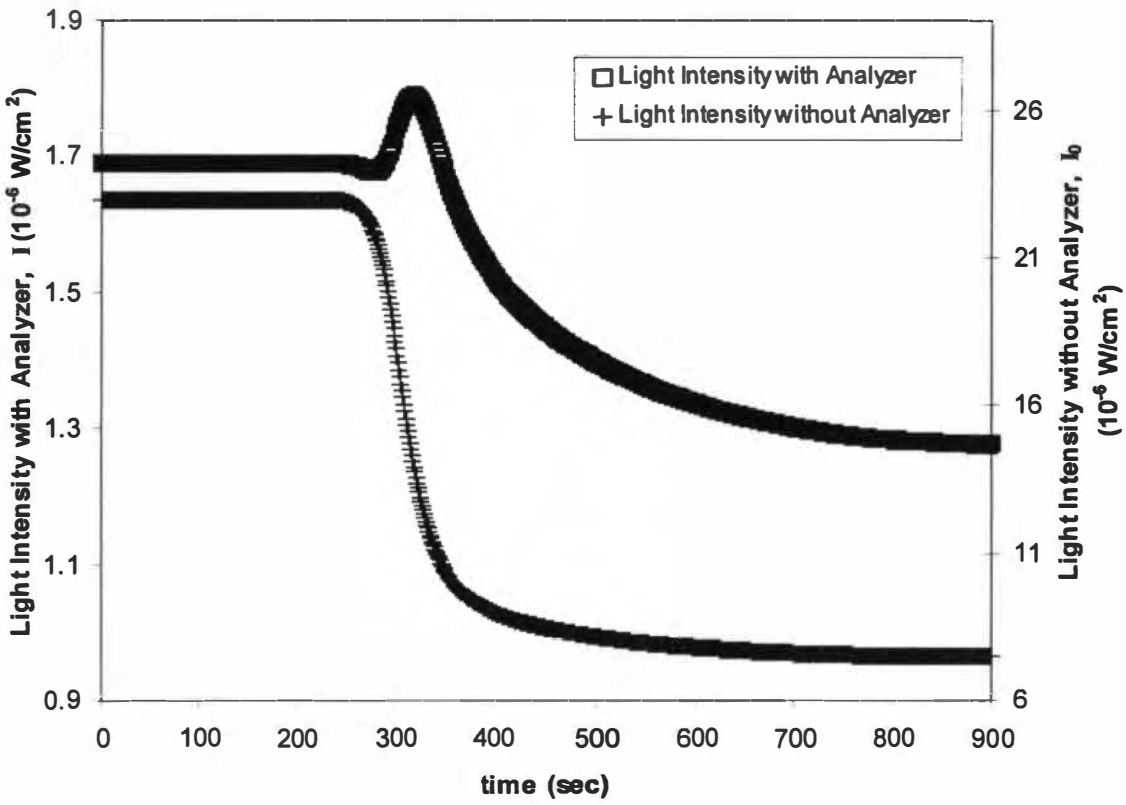

Figure 4.84: Typical Plot of I and I_0 for Copolyesters Crystallized Using Hotstage. In This Case the Data is Taken for a 7 mol% MPDiol at 10°C/min.

scattered away from the objective lens as the polymer reaches higher and higher degrees of crystallinity. Thus it is expected that this phenomena is related to the thickness of the specimen and that this effect would become less significant as sample thickness decreases.

It was observed that as the cooling rate increased the optical quality of the sample changed significantly with cooling rate. Samples crystallized using the hot-stage cooling rate appeared translucent, nearly opaque. However, as the cooling rate was increased the samples became more and more transparent until finally the samples appeared to be completely quenched. It should be noted that this general observation does not apply to the PET homopolymer samples. For PET homopolymer, the samples always appeared to be nearly opaque and only appeared slightly translucent at the highest measured cooling rates. This is undoubtedly due to the fact that these samples have been shown to contain $Ti0_2$, which in itself scatters light thus giving the polymer a white appearance, even when molten.

The change in optical properties with increasing cooling rate can be seen by examining the plots of I as a function of I_0 for samples crystallized under different cooling conditions. As is shown in Figures 3.5-3.8, samples crystallized at the lowest cooling rates showed a much steeper slope in the plot of I versus I_0 than those subjected to higher cooling rates. This increase in slope with decreasing cooling rate indicates that samples crystallized at the lower cooling rates were found to depolarize more light than those cooled at higher cooling rates. This is to be expected since as cooling rate is increased it is expected that the spherulite size and quality will decrease.

The third type of curve observed during this experiment was sometimes observed at the highest cooling rates using the nitrogen gas cooling method and is shown in Figure 4.85. These types of curves were most prevalent for samples that were crystallized at cooling rates somewhat near the critical quenching cooling rate. In these cases, again the plot of I_0 appears to not change significantly from that found earlier. However, the plot of I looks significantly different from that described earlier. In these cases, I also decreases with time. This is likely due to the fact that the spherulites never achieve the critical size required to sufficiently depolarize the light to the objective lens and thus the decrease in intensity is likely due to light being scattered away from the objective lens by the small spherulites.

Once the raw data was obtained equations 3.10 and 3.11 were used to convert the raw data to relative light intensity, R, and ultimately the reduced crystallinity, $\theta(t)$. Both the relative light intensity and the reduced crystallinity, plotted as functions of time, are shown in Figure 4.86 for PET homopolymer with a CRF=0.0069 sec^{-1}. In this figure it is evident that the two curves are identical in shape and differ only in magnitude.

Typical reduced crystallinity conversion curves as functions of temperature are shown in Figure 4.87 for PET homopolymer where it is evident that an increase in the cooling rate causes the conversion curves to shift to lower temperatures, much as was observed in the nonisothermal DSC experiment. Figure 4.88 shows these same conversion curves as functions of time (i.e. $t-t_0$ where t_0 is the time when crystallization is first detected) where it is evident that the rate of crystallization appears to increase with increasing cooling rate, as indicated by the slopes of these curves.

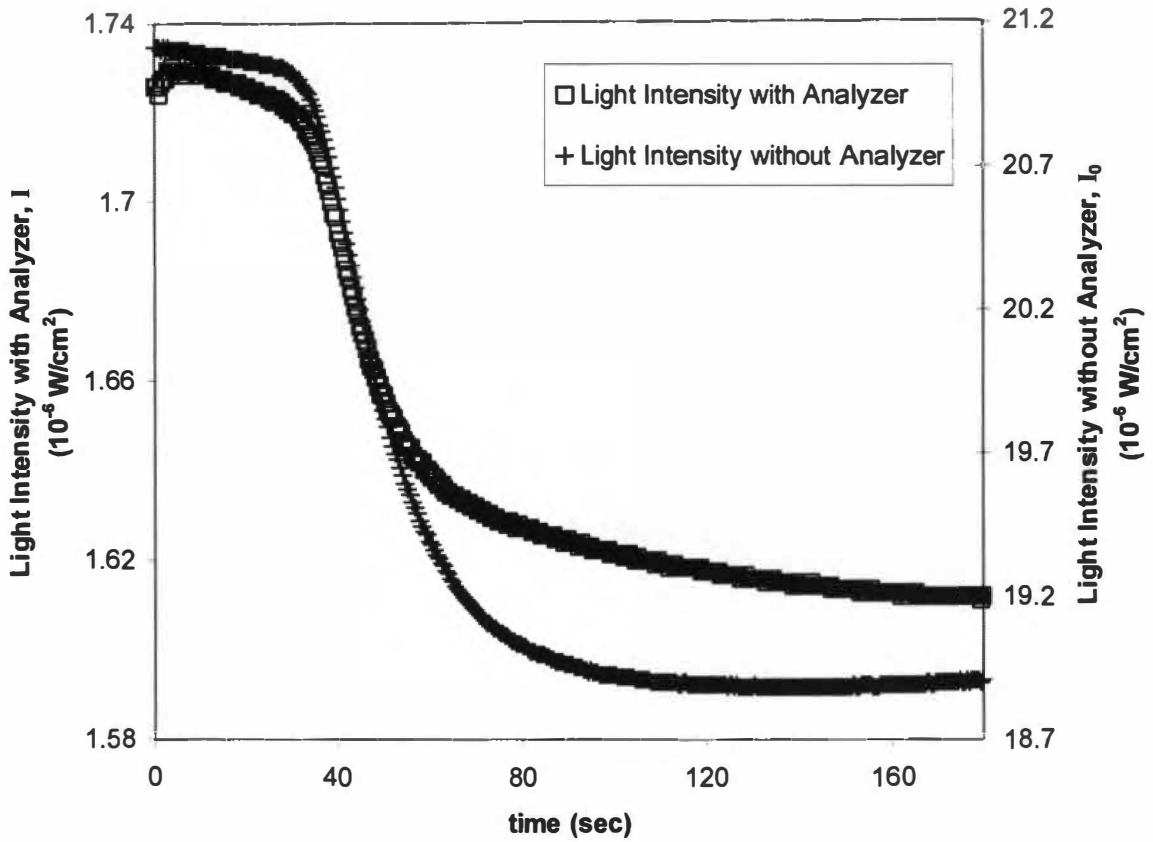

Figure 4.85: Observed Plot of I and I_0 for Copolyesters at Higher Cooling Rates Using Nitrogen Gas Cooling System. In this case the data is for PET-7 copolymer with CRF=0.02 sec^{-1}.

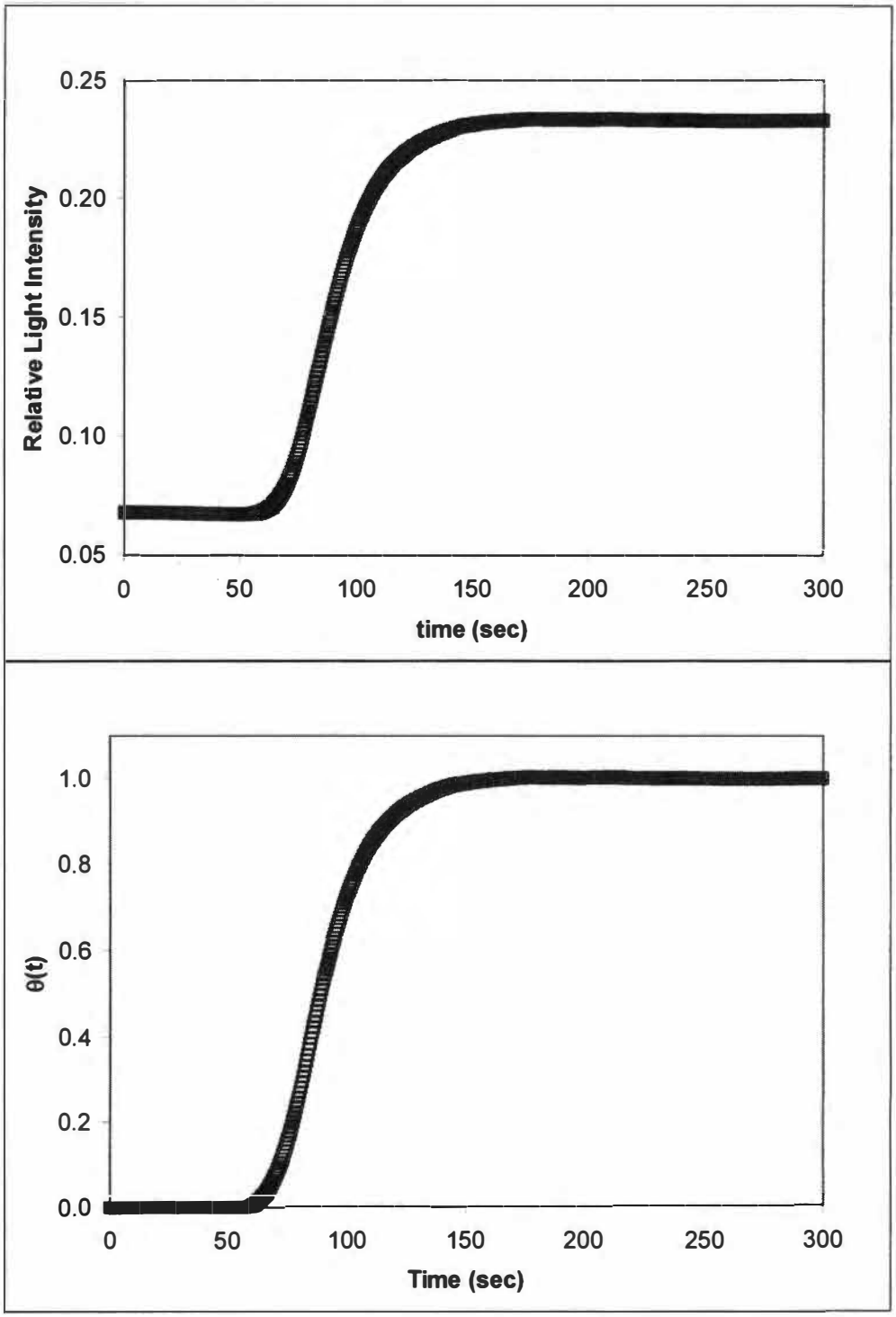

Figure 4.86: Relative Light Intensity and Relative Degree of Crystallinity for PET Homopolymer with CRF=0.0069 sec^{-1}

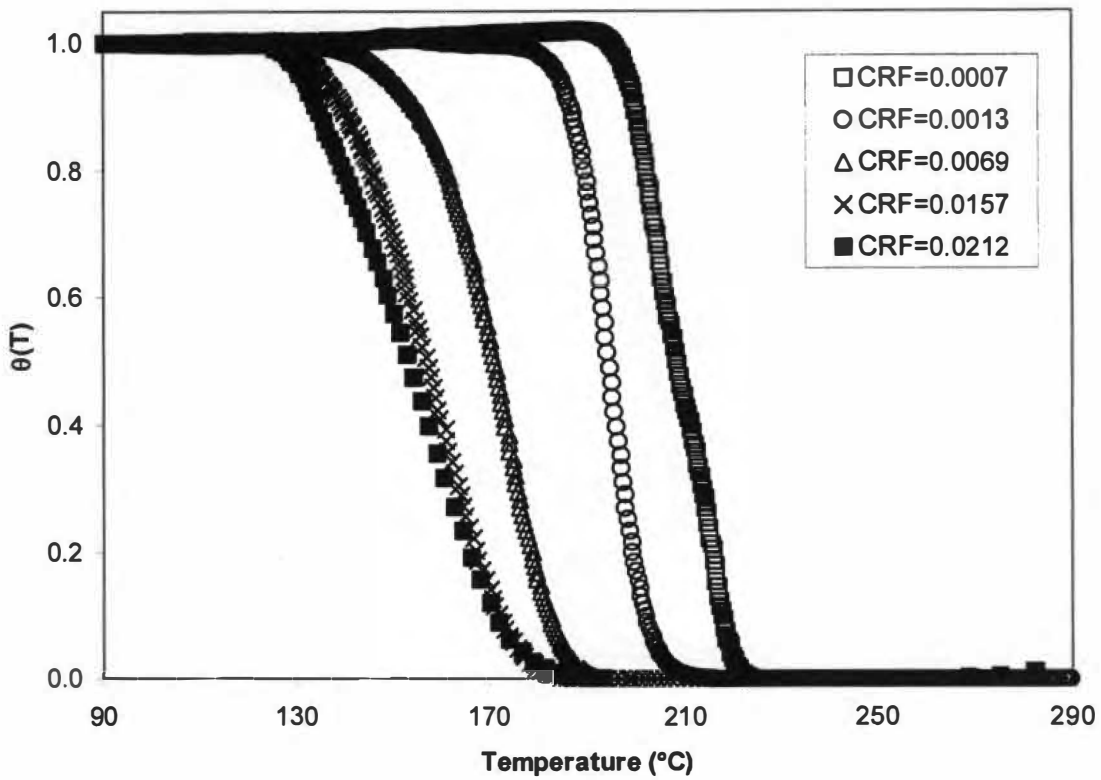

Figure 4.87: Conversion Curves as a Function of Temperature for PET Homopolymer Under Five Different Cooling Conditions

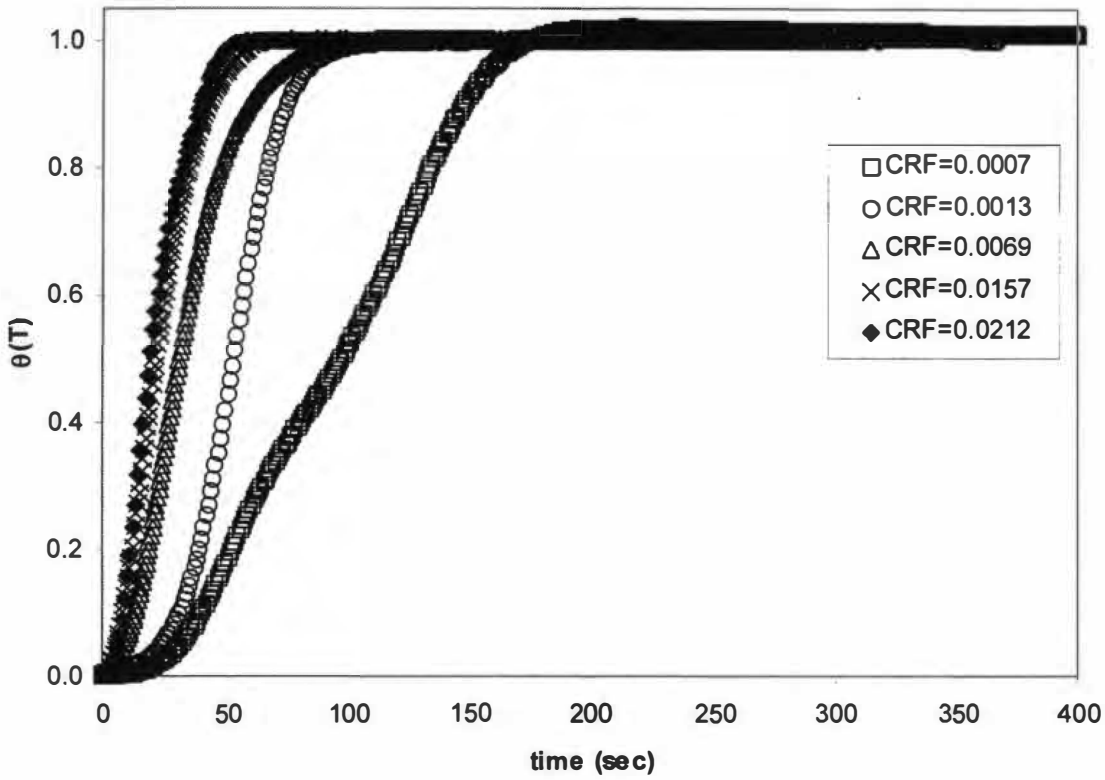

Figure 4.88: Conversion Curves as a Function of Time for PET Homopolymer at Five Different Cooling Conditions

As mentioned earlier, the CRF and CR were determined by the application of regression lines from the initial temperature (290°C) to the temperature where crystallization was first observed. Although this is considered to be best method for determining these quantities it is important to mention that this introduces some error with regard to the direct comparison of dissimilar materials (i.e. materials with different equilibrium melting temperatures).

Figure 4.89 shows a conversion plot for PET homopolymer and for a 10mol% MPDiol copolyester where it is evident that, although both of these samples are subjected to more or less the same calculated CRF, the temperature range over which crystallization occurs is significantly different. In general it was observed that as comonomer content is increased the temperature at which crystallization occurs is shifted to lower temperatures. Thus a PET homopolymer sample cooled at a given CRF will crystallize over a higher range of temperatures compared to that for the copolyester samples.

The fact that these materials crystallize at different temperatures has a profound effect on the values determined for CRF and CR. Figure 4.90 shows the cooling curves for PET homopolymer with CRF=0.0069 sec^{-1} along with the cooling curve for a PET-10 sample with CRF=0.0068 sec^{-1}. It is evident that, although the calculated value of CRF is nearly identical for these two curves, they are substantially different. This is reinforced by Figure 4.91 where the regression lines used to determine both CRF and CR for the two materials are shown. Here it is evident that not only is the cooling rate curve for the PET-10 sample initially much steeper than for the PET homopolymer sample, but also the best fit trend lines for the PET-10 sample appear to not fit the experimental data as well due to the fact that these lines are fit to a wider temperature range. Nevertheless, it

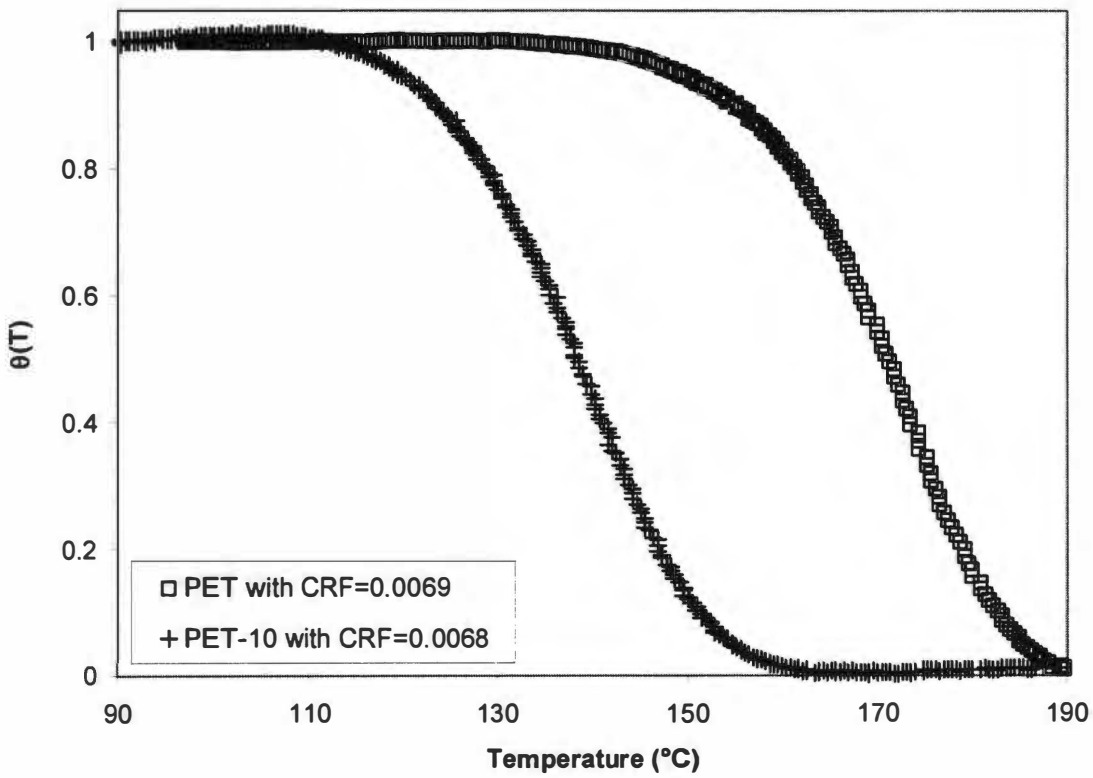

Figure 4.89: Plot of Reduced Crystallinity for PET and PET-10 at Nearly the Same CRF. Note CRF Units in sec^{-1}.

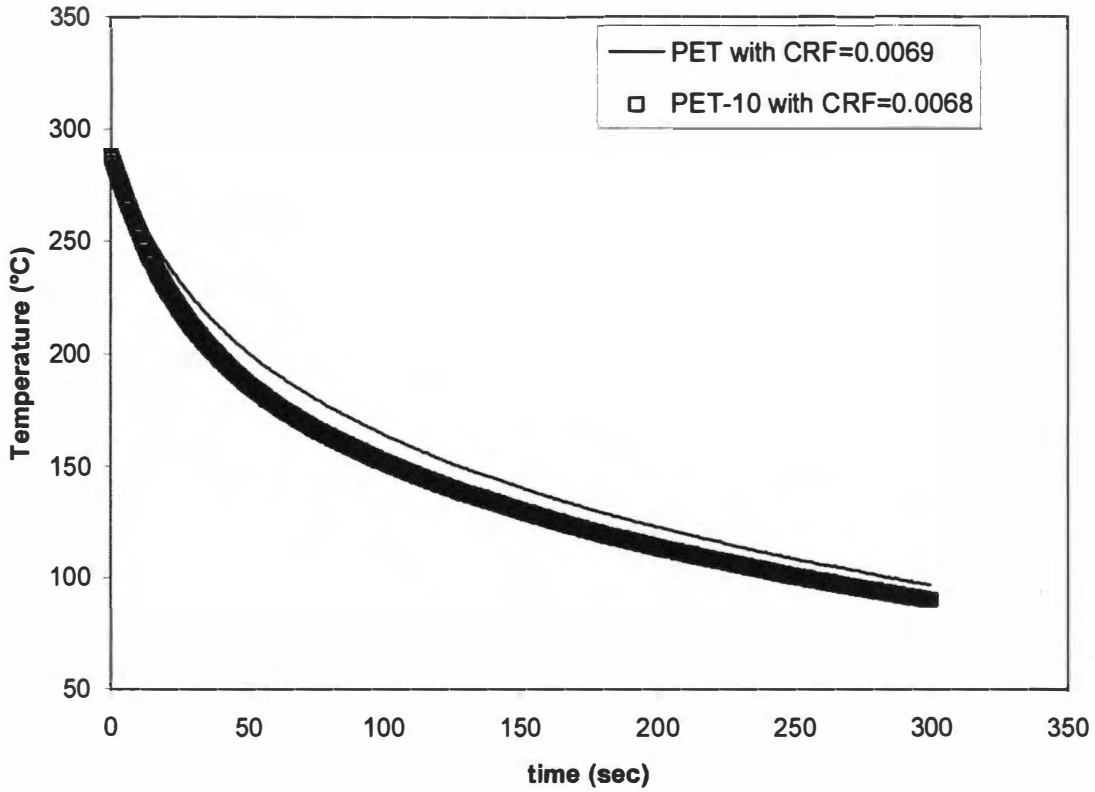

Figure 4.90: Cooling Plots for PET and PET-10 at Nearly the Same Calculated CRF Note CRF Units in sec^{-1}.

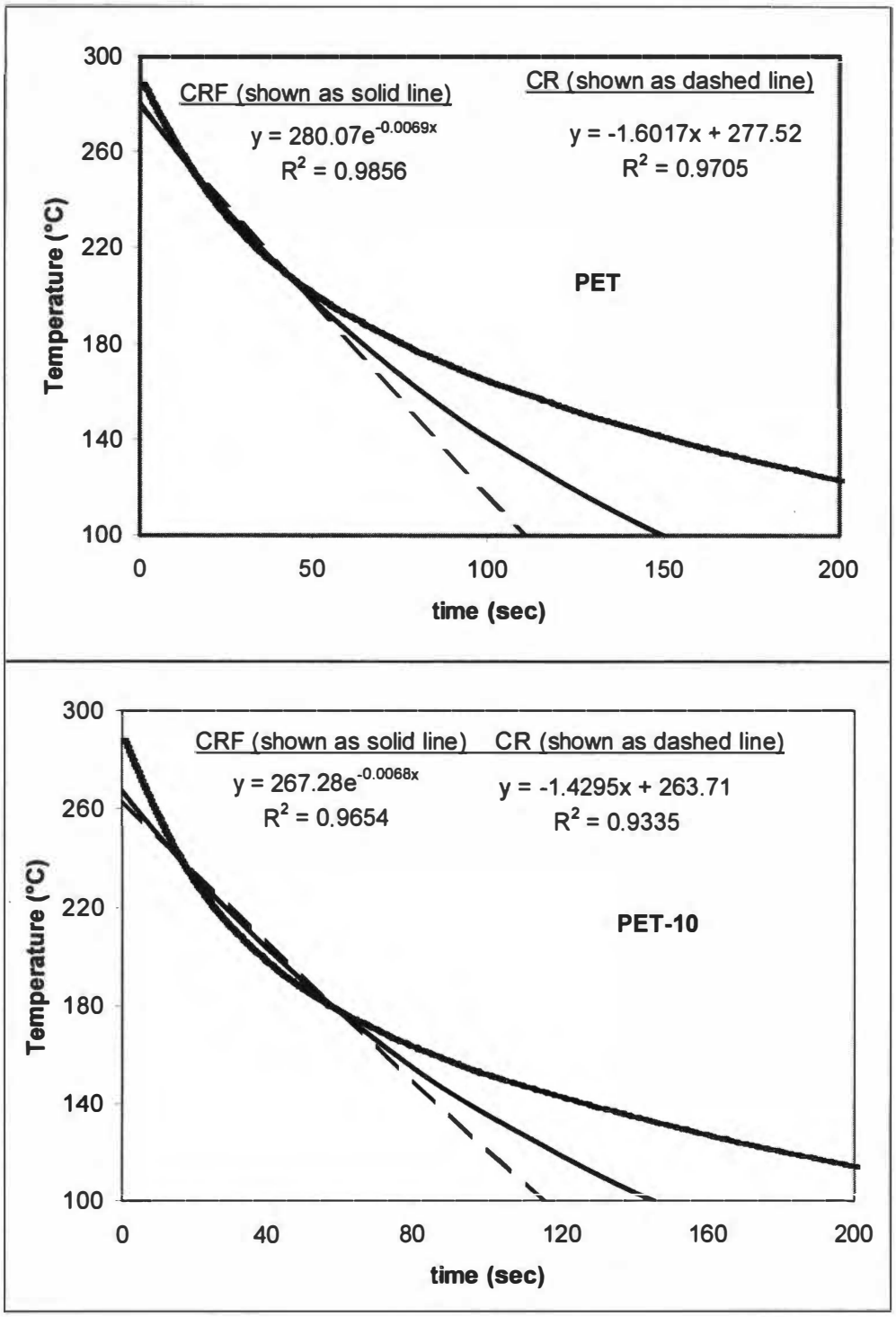

Figure 4.91: Zoomed View of PET and PET-10 Cooling Curves Illustrating Trend lines Used to Determine CR and CRF

was decided that this is likely the best method for comparing these materials with regard to cooling rate and therefore has been included in this analysis. As will be shown in the next section, an alternate method of comparing the crystallization kinetics of these materials will be to compare them on the basis of temperature.

Figure 4.92 shows a plot of the half time of crystallization when cooled from the initial temperature 290°C as a function of CRF, while Figure 4.93 shows a plot of the half time of crystallization determined as the time when $\theta(t)=0.50$ less the time taken for the sample to reach its equilibrium melting temperature when cooled from a standard temperature in the melt (ca. 290°C). Although Figures 4.92 and 4.93 appear to be nearly identical from a qualitative standpoint, it is believed that the representation of the data in Figure 4.93 is the most theoretical sound method for examining these data in that it takes undercooling into account. In either case however, it is apparent that PET homopolymer and the 4mol% copolyester crystallize at nearly the same rate at a given CRF value. Likewise it appears that the PET-7 samples crystallized just slightly less rapidly and that the 10mol% samples crystallized the slowest at a given cooling rate.

The half time data ($t_{0.5}$-t_0) for PET homopolymer appears to agree quite well with that found for the nonisothermal DSC experiments at 10°C/min. On the other hand it appears that the half-time data for the three copolyesters containing MPDiol do not agree well with that found during DSC experiments and suggests that these copolyesters are crystallizing much more rapidly than that observed during DSC experiments (as indicated by the $t_{0.5}$-t_0 data found in Tables 4.14 – 4.17). Although the cover slips were carefully cleaned with a clean cloth prior to sample preparation it is conceivable that contaminants

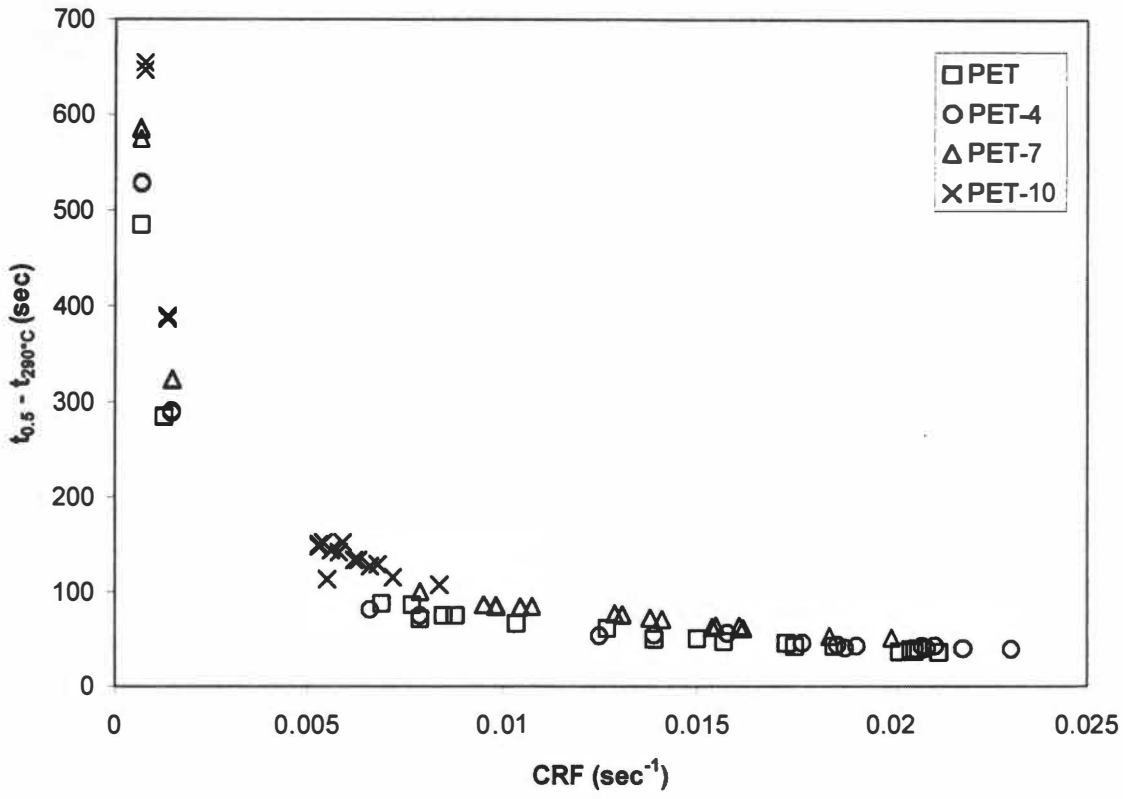

Figure 4.92: Plot of $t_{0.5}$-$t_{290°C}$ as a Function of CRF for Four Materials

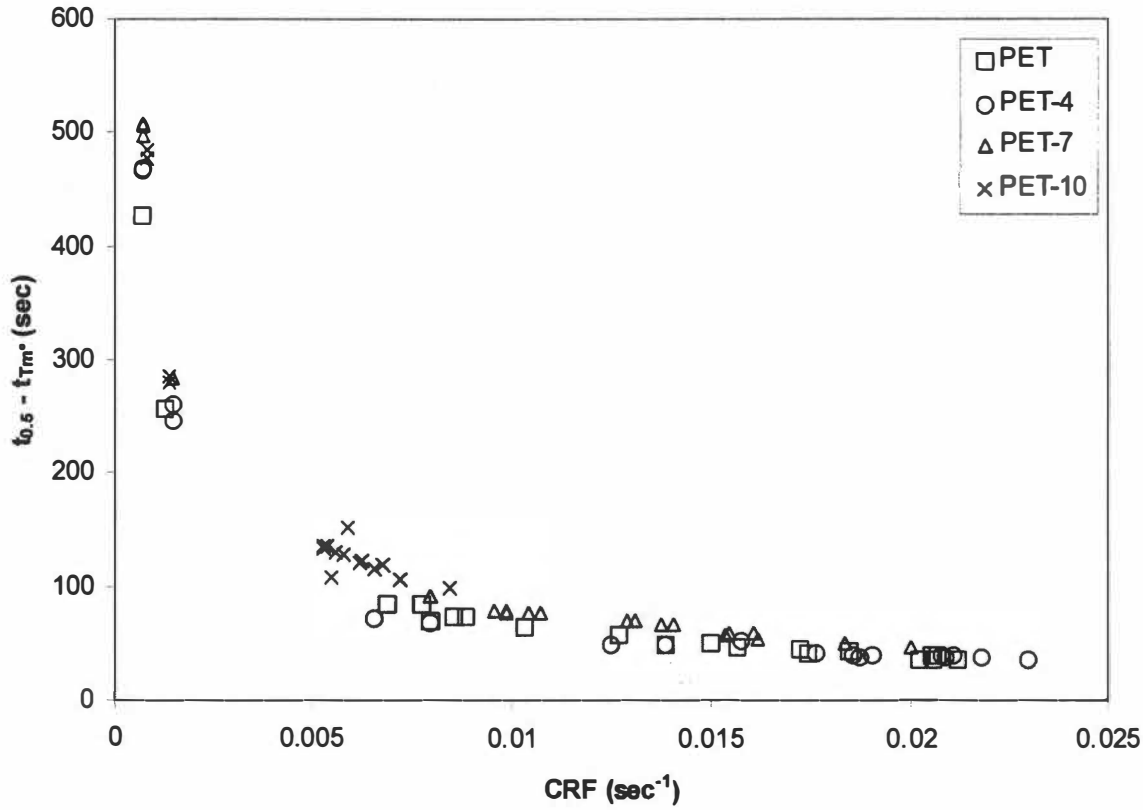

Figure 4.93: Plot of $t_{0.5}$-t_{Tm^o} as a Function of CRF for Four Materials

on the surface of the cover slips or on the surface of the imbedded thermocouple may have led to an enhanced nucleation rate for these materials.

4.3.2.2. Avrami Analysis

An Avrami analysis was applied to the experimental data over the range, $0.10 \leq \theta(t) \leq 0.80$ and is illustrated in Figure 4.94 for PET homopolymer. For clarity not all of the experimental data is shown in this figure. As is shown the Avrami equation appeared to fit the experimental data quite well over the specified range. As before, these plots suggest that as cooling rate is increased the Avrami data is shifted further and further to the left.

The results of the Avrami analysis are listed in Tables 4.18-4.21. Note that from Table 4.18, the Avrami analysis predicts that PET homopolymer cooled at 10°C/min (0.0007°C/sec) will crystallize more rapidly than at a CR= 20°C/min (0.0013°C/sec). This is known not to be the case as the slopes of the conversion curves shown in Figure 4.88 clearly suggest that the PET homopolymer sample crystallized at 20°C/min does crystallize much more rapidly than the sample crystallized at 10°C/min. This was also confirmed from the half-time data shown earlier. However, it would appear that the Avrami rate constant predicts just the opposite effect. This would suggest that, in this particular situation, it appears that the Avrami equation fails to accurately predict the actual crystallization kinetics of this polymer under these conditions. Some insight into this apparent discrepancy might be obtained by examining Figure 4.95 where a zoomed view of the Avrami plot for the PET homopolymer sample crystallized at 10°C/min

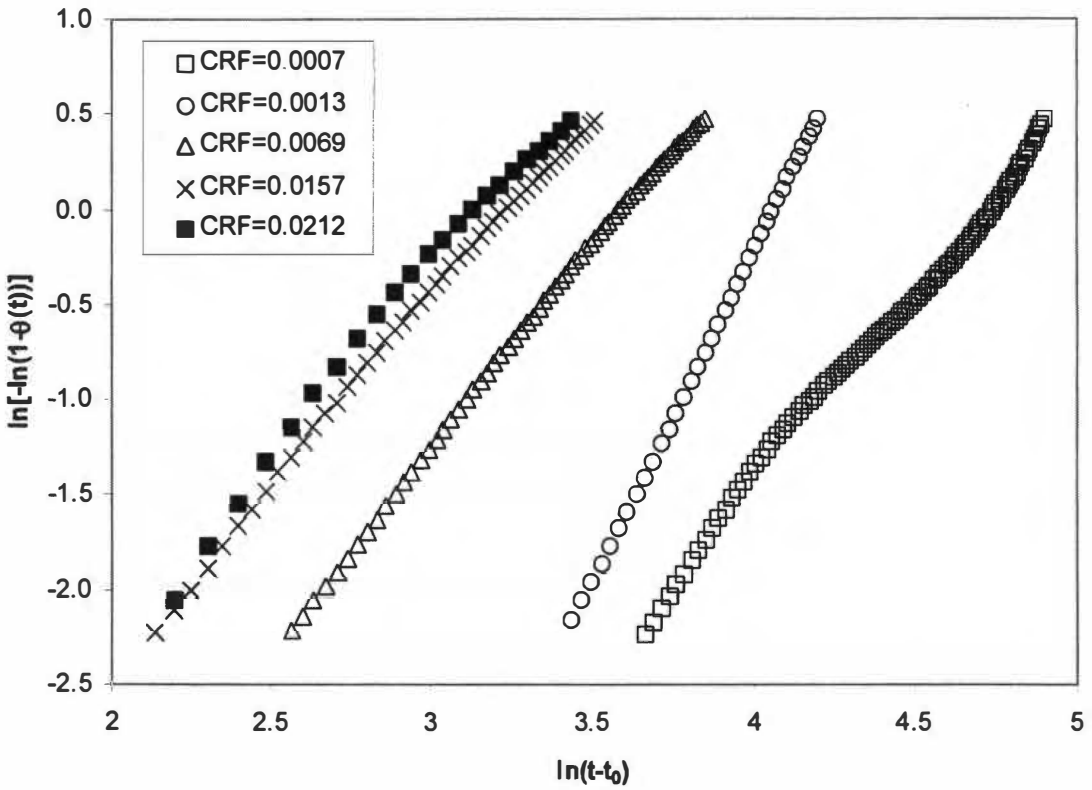

Figure 4.94: Typical Avrami Plots for PET Homopolymer at Five Cooling Rates (CRF)

Table 4.18: Avrami Summary Data for Nonisothermal Crystallization of PET Homopolymer Using LDM System

CRF (sec^{-1})	CR (°C/sec)	k (sec^{-n})	n	$k_{0.5}$ (sec^{-n})
0.0007	0.1676	7.10E-05	2.03	6.50E-05
0.0007	0.1681	9.11E-05	1.97	8.48E-05
0.0013	0.3331	7.41E-07	3.47	7.40E-07
0.0013	0.3333	2.79E-06	3.19	2.85E-06
0.0013	0.3332	8.58E-06	2.97	8.47E-06
0.0069	1.6017	5.12E-04	2.11	5.34E-04
0.0077	1.7716	3.14E-04	2.18	3.21E-04
0.0079	1.8530	2.05E-04	2.53	2.07E-04
0.0085	1.9857	5.85E-04	2.07	5.97E-04
0.0088	2.0528	7.18E-04	2.01	7.34E-04
0.0103	2.3852	1.00E-03	1.99	1.02E-03
0.0127	3.0328	9.55E-04	1.97	1.00E-03
0.0139	3.2045	2.03E-03	1.88	2.16E-03
0.0150	3.4761	1.16E-03	2.02	1.17E-03
0.0157	3.5970	1.82E-03	1.95	1.85E-03
0.0173	3.9736	3.96E-03	1.69	4.00E-03
0.0175	4.0052	4.05E-03	1.73	4.23E-03
0.0185	4.2073	2.13E-03	1.95	2.20E-03
0.0202	4.6711	4.28E-03	1.79	4.53E-03
0.0205	4.6513	1.91E-03	2.04	2.00E-03
0.0206	4.8783	1.56E-03	2.03	1.66E-03
0.0207	4.9093	1.66E-03	2.08	1.72E-03
0.0212	4.9304	1.91E-03	1.99	2.02E-03

Table 4.19: Avrami Summary Data for Nonisothermal Crystallization of PET-4 Copolyester Using LDM System

CRF (sec^{-1})	CR (°C/sec)	k (sec^{-n})	n	$k_{0.5}$ (sec^{-n})
0.0007	0.1656	2.54E-07	3.69	2.60E-07
0.0007	0.1658	1.96E-07	3.77	2.04E-07
0.0015	0.3329	3.37E-06	3.38	3.49E-06
0.0015	0.3343	2.90E-06	3.39	3.03E-06
0.0066	1.5510	2.63E-05	3.29	2.67E-05
0.0079	1.8119	1.36E-05	3.42	1.36E-05
0.0125	2.8475	4.05E-04	2.58	4.28E-04
0.0139	3.1913	4.56E-04	2.43	4.80E-04
0.0158	3.3932	6.47E-04	2.26	6.73E-04
0.0177	4.0422	4.94E-04	2.41	5.40E-04
0.0186	4.3135	2.15E-04	2.63	2.32E-04
0.0188	4.2600	5.50E-04	2.39	5.95E-04
0.0191	4.3901	3.38E-04	2.54	3.71E-04
0.0208	4.5185	2.46E-03	2.00	2.51E-03
0.0209	4.6566	1.14E-03	2.23	1.19E-03
0.0211	4.7588	1.45E-03	2.11	1.53E-03
0.0218	4.7736	2.86E-03	1.97	2.97E-03
0.0230	5.0485	2.94E-03	2.00	3.11E-03

Table 4.20: Avrami Summary Data for Nonisothermal Crystallization of PET-7 Copolyester Using LDM System

CRF (sec^{-1})	CR (°C/sec)	k (sec^{-n})	n	$k_{0.5}$ (sec^{-n})
0.0007	0.1668	7.31E-07	3.33	7.75E-07
0.0007	0.1667	3.79E-07	3.44	3.83E-07
0.0007	0.1668	2.36E-07	3.65	2.41E-07
0.0015	0.3333	6.12E-07	3.58	6.63E-07
0.0015	0.3347	8.01E-07	3.52	8.46E-07
0.0079	1.7355	7.54E-05	2.50	7.84E-05
0.0095	2.0579	4.40E-04	2.10	4.49E-04
0.0098	2.1237	2.63E-04	2.21	2.75E-04
0.0098	2.1170	5.24E-04	2.06	5.56E-04
0.0104	2.2467	5.05E-04	2.04	5.26E-04
0.0107	2.2952	6.63E-04	1.97	6.80E-04
0.0129	2.8586	4.75E-05	2.61	4.84E-05
0.0131	2.8634	1.54E-04	2.33	1.54E-04
0.0138	2.9437	7.23E-04	1.99	7.40E-04
0.0141	2.9427	2.54E-04	2.25	2.69E-04
0.0154	3.2155	1.21E-03	1.98	1.22E-03
0.0155	3.3130	9.47E-04	2.00	9.58E-04
0.0161	3.5438	2.99E-04	2.21	3.12E-04
0.0162	3.6420	4.00E-04	2.21	4.17E-04
0.0184	3.9067	7.82E-04	2.16	7.94E-04
0.0200	4.3273	1.22E-03	2.04	1.27E-03

Table 4.21: Avrami Summary Data for Nonisothermal Crystallization of PET-10 Copolyester Using LDM System

CRF (sec^{-1})	CR (°C/sec)	k (sec^{-n})	n	$k_{0.5}$ (sec^{-n})
0.0008	0.1671	1.24E-05	2.52	1.26E-05
0.0008	0.1678	2.53E-05	2.40	2.63E-05
0.0014	0.3351	2.94E-05	2.34	3.02E-05
0.0014	0.3342	3.38E-05	2.30	3.52E-05
0.0053	1.1384	1.58E-04	2.13	1.61E-04
0.0053	1.1373	1.67E-04	2.09	1.71E-04
0.0054	1.1943	6.21E-05	2.30	6.42E-05
0.0055	1.1968	1.57E-04	2.11	1.66E-04
0.0056	1.2079	9.96E-05	2.24	1.03E-04
0.0058	1.2062	1.68E-04	2.21	1.73E-04
0.0059	1.3280	1.23E-04	2.19	1.27E-04
0.0062	1.3388	2.31E-04	2.04	2.34E-04
0.0063	1.3495	1.82E-04	2.09	1.85E-04
0.0066	1.3988	1.94E-04	2.18	1.96E-04
0.0068	1.4295	1.32E-04	2.20	1.34E-04
0.0072	1.5172	1.64E-04	2.21	1.69E-04
0.0084	1.7793	9.61E-05	2.33	9.91E-05

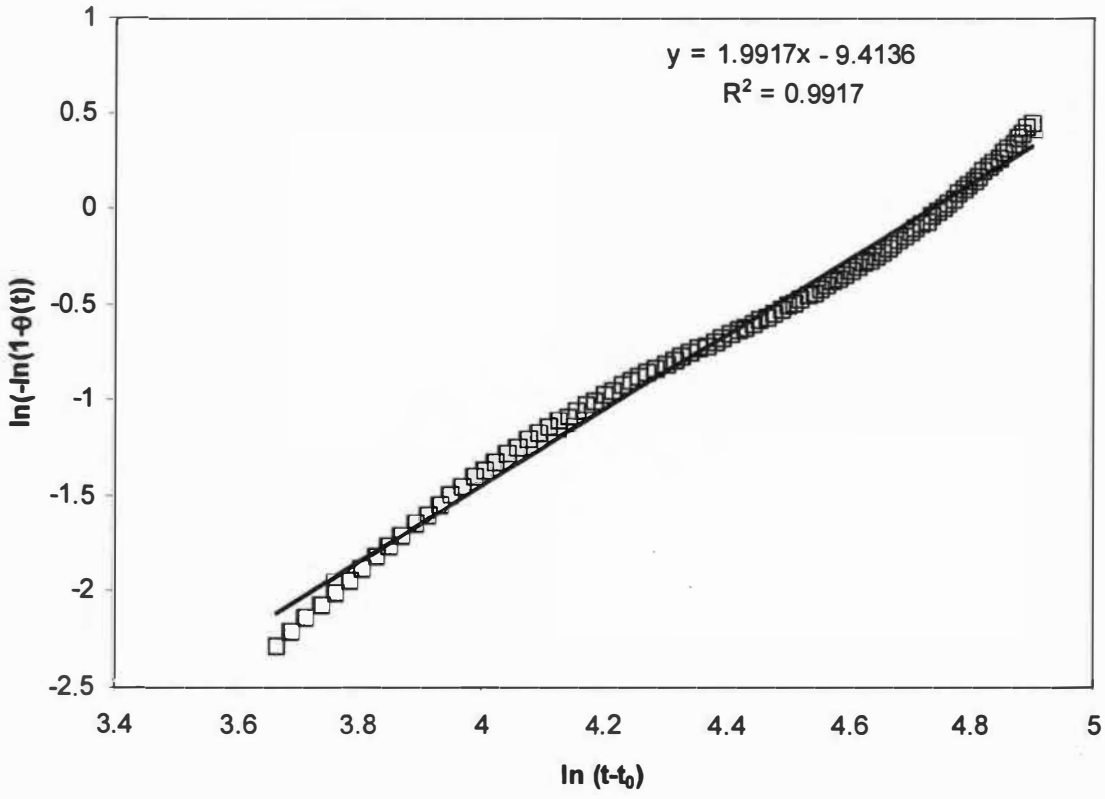

Figure 4.95: Typical Avrami Plot for PET Homopolymer Crystallized at 10C/min Using LDM method

is shown. Notice in this plot that, although the correlation coefficient is predicting good linearity, the line appears to contain several "wiggles" which appear to be much more prevalent than that found for the samples crystallized at higher cooling rates. Note also that these same wiggles are observed in the time based conversion curve shown in Figure 4.88. Wiggles in the Avrami curve such as that shown in Figure 4.95 are often attributed to secondary crystallization, although it was shown in the previous section using DSC that at 10°C/min, there did not appear to be a significant difference between the heat of crystallization and the heat of melting which signified that there was likely very little secondary crystallization at this particular cooling rate. The general shape of this curve may have something to do with the optical characteristics of the PET homopolymer crystallized under such slow conditions.

Figure 4.96 shows a plot of the Avrami rate constant, k, as a function of the crystallization half-time temperature, $T\{\theta(t)=0.50\}$. Again, although there does appear to be significant scatter in the experimental data it is quite evident that PET homopolymer crystallizes much more rapidly than the other copolymers at a given temperature, and that an increase in comonomer concentration serves to decrease the rate of crystallization. As before, the Avrami rate constant also appears to increase in an exponential type fashion.

The Avrami indices in this experiment were found to range from approximately 1.7 - 3.8 for the PET homopolymer, PET-4, and PET-7 samples which agrees reasonably well with that obtained by nonsiothermal crystallization using DSC. On the other hand, the PET-10 samples were found to have values of n ranging from 2.0 - 2.5. Although these values are somewhat lower than that observed in the Avrami analysis of the nonisothermal DSC data, they do agreed reasonably well with that observed for the

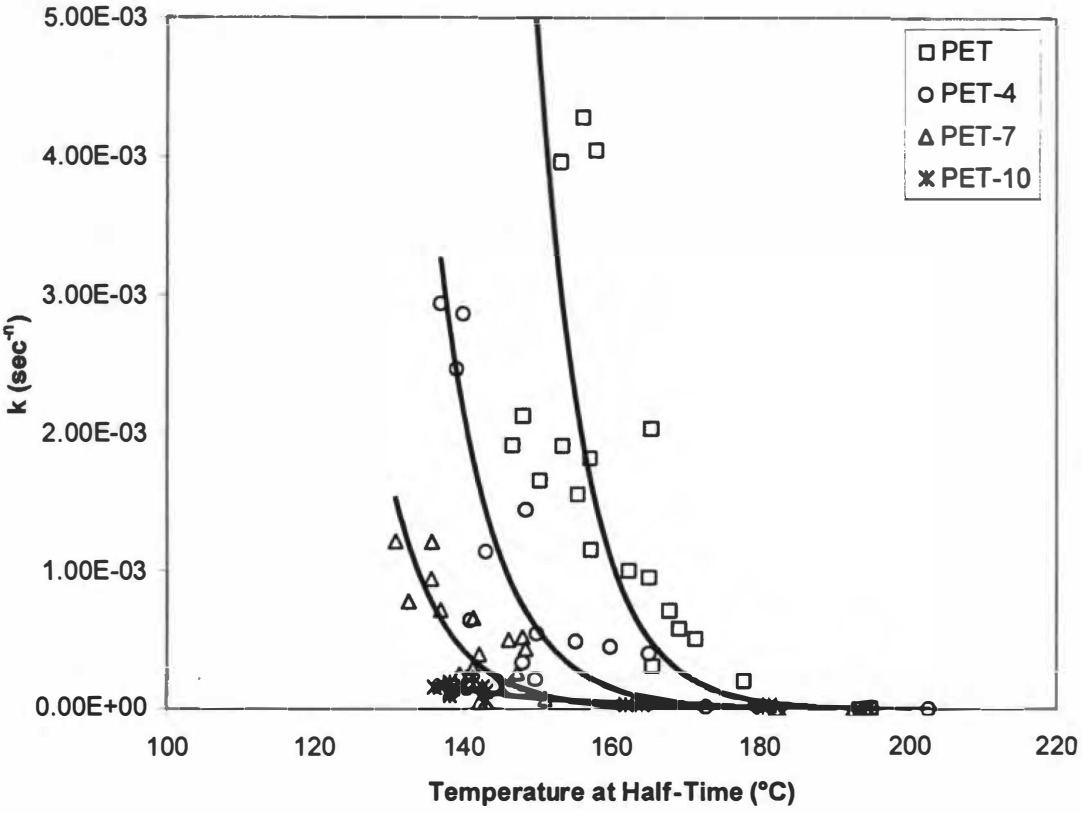

Figure 4.96: Plot of Avrami Rate Constant, k, as a Function of Temperature at Half Time of Crystallization

isothermal crystallization of these copolyesters, as well as that obtained in the Ozawa analysis.

Although there is significant scatter in the experimental data, Figure 4.97 shows the effect of cooling rate on the Avrami indices for these four materials. From this plot it appears that n decreases with increasing cooling rate. As would be expected n also appears to decrease with decreasing temperature, as is illustrated in Figure 4.98.

The results of this experiment would seem to indicate that, as before, the crystallization rate is impeded by the addition of the MPDiol comonomer even under these high cooling conditions. It is expected that this is likely due to the rejection of the comonomer from the parent PET homopolymer crystal.

4.3.2.3. Complications Associated with the Application of the LDM Technique to These Materials

The data does appear to indicate that the addition of MPDiol negatively influences the crystallizability and crystallization kinetics of PET copolymers at high cooling rates. However, it is important to point out that there is a need to refine the analysis of the LDM data for this particular class of materials.

As was discussed earlier, because these materials are capable of being quenched to the glassy state there is a dramatic change in the optical characteristics of these polymers with increasing cooling rate. At low cooling rates the crystallinity developed becomes so significant that a substantial portion of the light is absorbed and scattered away from the light detector, while at higher cooling rates, the materials become completely translucent and glassy. This drastic change in optical properties may lead to a

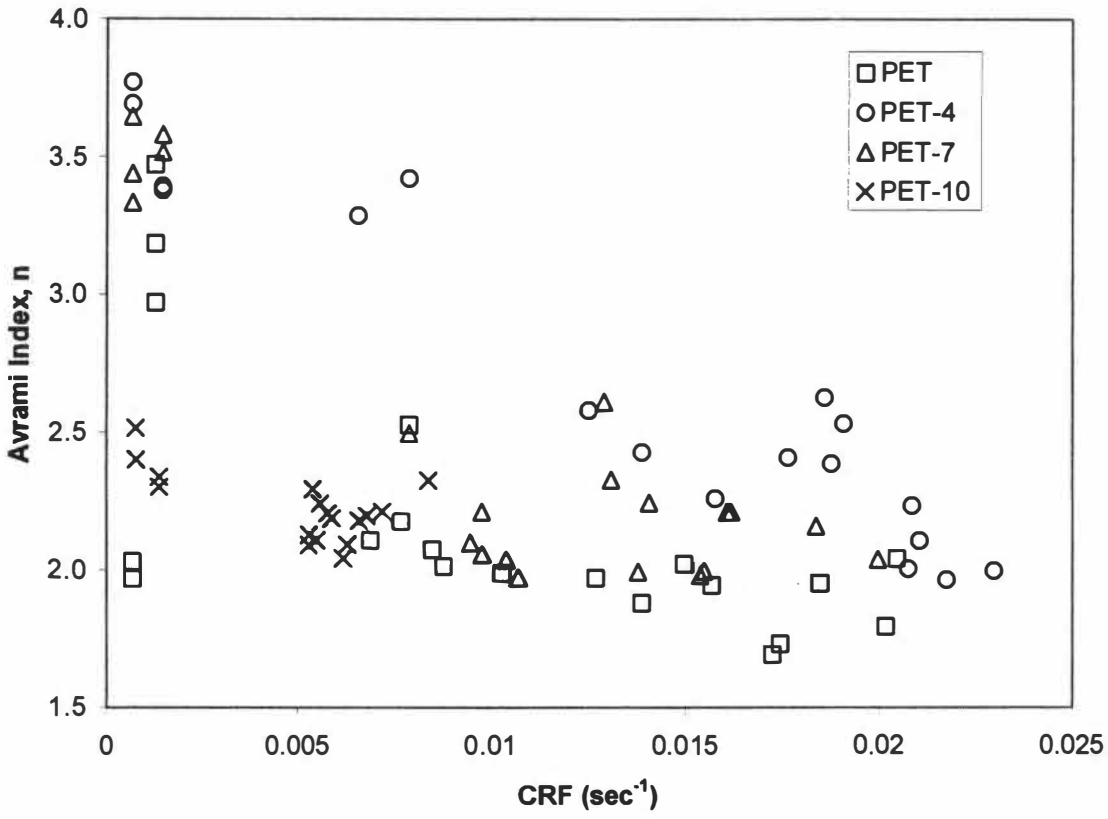

Figure 4.97: Relationship Between Avrami Index, n and CRF

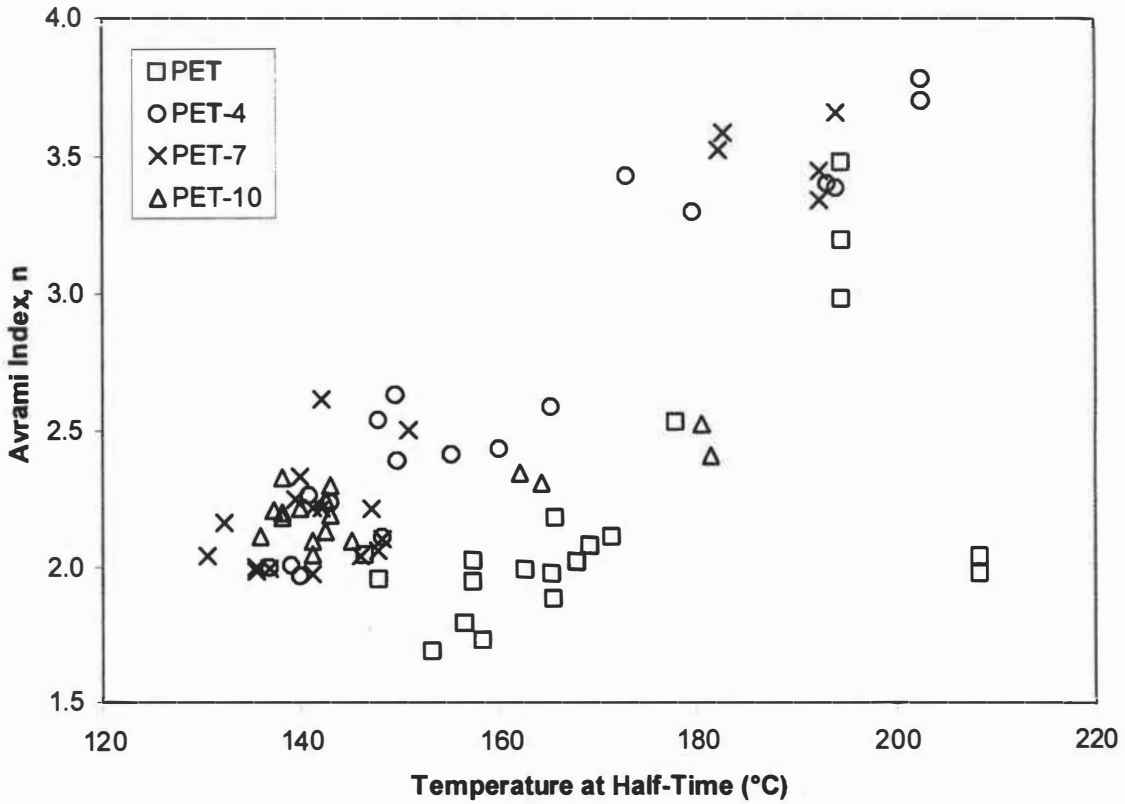

Figure 4.98: Relationship Between Avrami Index, n and the Temperature at Half Time

significant error in the value of the constant, C_2, as well as influence the results of this data.

The fact that these materials do not exhibit a plateau temperature would suggest that, unlike the materials that have been investigated by this technique in the past, the crystallization of these materials occurs over a wide range of temperatures. As was described earlier, PE and i-PP were both shown to exhibit the plateau temperature. Additionally, this plateau temperature was shown to occur over a substantial portion of the crystallization process. Thus in these cases, the materials could be treated as occurring under pseudoisothermal conditions. Unfortunately, with the materials tested here this is hardly the case. Thus some additional research is recommended to establish how to treat this unique kind of situation.

4.3.2.4. Estimation of Critical Cooling Rate for Quenching to the Glassy State and Determination of Continuous Cooling Transformation Diagram (CTT)

As described earlier, as the cooling rate is increased, the optical properties of these materials, with the exception of the PET homopolymer samples containing $Ti0_2$, shifted from nearly opaque to completely transparent when the material was quenched.

To approximate the critical quenching cooling rate (QCR) for each material samples were prepared as described earlier and subjected to higher and higher cooling rates until the sample appeared to be completely quenched when viewed under a microscope using crossed polars. The critical cooling rate was then determined by applying both a linear curve fit to determine CR and an exponential curve fit to determine CRF. Since there was no initial crystallization temperature to aid in establishing the

limits to apply the trend lines, all best-fit trend lines were applied over the same temperature range, namely from 290 to 190°C. This allowed not only for a consistent, reproducible method for determining the cooling rate, but also allows for a more direct comparison between these four materials.

While this technique would probably be sufficient for determining QCR for the MPDiol copolymer samples, in that the materials can be visually inspected after each cooling run, the PET samples which appear translucent, even in the molten state, required a somewhat different technique to approximate QCR. This was accomplished by examining the plots of I and I_0 as a function of both time and temperature for the copolyester samples that appeared to be quenched. A typical plot of I and I_0 as a function of time is shown in Figure 4.99 for a PET-4 sample cooled at a CRF=0.0449 sec^{-1}.

Although the sample appeared to be visually quenched, I and I_0 appear to be displaying a behavior that might lead to the conclusion that some crystallization is occurring during the cooling run. To investigate this behavior, a sample was prepared where the polymer sample and thermocouple arrangement was replaced by an additional cover slip sandwiched between two other cover slips. The sample was then placed in the LDM sample chamber, heated for three minutes, and then cooled rapidly to mock an actual experimental run. The results of this experiment are shown in Figure 4.100 where it is shown that there appears to be a significant amount of signal drift in these two curves. More surprising is the fact that the signal appears to shift so significantly that this could be misconstrued as a thermodynamic response of a real sample. It is conceivable that this phenomena might be caused by a change in the interface between the cover slips during cooling which might affect the light intensity measurements by means of a

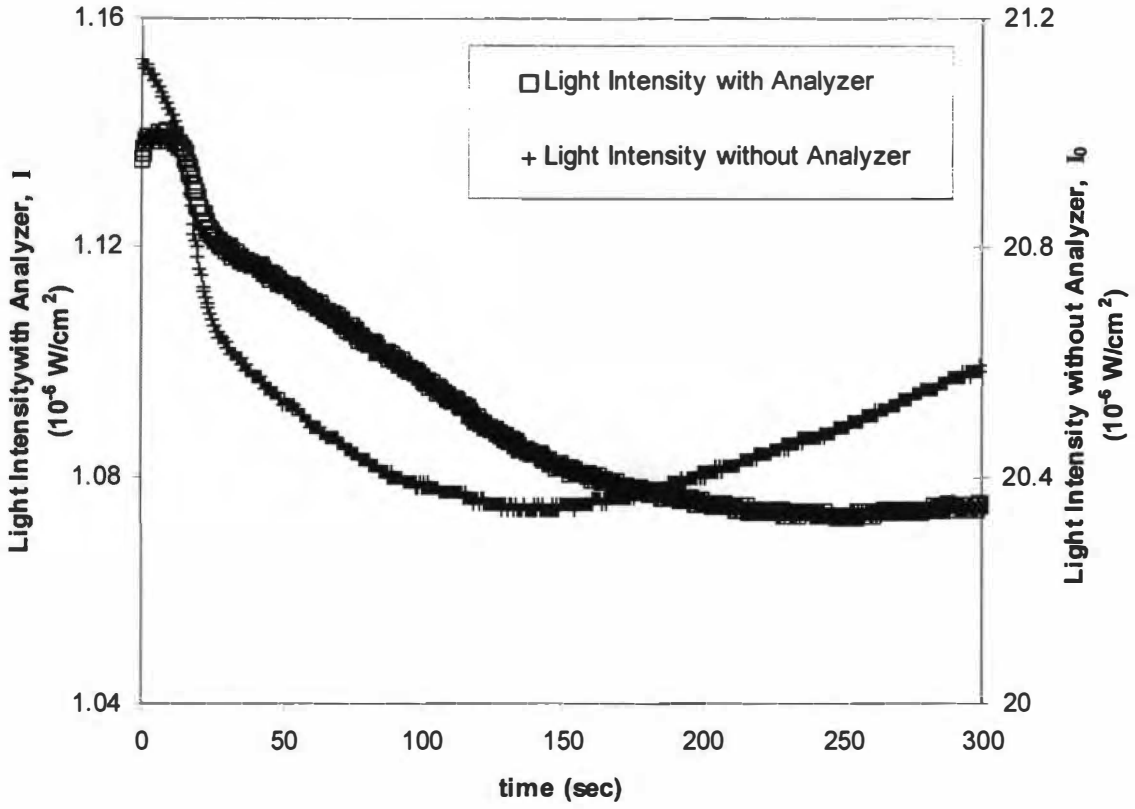

Figure 4.99: Typical Plot of I and I_0 as a Function of Time for Quenched PET-4 Sample

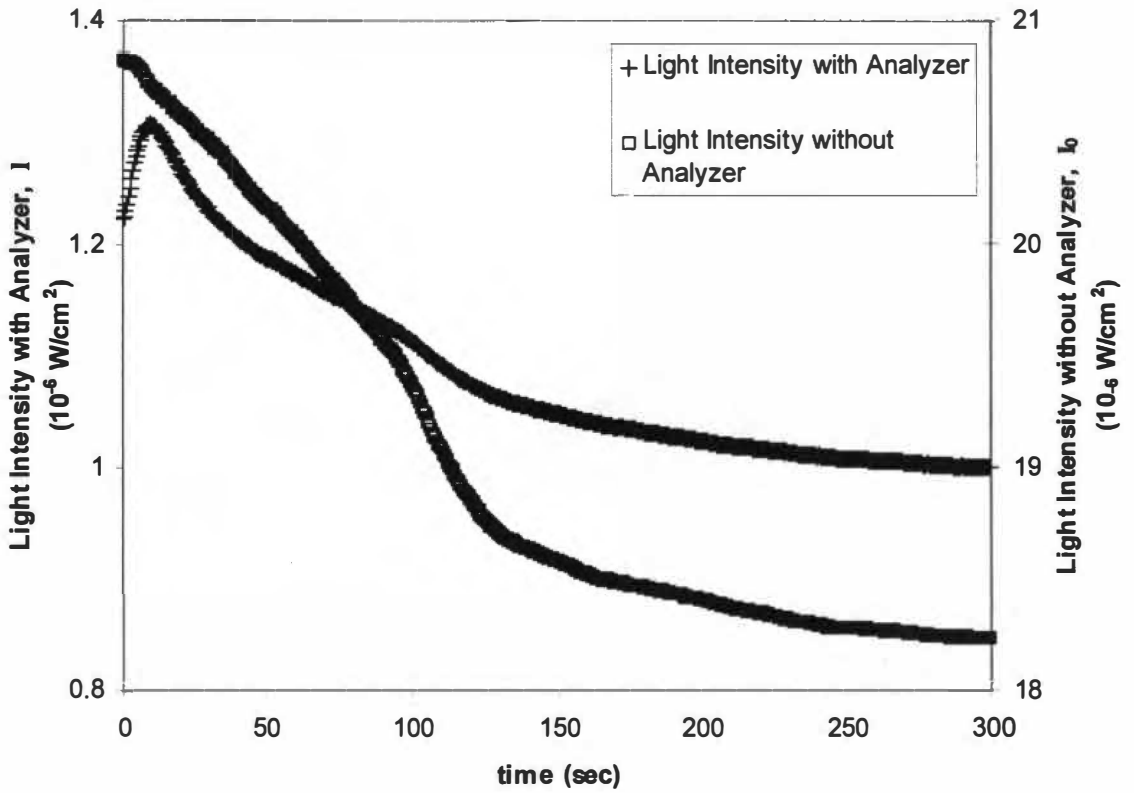

Figure 4.100: Resulting Plot of I and I_0 as a Function of Time for Cover Glass Sample

changing refractive index at the cover slip interface. The relative magnitude of the baseline response of this system would probably not be very significant for PP or PE or even PET at low cooling rates but surely might be responsible for some experimental error in these data, especially for those samples crystallized at the higher cooling rates.

To estimate QCR for these materials all of the plots were compared to Figure 4.100. Comparing Figures 4.99 and 4.100 it is evident that both the relative magnitude of the change in I and I_0, as well as the general qualitative shape of this plot resembles that found for the cover glass sample. Using these assumptions the QCR was estimated from the experimental data.

Figure 4.101 shows a typical "quenched" plot for PET homopolymer. Notice in this plot that again the relative magnitude of change in I and I_0 is similar to that obtained for the cover glass sample containing no polymer. However, notice also that qualitatively this plot looks somewhat different than that observed for the other copolyesters. However, examination of I and I_0 as functions of temperature, shown in Figure 4.102, would suggest that the inflection points in I and I_0 are not likely due to crystallization since it appears that this peak transition occurs very near the glass transition temperature and appears to continue on after the glass transition temperature has been reached. Since the glass transition temperature marks the point of the cessation of the molecular motions necessary for diffusion, any signal change that occurs and/or continues after reaching this temperature is likely due to some phenomena other than crystallization thus signifying that the polymer is likely quenched to the amorphous state.

While it is believed that the method employed to conduct this portion of the analysis is probably a close approximation to the actual value of QCR for each material,

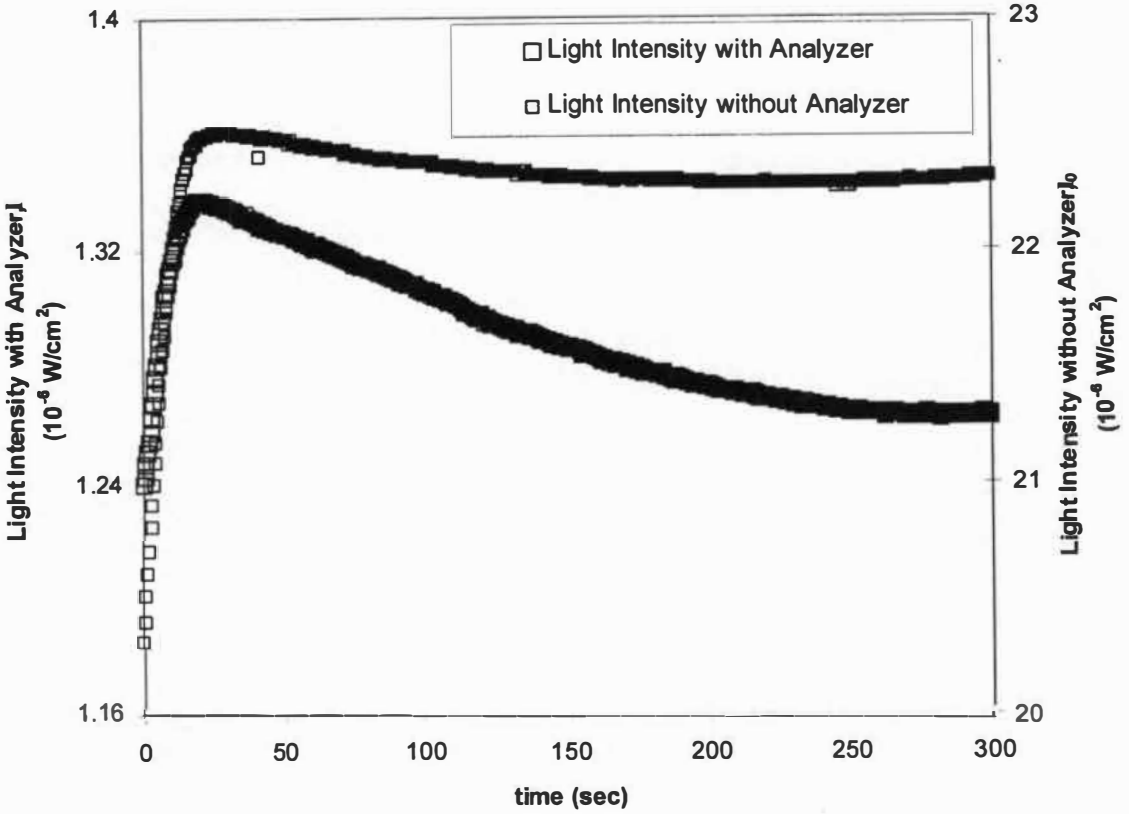

Figure 4.101: Typical Quench Plot of I and I_0 as a Function of Time for PET Homopolymer

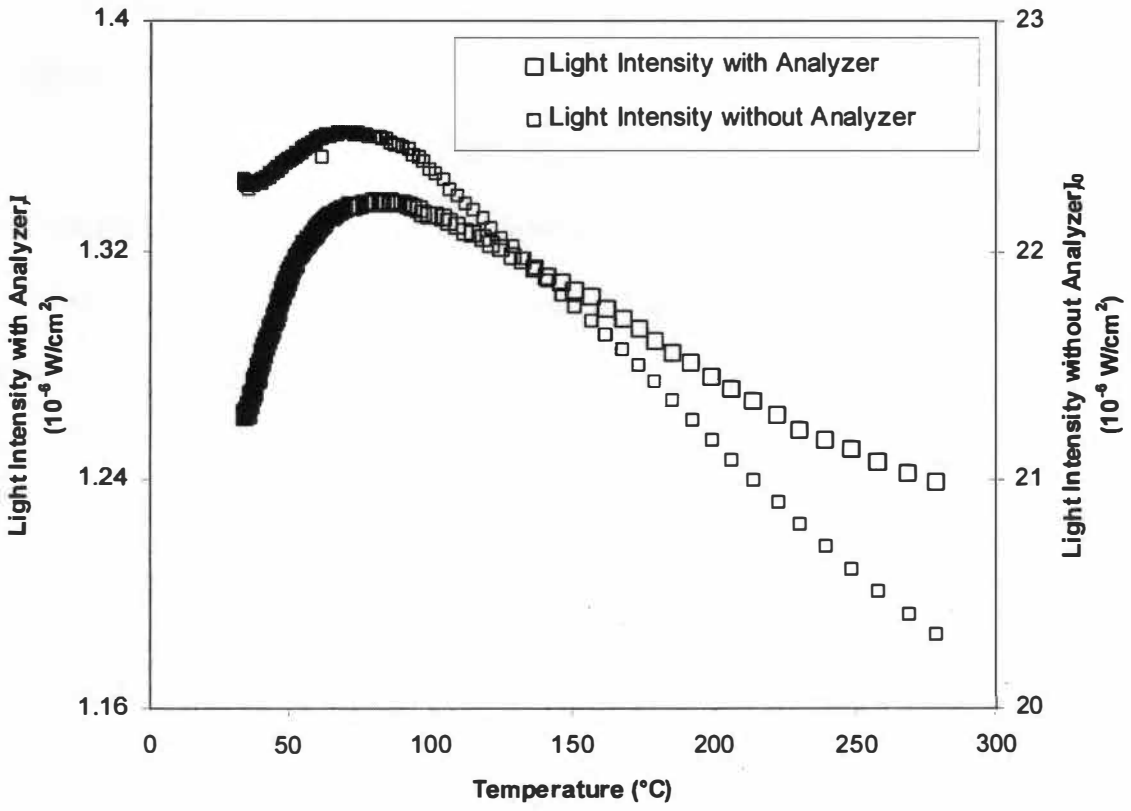

Figure 4.102: Typical Quench Plot of I and I_0 as a Function of Temperature for PET Homopolymer

an independent technique such as WAXD or DSC should be used to determine the precise value. It is possible that some crystallinity may have developed in the sample, or that at least some nuclei were developed during the rapid quenching process.

Once the QCR was determined for each material, the beginning and ending temperatures of crystallization, called T_s and T_f respectively, were plotted as a function of time to develop a Continuous Cooling Transformation (CCT) diagram for each material. These CCT diagrams are shown in Figures 4.103-4.106.

Although there is some scatter in the experimental data it does appear that the plot of temperature versus log time for these materials fits the data reasonably well. These plots could be used to estimate whether a particular cooling condition would be sufficient to obtain a particular morphology, much like a CCT diagram is applied in modern metallurgical practice. In particular this type of curve might be best utilized in a mathematical model used to predict whether, under certain processing conditions, one of these materials might crystallize. This might be applicable to the modeling of a blow molding process or possibly even a fiber spinning process where the degree of crystallinity as a function of cooling rate is crucial to ensure product performance and aesthetic considerations. It is important to note however that this investigation does not take into account for the effects of molecular orientation, which is known to drastically increase crystallization rate.

The QCR for each material are also shown in these figures along with the respective standard deviations. This data would indicate that an increase in MPDiol concentration significantly influences the crystallization behavior of the material at high cooling rates. Although these cooling rates are estimates, there does appear to be a

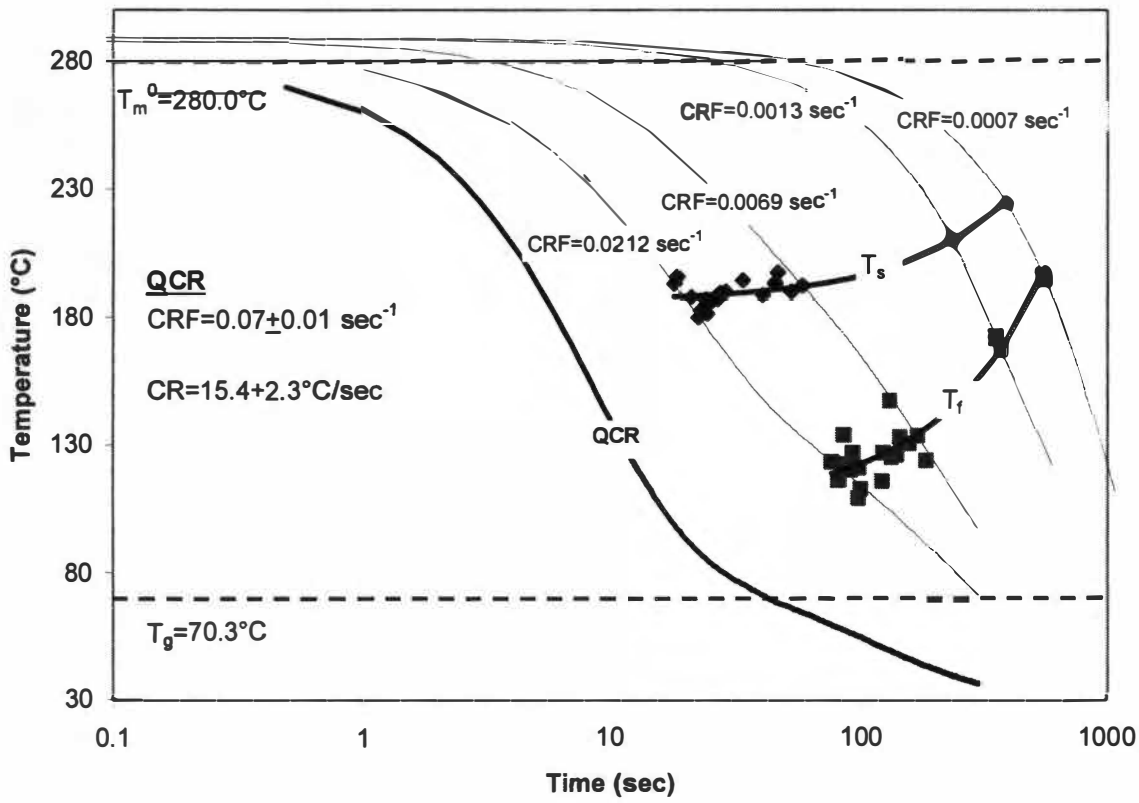

Figure 4.103: Proposed CCT Diagram for PET Homopolymer. Note that QCR Values Listed As +/- One Standard Deviation.

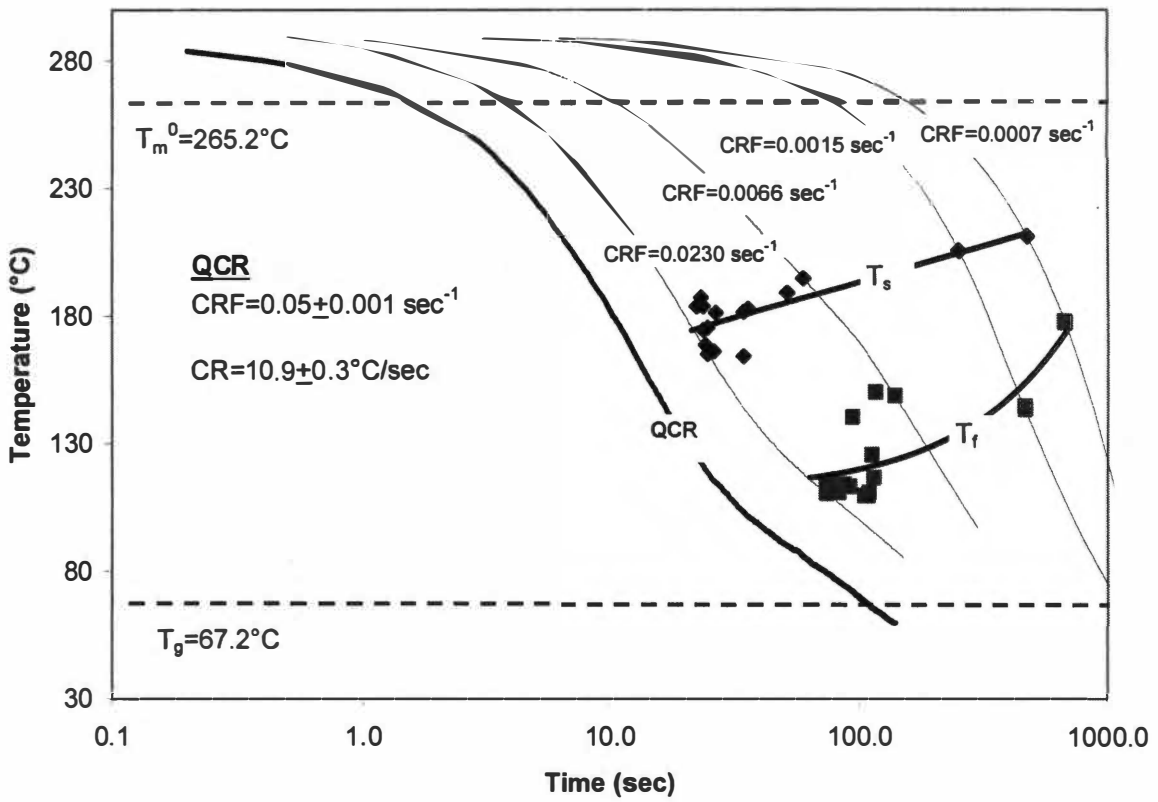

Figure 4.104: Proposed CCT Diagram for PET-4 Copolymer. Note that QCR Values Listed As +/- One Standard Deviation.

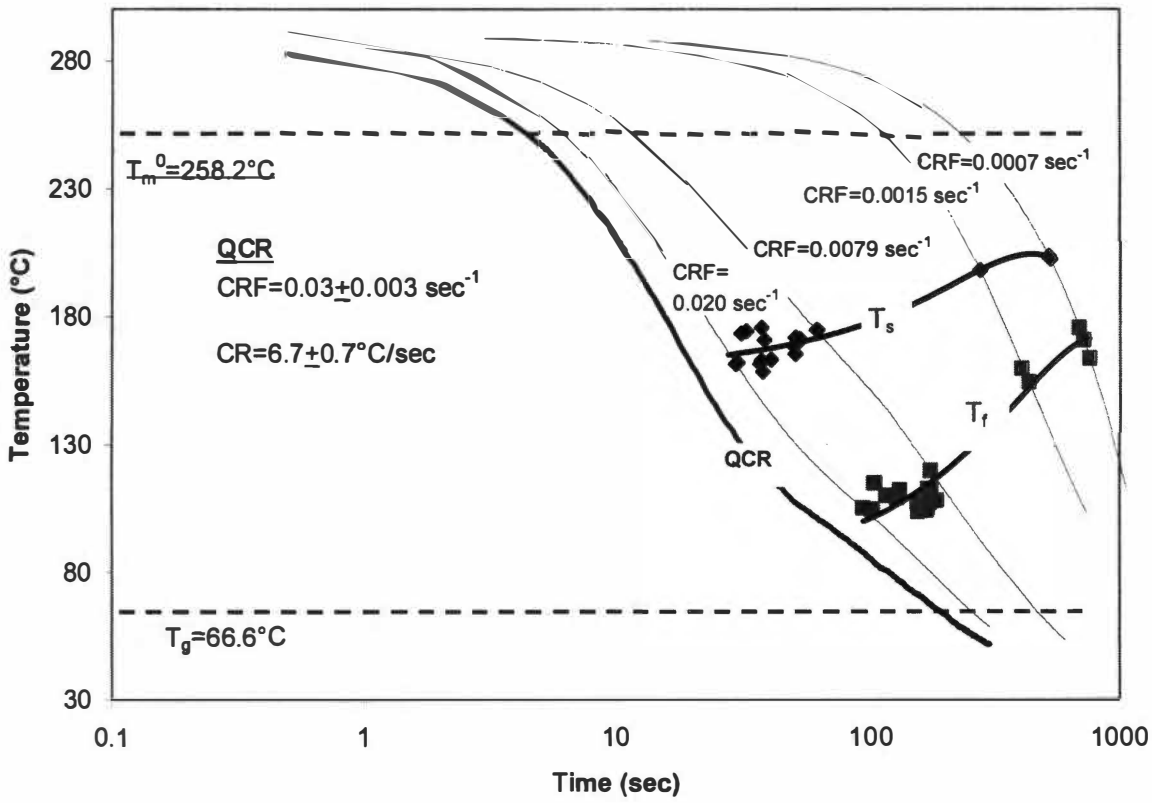

Figure 4.105: Proposed CCT Diagram for PET-7 Copolymer. Note that QCR Values Listed As +/- One Standard Deviation.

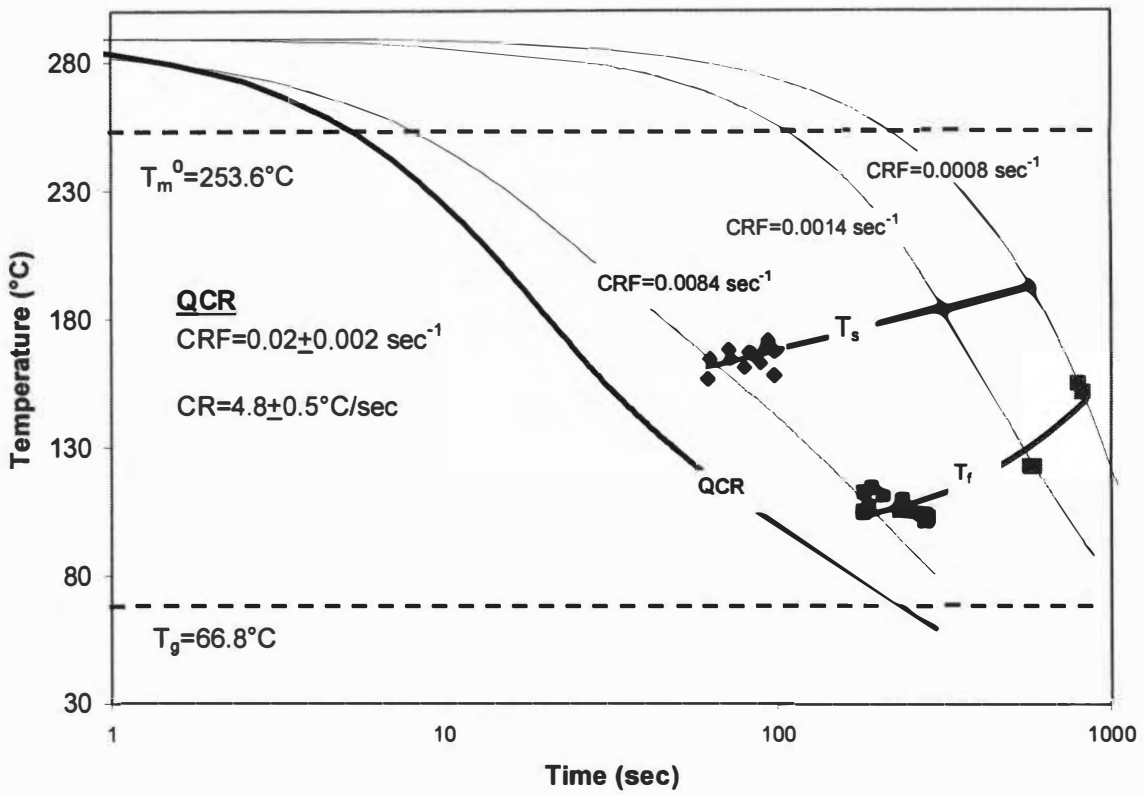

Figure 4.106: Proposed CCT Diagram for PET-10 Copolymer. Note that QCR Values Listed As +/- One Standard Deviation.

significant difference between each of these materials. The general trend of these data is that QCR decreases with increasing comonomer content. This would indicate that the addition of MPDiol comonomer requires that more time must be allowed for the necessary molecular rearrangement to initiate crystallization.

In Figure 4.107 the starting temperatures and cooling rates for the four materials are plotted on the same diagram further illustrating the effect of MPDiol concentration on PET. Here it is shown that not only does the QCR decrease with increasing comonomer concentration, but also the start times appear to be shifted to lower temperature with increasing comonomer concentration.

From examining these plots it is evident that there is a significant amount of unobtainable data, particularly when approaching the critical quenching cooling rate. Because these materials are capable of being quenched to the amorphous state the light signal to noise ratio becomes extremely crucial. At higher and higher cooling rates the signal change associated with the transition becomes immeasurable due to the high level of noise associated with that shown in Figure 4.100. Another source of error in this experiment is related to sample thickness. Although all samples were carefully prepared according to that described earlier, the viscosity of the material became sufficiently low enough at the higher temperatures to allow for some flow during the experiment. This caused the sample to "thin" during the experiment and prevented the samples from being used more than a few times before a fresh sample was required.

The cooling rates intermediate to those obtained with the hot-stage and those obtained with the nitrogen cooling system were also unable to be obtained due to an

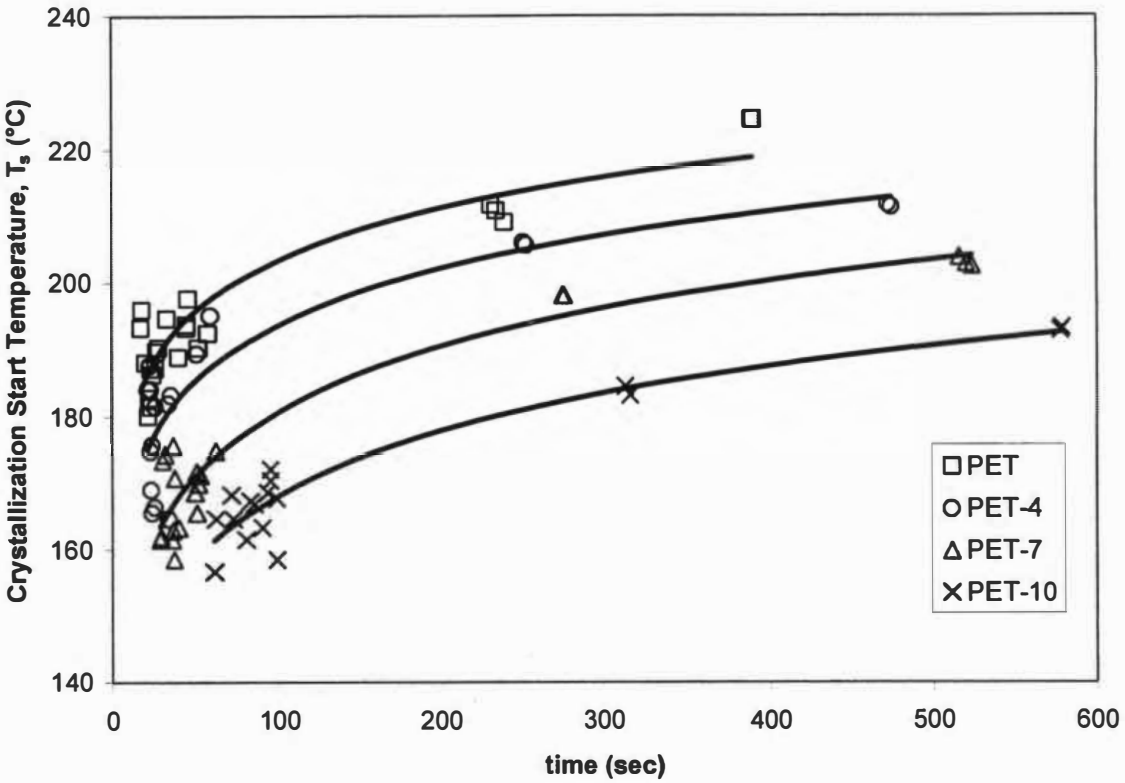

Figure 4.107: Relationship Between Crystallization Start Temperature, T_s, as a Function of Time

insufficient method of obtaining these fairly low cooling rates. The current gas metering system proved to be incapable of delivering a constant, steady flow of gas to the sample thus not allowing for these measurements to be made.

Nevertheless, this experiment has shown that under these high cooling conditions that the addition of MPDiol results in a significant decrease in the rate of crystallization. Additionally it was shown that the addition of MPDiol causes the crystallization process to be shifted to lower temperatures and that an increase in MPDiol concentration eases the ability of these materials to be quenched.

These results would seem to support the results obtained in the previously described DSC experiments. The negative impact of MPDiol's presence on the crystallization kinetics might suggest that more time is required for the molecular rearrangement of these polymer chains to allow for the exclusion of the MPDiol unit from the parent PET homopolymer crystal.

CHAPTER 5: CONCLUSIONS AND RECOMMENDATIONS

5.1. Summary and Conclusions

Differential Scanning Calorimetry (DSC) and a modified Light Depolarizing Microscopy (LDM) technique was used to evaluate the isothermal and nonisothermal crystallization kinetics of poly(ethylene terephthalate) (PET) copolymers containing 2-methyl-1,3-propanediol (MPDiol) as the comonomer unit.

It has been suggested by other investigators that PET copolymers containing certain short diols exhibit an enhanced rate of crystallization. The results of these experiments indicate that the rates of crystallization, both under isothermal and nonisothermal conditions, are reduced by the addition of this particular comonomer. The claim that the more flexible glycol group might increase crystallization rates by promoting chain folding during crystallization does not appear to be substantiated by these experiments, except when undercooling is taken into account for certain isothermally crystallized samples.

For isothermal crystallization experiments it was shown that PET copolymers containing less than or equal to 4mol% MPDiol did appear to show an enhanced rate of crystallization when comparing these materials on the basis of undercooling. It was also shown that the induction time as a function of undercooling was not significantly affected for this level of MPDiol concentration, as implied by the apparent induction times being nearly equal for the PET-4 and PET homopolymer samples.

The thermal characterization of these materials suggested that an increase in MPDiol content resulted in a decrease in the glass transition temperature, likely due to the incorporation of a more flexible unit. Additionally, the melting temperature of partially quenched samples was found to decrease with increasing MPDiol concentration. It was found that the melting temperatures were more strongly influenced by the addition of MPDiol than was the glass transition temperature. Thus the temperature region whereby crystallization is possible is reduced by the addition of MPDiol thus signifying that the crystallizability of these materials is impeded by the addition of MPDiol.

Under nonisothermal conditions it was observed that, even up to the point of quenching, that the incorporation of MPDiol appears to negatively influence the rate of crystallization of these materials. The moderate cooling experiments, conducted using a DSC, showed that PET homopolymer crystallizes more rapidly, and at a higher temperature at a given cooling rate, than any of the copolymer samples and that generally it was observed that an increase in MPDiol concentration shifted the exothermic crystallization peak to lower temperature.

The melting behavior was also examined where it was found that the inclusion of these commoners, as would be expected, served to decrease the observed melting temperature. The isothermal melting behavior was examined using a Hoffman-Weeks approach, showing very good linearity for all copolymers tested ($R^2 \approx 0.99$ in most cases) and predicted an equilibrium melting temperature of 280.0°C for PET homopolymer (well substantiated by other investigators). The remaining copolymers showed a marked decrease with increasing copolymer composition. The results of this analysis of the

melting behavior further support the claim that these comonomers are excluded from the polymer crystal during growth.

5.2. Recommendations for Further Study

There is a need to further refine the CCT diagrams shown in Chapter 4. Particularly it would be useful to obtain average values of the apparent degree of crystallinity at cooling rates along the T_{finish} curve so that the crystallinity as a function of cooling rate can be compared for each material.

Additionally, the use of an independent technique to determine the apparent degree of crystallinity would allow for a more precise value of the quenching rate required for quenching of the material to the glassy state.

With regard to the crystallization kinetics under higher cooling conditions it was previously explained that some more thought is required on exactly how the data should be treated for polymers capable of being quenched to the amorphous state. As was explained earlier, because the crystallization process occurs over such a wide range of temperatures, and because the heat released during crystallization occurs over a longer period of time, no plateau temperature was observed for these materials. Thus unlike many of the polyolefin systems previously studied using this technique, these materials do not achieve a pseudoisothermal crystallization region and therefore the experimental data should be handled much differently.

There is a need to determine the crystallization kinetics using LDM at cooling rates intermediate to that obtained in this experiment using the hotstage and nitrogen gas cooling methods. This could be accomplished by modifying the nitrogen gas cooling

system with a flow meter that allowed for slower gas flow rates to be used than was available with the current system.

Unfortunately, the bulk of this experimentation was required to be carried as an indirect observation, since microscopically the crystalline entities were apparently too small for direct observation. Small Angle X-Ray Scattering (SAXS) experiments and possibly Atomic Force Microscopy (AFM) could provide more detailed information relating to how the lamellae thickness changes with increasing MPDiol content at a given set of cooling and/or isothermal conditions. This would provide the necessary experimental evidence to test the hypothesis that MPDiol is excluded from the PET homopolymer crystal, as well as provide an alternate method for determining the equilibrium melting temperature.

The fact that PET homopolymer samples were found to contain TiO_2, while the copolymer samples did not, made direct comparisons of the experimental data obtained for these materials much more difficult. It is recommended that TiO_2 free PET homopolymer be tested and compared to the experimental data. Since the crystallization kinetics of PET homopolymer are known to be a function of many variables, including comonomer concentration, molecular weight, molecular weight distribution, and diethylene glycol content, it is not recommended that materials obtained from alternate sources be compared to the data shown here. One alternative might be to attempt to separate out the TiO_2 in these samples (possibly by placing the PET homopolymer pellets in solution and allowing the TiO_2 to settle out) and testing those materials.

REFERENCES

Arroyo, M., in "Handbook or Thermoplastics," (Olabisi, O., Ed.), Marcel Dekker, New York, Chapter 18 (1997).

Asano, T., Dzeick-Pickuth, A., and Zachmann, H.G., J. Mater. Sci., 24, 348 (1989).

Atkins, P.W., Physical Chemistry, 4th ed., W.H. Freeman and Co., New York, 1990.

Avrami, M. Journal of Chemical Physics, 7, 1103 (1939); 8, 212 (1940); 9, 177 (1941).

Baltá Calleja, F.J., Garcia Gutièrrez, M.C., Rueda, D.R., and Piccarolo, S., Polymer, 41, 4143 (2000).

Baranov, V.G., Kenarov, A.V., and Volkov, T.I., Journal of Polymer Science, Part C, 30, 271 (1970).

Baur, V.H., Makromol. Chem., 98, 297 (1966).

Baxter, R.A., in "Thermal Analysis," Vol. 1, (Schwenker, R.F., and Garn, P.D. Ed), Academic Press, New York, 65 (1969).

Bier, P., Binsak, R., Vernaleken, H., and Rempel, D., Angew Makromol Chem, 65, 1 (1977).

Boerio-Goates, J., and Callanan, J.E., in "Physical Methods of Chemistry," Vol. 6 (Rossiter, B.W., and Baetzold, R.C. Ed), Wiley, Chichester, 621 (1992).

Bouma, K., Regelink, M., and Gaymans, R.J., Journal of Applied Polymer Science, 80, 2676 (2001).

Bovey, F., in "Macromolecules," (Bovey F., and Winslow, H. Ed), Academic Press, New York, Chapter 5 (1979).

Boyd, R.H., and Phillips, P.J., The Science of Polymer Molecules, Cambridge University Press, Cambridge, 1993.

Carraher, C. Jr., Seymour/Carraher's Polymer Chemistry, 5th ed., Marcel Dekker, New York, 2000.

Chen, S., Lin, F., Chou, J., and Wang, H., Eur. Pat. EP0984086A (2000).

Connor, D., Allen, S., Collard, D., Liotta, C., and Schiraldi, D., Journal of Applied Polymer Science, 80, 2696 (2001).

Daubeny, R.P., Bunn, C.W., and Brown, C.J., Proc. Roy. Soc., Ser. A 226, 531 (1954).

Dietz, W., Colloid. Polym. Sci., 259, 413 (1981).

DiFiore, C., Leone, B., DeRosa, C., Guerra, G., Petraccone, V., DiDino, G., Bianchi, R., and Vosa, R., Journal of Applied Science, 48, 1997 (1993).

Ding, Z., Ph.D. Diss., University of Tenn., (1995).

Ding, Z., and Spruiell, J.E., Journal of Polymer Science: Part B: Polymer Physics, 34, 2783 (1996).

Ding, Z., and Spruiell, J.E., Journal of Polymer Science, 35, 1077 (1997).

Dixon, E.R., and Jackson, J.B., J. Materials Sci., 3, 464 (1968).

Elias, H., Macromolecules, Volume 1, Plenum Press, New York, 1977.

Eisenbach, C.D., Stadler, E., and Enkelmann, V. Macromol. Chem. Phys., 196, 833 (1995).

Evans, U.R., Trans. Faraday Soc., 41, 365 (1945).

Fakirov, S., Structure and Properties of Polymers, Sofia Press, Sofia, 1985.

Fakirov, S., in "Handbook or Thermoplastics," (Olabisi, O., Ed.), Marcel Dekker, New York, Chapter 19 (1997).

Fakirov, S., I., Seganov, I., and Kurdova, E., Makromol. Chem., 182, 185 (1985).

Fischer, E.W., and Schmidt, G., Angew. Chem., 74, 551 (1962).

Flory, P., J. Chem. Phys., 15, 684 (1947).

Flory, P., J. Chem. Phys., 51, 848 (1955).

Flory, P., Ibid., 84, 2857 (1962).

Flory, P., Principles of Polymer Chemistry, Cornell University Press, Ithaca, 1953.

Gallagher, P.K., in "Thermal Characterization of Polymeric Materials," 2nd ed., Vol. 1 (Turi, E.A., Ed), Academic Press, New York, Chapter 1 (1997).

Gan, Z., Zhang, J., and Jiang, B., Journal of Applied Polymer Science, 63, 1793 (1997).

Geil, P., in "Introduction to Polymer Science and Technology: An SPE Textbook," (Kaufman, H., and Falcetta, J. Ed), John Wiley & Sons, New York, Chapter 5 (1977).

Gowariker, V.R., Viswanathan, N.V., and Sreedhar, J., Polymer Science, John Wiley and Sons, New York, 1986.

Groeninckx, G., Berghmans, H., Overbergh, N., and Smets, G., Journal of Polymer Science Polymer Physics, 12, 303 (1974).

Gümther, B., and Zachmann, H.G., Polymer, 24, 1008 (1983).

Gupta, V.K., Man Made Text, 554 (1983).

Hartley, F.D., Lord, F.W., and Morgan, L.B., Phil. Trans. Ser. A, 247, 23 (1954).

Hay, J.N., Br. Polym. J., 3, 74 (1971).

Helfand, E., and Lauritzen, Jr., J., Macromolecules, 6, 631 (1973).

Hemminger, W.F., and Höhne, G.W.H., Calorimetry: Fundamentals and Practice, Verlag Chemie, Weinheim, 1984.

Hillier, I.H., Journal of Applied Polymer Science: Part A, 3, 3067 (1965).

Hoffman, J.D., Polymer, 24, 3 (1983).

Hoffman, J.D., Polymer, 25, 1763 (1985).

Hoffman, J.D., Polymer, 33, 2643 (1992).

Hoffman, J.D., SPE ANTEC Proc., 288 (1989).

Hoffman, J.D., Davies, G.T., and Lauritzen, J.I. Jr., in "Treatise in Solid State Chemistry," Vol. 3, (Hannay, N.B. Ed.), Plenum Press, New York, Chapter 7 (1976).

Hoffman, J.D., and Lauritzen, J.I. Jr., Journal of Research, 65A, 297 (1961).

Hoffman, J.D., Miller, R. L., Macromolecules, 21, 3038 (1988).

Hoffman, J.D., Miller, R. L., Marand, H., and Roitman, D.B., Macromolecules, 25, 2221 (1992).

Hoffman, J.D., and Weeks, J.J., Journal of Research of the National Bureau of Standards—A. Physics and Chemistry, 66A, 13 (1962).

Hoffman, J.D., and Weeks, J.J., J. Chem. Phys., 36, 1723 (1962b).

Hoffman, J.D., Weeks, J.J., and Murphey, W.M., Journal of Research of the National Bureau of Standards—A. Physics and Chemistry, 63A, 67 (1959).

Hybart, F.J. and Pepper, B., Journal of Applied Polymer Science, 13, 2643 (1969).

Jabarin, S.A., Polymer Science and Engineering, 29, 1259 (1989).

Jayakannan, M., and Ramakrishnan, S., Journal of Applied Polymer Science, 74, 59 (1999).

Kamal, M.R., and Chu, E., Polymer Engineering and Science, 23, 27 (1983).

Kämpf, G., Characterization of Plastics by Physical Methods, Hanser Publishers, Munich, 1986.

Karayannidis, G.P., Sideridou, I., Zamboulis, D., Bikiaris, D., and Sakalis, A., Journal of Applied Polymer Science, 78, 200 (2000).

Kargin, V.A., Sogolova, T. I., and Rubshtein V.M., Polymer Sci. USSR, 8, 645 (1966).

Keith, H.D., and Padden, F.J., Journal of Applied Physics, 35, 1270 (1964).

Keith, H.D., and Padden, F.J., Journal of Applied Physics, 35, 1286 (1964b).

Khanna, Y.P., and Taylor, T.J., Polymer Engineering and Science, 28, 1042 (1988).

Kim, S.P., and Kim, S.C., Polymer Engineering and Science, 31, 110 (1991).

Kim, M., Phillips, P.J, and Lin, J.S., Journal of Polymer Science: Part B: Polymer Physics, 38, 154 (2000).

Kiyotsukuri, T., Masuda, T., and Tsutsumi, N., Polymer, 35, 1274 (1994).

Kiyotsukuri, T., Masuda, T., Tsutsumi, N., Sakai, W., and Nagat, M., Polymer, 36, 2629 (1995).

Kong, X., Yang, X., Li, G., Zhao, X., Zhou, E., and Ma, D., European Polymer Journal, 37, 1855 (2000).

Lauritzen, J.I., Jr., Journal of Applied Physics, 44, 4353 (1973).

Lauritzen, J.I., Jr., and Hoffman, J.D., Journal of Applied Physics., 44, 4340 (1973).

Lawton, E.L., Polym. Eng. Sci., 25, 248 (1985).

Lenz, R., Organic Chemistry of Synthetic Polymers, John Wiley & Sons, New York, 1967.

Li, B., Yu, J., Lee, S., and Ree, M., European Polymer Journal, 35, 1607 (1999).

Li, B., Yu, J., Lee, S., and Ree, M., Polymer, 40, 5371 (1999b).

Liu, S., Yu, Y., Cui, Y., Zhang, H., and Mo, Z., Journal of Applied Polymer Science, 70, 2371 (1998).

Lu, X.F., and Hay, J.N., Polymer, 42, 9423 (2001).

Lu, X., and Windle, A.H., Polymer, 36, 451 (1995).

Lu, X., and Windle, A.H., Polymer, 37, 2027 (1996).

Malkin, A., Beghishev, V.P., Keapin, I.A., and Bolgov, S.A., Polymer Engineering and Science, 24, 1396 (1984).

Mandelkern, L., An Introduction to Macromolecules, Springer-Verlag, New York, 1972.

Mandelkern, L., in "History of Polymer Science and Technology," (Seymour, R. Ed.), Marcel Dekker, New York, 147 (1982).

McCrum, N.G., Buckley, C.P., and Bucknall, C.B., Principles of Polymer Engineering, 2nd ed., Oxford University Press, New York, 1997.

Medellín-Rodríguez, F. J., Phillips, P.J., and Lin, J.S., Macromolecules, 29, 7491 (1996).

Medellín-Rodríguez, F. J., Phillips, P.J., Lin, J.S., and Avila-Orta, C.A., Journal of Polymer Science, 36, 763 (1998).

Medellín-Rodríguez, F. J., Phillips, P.J., Lin, J.S., and Campos, R., Journal of Polymer Science, 35, 1757 (1997).

Mitchell, A.K., in "Modern Plastics Encyclopedia 95," McGraw-Hill, New York, B48, 1994.

Miyagi, A., and Wunderlich, B., Journal of Polymer Science Phys. Ed., 10, 2085 (1972).

Nakamura, K., Katayama, K., and Amano, T., Journal of Applied Polymer Science, 17, 1031 (1973).

Ohlberg, S.M., Roth, J., and Raff, R.A.V., Journal of Applied Polymer Science, 1, 114 (1959).

Ozawa, T., Polymer 12, 150 (1971).

Palys, L.H., and Phillips, P.J., Journal of Polymer Science, 18, 829 (1980).

Park, L.S., and Lee, D.C., Polymer Engineering and Science, 35, 1629 (1995).

Patel, R.M., Bheda, J.H., and Spruiell, J.E., Journal of Applied Polymer Science, 42, 1671 (1991).

Patel, R.M., and Spruiell, J.E., Polymer Engineering and Science, 31, 730 (1991).

Pérez, E., Benavente, R., Quijada, R., Narváez, A., and Barrera Galland, G., Journal of Polymer Science: Part B: Polymer Physics, 38, 1440 (2000).

Peeters, M., Goderis, B., Vonk, C., Reynaers, H., and Mathot, V., Journal of Polymer Physics: Part B: Polymer Physics, 35, 2689 (1997).

Phillips, P.J., and Tseng, H.T., Macromolecules, 22, 1649 (1989).

Phillips, P.J., Rep. Prog. Phys., 53, 549 (1990).

Poisson, S.D., Recherches sur la Probabilité des Jugements en matières criminelle et en matière civile, Bachelier, Paris, 1837.

Rabek, J., Experimental Methods in Polymer Chemistry, John Wiley & Sons, New York, 1980.

Richardson, T.L., Industrial Plastics: Theory and Application, 2nd ed., Delmar Publishers, Inc., Albany, 1989.

Righetti, M.C., Pizzoli, M., Lotti, N., and Munari, A., Macromol. Chem. Phys., 199, 2063 (1998).

Ross, G.S., Frolen, L. J., Journal of Res. Natl. Bur. Stand., 79A, 701 (1975).

Ross, G.S., Frolen, L. J., in "Polymers," Vol. 16 (Fava, R.A. Ed) Academic Press, New York, 339 (1980).

Sajkiewicz, P., Carpaneto, L., and Wasiak, A., 42, 5365 (2001).

Sakaguchi, Y., Polymer, 38, 2201, (1997).

Sakaguchi, Y., Okamoto, M., and Tanaka, I., Macromolecules 28, 6155 (1995).

Schultz, Polymer Materials Science, Prentice-Hall, Englewood Cliffs, 1974.

Sharples, A., Introduction to Polymer Crystallization, St. Martin's Press, New York, 1966.

Sogolova, T.I., Polymer Mech., 1, 1 (1965).

Sperling, L.H., Introduction to Physical Polymer Science, 2nd ed., John Wiley & Sons, New York, 1992.

Stein, R., and Tobolsky, A., in "Polymer Science and Materials," (Tobolsky, A., and Herman, M. Ed.), John Wiley & Sons, New York, Chapter 8 (1971).

Stevens, M., Polymer Chemistry, Oxford University Press, New York, 1990.

Stevens, M., in "Analytical Applications of Spectroscopy II (Davies, A.M.C., and Creaser, C.S. Ed), Royal Society of Chemistry, Cambridge, 79 (1991).

Strobl, G., The Physics of Polymers, 2nd ed., Springer-Verlag, New York, 1997.

Suh, J., M.S. Thesis, University of Tenn. (2001).

Sun, Y., and Liu, H., Journal of Applied Science, 81, 2754 (2001).

Supaphol, P., Journal of Applied Polymer Science, 78, 338 (2000).

Supaphol, P., M.S. Thesis, University of Tenn., (1996).

Supaphol, P., and Spruiell, J.E., Journal of Polymer Science: Part B: Polymer Physics, 36, 681 (1998).

Supaphol, P., and Spruiell, J.E., Journal of Applied Polymer Science, 75, 44 (2000).

Supaphol, P., and Spruiell, J.E., Polymer, 42, 699 (2001).

Tant, M.R., and Culberson, W.T., Polymer Engineering and Science, 33, 1152 (1993).

Taylor, G.W., Polymer, 3, 543 (1962).

Tobin, M.C., Journal of Polymer Science Polymer Physics, 12, 399 (1974); 14, 2253 (1976); 15, 2269 (1977).

Turnbull, D., and Fischer, J.C., J. Chem. Phys., 17, 71 (1949).

Ulrich, H., Introduction to Industrial Polymers, 2nd ed., Hanser, New York, 1993.

Urbanovici, E., Schneider, H.A., and Cantow, H.J., Journal of Polymer Science: Part B: Polymer Physics, 35, 359 (1997).

Van Antwerpen, F., and Van Krevelen, D.W., Journal of Polymer Science, 10, 2423 (1972).

Van Reenen, A.J. Brull, R., Wahner, U.M., Raubenheimer, H.G., Sanderson, R. D., and Pasch, H., Journal of Polymer Science: Part A: Polymer Chemistry, 38, 4110 (2000).

Varma, D.S., Radha, A., and Varma, I.K., Tex. Res. Jour., 56, 364 (1986).

Verhoyen, O., Dupret, F., and Legras, R., Polymer Engineering and Science, 38, 1597 (1998).

Vilanova P., Ribas, S., and Guzman, G., Polymer, 26, 423 (1985).

Wang, Z.-G., Hsiao, B.S., Sauer, B.B., and Kampert, W.G., Polymer, 40, 4615 (1999).

Ward, I.M., and Hadley, An Introduction to the Mechanical Properties of Solid Polymers, John Wiley & Sons, Chichester, 1993.

Watson, E.S., O'Neill, M.J., Justin, J., and Brenner, N., Anal. Chem., 36, 1233 (1964).

Weigel, P., and Zimmerman, H., Acta Polym., 30, 297 (1979).

Wendlandt, W.W., and Gallagher, P.K., in "Thermal Characterization of Polymeric Materials," (Turi, E.A., Ed), Academic Press, New York, Chapter 1 (1981).

Wendling, J., and Suter, U.W., Macromolecules, 31, 2516 (1998).

Wlochowicz, A., and Przygocki, W., Jounral of Applied Science, 17, 1197 (1973).

Woodward, A., Atlas of Polymer Morphology, Hanser Publishers, Munich, 1989.

Wunderlich, B., Macromolecular Physics, Vol. 2, Academic Press, New York, 1976.

Wunderlich, B., Macromolecular Physics, Vol. 3, Academic Press, New York, 1980.

Wunderlich, B., Thermal Analysis, Academic Press, San Diego, 1990.

Wunderlich, B., in "Thermal Characterization of Polymeric Materials," 2nd ed., Vol. 1 (Turi, E.A., Ed), Academic Press, New York, Chapter 2 (1997).

Xu, X., Xu, J., Feng, L., and Chen, W., Journal of Applied Polymer Science, 77, 1709 (2000).

Yingning, S.L., Yu, Y., Zhang, H., and Mo, Z., Journal of Applied Polymer Science, 70, 2371 (1998).

Young, R., Introduction to Polymers, Chapman and Hill, New York, 1981.

Zhang, Y., and Gu, L., European Polymer Journal, 36, 759 (2000).

Zhou, C., Clough, S.B., Polymer Engineering Science, 28, 65 (1988).

Ziabicki, A., Appl. Polym. Symp, 6, 1 (1967).

Ziabicki, A., Polymetry, 12, 405 (1967b).

Ziabicki, A., In Fundementals of Fiber Spinning, Wiley, New York, (1976).

VITA

Christopher L. Lewis was born to H. Lloyd and Diana Lewis in Williamsport, Pennsylvania on August 15, 1974. He obtained a Bachelor of Science degree in Plastics and Polymer Engineering Technology from the Pennsylvania College of Technology in May 1997. Upon graduation he obtained a position at AMP Inc. in Harrisburg, Pennsylvania where he worked as a Plastics Engineer until entering graduate school at the University of Tennessee in August, 1999. The Master of Science degree in Polymer Engineering will be officially awarded in May, 2002.